12-2008

Variational Asymptotic Micromechanics Modeling of Composite Materials

Tian Tang
Utah State University

VARIATIONAL ASYMPTOTIC MICROMECHANICS MODELING OF COMPOSITE MATERIALS

by

Tian Tang

A dissertation submitted in partial fulfillment
of the requirements for the degree

of

DOCTOR OF PHILOSOPHY

in

Mechanical Engineering

Approved:

Dr. Wenbin Yu Major Professor	Dr. Leijun Li Committee Member
Dr. Brent E. Stucker Committee Member	Dr. Thomas H. Fronk Committee Member
Dr. David E. Richardson Committee Member	Dr. Byron R. Burnham Dean of Graduate Studies

UTAH STATE UNIVERSITY
Logan, Utah

2008

Abstract

Variational Asymptotic Micromechanics Modeling of Composite Materials

by

Tian Tang, Doctor of Philosophy

Utah State University, 2008

Major Professor: Dr. Wenbin Yu
Department: Mechanical and Aerospace Engineering

The issue of accurately determining the effective properties of composite materials has received the attention of numerous researchers in the last few decades and continues to be in the forefront of material research. Micromechanics models have been proven to be very useful tools for design and analysis of composite materials. In the present work, a versatile micromechanics modeling framework, namely, the ***V***ariational ***A***symptotic ***M***ethod for ***U***nit ***C***ell ***H***omogenization (VAMUCH), has been invented and various micromechancis models have been constructed in light of this novel framework. Considering the periodicity as a small parameter, we can formulate the variational statements of the unit cell through an asymptotic expansion of the energy functional. It is shown that the governing differential equations and periodic boundary conditions of mathematical homogenization theories (MHT) can be reproduced from this variational statement. Finally, we employed the finite element method to solve the numerical solution of the constrained minimization problem. If the local fields within the unit cell are of interest, the proposed models can also accurately recover those fields based on the global behavior. In comparison to other existing models, the advantages of VAMUCH are: (1) it invokes only two essential assumptions within the concept of micromechanics for heterogeneous material with identifiable unit cells; (2) it has an inherent variational nature and its numerical implementation is shown to be straightforward; (3) it calculates the different material properties in different directions simultaneously, which is more efficient than those approaches requiring multiple runs under different loading conditions; and (4) it calculates the effective properties and the local fields directly with the

same accuracy as the fluctuation functions. No postprocessing calculations such as stress averaging and strain averaging are needed.

The present theory is implemented in the computer program VAMUCH, a versatile engineering code for the homogenization of heterogeneous materials. This new micromechanics modeling approach has been successfully applied to predict the effective properties of composite materials including elastic properties, coefficients of thermal expansion, and specific heat and the effective properties of piezoelectric and electro-magneto-elastic composites. This approach has also been extended to the prediction of the nonlinear response of multiphase composites. Numerous examples have been utilized to clearly demonstrate its application and accuracy as a general-purpose micromechanical analysis tool.

(280 pages)

Acknowledgments

I am deeply grateful and indebted to my advisor, Professor Wenbin Yu, for his consistent guidance, support, and encouragement during my graduate studies at Utah State University. Without his help and patience, this work would not have been possible to reach its final stage. In addition to introducing me to the subject of micromechanics, the most important skill that he helped me obtain was how to be an effective researcher.

I would like to thank my committee members, Dr. Brent E. Stucker, Dr. Leijun Li, Dr. Thomas H. Fronk, and Dr. David E. Richardson, for their guidance, criticisms, and insightful comments on my dissertation.

I would like to thank our academic advisor, Bonnie Ogden, for her enthusiasm and great help.

I would also like to thank our department head, Dr. Byard Wood, for his encouragements and writing the recommendation letter for my application for a dissertation fellowship.

This work is supported, in part, by the National Science Foundation under Grant DMI-0522908 and the State of Utah Community/University Research Initiative Grant. This support is gratefully acknowledged.

Special thanks go to Dr. Harald Berger from Otto-von-Guericke-University of Magdeburg, Germany, for technical discussions and kindly providing the ANSYS macro files and the data of the effective properties of PZT-7A fiber reinforced composites.

Finally, I would like to express particular gratitude to my wife, Yanqing Yang, for her endless loving, caring, support, and encouragements.

Tian Tang

Contents

List of Tables

List of Figures

Chapter 1

Introduction

The main impetuses of using composite materials are low weight-stiffness ratio, enhanced fatigue life, and corrosion resistance. Other thrusts of applications in some special fields include wear resistance, thermal-acoustical insulation, low thermal expansion, and low thermal conductivity, etc. In recent years, more and more engineering structures are made of composite materials to achieve better performance. The increased complexity of composite structure at the microlevel, however, greatly complicates the analysis of the structural behavior, which is indispensable for the rational design of these structures. Direct analysis of such structures, although possible, is computationally intensive and unrealistic. One way of determining the properties of composite materials can be accomplished by experimental tests. In many cases, it is not practical that experimental determinations are performed for all possible reinforcement types due to the volume and cost of the required tests. Fortunately, composite materials have a necessary characteristic, namely, statistical homogeneity (SH) [1] so that we can define a representative volume element (RVE), which is, as indicated by Hill [2], structurally entirely typical of the whole mixture on average and contains a sufficient number of inclusions for the apparent overall moduli to be effectively independent of the boundary conditions. In the present investigation, the RVE is conceptually similar to the crystallographic unit cell (UC) [3] and is the building block of the "lattice" of composite materials, namely, a periodic volume element. Based on the fundamental concept of RVE, micromechanics models are employed to simplify the analysis without significant loss of accuracy. As illustrated in Fig. 1.1, micromechanics models enable us to decouple the analysis for composites with heterogeneous microstructures into a local micromechanical analysis over the microstructures and a global analysis of the material without microstructural details. The global analysis requires effective properties obtained from the micromechanical analysis. The responses calculated by the global analysis can be fed into the recovery relations provided by the micromechanical analysis to calculate the pointwise information within the microstructure.

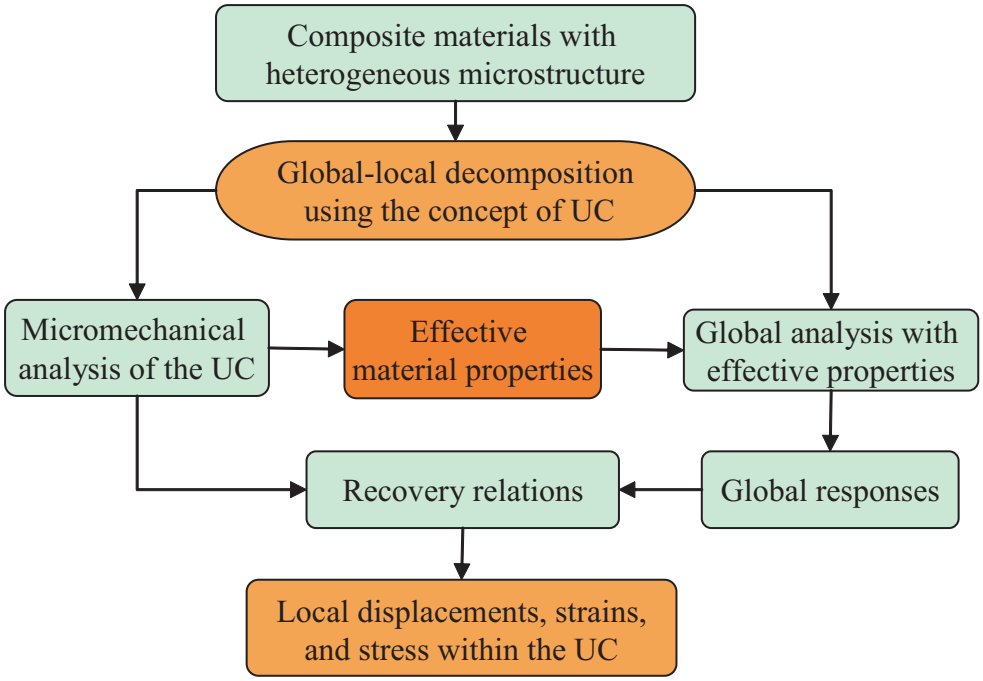

Fig. 1.1: The basic steps of structure analysis with heterogeneous microstructures using the concept of unit cell.

1.1 Literature Review on Micromechanics

The study of micromechanics has been an active research area for many decades and continues to be the forefront of analysis of composite materials. Excellent reviews of micromechanics were given in Hashin [1], Nemat-Nasser and Hori [4], Milton [5], Christensen [6], and Mura [7]. In the following of this chapter, a review of micromechanics from open literature is presented.

1.1.1 Volume Averaging and Effective Properties

The property "averages" of different RVE are statistically indistinguishable. Thus, the heterogeneous composites can be homogenized into equivalent homogeneous materials having effective properties. This homogenization is performed in terms of volume averaging. The average stresses and average strains over the RVE are expressed as:

$$\bar{\sigma}_{ij} = \frac{1}{\Omega}\int_{\Omega} \sigma_{ij}\, \mathrm{d}\Omega \tag{1.1}$$

$$\bar{\epsilon}_{ij} = \frac{1}{\Omega}\int_{\Omega} \epsilon_{ij}\, \mathrm{d}\Omega \tag{1.2}$$

where Ω is the volume of RVE.

One of the central goals of micromechanics is to obtain effective properties. The definitions of effective properties of composite materials can be defined by means of direct or energy expressions.

- **Direct expressions:**

Elastic constitutive equations

$$\begin{aligned} \bar{\sigma}_{ij} &= C^*_{ijkl}\bar{\epsilon}_{kl} \\ \bar{\epsilon}_{ij} &= S^*_{ijkl}\bar{\sigma}_{kl} \end{aligned} \tag{1.3}$$

Thermoelastic constitutive equations

$$\begin{aligned} \bar{\sigma}_{ij} &= C^*_{ijkl}\bar{\epsilon}_{kl} - C^*_{ijkl}\alpha^*_{kl}\bar{\theta} \\ \bar{\epsilon}_{ij} &= S^*_{ijkl}\bar{\sigma}_{kl} + \alpha^*_{ij}\bar{\theta} \end{aligned} \tag{1.4}$$

Piezoelectric constitutive equations

$$\begin{aligned} \bar{\sigma}_{ij} &= C^*_{ijkl}\bar{\epsilon}_{kl} - e^*_{ijk}\bar{E}_k \\ \bar{T}_i &= e^*_{ijk}\bar{\epsilon}_{kl} + k^*_{ij}\bar{E}_j \end{aligned} \tag{1.5}$$

Electro-magneto-elastic constitutive equations

$$\begin{aligned} \bar{\sigma}_{ij} &= C^*_{ijkl}\bar{\epsilon}_{kl} - e^*_{ijk}\bar{E}_k - q^*_{ijk}\bar{H}_k \\ \bar{T}_i &= e^*_{ikl}\bar{\epsilon}_{kl} + k^*_{ij}\bar{E}_j + a^*_{ij}\bar{H}_j \\ \bar{B}_i &= q^*_{ikl}\bar{\epsilon}_{kl} + a^*_{ij}\bar{E}_j + \mu^*_{ij}\bar{H}_j \end{aligned} \tag{1.6}$$

Fourier law of heat conduction

$$\bar{q}_i = -K^*_{ij}\bar{\phi}_{,j} \tag{1.7}$$

where the C_{ijkl} and S_{ijkl} are the stiffness and compliances; α_{ij} are the thermal expansion coefficients; e_{ijk} and q_{ijk} are the piezoelectric and piezomagnetic third order tensors, respectively; k_{ij}, μ_{ij}, and a_{ij} are the dielectric permittivity, magnetic permeability, and magneto-electric second order tensors; K_{ij} are the components of

the second-order thermal conductivity tensor; σ_{ij}, ϵ_{ij} are the tensors of stresses and strains, respectively; T_i, E_i, B_i, H_i, q_i, and $\phi_{,j}$ denote the vectors of the electric flux density (or electric displacement), the electric field, magnetic flux density, magnetic field, heat flux, and temperature gradients, respectively. The "over-bars" stand for volume average values of the field variables over the volume of RVE. Superscripts "*" denote effective properties whose calculation are determined by the micromechanics model one employs.

- **Energy expressions:**

  Elastic strain and complementary strain energy

$$\int_\Omega \frac{1}{2} C_{ijkl}\ \epsilon_{ij}\ \epsilon_{kl} \mathrm{d}\Omega = \frac{1}{2} C^*_{ijkl}\ \bar{\epsilon}_{ij}\ \bar{\epsilon}_{kl} \Omega \tag{1.8}$$

$$\int_\Omega \frac{1}{2} S_{ijkl}\ \sigma_{ij}\ \sigma_{kl} \mathrm{d}\Omega = \frac{1}{2} S^*_{ijkl}\ \bar{\sigma}_{ij}\ \bar{\sigma}_{kl} \Omega \tag{1.9}$$

  Helmholtz free energy

$$\frac{1}{2}\int_\Omega (C_{ijkl}\ \epsilon_{ij}\ \epsilon_{kl} + 2\beta_{ij}\ \epsilon_{ij}\ \theta + c_v\ \frac{\theta^2}{T_0}) \mathrm{d}\Omega = \frac{1}{2}(C^*_{ijkl}\ \bar{\epsilon}_{ij}\ \bar{\epsilon}_{kl} + 2\beta^*_{ij}\ \bar{\epsilon}_{ij}\ \bar{\theta} + c^*_v\ \frac{\bar{\theta}^2}{T_0})\Omega \tag{1.10}$$

  where

$$\beta^*_{ij} = -C^*_{ijkl}\alpha^*_{kl} \tag{1.11}$$

  Electric enthalpy of piezoelectric materials

$$\int_\Omega \epsilon^T D \epsilon \mathrm{d}\Omega = \bar{\epsilon}^T D^* \bar{\epsilon} \Omega \tag{1.12}$$

  where

$$\epsilon = \lfloor \epsilon_{11}\ \ 2\epsilon_{12}\ \ \epsilon_{22}\ \ 2\epsilon_{13}\ \ 2\epsilon_{23}\ \ \epsilon_{33}\ \ E_1\ \ E_2\ \ E_3 \rfloor^T \tag{1.13}$$

  and D is a 9×9 matrix including the elastic, piezoelectric, and dielectric matrix and is expressed as

$$D = \begin{bmatrix} \boldsymbol{C} & -\boldsymbol{e} \\ -\boldsymbol{e}^T & -\boldsymbol{k} \end{bmatrix} \tag{1.14}$$

  where $\boldsymbol{C}$ is a 6×6 elastic stiffness matrix; $\boldsymbol{e}$ is a 6×3 piezoelectric coupling matrix; and $\boldsymbol{k}$ is a 3×3 dielectric constant matrix.

Electromagnetic enthalpy of electro-magneto-elastic materials

$$\int_{\Omega} \epsilon_{||}^{T} \widehat{D} \epsilon_{||} \mathrm{d}\Omega = \bar{\epsilon}^{T} \widehat{D}^{*} \bar{\epsilon} \Omega \tag{1.15}$$

where

$$\epsilon_{||} = \lfloor \epsilon_{11} \;\; 2\epsilon_{12} \;\; \epsilon_{22} \;\; 2\epsilon_{13} \;\; 2\epsilon_{23} \;\; \epsilon_{33} \;\; E_1 \;\; E_2 \;\; E_3 \;\; H_1 \;\; H_2 \;\; H_3 \rfloor^{T} \tag{1.16}$$

and $\widehat{D}$ is a 12×12 matrix including the elastic, piezoelectric, dielectric, piezomagnetic, magneto-electric, and magnetic permeability properties and is expressed as

$$\widehat{D} = \begin{bmatrix} \boldsymbol{C} & -\boldsymbol{e} & -\boldsymbol{q} \\ -\boldsymbol{e}^{T} & -\boldsymbol{k} & -\boldsymbol{a} \\ -\boldsymbol{q}^{T} & -\boldsymbol{a}^{T} & -\boldsymbol{\mu} \end{bmatrix} \tag{1.17}$$

where $\boldsymbol{C}$ is a 6×6 elastic stiffness matrix; $\boldsymbol{e}$ is a 6×3 piezoelectric coupling matrix; $\boldsymbol{k}$ is a 3×3 dielectric constant matrix; $\boldsymbol{q}$ is a 6×3 piezomagnetic matrix; $\boldsymbol{a}$ is a 3×3 magneto-electric coupling matrix; and $\boldsymbol{\mu}$ is a 3×3 magnetic permeability matrix

Energy integral (define effective thermal conductivity)

$$\frac{1}{2} \int_{\Omega} K_{ij} \; \phi_{,i} \; \phi_{,j} \mathrm{d}\Omega = \frac{1}{2} K_{ij}^{*} \; \bar{\phi}_{,i} \; \bar{\phi}_{,j} \Omega \tag{1.18}$$

1.1.2 Rigorous Bounds

(1) Rules of Mixtures

Voigt's and Reuss' *rules of mixtures* provide the effective properties of composites in terms of the quantity, and properties of its constituents based on simplifying assumptions which are that strain is uniform or stress is uniform. Their use is tempered with extreme caution and they only offer the upper and lower bounds with big difference in most cases.

It is well known that the properties of fiber-reinforced composites are controlled by the volume fraction, properties and spatial array of constituents. Figure 1.2 is a typical RVE of fiber-reinforced composites with fiber square array. The fiber is infinitely long perpendicular to the paper. It will be used to illustrate the rules of mixtures for obtaining the effective properties.

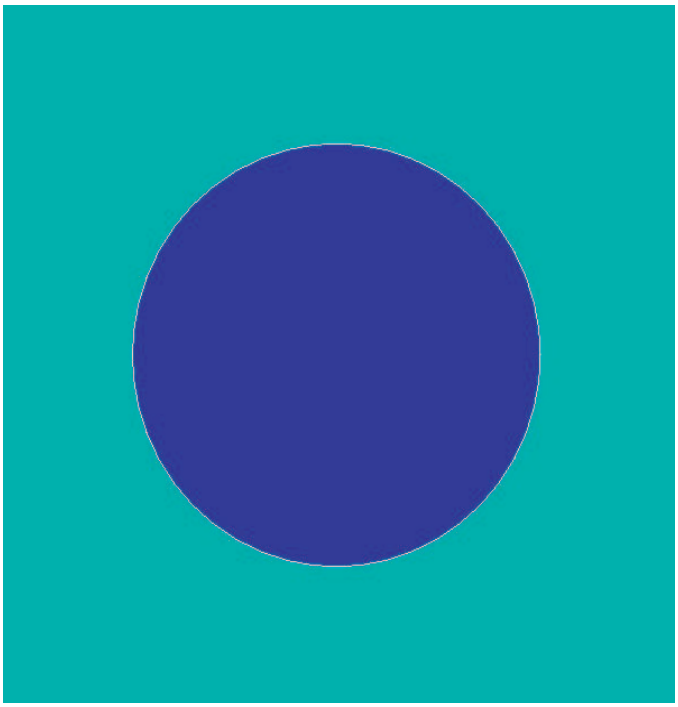

Fig. 1.2: RVE of fiber-reinforced composites with fiber square array.

I. Voigt's rule of mixture According to Voigt, the strain is assumed to be uniform in the composites, i.e., $\epsilon_{ij} = \bar{\epsilon}_{kl}$. Then, the generalized Hookie's law may be expressed as

$$\sigma_{ij} = C_{ijkl}\epsilon_{kl} = C_{ijkl}\bar{\epsilon}_{kl} \tag{1.19}$$

where σ_{ij}, C_{ijkl}, and ϵ_{kl} are the functions of coordinates.

In terms of the concepts of macroscopically average stress and strain of the composites, the following expressions can be obtained

$$\bar{\sigma}_{ij} = \frac{1}{\Omega}\int_{\Omega} C_{ijkl}\bar{\epsilon}_{kl}\,\mathrm{d}\Omega = \left(\frac{1}{\Omega}\int_{\Omega} C_{ijkl}\,\mathrm{d}\Omega\right)\bar{\epsilon}_{kl} = \bar{C}_{ijkl}\bar{\epsilon}_{kl} \tag{1.20}$$

where $\bar{C}_{ijkl}$ are the volume average of stiffness constants of the composites.

The effective stiffness constants C^*_{ijkl} of the homogenized material are the linear constants linking the average stresses and average strains of the composites. It is known that the constitutive relation of the homogenized material is,

$$\bar{\sigma}_{ij} = C^*_{ijkl}\bar{\epsilon}_{kl} \tag{1.21}$$

It is easy to get the below corollary from Eqs. (1.20) and (1.21),

$$C^*_{ijkl} = \bar{C}_{ijkl} = V_f C^{(f)}_{ijkl} + V_m C^{(m)}_{ijkl} \tag{1.22}$$

where V_f and V_m are the volume fraction of the fiber and matrix, respectively; $C^{(f)}_{ijkl}$ and $C^{(m)}_{ijkl}$ are the elastic stiffness constants of the fiber and matrix, respectively.

II. Reuss' rule of mixture According to Reuss, the stress is assumed to be uniform in the composites, the strain-stress relation can be written in terms of compliance constants, such that

$$\epsilon_{ij} = S_{ijkl}\sigma_{kl} = S_{ijkl}\bar{\sigma}_{kl} \tag{1.23}$$

By virtue of the concept of average strain, we obtain the following:

$$\bar{\epsilon}_{ij} = \frac{1}{\Omega}\int_\Omega S_{ijkl}\bar{\sigma}_{kl}\,\mathrm{d}\Omega = \left(\frac{1}{\Omega}\int_\Omega S_{ijkl}\,\mathrm{d}\Omega\right)\bar{\sigma}_{kl} = \bar{S}_{ijkl}\bar{\sigma}_{kl} \tag{1.24}$$

where $\bar{S}_{ijkl}$ are the volume average of compliance constants of composites.

The constitutive relation of the homogenized material using the compliance matrix is described as

$$\bar{\epsilon}_{ij} = S^*_{ijkl}\bar{\sigma}_{kl} \tag{1.25}$$

From Eqs. (1.24) and (1.25) , we can conclude

$$S^*_{ijkl} = \bar{S}_{ijkl} = V_f S^{(f)}_{ijkl} + V_m S^{(m)}_{ijkl} \tag{1.26}$$

where V_f and V_m are the volume fraction of the fiber and matrix, respectively; $S^{(f)}_{ijkl}$ and $S^{(m)}_{ijkl}$ are the elastic compliance constants of the fiber and matrix, respectively.

(2) Hashin-Shtrikman-Type Variational Bounds

Variational bounds use energy principles to determine the bounds for effective properties. Paul [8] obtained the bounds for alloyed materials based on the principle of minimum potential and complementary energy. *Hashin-Shtrikman-type* bounds are thought of as the best possible bounds when the only available geometric information is the volume fraction. However, such bounds can be improved if additional information such as shape of inclusions

and geometry of the microstructure are added into the formulation. Further developments of such bounds are discussed in [1, 9]. A brief summary of the Hashin-Shtrikman bounds is given in this section.

Cubic Polycrystals Hashin-Shtrikman [10] established more improved bounds than the rules of mixtures for effective shear moduli of an aggregate of cubic crystals in terms of a variational method,

- Lower bound

$$G^*_{(-)} = G_1 + 3\left(\frac{5}{G_2 - G_1} - 4\beta_1\right)^{-1} \tag{1.27}$$

- Upper bound

$$G^*_{(+)} = G_2 + 2\left(\frac{5}{G_1 - G_2} - 6\beta_2\right)^{-1} \tag{1.28}$$

where G_1 and G_2 are the two shear moduli of a crystal of cubic symmetry. While β_1 and β_2 are defined as

$$\beta_1 = -\frac{3\left(K + 2G_1\right)}{5G_1\left(3K + 4G_1\right)} \tag{1.29}$$

$$\beta_2 = -\frac{3\left(K + 2G_2\right)}{5G_2\left(3K + 4G_2\right)} \tag{1.30}$$

where K is the bulk modulus of polycrystals. K is the same as the bulk modulus of a single cubic crystal and is expressed as:

$$K = \frac{1}{3}\left(C_{11} + C_{12}\right) \tag{1.31}$$

where C_{11} and C_{12} are the elastic moduli of a single cubic crystal. In comparison, the bounds obtained from rules of mixtures are also listed here:

- Lower bound (Reuss bound)

$$G^*_{(-)} = \frac{5G_1G_2}{2G_2 + 3G_1} \tag{1.32}$$

- Upper bound (Voigt bound)

$$G^*_{(+)} = \frac{1}{5}\left(2G_1 + 3G_2\right) \tag{1.33}$$

Statistically Isotropic Composites The bounds [11] for statistically isotropic composites is established on the basis of the concept of a polarization field. The bounds for the bulk modulus and the shear modulus of two-phase statistical homogeneous composites are given by

$$K^*_{(-)} = K_1 + \frac{V_2}{\frac{1}{K_2-K_1} + \frac{3V_1}{3K_1+4G_1}} \tag{1.34}$$

$$K^*_{(+)} = K_2 + \frac{V_1}{\frac{1}{K_1-K_2} + \frac{3V_2}{3K_2+4G_2}} \tag{1.35}$$

$$G^*_{(-)} = G_1 + \frac{V_2}{\frac{1}{G_2-G_1} + \frac{6V_1(K_1+2G_1)}{5G_1(3K_1+4G_1)}} \tag{1.36}$$

$$G^*_{(+)} = G_2 + \frac{V_1}{\frac{1}{G_1-G_2} + \frac{6V_2(K_2+2G_2)}{5G_2(3K_2+4G_2)}} \tag{1.37}$$

when

$$K_1 < K_2 \tag{1.38}$$

$$G_1 < G_2 \tag{1.39}$$

where K_1 and K_2 are the bulk modulus of the phases, respectively; G_1 and G_2 are the shear modulus of the phases, respectively; and V_1 and V_2 are the volume fraction of the phases, respectively.

Fiber-reinforced Composites The bounds [12] for the plane strain bulk modulus and the transverse shear moduli of two-phase composites are found to be

$$K^*_{(-)} = K_1 + \frac{V_2}{\frac{1}{K_2-K_1} + \frac{V_1}{K_1+G_1}} \tag{1.40}$$

$$K^*_{(+)} = K_2 + \frac{V_1}{\frac{1}{K_1-K_2} + \frac{V_2}{K_2+G_2}} \tag{1.41}$$

$$G^*_{(-)} = G_1 + \frac{V_2}{\frac{1}{G_2-G_1} + \frac{V_1(K_1+2G_1)}{2G_1(K_1+G_1)}} \tag{1.42}$$

$$G^*_{(+)} = G_2 + \frac{V_1}{\frac{1}{G_1 - G_2} + \frac{V_2(K_2+2G_2)}{2G_2(K_2+G_2)}} \tag{1.43}$$

where K_1 and K_2 are the plane strain bulk moduli, respectively; and G_1 and G_2 are the plane strain transverse shear modulus, respectively; These bounds are developed in terms of phase moduli and phase volume fraction.

(3) Improved Bounds

Improved bounds depend nontrivially on two-point or high-order correlation functions and require more geometrical information besides volume fractions [13, 14]. For the conductivity and elastic moduli of isotropic two-phase media, they are bounds that are tighter than the Hashin-Shtrikman bounds.

Milton [15] derived the bounds for effective properties of two-component macroscopically homogeneous and isotropic composites, which improved upon Hashin-Shtrikman bounds in terms of geometrical parameters, i.e., ζ_1 and η_1, as well as volume fraction of the constituents. ζ_1 and η_1 range from 0 to 1, which incorporate three-point correlation functions. Milton also developed four-point bounds on the effective axial shear modulus of transversely isotropic two-phase composites [16]. However, higher order bounds such as three- and four-point bounds diverge with increasing contrast of constituent properties, even though they are definitely an improvement over the two-point bounds. Further discussions of improved bounds have been given in [9, 13, 14].

1.1.3 Analytical Methods

The bounds provide approximate assessments of effective properties, while the analytical methods are aimed to determine unique solutions for the effective properties of a heterogeneous medium.

(1) Dilute Concentration

Dilute concentration problems involve a single particle embedded in an infinite medium in one RVE . The volume fraction of particles are very small and the particles are far apart. Consequently, the interactions between particles can be ignored. The exact solutions for effective shear modulus and bulk modulus have been developed by Dewey [17].

- Shear modulus

$$\frac{G^*}{G_m} = 1 - \frac{15\left(1-\nu_m\right)\left[1-\frac{G_p}{G_m}\right]V_p}{7-5G_m+2\left(4-5\nu_m\right)\frac{G_p}{G_m}} \tag{1.44}$$

- Bulk modulus

$$K^* = K_m + \frac{\left(K_p - K_m\right)V_P}{1+\frac{K_p-K_m}{K_m+\frac{3}{4}\mu_m}} \tag{1.45}$$

(2) Composite Sphere Assemblage Model

For high volume fraction particle composites, Hashin [18] introduced a composite sphere assemblage model, which consists of various sizes of particles embedded in continuous matrix. The composites are idealized as the assemblage of coated spheres. Each coated sphere is composed of a spherical particle and a concentric matrix shell. The ratio of the volume of the individual spherical particle to the total volume of the corresponding individual coated sphere reflects the volume fraction of the composites. However, this model is only available for the effective bulk modulus, which is given by

$$K^* = K_m + \frac{V_p}{\frac{1}{K_p-K_m}+\frac{3V_m}{3K_m+4G_m}} \tag{1.46}$$

where K_p and K_m are the bulk modulus of the particles and matrix, respectively; G_p and G_m are the shear modulus of the particles and matrix, respectively; and V_p and V_m are the volume fraction of the particles and matrix, respectively.

(3) Composite Cylinder Assemblage Model

The composite cylinder model introduced by Hashin and Rosen [19] is used to obtain five independent effective properties of fiber-reinforced composites when the composites are assumed to be transversely isotropic materials. This model considers the composites as the assemblage of coated cylinders. Each coated cylinder consists of cylindrical fiber (with radius a) with an annulus of matrix (with radius b). For each coated cylinder, the ratio of a to b is constant and reflect the volume fraction of composites. By use of this model, the axial effective Young's modulus and Poisson's ratio are found to be

$$E_{11}^* = V_f E_f + \left(1-V_f\right)E_m + \frac{4V_f\left(1-V_f\right)\left(\nu_f-\nu_m\right)^2 G_m}{\frac{\left(1-V_f\right)G_m}{K_f+\frac{G_f}{3}}+\frac{V_f G_m}{K_m+\frac{G_m}{3}}+1} \tag{1.47}$$

$$\nu_{12}^{*} = (1 - V_f)\,\nu_m + V_f \nu_f + \frac{V_f\,(1 - V_f)\,(\nu_f - \nu_m)\left(\frac{G_m}{K_m + \frac{G_m}{3}} - \frac{G_m}{K_f + \frac{G_f}{3}}\right)}{\frac{(1-V_f)G_m}{K_f + \frac{G_f}{3}} + \frac{V_f G_m}{K_m + \frac{G_m}{3}} + 1} \tag{1.48}$$

where K_f and K_m are the bulk modulus of the fibers and matrix, respectively; G_f and G_m are the shear modulus of the fibers and matrix, respectively; and V_f and V_m are the volume fraction of the fibers and matrix, respectively.

(4) Self-Consistent Method

All self-consistent methods are based on the Eshelby result [20], which is valid for ellipsoidal inclusions and assumes a perfect bonding between the phases.

The original work of developing the self-consistent scheme was performed by Hershey [21], Kröner [22], and Kerner [23] to model the behavior of single or polycrystalline materials. Hill [24] and Budiansky [25] simultaneously extended the self-consistent method to high concentration multiphase media. They used the idea of a single inclusion embedded within an effective matrix having the effective elastic moduli of the composites, and thus the interactions of the inclusions are accounted for.

It should be noted that the self-consistent methods are implicit methods which compute the solutions by iteration, since the effective properties of the composites are imbedded directly in the formulation.

Generally speaking, these methods are not suitable for materials with both a high volume fraction of inclusions as well as a high modulus contrast between the constituents [26]. Another difficulty associated with these methods can be observed in rigid inclusions and porous composites. They fail to give correct estimations of shear modulus at a volume fraction of $\frac{1}{2}$ in the case of voids and at a volume fraction of $\frac{2}{5}$ in the case of rigid inclusions [6].

(4) Mori-Tanaka Method

Another analytical model which is also based on the Eshelby Tensor is the Mori-Tanaka method [27]. Benveniste [28] reformulated the application of the Mori-Tanaka's theory to the calculation of the effective properties of composites in terms of the equivalent inclusion

idea of Eshelby and the concept of "average stress" in the matrix of Mori and Tanaka. The central assumption of this method is that the average strain in the interacting inclusions can be approximated by that of a single inclusion embedded in an infinite matrix subjected to the uniform average matrix strain. This method providevs an explicit formulation for the calculation of effective properties of composites, thus it allow one to perform homogenization analysis at minimum computational cost. Berryman and Berge [29] provided an excellent comparison and contrast between self-consistent methods and the Mori-Tanaka approximation. They concluded that explicit methods of Mori-Tanaka and Kuster-Toksöz [30] are suitable to predict the effective elastic moduli of multiphase composites in which the volume fraction of host materials is $70 - 80\%$ or more.

One important characteristic of this method is that it permits full packing of reinforcement inclusions with $0 \leq c \leq 1$, where c is the volume fraction of inclusions. At all volume fractions, the Mori-Tanka method describes the microstructure of composites as aligned ellipsoidal inhomogeneities embedded in a matrix, which can be thought of as affinely deformed version of the composite sphere assemblage (CSA) of Hashin [31]. Therefore, this scheme is well suited for composites with aligned matrix-inclusion microtopologies. Recently, there are many extensions of this method that have been developed for nonaligned cases.

(5) Three-phase Model

To obtain the effective properties of two-phase composite materials, Hashin devised two common idealized geometric models, namely, composite sphere assemblage (CSA) and composite cylinder assemblage (CCA) [18, 19]. However, Hashin methods can not provide all the exact solutions for effective properties even though they are exact elasticity methods instead of self-consistent methods. Both models can only offer bounds for the transverse shear modulus. Christensen and Lo [32] later developed a so-called three-phase model used to offer an exact solution for the remaining transverse shear modulus. Three-phase model is based on the elasticity solution for spherical or cylindrical geometries, and thus it does not rely on the Eshelby solution for inclusions. Christensen [33] also performed a critical evaluation of the Mori-Tanaka scheme, differential method, and three-phase model and concluded that only the three-phase model provides reasonable results at high concentration. The range of validity of the Mori-Tanaka method was established in terms of the results of the

three-phase Model as rigorous results [34]. This model has also been successfully employed to calculation of effective thermal conductivity of composites [35, 36]. It is interesting to note that the three-phase model is often referred to as the generalized self-consistent method despite in fact that it is not a self-consistent method.

1.1.4 Numerical Methods

The effective properties of composites can be approximately obtained by numerically solving the governing equations over RVE associated with appropriate boundary conditions. Numerous numerical methods have been employed for resolving the microfields, such as early finite difference methods, boundary element methods, and finite element methods (FEM). There are many micromechanics models that deal actually with the composites with the assumption of periodic microstructures. The reinforcements are arranged in rectangular, square, hexagonal array, or some other pattern of array. The smallest element is taken as RVE with periodic boundary conditions. Different RVE undergoes identical deformation when the composite medium is subjected to uniform far field loading. These approaches include fast Fourier transforms [37], discrete Fourier transforms [38], the tranformation field analysis [39], method of cells (MOC) developed by Aboudi [40, 41, 42, 43], and RVE-based finite element methods [44]. In this section, we give a brief review of the MOC and the finite element methods.

(1) MOC and its Variants

For unidirectional fiber reinforced composites, the microstructure of the composite materials are assumed to be periodic, namely, the fibers are in a periodical array in the matrix. Due to characteristics of periodic arrangement, the composites can be analyzed using a single repeating cell, which is divided into four subcells. One of the subcells represents fiber, while the others stand for the matrix. The basic assumption of MOC that the displacement vector within each subcell varies linearly with local coordinates. The continuity condition of displacements and tractions is imposed at the interfaces between subcells as well as between the repeating cells on average sense. The applications of MOC are summarized in Aboudi [45].

Generalized Method of Cells (GMC) [46] is the further generalized MOC, in which the repeating unit cell consists of an arbitrary number of subcells. It extends the capability

of MOC in many aspects including the inelastic thermomechanical behavior of multiphase metal matrix composites, modeling various fiber shapes and arrays, porous composites and damage, and the interfacial region around reinforcement inclusions. However, the basic assumption of GMC is the same as that of MOC, i.e., the displacement vector within the subcell is linearly dependent on local coordinates.

The obvious advantage of GMC is that the complete set of effective properties can be obtained just within one step analysis. This model is more computationally efficient than finite elements for modeling fiber composites. However, the deficiency of MOC and GMC is that they can not estimate the local stress and strain accurately due to the lack of so-called shear coupling resulting from the linear assumption of displacement fields. To overcome the shortcoming, a new micromechanics model, i.e., high fidelity GMC (HFGMC) [47] has been developed by incorporating the mathematical homogenization technique and second order expansion of displacement within each subcell. HFGMC has been employed to model the elastic, thermoelastic [47], thermoinelastic [48, 49], and local fiber-matrix debonding [50].

(2) Finite Element Method

The finite element method (FEM) is a commonly used numerical scheme for determining both global response and the local fields. It is thought of as one of the most accurate method and is usually adopted as a benchmark to verify the validity of other schemes. The main advantages of this method are the geometrical versatility and the capability of modeling a wide class of constitutive models for constituents. Its computational expense is high for three-dimensional models. Therefore, sometimes the simplification is adopted to reduce the 3D model to a 2D axisymmetric or planar one.

Sun and Vaidya [44] proposed a vigorous micromechanics method for using a representative volume element (RVE) to predict the mechanical properties of unidirectional fiber composites. The determination of composite moduli in this model is based on the equivalence in strain energy between the equivalent homogeneous material and the original heterogeneous material. The correct boundary conditions imposed on RVE is paramount. The plane sections of RVE remain plane when it is subjected to normal loading, while in two dimensional plane strain shear analysis the edges of RVE do not remain straight and just satisfy periodicity and symmetry. This approach has demonstrated its prediction accuracy.

Ghosh and coworkers [51, 52, 53] developed the *Voronoi cell finite element method*

(VCFEM) in order to computationally model arbitrary heterogeneous materials. This method is based on the Dirichlet tessellation of microstructural material elements into a network of multi-sided convex Voronoi polygons. This VCFEM has inherent computational advantages over the conventional finite element method, especially in the case of simulating the realistic microstructure of unidirectional composites [54, 55].

1.2 Motivation and Objective

From the background in the last section, numerous micromechanics models have been developed and many of the existing approaches are based on various *ad hoc* assumptions. However, a good theory should minimize the use of assumptions, particularly those which are not absolutely needed. According to the author's understanding, there are only two essential assumptions within the concept of micromechanics for composite materials with identifiable UCs:

- **Assumption 1** The exact solutions of the field variables have volume averages over the UC.
- **Assumption 2** The effective material properties obtained from the micromechanical analysis of the UC are independent of the geometry, the boundary conditions, and loading conditions of the macroscopic structure, which means that effective material properties are assumed to be the intrinsic properties of the material when viewed macroscopically.

Note that these assumptions are not restrictive. The mathematical meaning of the first assumption is that the exact solutions of the field variables are integrable over the domain of the UC, which is true almost all the time. The second assumption implies that we can neglect the size effects of the material properties in the macroscopic analysis, which is an assumption often made in conventional continuum mechanics. Of course, the micromechanical analysis of the UC is only needed and appropriate if $\eta = h/l \ll 1$, with h as the characteristic size of the UC and l as the macroscopic size of the macroscopic material. *All the others assumptions such as particular geometry shape and arrangement of the constituents, specific boundary conditions, and prescribed relations between local fields and global fields are convenient but not essential.*

Among the existing micromechanics approaches, the method of cells and its developments established by Aboudi have been shown to be general methods. Commercial finite element software such as ANSYS and ABAQUS can also be general-purpose tools for modeling of composites. However, the prediction of effective properties of composite materials using commercial software is not efficient enough. The drawbacks of commercial software are as follows:

1. The different linear material properties in different directions can not be obtained simultaneously. It requires multiple runs under different boundary conditions.

2. For modeling some properties of heterogeneous materials, for example, thermal conductivity, with constituents having full anisotropy, ANSYS and other FEM package can only handle constituents up to orthotropic materials, which is an unnecessary restriction.

3. Postprocessing calculations which introduce more approximations, such as averaging stress and strain, are needed.

Therefore, the primary objective of the present research is to develop a new general-purpose micromechanics tool to predict the effective properties and behavior of composite materials using the variational asymptotic method (VAM) [56] and two essential assumptions within the concept of micromechanics. VAM simplifies the procedure of solving physical problems that can be formulated in terms of a variational statement involving one or more small parameters. In contrast to conventional asymptotic methods, VAM carries out asymptotic analysis of the variational statement, synthesizing both merits of variational methods (*viz.*, systematic, simple, and easy to be implemented numerically) and asymptotic methods (*viz.*, without *ad hoc* assumptions). VAM has been used extensively to construct efficient high-fidelity structural models for composite beams [57], composite and smart plates [58, 59, 60], and composite and smart shells [61, 62], achieving an excellent compromise between accuracy and efficiency.

1.3 Outline of the Dissertation

The present dissertation is organized in the following way:

- Chapter 2 is a journal article to be submitted. In this paper, a micromechanics model was developed for the prediction of the effective properties and the distribution of local fields of smart materials which are responsive to fully coupled electric, magnetic, thermal, and mechanical fields.

- Chapter 3 is a journal article entitled "Variational Asymptotic Homogenization of Heterogeneous Electromagnetoelastic Materials." In this paper, the variational asymptotic method is used to develop a micromechanics model for predicting the effective properties and local fields of heterogeneous electromagnetoelastic materials

- Chapter 4 is a journal article entitled "Variational Asymptotic Micromechanics Modeling of Heterogeneous Piezoelectric Materials," which presents the derivation and application of a new micromechanics model for predicting the effective properties and local fields of heterogeneous piezoelectric materials.

- Chapter 5 is a journal article entitled "A Variational Asymptotic Micromechanics Model for Predicting Conductivity of Composite Materials." In this paper, a novel micromechanics model was constructed to obtain both effective conductivity and the local fields of the heterogeneous materials in light of the variational asymptotic method.

- Chapter 6 is a journal article (under review) entitled "Asymptotical Approach to Initial Yielding Surface and Elastoplasticity of Metal Matrix Composites." The focus of this paper is to develop a micromechanics model for predicting the initial yielding surface, overall instantaneous moduli, and elastoplastic behavior of metal matrix composites.

- Chapter 7 is a journal article to be submitted. The primary objective of this paper is to develop a micromechanics model for predicting the nonlinear behavior of the electrostrictive multiphase composites.

- Chapter 8 presents the conclusions and proposes the future work.

- All of the work described in Chapter 2 to Chapter 7 are based on the framework of the ***V***ariational ***A***symptotic ***M***ethod for ***U***nit ***C***ell ***H***omogenization (VAMUCH). The original theory and formulation of the VAMUCH are contained in Appendix A and

B. Appendix C perform a critical evaluation of the predictive capabilities of various advanced micromechanics models using several case studies.

References

1. Hashin, Z., "Analysis of composite materials-a survey," *Journal of Applied Mechanics*, Vol. 50, 1983, pp. 481-505.

2. Hill, R., "Elastic properties of reinforced solids: Some theoretical principles," *Journal of the Mechanics and Physics of Solids*, Vol. 11, 1963, pp. 357–372.

3. Holliday, L. and Thackray, G., "Heterogeneity in complex materials and the concept of the representative cell," *Nature*, Vol. 201, 1964, pp. 270-272.

4. Nemat-Nasser, S. and Hori, M., *Micromechanics: Overall Properties of Heterogeneous Materials*, 2nd ed., North-Holland, Amsterdam, 1993.

5. Milton, G.W., *Theory of Composites*, Cambridge University Press, 2001.

6. Christensen, R.M., *Mechanics of Composite Materials*, Dover Publication, Inc., New York, 1979.

7. Mura, T., *Micromechanics of Defects in Solids*, Martinus Nijhoff, Dordrecht, 1987.

8. Paul, B., "Prediction of elastic constants of multiphase materials," *Transactions of the metallurgical society of AIME*, Vol. 218, 1960, pp. 36-41.

9. Böhm, H.J., *Mechanics of Microstructured Materials*, Springer Wien, NewYork, 2004.

10. Hashin, Z. and Shtrikman, S., "A variational approach to the theory of the elastic behavior of polycrystals," *Journal of the Mechanics and Physics of Solids*, Vol. 10, 1962, pp. 343-352.

11. Hashin, Z. and Shtrikman, S., "A variational approach to the theory of the elastic behavior of multiphase materials," *Journal of the Mechanics and Physics of Solids*, Vol. 11, 1963, pp. 127-140.

12. Hashin, Z., "On elastic behavior of fiber reinforced materials of arbitrary transverse phase geometry," *Journal of the Mechanics and Physics of Solids*, Vol. 13, 1965, pp. 119-134.

13. Torquato, S., "Random heterogeneous media: Microstructure and improved bounds on effective properties," *Applied Mechanics Review*, Vol. 44, 1991, pp. 37-76.

14. Torquato, S., "Morphology and effective properties of disordered heterogeneous media," *International Journal of Solids and Structures*, Vol. 35, 1998, pp. 2385-2406.

15. Milton, G.W., "Bounds on the electromagnetic, elastic, and other properties of two-component composites," *Physical Review Letters*, Vol. 46, 1981, pp. 542-545.

16. Milton, G.W., "Bounds on the elastic and transport properties of two-component composites," *Journal of Mechanics and Solids*, Vol. 30, 1982, pp. 177-191.

17. Dewey, J.M., "The elastic constants of materials loaded with non-rigid fillers," *Journal of Applied Physics*, Vol. 18, 1947, pp. 578-581.

18. Hashin, Z., "The elastic moduli of heterogeneous materials," *ASME Jouranl of Applied Mechanics*, Vol. 29, 1962, pp. 143-150.

19. Hashin, Z. and Rosen, B.W., "The elastic moduli of fiber-reinforced materials," *ASME Jouranl of Applied Mechanics*, Vol. 31, 1964, pp. 223-232.

20. Eshelby, J., "The determination of the elastic field of an ellipsoidal inclusion, and related problems," *Proceedings of the Royal Society of London, Series A*, Vol. 241, 1957, pp. 376-396.

21. Hershey, A.V., "The elasticity of an isotropic aggregate of anisotropic cubic crystals," *Journal of Applied Mechanics*, Vol. 21, 1954, pp. 236.

22. Kröner, E., "Berechnung der elastischen Konstanten des Vielkristalls aus den Konstanten des Einkristalls," *Zeitschrift fr Physik A Hadrons and Nuclei*, Vol. 151, 1958, pp. 504.

23. Kerner, E.H., "The elastic and thermoelastic properties of composite media," *Proceedings of the Physical Society*, Vol. 69, 1956, pp. 808.

24. Hill, R., "A self-consistent mechanics of composite materials," *Journal of the Mechanics and Physics of Solids*, Vol. 13, 1965, pp. 213-222.

25. Budiansky, B., "On the elastic moduli of some heterogeneous materials," *Journal of the Mechanics and Physics of Solids*, Vol. 13, 1965, pp. 223-227.

26. Banerjee, B., *Micromechanics-based prediction of thermoelastic properties of high energy materials*. University of Utah, Ph.D thesis, 2002.

27. Mori, T. and Tanaka, K., "Average stress in matrix and average elastic energy of materials with misfitting inclusions," *Acta Metallurgica*, Vol. 21, 1973, pp. 571-574.

28. Benveniste, Y., "A new approach to the application of Mori-Tanaka's theory in composite materials," *Mechanics of Materials*, Vol. 6, 1987, pp. 147-157.

29. Berryman, J.G. and Berge, P.A., "Critique of two explicit schemes for estimating elastic properties of multiphase composites," *Mechanics of Materials*, Vol. 22, 1996, pp. 149-164.

30. Kuster, G.T. and Toksöz, M.N., "Velocity and attenuation of seismic waves in two-phase media: I. theoretical formulation," *Geophysics*, Vol. 39, 1974, pp. 587-606.

31. Böhm, H.J., *A short Introduction to Basic Aspects of Continuum Micromechanics*, ILSB Report, Vienna University of Technology, 2007.

32. Christensen, R.M. and Lo, K.H., "Solutions for effective shear properties in three phase sphere and cylinder models," *Journal of the Mechanics and Physics of Solids*, Vol. 27, 1979, pp. 315-330.

33. Christensen, R.M., "A critical evaluation for a class of micromechanics models," *Journal of the Mechanics and Physics of Solids*, Vol. 38, 1990, pp. 379-404.

34. Christensen, R.M., "On the range of validity of the Mori-Tanaka method," *Journal of the Mechanics and Physics of Solids*, Vol. 40, 1992, pp. 69-73.

35. Hashin, Z., "Assessment of the self-consistent scheme approximation: conductivity of particulate composites," *Journal of Composite Materials*, Vol. 2, 1968, pp. 284-300.

36. Lee, Y.M., Yang, R.B., and Gau, S.S., "A generalized self-consistent method for calculation of effective thermal conductivity of composites with interfacial contact conductance," *International Communication in Heat and Mass Transfer*, Vol. 33, 2006, pp. 142-150.

37. Moulinec, H. and Suquet, P., "A fast numerical method for computing the linear and nonlinear mechanical properties of composites," *Comptes rendus de l'Acadmie des sciences, Srie II*, Vol. 318, 1994, pp. 1417-1423.

38. Müller, W.H., "Mathematical versus experimental stress analysis of inhomogeneities in solids," *Journal of Physics IV*, Vol. 6, 1996, pp. 1-139-C1-148.

39. Dvorak, G.J., "Transformation field analysis of inelastic composite materials," *Proceedings of the Royal Society of London A*, Vol. 437, 1992, pp. 311-327.

40. Aboudi, J., "A continuum theory for fiber-reinforced elastic-viscoplastic composites," *International Journal of Engineering Science*, Vol. 20, 1982, pp. 605-621.

41. Aboudi, J., "Closed form constitutive equations for metal matrix composites," *International Journal of Engineering Science*, Vol. 25, 1987, pp. 1229-1240.

42. Aboudi, J., "Micromechanical analysis of composites by method of cells," *Applied Mechancis Review*, Vol. 42, 1989, pp. 193-221.

43. Aboudi, J., "Micromechanical analysis of composites by method of cells-update," *Applied Mechancis Review*, Vol. 49, 1996, pp. S83-S91.

44. Sun, C.T. and Vaidya, R.S., "Prediction of composite properties from a representative volume element," *Composites Science and Technology*, Vol. 56, 1996, pp. 171-179.

45. Aboudi, J., *Mechanics of Composite Materials-A unified micromechanics approach*, Elsevier, 1991.

46. Paley, M. and Aboudi, J., "Micromechanical analysis of composites by the generalized cells model," *Mechanics of Materials*, Vol. 14, 1992, pp. 127-139.

47. Aboudi, J., Pindera, M.J., and Arnold, S.M., "Linear thermoelastic higher-order theory for periodic multiphase materials," *Journal of Applied Mechanics*, Vol. 68, 2001, pp. 697-707.

48. Aboudi, J., Pindera, M.J., and Arnold, S.M., "Higher-order theory for periodic multiphase materials with inelastic phases," *International Journal of Plasticity*, Vol. 19, 2003, pp. 805-847.

49. Aboudi, J., Pindera, M.J., and Arnold, S.M., *High-Fidelity Generalized Method of Cells for inelastic periodic multiphase materials*, NASA, TM-2002-211469, 2002.

50. Bednarcyk, B.A., Arnold, S.M., Aboudi, J., and Pindera, M.J., "Local field effects in titanium matrix composites subjected to fiber-matrix debonding," *International Journal of Plasticity*, Vol. 20, 2004, pp. 1707-1737.

51. Ghosh, S. and Mallet, R.L., "Voronoi cell finite elements," *Computers and Structures*, Vol. 50, 1994, pp. 33-46.

52. Ghosh, S. and Moorthy, S., Elastic-plastic analysis of heterogeneous microstructures using the Voronoi cell finite element method. *Computer Methods in Applied Mechanics and Engineering*, Vol. 12, 1994, pp. 373-409.

53. Ghosh, S., Lee, K., and Moorthy, S., "Multiple scale analysis of heterogeneous elastic structures using homogenization theory and Voronoi cell finite element method," *International Journal of Solids and Structures*, Vol. 32, 1995, pp. 27-62.

54. Chung, P.W., Tamma, K.K., and Namburu, R.R., "Asymptotic expansion homogenization for heterogeneous media: computational issues and applications," *Composites: Part A*, Vol. 32, 2001, pp. 1291-1301.

55. Ghosh, S., Moorthy, S., and Lee, K., "Microstructural characterization, meso-scale modeling and multiple-scale analysis of discretely reinforced materials," *Materials Science and Engineering A: Struct Mater Prop Microstruct Process*, Vol. 249, 1998, pp. 62-70.

56. Berdichevsky, V.L., "Variational-asymptotic method of constructing a theory of shells," *PMM*, Vol. 43, No. 4, 1979, pp. 664-687.

57. Yu, W., Hodges, D.H., Volovoi, V.V., and Cesnik, C.E.S., "Timoshenko-like modeling of initially curved and twisted composite beams," *International Journal of Solids and Structures*, Vol. 39, No. 19, 2002, pp. 5101-5121.

58. Yu, W., Hodges, D.H., and Volovoi, V.V., "Asymptotic construction of reissner-like models for composite plates with accurate strain recovery," *International Journal of Solids and Structures*, Vol. 39, No. 20, 2002, pp. 5185-5203.

59. Yu, W. and Hodges, D.H., "An asymptotic approach for thermoelastic analysis of laminated composite plates," *Journal of Engineering Mechanics*, Vol. 130, No. 5, 2004, pp. 531-540.

60. Yu, W. and Hodges, D.H., "A simple thermopiezoelastic model for composite plates with accurate stress recovery," *Smart Materials and Structures*, Vol. 13, No. 4, pp. 926-938.

61. Yu, W., Hodges, D.H., and Volovoi, V.V., "Asymptotic generalization of Reissner-Mindlin theory: accurate three-dimensional recovery for composite shells," *Computer Methods in Applied Mechanics and Engineering*, Vol. 191, No. 44, 2002, pp. 5087-5109.

62. Yu, W. and Hodges, D.H., "Mathematical construction of an engineering thermopiezoelastic model for smart composite shells," *Smart Materials and Structures*, Vol. 14, No. 1, 2005, pp. 43-55.

Chapter 2

A Multiphysics Micromechanics Model of Smart Materials Using the Variational Asymptotic Method

[1]

Abstract

The primary objective of the present paper is to develop a micromechanics model for the prediction of the effective properties and the distribution of local fields of smart materials which are responsive to fully coupled electric, magnetic, thermal and mechanical fields. This work is based on the framework of the variational asymptotic method for unit cell homogenization (VAMUCH), a recently developed micromechanics modeling scheme. For practicle use of this theory, we implement this new model using the finite element method into the computer program VAMUCH. For validation, several examples will be presented to compare with the existing models and demonstrate the application and advantages of the new model.

2.1 Introduction

Smart materials are responsive to multiple physical fields, such as electric, magnetic, or thermal fields, in additional to the traditional mechanical field. Behavior of such materials will be multiphysical and predictive tools are essential for effective design and analysis of such materials. Usually, one single constituent will not be sufficient to create desirable properties needed for real applications. Often times, two or more constituents are used to engineering the microstructure of the smart material to achieve better properties. Furthermore, such heterogenous materials might exhibit new properties not existing in any of the constituents due to the coupling of different fields. For example, the most interesting behavior of smart composites consisting of piezoelectric and piezomagnetic constituents is that the magnetoelectric effect, which is only present in composites but absent in constituent phases,

[1] Coauthored by: Tian Tang and Wenbin Yu.

is created by the interaction between the constituent phases, a result of the so-called product property [1]. The mechanical constitutive response of the active materials is coupled with the non-mechanical effects [2]. For example, the continuum of thermo-piezoelectric can exhibit mechanical-electric coupling and pyroelectric effect. The thermo-piezomagnetic material is able to exhibit mechanical-magnetic coupling and pyromagnetic effect. Generally speaking, smart materials could have fully coupled electro-magneto-thermo-elastic behavior which exhibit both mechanical-electric and mechanical-magnetic coupling effects as well as pyroelectric, pyromagnetic, and the magnetoelectric effects.

The constitutive equations of thermo-elastic material, thermo-piezoelectric material, thermo-piezomagnetic material, and fully coupled electro-magneto-thermo-elastic material are expressed using Eqs. (2.1), (2.2), (2.3), and (2.4), respectively:

- Thermo-elastic constitutive equations

$$\sigma_{ij} = C_{ijkl}\epsilon_{kl} - \Lambda_{ij}\theta \tag{2.1}$$

- Thermo-piezoelectric constitutive equations

$$\begin{aligned} \sigma_{ij} &= C_{ijkl}\epsilon_{kl} - e_{kij}E_k - \Lambda_{ij}\theta \\ D_i &= e_{ikl}\epsilon_{kl} + \kappa_{ik}E_k + p_i\theta \end{aligned} \tag{2.2}$$

- Thermo-piezomagnetic constitutive equations

$$\begin{aligned} \sigma_{ij} &= C_{ijkl}\epsilon_{kl} - q_{kij}H_k - \Lambda_{ij}\theta \\ B_i &= q_{ikl}\epsilon_{kl} + \mu_{ik}H_k + m_i\theta \end{aligned} \tag{2.3}$$

- Thermo-electric-magnetic-elastic constitutive equations

$$\begin{aligned} \sigma_{ij} &= C_{ijkl}\epsilon_{kl} - e_{kij}E_k - q_{kij}H_k - \Lambda_{ij}\theta \\ D_i &= e_{ikl}\epsilon_{kl} + \kappa_{ik}E_k + a_{ik}H_k + p_i\theta \\ B_i &= q_{ikl}\epsilon_{kl} + a_{ik}E_k + \mu_{ik}H_k + m_i\theta \end{aligned} \tag{2.4}$$

where C_{ijkl}, e_{kij}, q_{kij}, and Λ_{ij} are the elastic, the piezoelectric, the piezomagnetic, and the thermal stress tensors, respectively (Note that $\Lambda_{ij} = -C_{ijkl}\alpha_{kl}$, where α_{kl} is the thermal

expansion coefficients); κ_{ik}, a_{ik}, and p_i are the dielectric, magnetoelectric, and pyroelectric tensors, respectively; and μ_{ik} and m_i are the magnetic permeability and pyromagnetic tensors.

Li and Dunn [3] employed the Mori-Tanaka method [4] for the micromechanics analysis of the average fields and effective moduli of fully coupled magneto-electro-elastic composites where the closed-form expressions are obtained for effective magneto-electro-elastic properties of circular cylinder fibrous and laminated two-phase composites. Aboudi [5] developed a homogenization method for the prediction of the effective properties of magneto-electro-thermo-elastic composites using the framework of high-fidelity generalized method of cells. The predictions of this model agree with those of Mori-Tanaka model well. Lee *et al.* [6] developed a finite element analysis-based micromechanics approach through averaging of the representative volume element (RVE) to determine the effective dielectric, magnetic, mechanical, and coupled-field properties of this composites as functions of the phase volume fractions, the fiber arrangements in RVE, and the fiber material properties with special emphasis on the poling directions of the piezoelectric and piezomagnetic fibers. The authors recently constructed a micromechanics approach for the prediction of the effective properties and local fields of heterogeneous electromagnetoelastic materials [7]. The work is based on the framework of variational asymptotic method for unit cell homogenization (VAMUCH) [8-12]. None of the above approach involve the effective specific heat for smart heterogeneous materials, which is, as pointed out by Rosen and Hashin [13], the quantity of heat necessary to produce a uniform temperature rise under the conditions of constant surface boundary conditions. The effective specific heats of the composite are not the simple weighted averages of the specific heat of components because the values of the local fields may change although the values of the global fields are kept constant when the smart material is subjected to fixed surface boundary conditions and a uniform temperature rise.

The primary objective of the present paper is to enable VAMUCH for smart heterogeneous composites to capture the fully coupled multiphyiscal behavior including electric, magnetic, thermal, and elastic behavior and their interactions. The resulting theory and companion code will be able to predict effective multiphysical properties (including the effective elastic, piezoelectic, piezomagnetic, and magnetoelectric coupling coefficients as well as the thermal stress coefficients, pyroelectric constants, pyromagnetic constants, and specific heats) and calculate the local multiphysical field distribution within the microstructure.

This work is build upon the variational asymptotic method [14] along with two essential assumptions within the concept of micromechanics for heterogeneous with an identifiable unit cell (UC):

- **Assumption 1** The exact solutions of the field variables have volume averages over the UC. For example, if u_i, ϕ^e, and ϕ^m are the exact displacements, electric potential, and magnetic potential within the UC occupying a volume Ω, respectively, there exist v_i, ψ^e, and ψ^m such that

$$\begin{aligned} v_i &= \frac{1}{\Omega}\int_\Omega u_i \, \mathrm{d}\Omega \equiv \langle u_i \rangle \\ \psi^e &= \frac{1}{\Omega}\int_\Omega \phi^e \, \mathrm{d}\Omega \equiv \langle \phi^e \rangle \\ \psi^m &= \frac{1}{\Omega}\int_\Omega \phi^m \, \mathrm{d}\Omega \equiv \langle \phi^m \rangle \end{aligned} \tag{2.5}$$

- **Assumption 2** The effective material properties obtained from the micromechanical analysis of the UC are independent of the geometry, the boundary conditions, and loading conditions of the macroscopic structure, which means that effective properties are assumed to be the intrinsic properties of the material when viewed macroscopically.

Note that these assumptions are not restrictive. The mathematical meaning of the first assumption is that the exact solutions of the field variables can be integrated over the domain of UC, which is true almost all the time. The second assumption implies that we will neglect the size effects of the material properties in the macroscopic analysis, which is an assumption often made in the conventional continuum mechanics. Of course, the micromechanical analysis of the UC is only needed and appropriate if $\eta = h/l \ll 1$, with h as the characteristic size of the UC and l as the macroscopic size of the material. Others assumptions such as particular geometry shape and arrangement of the constituents, specific boundary conditions applied to the UC, and prescribed relations between local fields and global fields are not needed for this study.

2.2 Theoretical Formulation

Three coordinates are used in our formulation: two cartesian coordinates $\mathbf{x} = (x_1, x_2, x_3)$ and $\mathbf{y} = (y_1, y_2, y_3)$, and an integer-valued coordinate $\mathbf{n} = (n_1, n_2, n_3)$ (see Fig. 2.1). We use x_i as the global coordinates to describe the macroscopic structure and y_i parallel to x_i

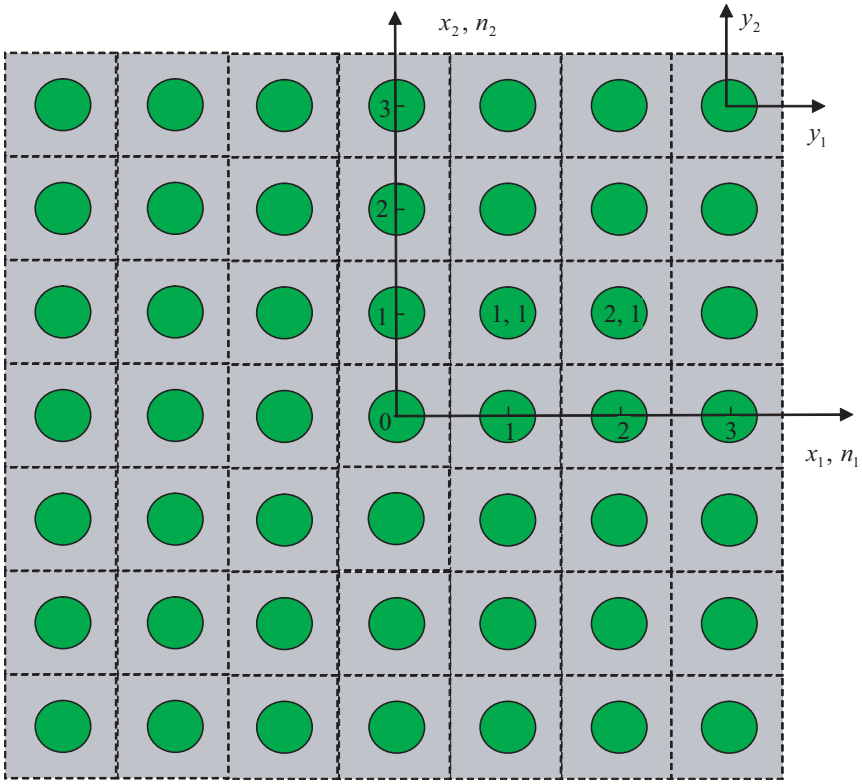

Fig. 2.1: Coordinate systems for heterogenous materials (only two-dimensional (2D) UC is drawn for clarity).

as the local coordinates to describe the UC (Here and throughout the paper, Latin indices assume 1, 2, and 3 and repeated indices are summed over their range except where explicitly indicated). We choose the origin of the local coordinates y_i to be the geometric center of UC. For example, if the UC is a cube with dimensions as d_i, then $y_i \in [-\frac{d_i}{2}, \frac{d_i}{2}]$. To uniquely locate a UC in the heterogeneous material we also introduce integer coordinates n_i. The integer coordinates are related to the global coordinates in such a way that $n_i = x_i/d_i$ (no summation over i). It is emphasized although only square array is sketched in Fig. 2.1, the present theory has no such limitations.

The same effective properties can be calculated from an imaginary, unbounded, and unloaded heterogeneous material with the same microstrucutre as the real, loaded, and bounded one in light of the essential assumption 2. Therefore, the micromechanics model could be developed from an imaginary, unloaded, heterogeneous material which completely occupies the three-dimensional (3D) space $\mathcal{R}$ and composes of infinite many repeating UCs. The total potential energy of this imaginary material is equal to the summation of the

Helmholtz free energy stored in all the UCs, which is

$$\Pi = \sum_{n=-\infty}^{\infty} \int_{\Omega} \left(\frac{1}{2} \epsilon^T D \epsilon + \epsilon^T \eta \theta + \frac{1}{2} c_v \frac{\theta^2}{T_0} \right) \mathrm{d}\Omega \tag{2.6}$$

where

$$\epsilon = \lfloor \epsilon_{11}, 2\epsilon_{12}, \epsilon_{22}, 2\epsilon_{13}, 2\epsilon_{23}, \epsilon_{33}, E_1, E_2, E_3, H_1, H_2, H_3 \rfloor^T \tag{2.7}$$

containing the 3D strain field ϵ_{ij}, the 3D electric field E_i, and the 3D magnetic field H_i, which are defined for a linear theory as:

$$\epsilon_{ij}(\mathbf{n}; \mathbf{y}) = \frac{1}{2} \left[\frac{\partial u_i(\mathbf{n}; \mathbf{y})}{\partial y_j} + \frac{\partial u_j(\mathbf{n}; \mathbf{y})}{\partial y_i} \right] \tag{2.8}$$

$$E_i(\mathbf{n}; \mathbf{y}) = -\frac{\partial \phi^e(\mathbf{n}; \mathbf{y})}{\partial y_i} \tag{2.9}$$

$$H_i(\mathbf{n}; \mathbf{y}) = -\frac{\partial \phi^m(\mathbf{n}; \mathbf{y})}{\partial y_i} \tag{2.10}$$

and D is a 12×12 matrix containing all the necessary material constants for characterizing the fully coupled thermoelectromagnetoelastic materials such that

$$D = \begin{bmatrix} \boldsymbol{C} & -\boldsymbol{e} & -\boldsymbol{q} \\ -\boldsymbol{e}^T & -\boldsymbol{k} & -\boldsymbol{a} \\ -\boldsymbol{q}^T & -\boldsymbol{a}^T & -\boldsymbol{\mu} \end{bmatrix} \tag{2.11}$$

where $\boldsymbol{C}$ is a 6×6 submatrix for elastic constants, $\boldsymbol{e}$ is a 6×3 submatrix for piezoelectric coefficients, $\boldsymbol{q}$ is a 6×3 submatrix for piezomagnetic coefficients, $\boldsymbol{k}$ is a 3×3 submatrix for dielectric permeability, $\boldsymbol{a}$ is a 3×3 submatrix for electromagnetic coefficients, and $\boldsymbol{\mu}$ is a 3×3 submatrix for magnetic permeability.

Other terms in Eq. (2.6) include η, which is a 12×1 matrix containing the second-order of thermal stress tensor Λ_{ij}, vectors of pyroelectric p_i, and vectors of pyromagnetic m_i; c_v is the specific heat per unit volume at constant volume, T_0 is the reference temperature at which the constituent material is stress free, θ denotes the difference between the actual temperature and the reference temperature.

Since the infinite many UCs form a continuous heterogenous material, we need to enforce the continuity of the displacement field u_i, the electric potential field ϕ^e, and the

magnetic potential ϕ^m on the interface between adjacent UCs, which are:

$$\begin{aligned}
u_i(n_1, n_2, n_3; d_1/2, y_2, y_3) &= u_i(n_1+1, n_2, n_3; -d_1/2, y_2, y_3) \\
u_i(n_1, n_2, n_3; y_1, d_2/2, y_3) &= u_i(n_1, n_2+1, n_3; y_1, -d_2/2, y_3) \\
u_i(n_1, n_2, n_3; y_1, y_2, d_3/2) &= u_i(n_1, n_2, n_3+1; y_1, y_2, -d_3/2) \\
\phi^e(n_1, n_2, n_3; d_1/2, y_2, y_3) &= \phi^e(n_1+1, n_2, n_3; -d_1/2, y_2, y_3) \\
\phi^e(n_1, n_2, n_3; y_1, d_2/2, y_3) &= \phi^e(n_1, n_2+1, n_3; y_1, -d_2/2, y_3) \\
\phi^e(n_1, n_2, n_3; y_1, y_2, d_3/2) &= \phi^e(n_1, n_2, n_3+1; y_1, y_2, -d_3/2) \\
\phi^m(n_1, n_2, n_3; d_1/2, y_2, y_3) &= \phi^m(n_1+1, n_2, n_3; -d_1/2, y_2, y_3) \\
\phi^m(n_1, n_2, n_3; y_1, d_2/2, y_3) &= \phi^m(n_1, n_2+1, n_3; y_1, -d_2/2, y_3) \\
\phi^m(n_1, n_2, n_3; y_1, y_2, d_3/2) &= \phi^m(n_1, n_2, n_3+1; y_1, y_2, -d_3/2)
\end{aligned} \tag{2.12}$$

The smart heterogeneous materials considered here is subjected to a uniform temperature deviation θ. Therefore, the continuity condition for temperature field between adjacent UCs is automatically satisfied. The exact solution of the present problem will minimize the summation of Helmholtz free energy in Eq. (2.6) under the conditions in Eqs. (2.5) and (2.12). To avoid the difficulty associated with discrete integer arguments, we can reformulate the problem, including Eqs. (2.6), (2.8), (2.9), (2.10), and (2.12) in terms of continuous functions using the idea of quasicontinuum [15]. The corresponding formulas are listed below.

$$\Pi = \int_{\mathcal{R}} \left\langle \frac{1}{2}\epsilon^T D\epsilon + \epsilon^T \eta\theta + \frac{1}{2}c_v \frac{\theta^2}{T_0} \right\rangle \mathrm{d}\mathcal{R} \tag{2.13}$$

$$\epsilon_{ij}(\mathbf{x};\mathbf{y}) = \frac{1}{2}\left[\frac{\partial u_i(\mathbf{x};\mathbf{y})}{\partial y_j} + \frac{\partial u_j(\mathbf{x};\mathbf{y})}{\partial y_i}\right] \equiv u_{(i|j)} \tag{2.14}$$

$$E_i(\mathbf{x};\mathbf{y}) = -\frac{\partial \phi^e(\mathbf{x};\mathbf{y})}{\partial y_i} \tag{2.15}$$

$$H_i(\mathbf{x};\mathbf{y}) = -\frac{\partial \phi^m(\mathbf{x};\mathbf{y})}{\partial y_i} \tag{2.16}$$

and

$$
\begin{aligned}
u_i(x_1,x_2,x_3;d_1/2,y_2,y_3) &= u_i(x_1+d_1,x_2,x_3;-d_1/2,y_2,y_3)\\
u_i(x_1,x_2,x_3;y_1,d_2/2,y_3) &= u_i(x_1,x_2+d_2,x_3;y_1,-d_2/2,y_3)\\
u_i(x_1,x_2,x_3;y_1,y_2,d_3/2) &= u_i(x_1,x_2,x_3+d_3;y_1,y_2,-d_3/2)\\
\phi^e(x_1,x_2,x_3;d_1/2,y_2,y_3) &= \phi^e(x_1+d_1,x_2,x_3;-d_1/2,y_2,y_3)\\
\phi^e(x_1,x_2,x_3;y_1,d_2/2,y_3) &= \phi^e(x_1,x_2+d_2,x_3;y_1,-d_2/2,y_3)\\
\phi^e(x_1,x_2,x_3;y_1,y_2,d_3/2) &= \phi^e(x_1,x_2,x_3+d_3;y_1,y_2,-d_3/2)\\
\phi^m(x_1,x_2,x_3;d_1/2,y_2,y_3) &= \phi^m(x_1+d_1,x_2,x_3;-d_1/2,y_2,y_3)\\
\phi^m(x_1,x_2,x_3;y_1,d_2/2,y_3) &= \phi^m(x_1,x_2+d_2,x_3;y_1,-d_2/2,y_3)\\
\phi^m(x_1,x_2,x_3;y_1,y_2,d_3/2) &= \phi^m(x_1,x_2,x_3+d_3;y_1,y_2,-d_3/2)
\end{aligned}
\tag{2.17}
$$

Introducing Lagrange multipliers, we can pose the variational statement of the micromechanical analysis of UC as a stationary value problem of the following functional:

$$
\begin{aligned}
J = \int_{\mathcal{R}} \Bigg\{ & \left\langle \frac{1}{2}\epsilon^T D\epsilon + \epsilon^T\eta\theta + \frac{1}{2}c_v\,\frac{\theta^2}{T_0}\right\rangle + \lambda_i(\langle u_i\rangle - v_i)\\
& + \lambda^e(\langle\phi\rangle^e - \psi^e) + \lambda^m(\langle\phi\rangle^m - \psi^m)\\
& + \int_{S_1}\gamma_{i1}\left[u_i(x_j;d_1/2,y_2,y_3) - u_i(x_j+\delta_{j1}d_1;-d_1/2,y_2,y_3)\right]\mathrm{d}S_1\\
& + \int_{S_2}\gamma_{i2}\left[u_i(x_j;y_1,d_2/2,y_3) - u_i(x_j+\delta_{j2}d_2;y_1,-d_2/2,y_3)\right]\mathrm{d}S_2\\
& + \int_{S_3}\gamma_{i3}\left[u_i(x_j;y_1,y_2,d_3/2) - u_i(x_j+\delta_{j3}d_3;y_1,y_2,-d_3/2)\right]\mathrm{d}S_3\\
& + \int_{S_1}\alpha_1\left[\phi^e(x_j;d_1/2,y_2,y_3) - \phi^e(x_j+\delta_{j1}d_1;-d_1/2,y_2,y_3)\right]\mathrm{d}S_1\\
& + \int_{S_2}\alpha_2\left[\phi^e(x_j;y_1,d_2/2,y_3) - \phi^e(x_j+\delta_{j2}d_2;y_1,-d_2/2,y_3)\right]\mathrm{d}S_2\\
& + \int_{S_3}\alpha_3\left[\phi^e(x_j;y_1,y_2,d_3/2) - \phi^e(x_j+\delta_{j3}d_3;y_1,y_2,-d_3/2)\right]\mathrm{d}S_3\\
& + \int_{S_1}\beta_1\left[\phi^m(x_j;d_1/2,y_2,y_3) - \phi^m(x_j+\delta_{j1}d_1;-d_1/2,y_2,y_3)\right]\mathrm{d}S_1\\
& + \int_{S_2}\beta_2\left[\phi^m(x_j;y_1,d_2/2,y_3) - \phi^m(x_j+\delta_{j2}d_2;y_1,-d_2/2,y_3)\right]\mathrm{d}S_2\\
& + \int_{S_3}\beta_3\left[\phi^m(x_j;y_1,y_2,d_3/2) - \phi^m(x_j+\delta_{j3}d_3;y_1,y_2,-d_3/2)\right]\mathrm{d}S_3\Bigg\}\mathrm{d}\mathcal{R}
\end{aligned}
\tag{2.18}
$$

where λ_i, λ^e, λ^m, γ_{ij}, α_i, and β_i are Lagrange multipliers introduced to enforce the constraints in Eqs. (2.5) and (2.17), S_i are the surfaces with $n_i = 1$, x_j represents the triplet

of x_1, x_2, x_3, and δ_{ij} is the Kronecker delta. Following the general procedure of VAMUCH, we can obtain the following change of variables for u_i, ϕ^e, and ϕ^m:

$$u_i(\mathbf{x};\mathbf{y}) = v_i(\mathbf{x}) + y_j\frac{\partial v_i}{\partial x_j} + \chi_i(\mathbf{x};\mathbf{y}) \tag{2.19}$$

$$\phi^e(\mathbf{x};\mathbf{y}) = \psi^e(\mathbf{x}) + y_i\frac{\partial \psi^e}{\partial x_i} + \zeta^e(\mathbf{x};\mathbf{y}) \tag{2.20}$$

$$\phi^m(\mathbf{x};\mathbf{y}) = \psi^m(\mathbf{x}) + y_i\frac{\partial \psi^m}{\partial x_i} + \zeta^m(\mathbf{x};\mathbf{y}) \tag{2.21}$$

where χ_i, ζ^e, and ζ^m are the fluctuation functions, satisfying the following constraints in view of Eqs. (2.5) when the origin of the local coordinate system is chosen to be the center of UC:

$$\langle\chi_i\rangle = 0 \qquad \langle\zeta^e\rangle = 0 \qquad \langle\zeta^m\rangle = 0 \tag{2.22}$$

Substituting Eqs. (2.19), (2.20), and (2.21) into Eq. (2.18), we obtain a stationary value problem of a functional defined over UC for χ_i, ζ^e, and ζ^m according to the variational asymptotic method [14], such that:

$$\begin{aligned} J_\Omega = &\left\langle \frac{1}{2}\epsilon^T D\epsilon + \epsilon^T\eta\theta + \frac{1}{2}c_v\frac{\theta^2}{T_0}\right\rangle + \lambda_i\langle\chi_i\rangle + \lambda^e\langle\zeta^e\rangle \\ &+ \lambda^m\langle\zeta^m\rangle + \sum_{j=1}^{3}\int_{S_j}\gamma_{ij}(\chi_i^{+j} - \chi_i^{-j})\mathrm{d}S_j \\ &+ \sum_{j=1}^{3}\int_{S_j}\alpha_j(\zeta_{+j}^e - \zeta_{-j}^e)\mathrm{d}S_j + \sum_{j=1}^{3}\int_{S_j}\beta_j(\zeta_{+j}^m - \zeta_{-j}^m)\mathrm{d}S_j \end{aligned} \tag{2.23}$$

with

$$\chi_i^{+j} = \chi_i|_{y_j=d_j/2},\ \chi_i^{-j} = \chi_i|_{y_j=-d_j/2} \quad \text{for} \quad j=1,2,3$$

$$\zeta_{+j}^e = \zeta^e|_{y_j=d_j/2},\ \zeta_{-j}^e = \zeta^e|_{y_j=-d_j/2} \quad \text{for} \quad j=1,2,3$$

$$\zeta_{+j}^m = \zeta^m|_{y_j=d_j/2},\ \zeta_{-j}^m = \zeta^m|_{y_j=-d_j/2} \quad \text{for} \quad j=1,2,3$$

Matrix ϵ can be expressed as

$$\epsilon = \bar{\epsilon} + \epsilon_1 \tag{2.24}$$

with

$$\begin{aligned}\bar{\epsilon} &= \lfloor \bar{\epsilon}_{11} \;\; 2\bar{\epsilon}_{12} \;\; \bar{\epsilon}_{22} \;\; 2\bar{\epsilon}_{13} \;\; 2\bar{\epsilon}_{23} \;\; \bar{\epsilon}_{33} \;\; \bar{E}_1 \;\; \bar{E}_2 \;\; \bar{E}_3 \;\; \bar{H}_1 \;\; \bar{H}_2 \;\; \bar{H}_3 \rfloor^T \\ \epsilon_1 &= \lfloor \hat{\epsilon}_{11} \;\; 2\hat{\epsilon}_{12} \;\; \hat{\epsilon}_{22} \;\; 2\hat{\epsilon}_{13} \;\; 2\hat{\epsilon}_{23} \;\; \hat{\epsilon}_{33} \;\; \hat{E}_1 \;\; \hat{E}_2 \;\; \hat{E}_3 \;\; \hat{H}_1 \;\; \hat{H}_2 \;\; \hat{H}_3 \rfloor^T \end{aligned} \tag{2.25}$$

and

$$\begin{aligned} \bar{\epsilon}_{ij} &= \frac{1}{2}\left(\frac{\partial v_i}{\partial x_j} + \frac{\partial v_j}{\partial x_i}\right) \qquad \bar{E}_i = -\frac{\partial \psi^e}{\partial x_i} \qquad \bar{H}_i = -\frac{\partial \psi^m}{\partial x_i} \\ \hat{\epsilon}_{ij} &= \frac{1}{2}\left(\frac{\partial \chi_i}{\partial y_j} + \frac{\partial \chi_j}{\partial y_i}\right) \qquad \hat{E}_i = -\frac{\partial \zeta^e}{\partial y_i} \qquad \hat{H}_i = -\frac{\partial \zeta^m}{\partial y_i} \end{aligned} \tag{2.26}$$

where $\bar{\epsilon}$ will be shown later to be the global field variable array containing the strain field, the electric field, and the magnetic field for the material with homogenized effective material properties. The functional J_Ω in Eq. (2.23) forms the backbone of the present theory. This stationary value of this functional can be solved analytically for very simple cases such as binary composites, however, for general cases we need to use numerical techniques such as the finite element method (FEM) to seek numerical solutions.

2.3 Finite Element Implementation

It is not efficient to perform the FEM soultion in light of Eq. (2.23) because the Lagrange multipliers increase the number of unknowns. In practice, we minimized the following functional

$$\Pi_\Omega = \frac{1}{\Omega}\int_\Omega \left(\frac{1}{2}\epsilon^T D\epsilon + \epsilon^T \eta\theta + \frac{1}{2}c_v\,\frac{\theta^2}{T_0}\right) \mathrm{d}\Omega \tag{2.27}$$

under the following constraints

$$\chi_i^{+j} = \chi_i^{-j} \quad , \quad \zeta_{+j}^e = \zeta_{-j}^e \quad \text{, and} \quad \zeta_{+j}^m = \zeta_{-j}^m \quad \text{for} \quad j = 1, 2, 3 \tag{2.28}$$

The constraints in Eqs. (2.22) do not affect the minimum values of Π_Ω but help uniquely determine χ_i, ζ^e, and ζ^m. We actually constrain the fluctuation function at an arbitrary node to be zero and later use this constraint to recover the unique fluctuation functions. The degrees of freedom of the nodes on the positive boundary surface (*i.e.*, $y_i = d_i/2$) are slave to the nodes on the opposite negative boundary surface (*i.e.*, $y_i = -d_i/2$). By assembling all the independent active degrees of freedom (DOFs), we can implicitly and

exactly incorporate the constraints in Eqs. (2.28).

Introduce the following matrix notation

$$\epsilon_1 = \begin{bmatrix} \frac{\partial}{\partial y_1} & 0 & 0 & 0 & 0 \\ \frac{\partial}{\partial y_2} & \frac{\partial}{\partial y_1} & 0 & 0 & 0 \\ 0 & \frac{\partial}{\partial y_2} & 0 & 0 & 0 \\ \frac{\partial}{\partial y_3} & 0 & \frac{\partial}{\partial y_1} & 0 & 0 \\ 0 & \frac{\partial}{\partial y_3} & \frac{\partial}{\partial y_2} & 0 & 0 \\ 0 & 0 & \frac{\partial}{\partial y_3} & 0 & 0 \\ 0 & 0 & 0 & -\frac{\partial}{\partial y_1} & 0 \\ 0 & 0 & 0 & -\frac{\partial}{\partial y_2} & 0 \\ 0 & 0 & 0 & -\frac{\partial}{\partial y_3} & 0 \\ 0 & 0 & 0 & 0 & -\frac{\partial}{\partial y_1} \\ 0 & 0 & 0 & 0 & -\frac{\partial}{\partial y_2} \\ 0 & 0 & 0 & 0 & -\frac{\partial}{\partial y_3} \end{bmatrix} \begin{Bmatrix} \chi_1 \\ \chi_2 \\ \chi_3 \\ \zeta^e \\ \zeta^m \end{Bmatrix} \equiv \Gamma_h \chi \tag{2.29}$$

where Γ_h is an operator matrix. The χ is discretized using the finite elements as

$$\chi(x_i; y_i) = S(y_i)\mathcal{X}(x_i) \tag{2.30}$$

with S representing the shape functions and $\mathcal{X}$ is a column matrix of the nodal values of the mechanical, electric, and magnetic fluctuation functions. Substituting Eqs. (2.29) and (2.30) into Eq. (2.27), the discretized version of the functional is obtained as

$$\begin{aligned} \Pi_\Omega = \frac{1}{2\Omega}(&\mathcal{X}^T E \mathcal{X} + 2\mathcal{X}^T D_{h\epsilon}\bar{\epsilon} + \bar{\epsilon}^T D_{\epsilon\epsilon}\bar{\epsilon} \\ &+ 2\mathcal{X}^T D_{h\theta}\theta + 2\bar{\epsilon}^T D_{\epsilon\theta}\theta + D_{\theta\theta}\frac{\theta^2}{T_0}) \end{aligned} \tag{2.31}$$

where

$$E = \int_\Omega (\Gamma_h S)^T D (\Gamma_h S) \mathrm{d}\Omega \qquad D_{h\epsilon} = \int_\Omega (\Gamma_h S)^T D \mathrm{d}\Omega$$

$$D_{\epsilon\epsilon} = \int_\Omega D \mathrm{d}\Omega \qquad D_{h\theta} = \int_\Omega (\Gamma_h S)^T \beta \mathrm{d}\Omega$$

$$D_{\epsilon\theta} = \int_\Omega \beta \mathrm{d}\Omega \qquad D_{\theta\theta} = \int_\Omega c_v \mathrm{d}\Omega$$

Minimizing Π_Ω in Eq. (2.31), we obtain the following linear system

$$E\mathcal{X} = -D_{h\epsilon}\bar{\epsilon} - D_{h\theta}\theta \tag{2.32}$$

The fluctuation function $\mathcal{X}$ in Eq. (2.32) is linearly proportional to $\bar{\epsilon}$ and θ so that the solution can be written symbolically as

$$\mathcal{X} = \mathcal{X}_0\bar{\epsilon} + \mathcal{X}_\theta\theta \tag{2.33}$$

Substituting Eq. (2.33) into Eq. (2.31), we obtain the Helmholtz free energy density of the UC as

$$\Pi_\Omega = \frac{1}{2}\bar{\epsilon}^T\bar{D}\bar{\epsilon} + \bar{\epsilon}^T\bar{\eta}\theta + \frac{1}{2}\bar{c}_v\frac{\theta^2}{T_0} \tag{2.34}$$

with

$$\begin{aligned}
\bar{D} &= \frac{1}{\Omega}(\mathcal{X}_0^T D_{h\epsilon} + D_{\epsilon\epsilon}) \\
\bar{\eta} &= \frac{1}{\Omega}\left[\frac{1}{2}(D_{h\epsilon}^T\mathcal{X}_\theta + \mathcal{X}_0^T D_{h\theta}) + D_{\epsilon\theta}\right] \\
\bar{c}_v &= \frac{1}{\Omega}\left[\mathcal{X}_\theta^T D_{h\theta}T_0 + D_{\theta\theta}\right]
\end{aligned}$$

where $\bar{\epsilon}$ is a column matrix containing the global strains, global electric fields, and global magnetic fields; $\bar{D}$ in Eq. (2.34) is a 12×12 effective material matrix containing the effective material properties which can be expressed as

$$\bar{D} = \begin{bmatrix} \boldsymbol{C}^* & -\boldsymbol{e}^* & -\boldsymbol{q}^* \\ -\boldsymbol{e}^{*T} & -\boldsymbol{k}^* & -\boldsymbol{a}^* \\ -\boldsymbol{q}^{*T} & -\boldsymbol{a}^* & -\boldsymbol{\mu}^* \end{bmatrix} \tag{2.35}$$

$\bar{\eta}$ is a 12×1 effective matrix containing the second-order thermal stress tensor Λ_{ij}, the pyroelectric vectors p_i, and the pyromagnetic vectors m_i; and $\bar{c}_v$ is the effective specific heat.

After solving the fluctuation function χ, we can recover the local fields, such as local displacements, electric potential, magnetic potential, stresses, electric displacements, and magnetic flux density in terms of the macroscopic behavior including the global displacements v_i, the global electric potential ψ^e, the global magnetic potential ϕ^m, and the global

field variables contained in $\bar{\epsilon}$. First, the fluctuation functions should be uniquely determined using the constraints in Eq. (2.22). Then, we can recover the local displacements, electric potential, and magnetic potential using Eqs. (2.19), (2.20), and (2.21) as

$$\begin{Bmatrix} u_1 \\ u_2 \\ u_3 \\ \phi^e \\ \phi^m \end{Bmatrix} = \begin{Bmatrix} v_1 \\ v_2 \\ v_3 \\ \psi^e \\ \psi^m \end{Bmatrix} + \begin{bmatrix} \frac{\partial v_1}{\partial x_1} & \frac{\partial v_1}{\partial x_2} & \frac{\partial v_1}{\partial x_3} \\ \frac{\partial v_2}{\partial x_1} & \frac{\partial v_2}{\partial x_2} & \frac{\partial v_2}{\partial x_3} \\ \frac{\partial v_3}{\partial x_1} & \frac{\partial v_3}{\partial x_2} & \frac{\partial v_3}{\partial x_3} \\ \frac{\partial \psi^e}{\partial x_1} & \frac{\partial \psi^e}{\partial x_2} & \frac{\partial \psi^e}{\partial x_3} \\ \frac{\partial \psi^m}{\partial x_1} & \frac{\partial \psi^m}{\partial x_2} & \frac{\partial \psi^m}{\partial x_3} \end{bmatrix} \begin{Bmatrix} y_1 \\ y_2 \\ y_3 \end{Bmatrix} + \bar{S}\bar{\mathcal{X}} \tag{2.36}$$

Here $\bar{S}$ is different from S due to the recovery of slave nodes and the constrained node. The local strain field, the electric field, and the magnetic field can be recovered using Eq. (2.24) along with Eq. (2.29) as

$$\epsilon = \bar{\epsilon} + \Gamma_h \bar{S}\bar{\mathcal{X}} \tag{2.37}$$

The local stress, the electric displacement field, and the magnetic flux density can be recovered straightforwardly using the 3D constitutive relations for the constituent material as

$$\sigma = D\epsilon + \eta\theta \tag{2.38}$$

where σ is a column matrix containing 3D stresses, electric displacements, and magnetic flux density such that

$$\sigma = \lfloor \sigma_{11} \;\; \sigma_{12} \;\; \sigma_{22} \;\; \sigma_{13} \;\; \sigma_{23} \;\; \sigma_{33} \;\; -T_1 \;\; -T_2 \;\; -T_3 \;\; -B_1 \;\; -B_2 \;\; -B_3 \rfloor^T \tag{2.39}$$

where σ_{ij}, T_i, and B_i denote the stress tensor, the electric flux density vector, and the magnetic flux density vector, respectively.

2.4 Numerical Results

The predictive capability of the effective properties of VAMUCH has been demonstrated using many examples [11]. In this section, we will use VAMUCH to predict the effective elastic, piezoelectric, piezomagnetic, dielectric, magnetic permeability, and electromagnetic coupling constants as well as the thermal stress coefficients, pyroelectric, pyromagnetic coefficients, and specific heat, and recover the distribution of the local fields.

Table 2.1: Material properties of the composite constituents ($BaTiO_3$, $CoFe_2O_4$, and epoxy)

	$BaTiO_3$	$CoFe_2O_4$	Epoxy
C_{11}(GPa)	162	269.5	5.53
C_{12}(GPa)	78	170	2.97
C_{23}(GPa)	77	173	2.97
C_{22}(GPa)	166	286	5.53
C_{55}(GPa)	43	45.3	1.28
k_{11}(C/Vm)	12.6×10^{-9}	0.093×10^{-9}	0.1×10^{-9}
k_{33}(C/Vm)	11.2×10^{-9}	0.08×10^{-9}	0.1×10^{-9}
μ_{11}(Ns^2/C^2)	0.1×10^{-4}	1.57×10^{-4}	0.01×10^{-4}
μ_{33}(Ns^2/C^2)	0.05×10^{-4}	-5.9×10^{-4}	0.01×10^{-4}
e_{11}(C/m^2)	18.6	0	0
e_{21}(C/m^2)	-4.4	0	0
e_{51}(C/m^2)	11.6	0	0
q_{11}(N/Am)	0	699.7	0
q_{21}(N/Am)	0	580.3	0
q_{51}(N/Am)	0	550	0
α_{11}(1/K)	6.4×10^{-6}	10×10^{-6}	54×10^{-6}
α_{22}(1/K)	15.7×10^{-6}	10×10^{-6}	54×10^{-6}
α_{33}(1/K)	15.7×10^{-6}	10×10^{-6}	54×10^{-6}
c_v(kJ/m^3.K)	3193.62	2000	-

2.4.1 Two-phase composites

We consider a two-phase composite composed of a $CoFe_2O_4$ piezomagnetic matrix reinforced by $BaTiO_3$ piezoelectric fibers which is an example extensively investigated in [3], [6], and [11]. The piezoelectric fibers are of circular shape and arranged in a square array. Both constituents are transversely isotropic with the axis of symmetry oriented in the 1-direction. The independent material constants of constituents are given in Table 2.1.

Fig. 2.2 and 2.3 show the effective CTEs and specific heat varying with volume fraction of $CoFe_2O_4$. The effective pyroelectric and pyromagnetic constants of the composite are illustrated in Fig. 2.4 and 2.5, respectively, although they are absent in either of the individual phase. The current program can also accurately recover the local distribution of the field variables resulting from the application of certain external loading conditions. Fig. 2.6 and 2.7 show the contour plots of the distributions of σ_{22} and von Mises stress within UC (VOF 20%) which are induced by the applied boundary conditions of $\epsilon_{22} = 0.1\%$, $E_2 = 100$V/m, and 100K uniform temperature rise from stress free state.

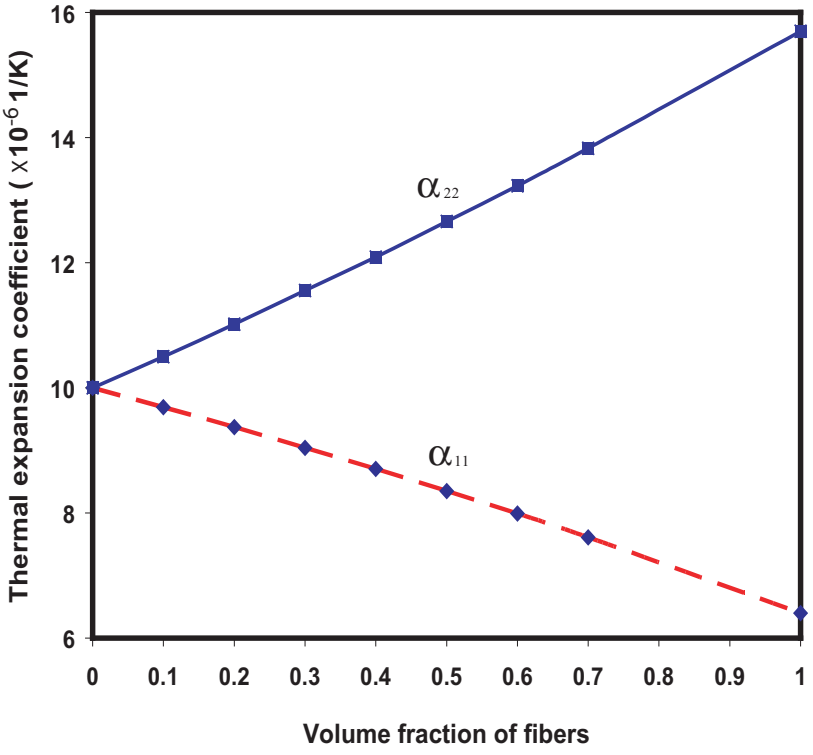

Fig. 2.2: Effective thermal expansion coefficients.

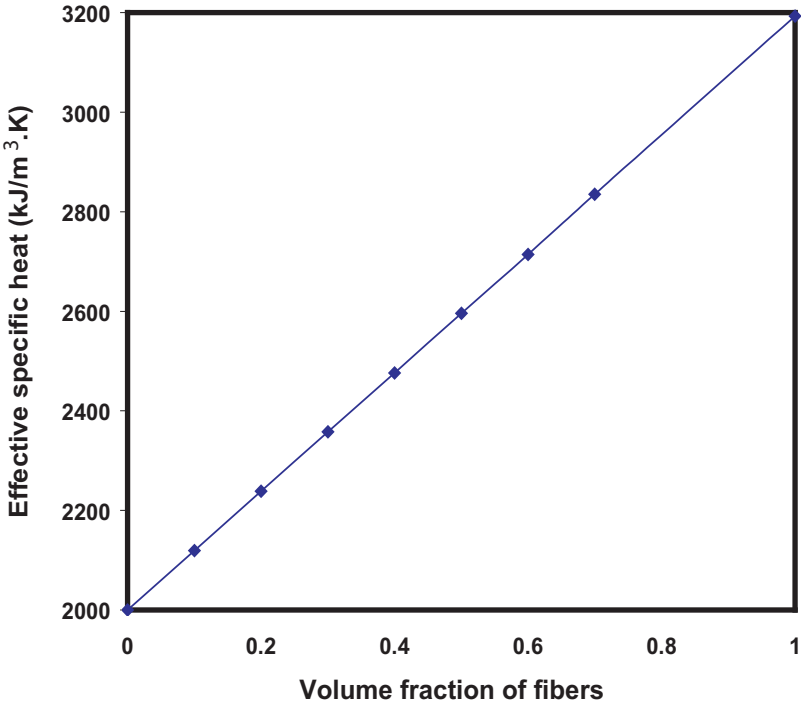

Fig. 2.3: Effective specific heat.

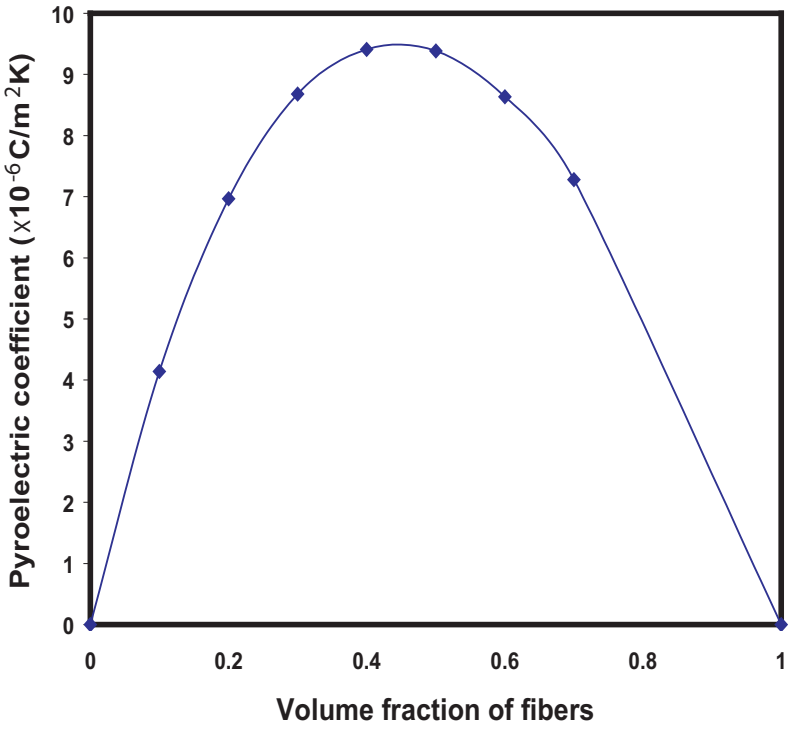

Fig. 2.4: Effective pyroelectric constants.

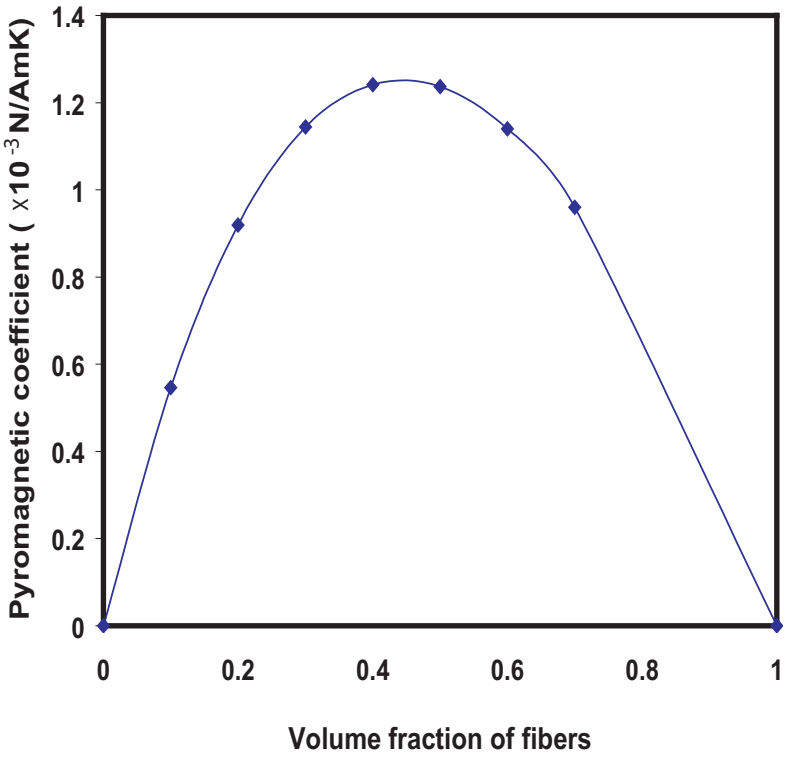

Fig. 2.5: Effective pyromagnetic constants.

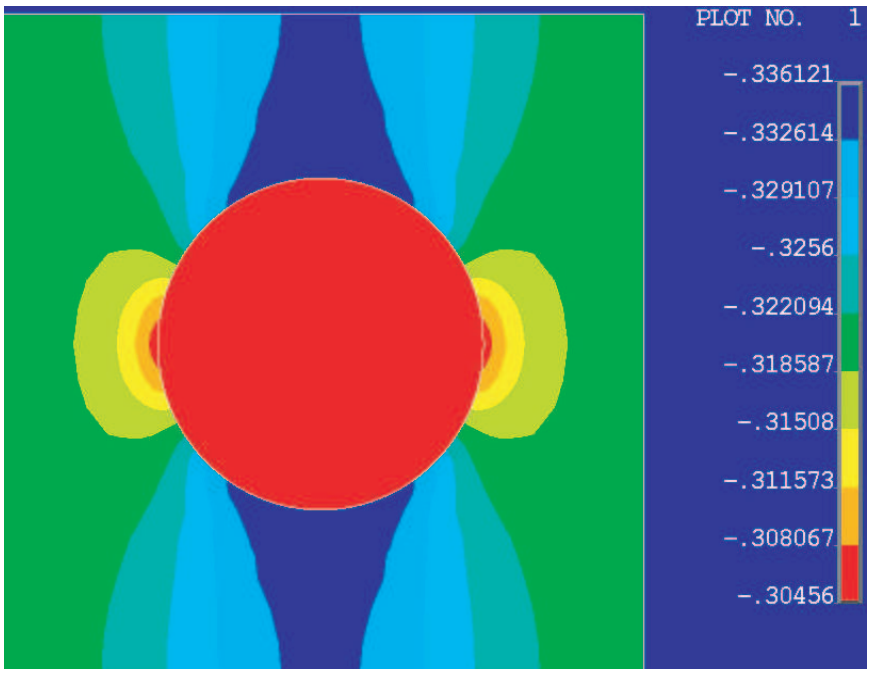

Fig. 2.6: Contour plot of σ_{22} (GPa).

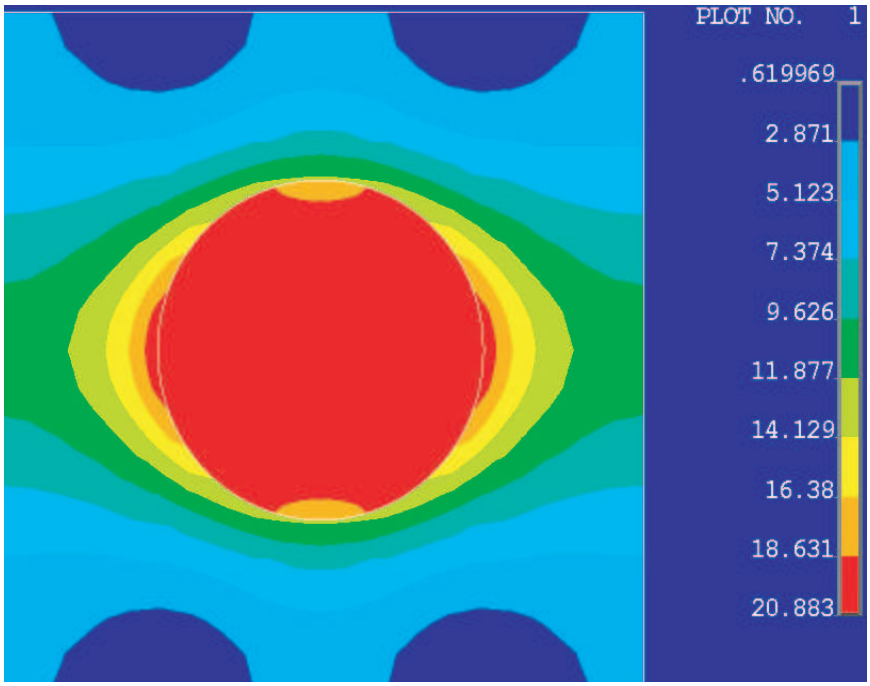

Fig. 2.7: Contour plot of von Mises stress (GPa).

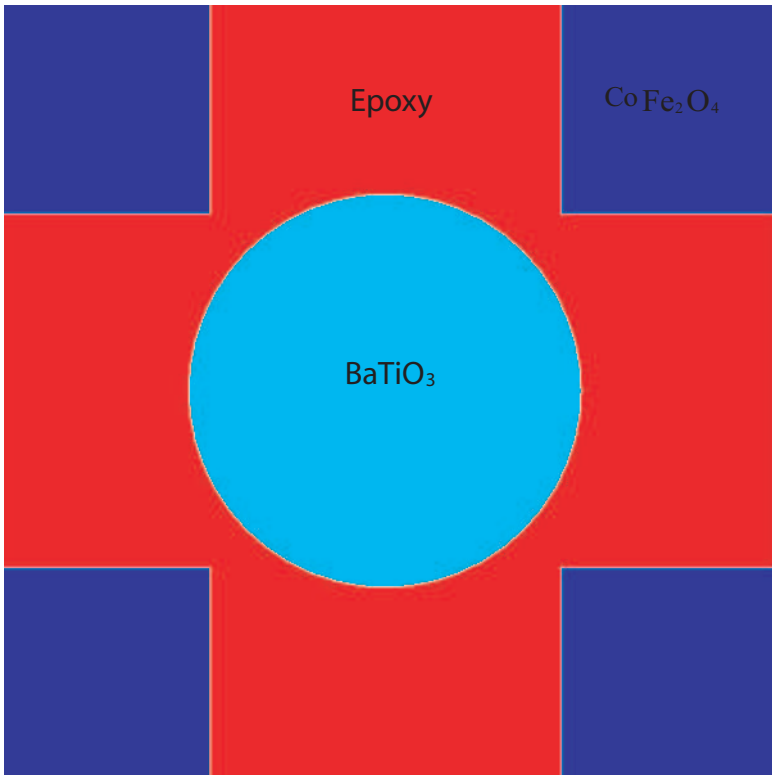

Fig. 2.8: Unit cell of three phase composites.

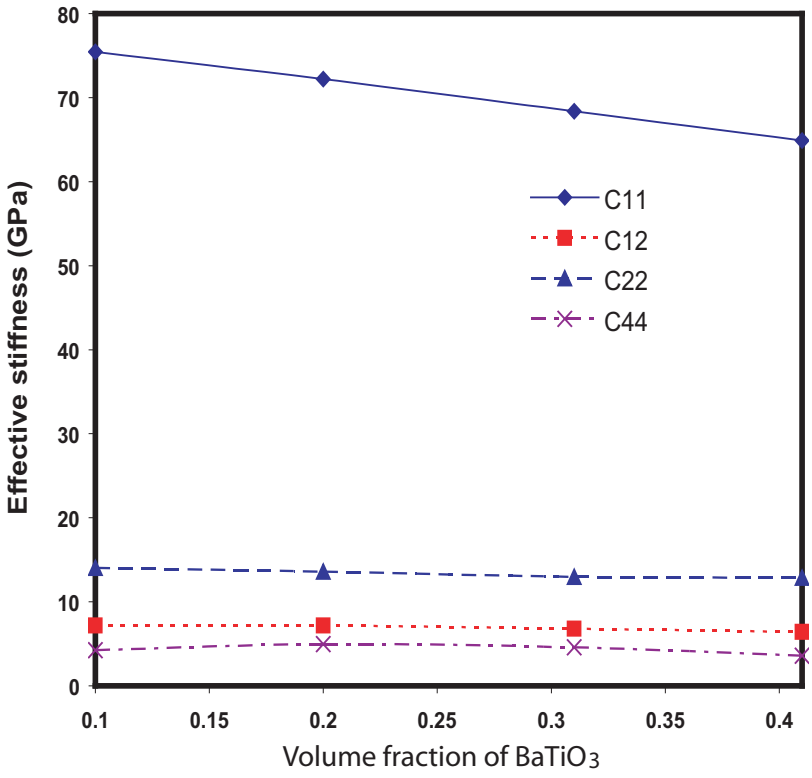

Fig. 2.9: Effective stiffness.

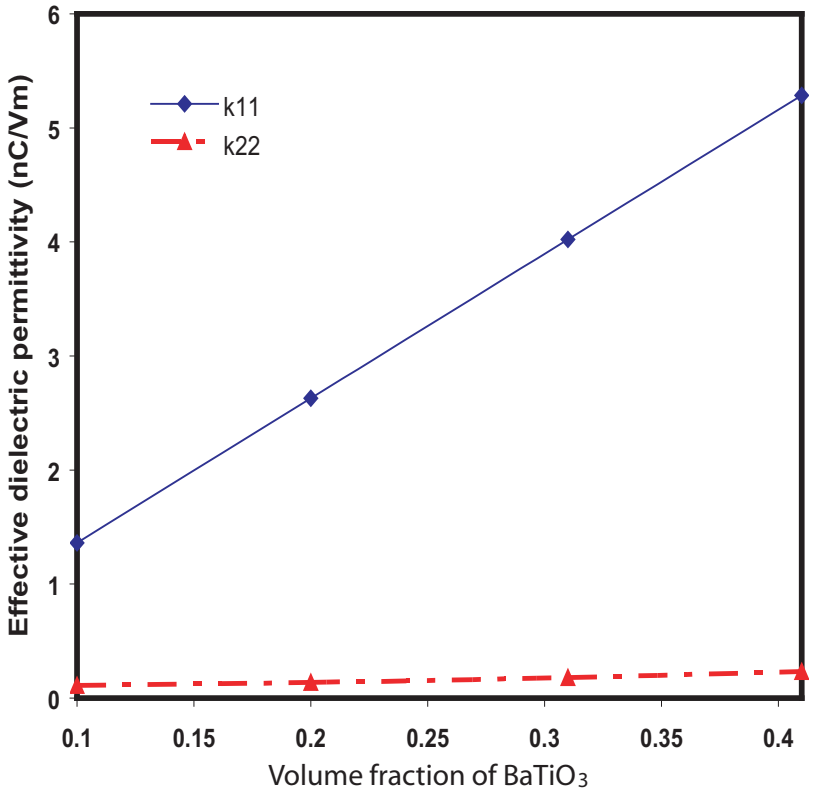

Fig. 2.10: Effective dielectric permittivity.

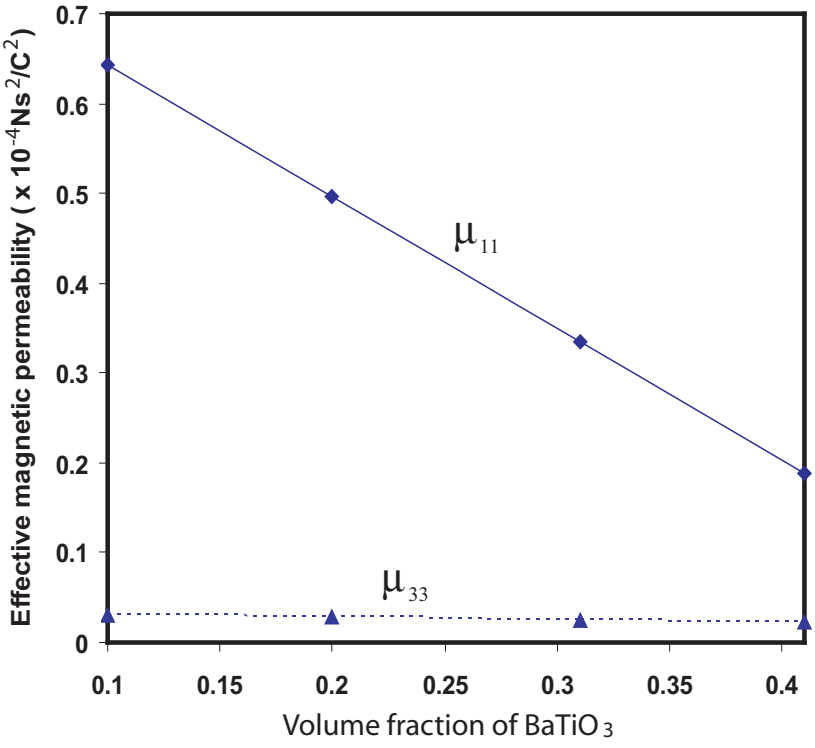

Fig. 2.11: Effective dielectric permittivity.

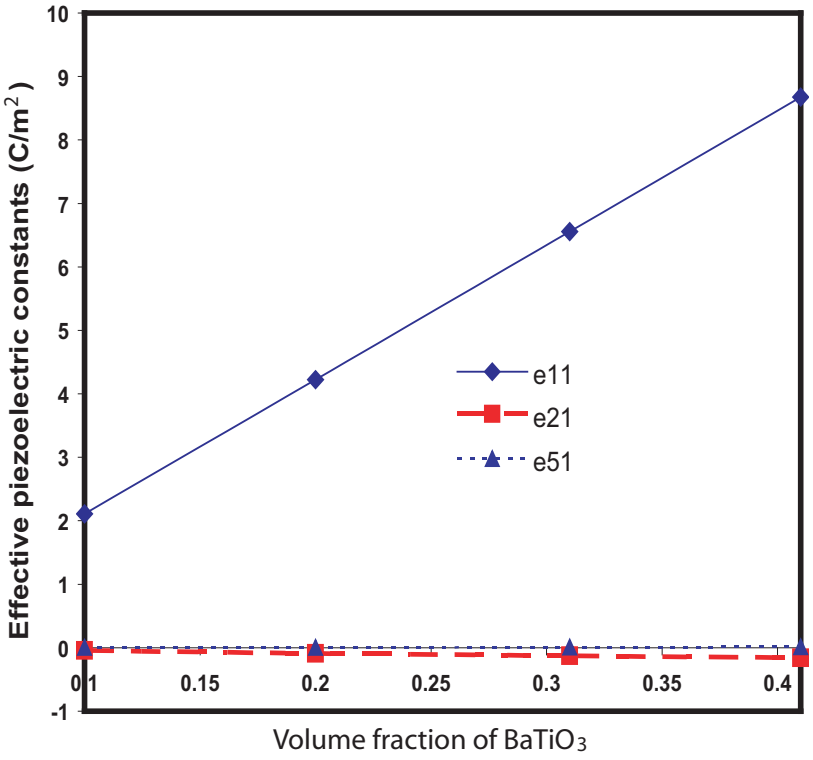

Fig. 2.12: Effective piezoelectric constants.

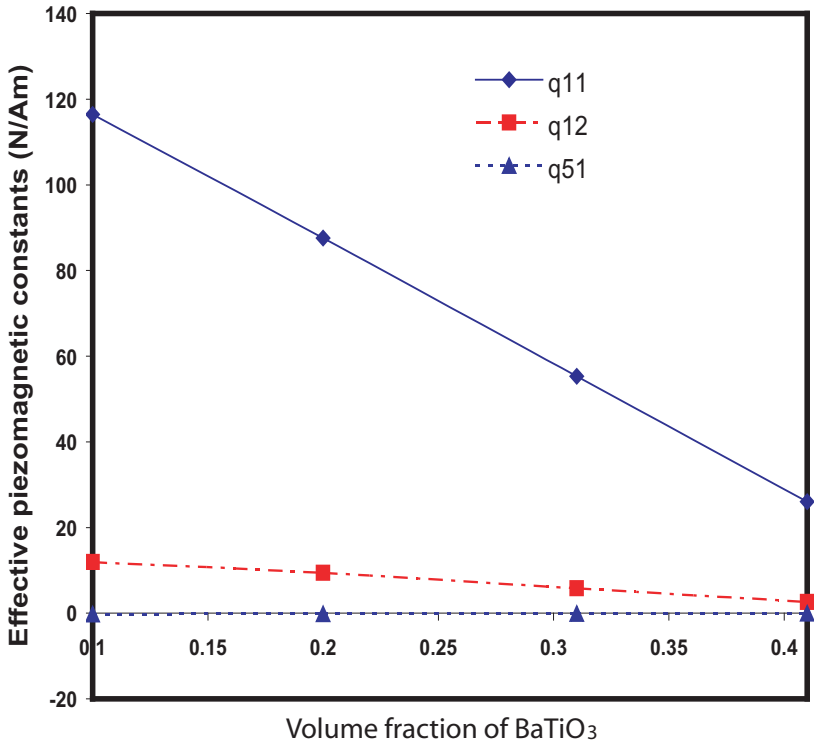

Fig. 2.13: Effective piezomagnetic constants.

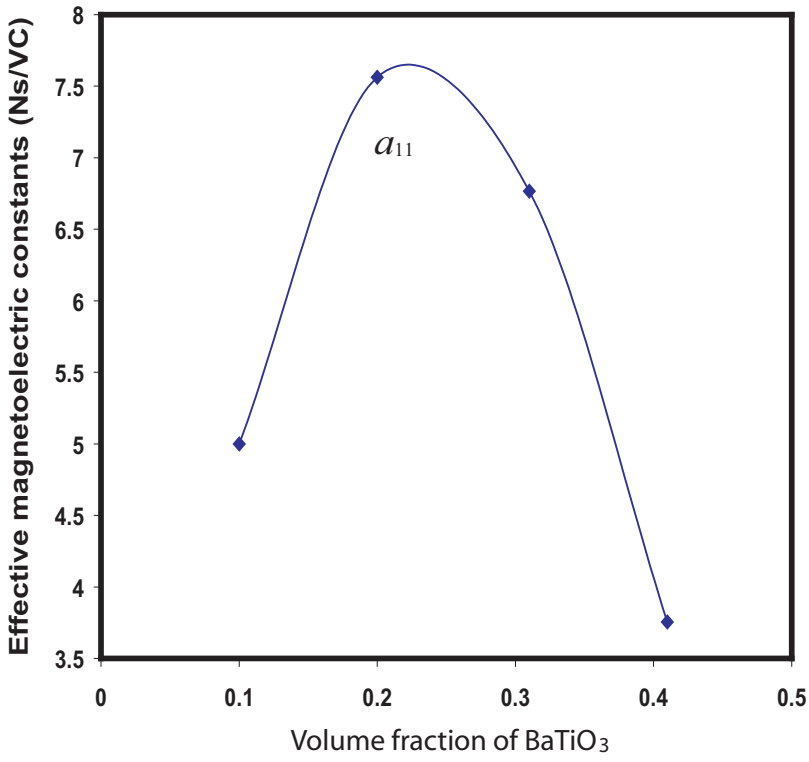

Fig. 2.14: Effective electromagnetic constants (a_{11}).

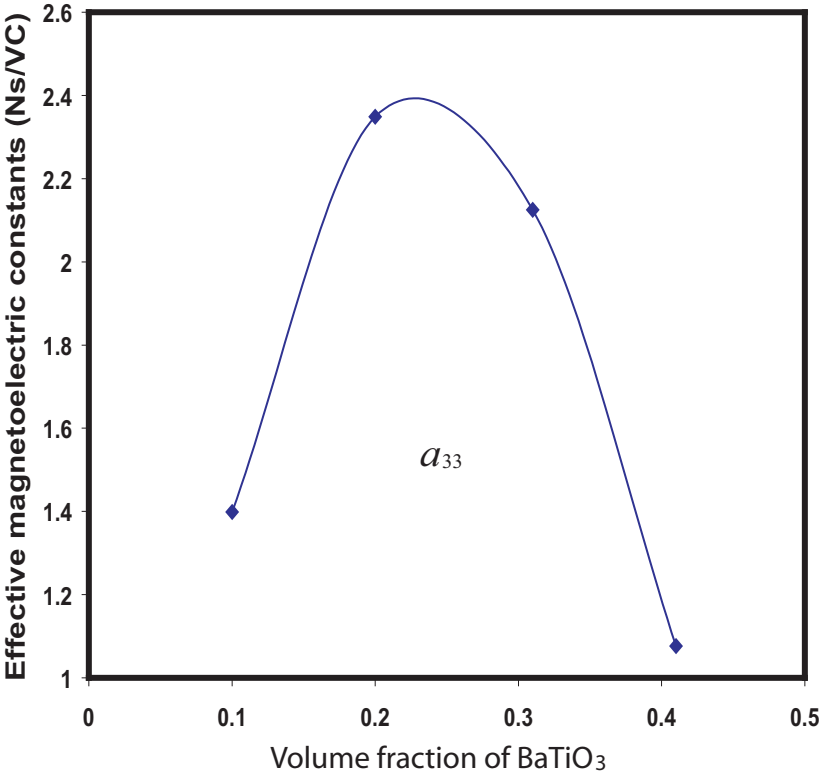

Fig. 2.15: Effective electromagnetic constants (a_{33}).

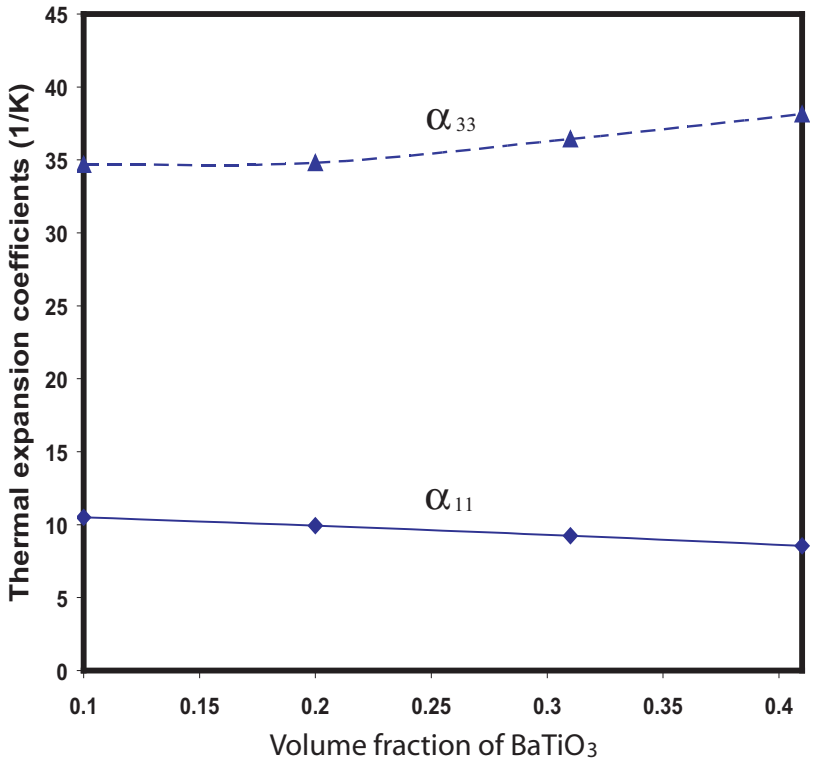

Fig. 2.16: Effective CTEs.

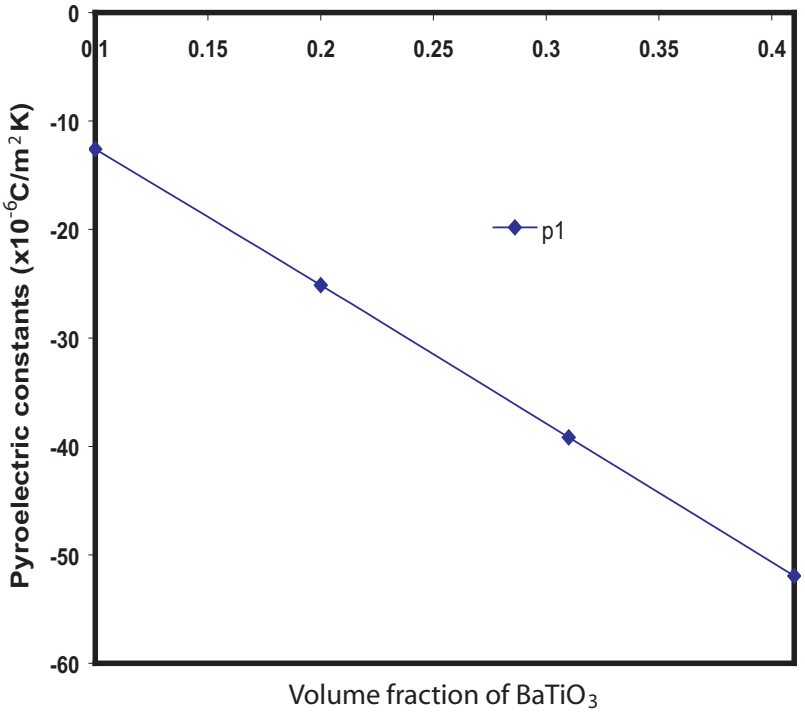

Fig. 2.17: Effective pyroelectric coefficients.

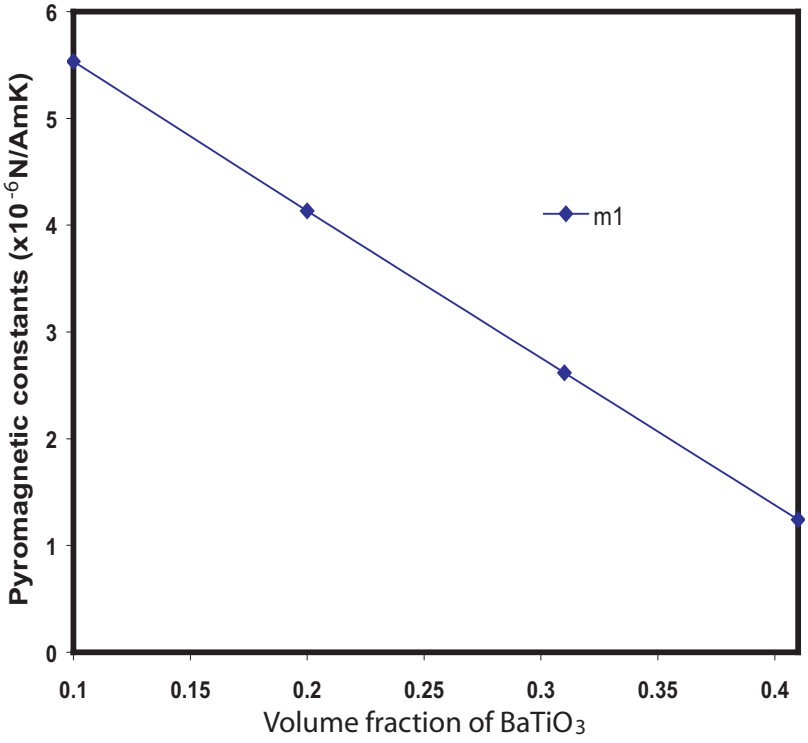

Fig. 2.18: Effective pyromagnetic coefficients.

2.4.2 Three-phase composites

The three-phase electromagnetoelastic composite considered consists of an elastic epoxy matrix reinforced with piezoelectric ($BaTiO_3$) and piezomagnetic fibers ($CoFe_2O_4$). The piezoelectric fiber is of circular shape and at the center of the unit cell while the piezomagnetic fibers in the shape of quarter squares are located at the four corners of unit cell as shown in Fig. 2.8. The material properties of the three constituents are listed in Table 2.1. Fig. 2.9-2.18 show that the variation of the effective properties of composites with respect to the volume fractions of the piezoelectric fibers ($BaTiO_3$) when the matrix volume fraction is fixed at 0.5. Effective material properties include elastic constants, dielectric coefficients, magnetic permeability coefficients, piezoelectric coefficients, piezomagnetic coefficients and electromagnetic coefficients as well as thermal stress coefficients, pyroelectric, and pyromagnetic coefficients.

2.5 Conclusion

A fully coupled micromecahnics model has been constructed for predicting the effective properties of smart composites. It can also accurately recover the distribution of the local

fields. It provides a convenient tool for the investigation of smart composite materials.

References

1. Nan, C. W., "Magnetoelectric effect in composites of piezoelectric and piezomagnetic phases," *Physical Review B*, Vol. 50, No. 9, 1994, pp. 6082-6088.

2. Lagoudas, D. C., Boyd, J. G., and Bo, Z., "Micromechanics of active composites with sma fibers," *Journal of Engineering Materials and Technology*, Vol. 116, 1994, pp. 337–345.

3. Li, J. Y. and Dunn, M. L., "Micromechanics of magnetoelectroelastic composite materials: average fields and effective behavior," *Journal of Intelligent Material Systems and Structures*, Vol. 9, 1998, pp. 404-416.

4. Mori, T. and Tanaka, K., "Average stress in matrix and average elastic energy of materials with misfitting inclusions," *Acta Metallurgica*, Vol. 21, 1973, pp. 571-574.

5. Aboudi, J., "Micromechanical analysis of fully coupled electro-magneto-thermo-elastic multiphase composites," *Smart Materials and Structures*, Vol. 10, 2001, pp. 867-877.

6. Lee, J. S., Boyd, J. G., and Lagoudas, D. C., "Effective properties of three-phase electro-magneto-elastic composites," *International Journal of Engineering Science*, Vol. 43, No. 10, 2005, pp. 790–825.

7. Tang, T. and Yu, W., "Variational asymptotic micromechanics modeling of heterogeneous piezoelectric materials," *Mechanics of Materials*, Vol. 40, 2008, pp. 812-824.

8. Yu, W. and Tang, T., "Variational asymptotic method for unit cell homogenization of periodically heterogeneous materials," *International Journal of Solids and Structures*, Vol. 44, 2007, pp. 3738-3755.

9. Yu, W. and Tang, T., "A variational asymptotic micromechanics model for predicting thermoelastic properties of heterogeneous materials," *International Journal of Solids and Structures*, Vol. 44, No. 22-23, 2007, pp. 7510-7525.

10. Tang, T. and Yu, W., "A variational asymptotic micromechanics model for predicting conductivity of composite materials," *Journal of Mechanics of Materials and Structures*, Vol. 2, No. 9, 2007, pp. 1813-1830.

11. Tang, T. and Yu, W., "Variational asymptotic homogenization of heterogeneous electromagnetoelastic materials," *International Journal of Engineering Science*, Vol. 46, No. 8, 2008, pp. 741-757.

12. Tang, T. and Yu, W., "A variational asymptotic model for predicting initial yielding surface and elastoplastic behavior of metal matrix composite materials," *Proceedings of the 2007 ASME International Mechanical Engineering Congress and Exposition*, Seattle, Washington, Nov. 2007.

13. Rosen, B. W. and Hashin, Z., "Effective thermal expansion coefficients and specific heats of composite materials," *International Journal of Engineering Science*, Vol. 8, 1970, pp. 157–173.

14. Berdichevsky, V. L., "On averaging of periodic systems," *PMM*, Vol. 41, No. 6, 1977, pp. 993-1006.

15. Kunin, I., *Theory of elastic media with microstructure*, vols. 1 and 2, Springer Verlag, 1982.

Chapter 3

Variational Asymptotic Homogenization of Heterogeneous Electromagnetoelastic Materials

[1]

This chapter is a journal paper published in the *International Journal of Engineering Science*, Vol. 46, No. 8, 2008, pp. 741-757.

Abstract

The variational asymptotic method is used to develop a micromechanics model for predicting the effective properties and local fields of heterogeneous electromagnetoelastic materials. Starting from the total electromagnetic enthalpy of the heterogenous continuum, we formulate the micromechanics model as a constrained minimization problem taking advantage of the fact that the size of the microstructure is small compared to the macroscopic size of the material. To handle real microstructures in engineering applications, we implement this new model using the finite element method. A few examples are used to demonstrate the application and accuracy of this theory and the companion computer program, VAMUCH. The present results are compared with those available in the literature.

3.1 Introduction

The smart composites consisting of piezoelectric and piezomagnetic constituents have received significant attention due to their extensive applications in broadband magnetic field probes, electronic packaging, acoustic devices, hydrophones, sensors, and actuators. The magnetoelectric effect in composites, which is absent in constituents, is created by the interaction between the constituent phases, a result of the so-called product property. Van Ran *et al.* [1] reported that the electromagnetic coefficient obtained in $BaTiO_3 - CoFe_2O_4$ composites is two orders larger than that of Cr_2O_3, which had the highest electromagnetic coefficient among single-phase materials known at that time. A broadband electromagnetic transducer with a flat frequency response is also achieved using composites in [2]. Since

[1] Coauthored by: Tian Tang and Wenbin Yu.

then, many theoretical and experimental studies have been performed on the electromagnetic coupling in the piezoelectric-piezomagnetic composite materials [3-11]. Harshe and his co-workers [3,4] investigated the 3-0/0-3 electromagnetic composites in terms of simple geometrical model by assuming that the particles embedded in matrix are small cubes. Nan [5] proposed a non-self-consistent model to predict the effective properties of piezoelectric-piezomagnetic two-phase composites which fails to satisfy the exact relations derived in [6]. Li and Dunn [7] solved the inclusion problem for an infinite electromagnetoelastic medium to obtain the generalized Eshelby tensors which can be used to predict the effective properties of electromagnetoelastic composites. For example, The Mori-Tanaka mean field method is used in [8] to study the average fields and effective moduli of composites that exhibit full coupling between elastic, electric, and magnetic fields, where closed-form expressions are obtained for effective electromagnetoelastic properties of circular cylinder fibrous and laminated two-phase composites. The Mori-Tanaka method is also used in [9] to derive a closed-form solution for effective moduli of piezoelectric-piezomagnetic two-phase composites for four practical inclusions: elliptical cylinder, circular cylinder, penny shape, and ribbon. Huang *et al.* [10] analytically obtained the optimum fiber volume fractions at which these coefficients reach their maximum values. Li [11] studied the average electromagnetoelastic field in a multi-inclusion or inhomogeneity embedded in an infinite matrix and developed a numerical algorithm to evaluate electromagnetoelastic Eshelby tensors. Aboudi [12] developed a homogenization method to predict the effective properties of electromagnetothermoelastic composites using the framework of high-fidelity generalized method of cells. The predictions of this model agree with those of Mori-Tanaka model well.

As suggested in [13], adding an elastic polymer matrix into the two-phase electromagnetoelastic composite will increase the ductility and formability of the composites. To perform a micromechanical modeling of this three-phase electromagnetoelastic composites, Lee *et al.* [14] developed a finite element analysis-based micromechanics approach through averaging of the representative volume element (RVE) to determine the effective dielectric, magnetic, mechanical, and coupled-field properties of this composites as functions of the phase volume fractions, the fiber arrangements in RVE, and the fiber material properties with special emphasis on the poling directions of the piezoelectric and piezomagnetic fibers.

The objective of this paper is to develop a micromechanics model based on the framework of variational asymptotic method for unit cell homogenization (VAMUCH) for pre-

dicting the effective properties and local fields of electromagnetoelastic composites. This framework is build upon the variational asymptotic method [15] along with two essential assumptions within the concept of micromechanics for composites with an identifiable unit cell (UC):

- **Assumption 1** The exact solutions of the field variables have volume averages over the UC. For example, if u_i, ϕ^e, and ϕ^m are the exact displacements, electric potential, and magnetic potential within the UC occupying a volume Ω, respectively, there exist v_i, ψ^e, and ψ^m such that

$$\begin{aligned} v_i &= \frac{1}{\Omega}\int_\Omega u_i \, \mathrm{d}\Omega \equiv \langle u_i \rangle \\ \psi^e &= \frac{1}{\Omega}\int_\Omega \phi^e \, \mathrm{d}\Omega \equiv \langle \phi^e \rangle \\ \psi^m &= \frac{1}{\Omega}\int_\Omega \phi^m \, \mathrm{d}\Omega \equiv \langle \phi^m \rangle \end{aligned} \tag{3.1}$$

- **Assumption 2** The effective material properties obtained from the micromechanical analysis of the UC are independent of the geometry, the boundary conditions, and loading conditions of the macroscopic structure, which means that effective properties are assumed to be the intrinsic properties of the material when viewed macroscopically.

Note that these assumptions are not restrictive. The mathematical meaning of the first assumption is that the exact solutions of the field variables can be integrated over the domain of UC, which is true almost all the time. The second assumption implies that we will neglect the size effects of the material properties in the macroscopic analysis, which is an assumption often made in the conventional continuum mechanics. Of course, the micromechanical analysis of the UC is only needed and appropriate if $\eta = h/l \ll 1$, with h as the characteristic size of the UC and l as the macroscopic size of the material. Other assumptions such as particular geometry shape and arrangement of the constituents, specific boundary conditions applied to the UC, and prescribed relations between local fields and global fields are not needed for this study.

This VAMUCH modeling framework has been successfully applied to predict effective thermoelastic properties including elastic constants, specific heats, and coefficients of thermal expansions, and effective thermal conductivity and associated local fields [16-18]. It is

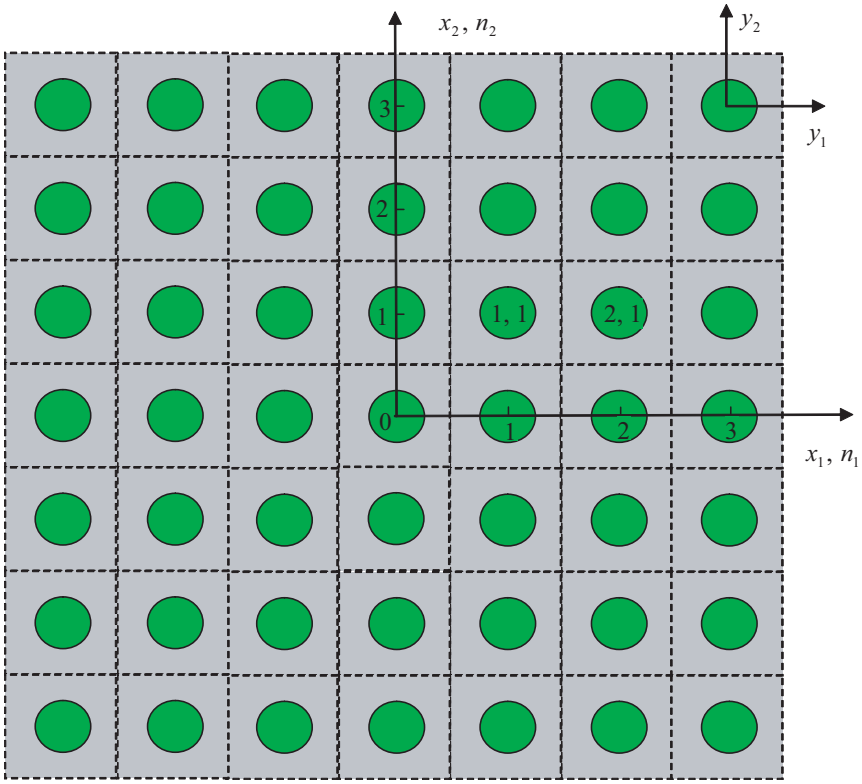

Fig. 3.1: Coordinate systems for heterogenous materials (only two-dimensional (2D) UC is drawn for clarity).

also applied to accurately predict the initial yielding surface and elastoplastic behavior of metal matrix composites [19].

3.2 Theoretical Formulation

Three coordinates are used in our formulation: two cartesian coordinates $\mathbf{x} = (x_1, x_2, x_3)$ and $\mathbf{y} = (y_1, y_2, y_3)$, and an integer-valued coordinate $\mathbf{n} = (n_1, n_2, n_3)$ (see Fig. 3.1). We use x_i as the global coordinates to describe the macroscopic structure and y_i parallel to x_i as the local coordinates to describe the UC (Here and throughout the paper, Latin indices assume 1, 2, and 3 and repeated indices are summed over their range except where explicitly indicated). We choose the origin of the local coordinates y_i to be the geometric center of UC. For example, if the UC is a cube with dimensions as d_i, then $y_i \in [-\frac{d_i}{2}, \frac{d_i}{2}]$. To uniquely locate a UC in the heterogeneous material we also introduce integer coordinates n_i. The integer coordinates are related to the global coordinates in such a way that $n_i = x_i/d_i$ (no summation over i). It is emphasized although only square array is sketched in Fig. 3.1, the present theory has no such limitations.

As implied by Assumption 2, we can obtain the same effective properties from an

imaginary, unbounded, and unloaded heterogeneous material with the same microstrucutre as the real, loaded, and bounded one. Hence we could derive the micromechanics model from a imaginary, unloaded, heterogeneous material which completely occupies the three-dimensional (3D) space $\mathcal{R}$ and composes of infinite many repeating UCs. For composites containing piezoelectric and piezomagnetic phases, the total electromagnetic enthalpy is equal to the summation of the electromagnetic enthalpy [20] stored in all the UCs, which is

$$\Pi = \sum_{n=-\infty}^{\infty} \int_{\Omega} 2H \mathrm{d}\Omega \tag{3.2}$$

where $2H$ is twice the electromagnetic enthalpy, given by

$$2H = \epsilon^T D \epsilon \tag{3.3}$$

where

$$\epsilon = \lfloor \epsilon_{11} \;\; 2\epsilon_{12} \;\; \epsilon_{22} \;\; 2\epsilon_{13} \;\; 2\epsilon_{23} \;\; \epsilon_{33} \;\; E_1 \;\; E_2 \;\; E_3 \;\; H_1 \;\; H_2 \;\; H_3 \rfloor^T \tag{3.4}$$

containing the 3D strain field ϵ_{ij}, the 3D electric field E_i, and the 3D magnetic field H_i, which are defined for a linear theory as:

$$\epsilon_{ij}(\mathbf{n};\mathbf{y}) = \frac{1}{2}\left[\frac{\partial u_i(\mathbf{n};\mathbf{y})}{\partial y_j} + \frac{\partial u_j(\mathbf{n};\mathbf{y})}{\partial y_i}\right] \tag{3.5}$$

$$E_i(\mathbf{n};\mathbf{y}) = -\frac{\partial \phi^e(\mathbf{n};\mathbf{y})}{\partial y_i} \tag{3.6}$$

$$H_i(\mathbf{n};\mathbf{y}) = -\frac{\partial \phi^m(\mathbf{n};\mathbf{y})}{\partial y_i} \tag{3.7}$$

and D is a 12×12 matrix containing all the necessary material constants for characterizing completely coupled electromagnetoelastic materials such that

$$D = \begin{bmatrix} \boldsymbol{C} & -\boldsymbol{e} & -\boldsymbol{q} \\ -\boldsymbol{e}^T & -\boldsymbol{k} & -\boldsymbol{a} \\ -\boldsymbol{q}^T & -\boldsymbol{a}^T & -\boldsymbol{\mu} \end{bmatrix} \tag{3.8}$$

where $\boldsymbol{C}$ is a 6×6 submatrix for elastic constants, $\boldsymbol{e}$ is a 6×3 submatrix for piezoelectric coefficients, $\boldsymbol{q}$ is a 6×3 submatrix for piezomagnetic coefficients, $\boldsymbol{k}$ is a 3×3 submatrix for dielectric permeability, $\boldsymbol{a}$ is a 3×3 submatrix for electromagnetic coefficients, and $\boldsymbol{\mu}$

is a 3×3 submatrix for magnetic permeability. $\boldsymbol{C}$, $\boldsymbol{k}$, and $\boldsymbol{\mu}$ will not vanish all the time, while other coefficients including $\boldsymbol{e}$, $\boldsymbol{q}$, $\boldsymbol{a}$ will vanish if the corresponding coupling does not exist. For example, if the magnetic field is not coupled with the electric field, then $\boldsymbol{a} = 0$. If the magnetic field is not coupled with the mechanical field, then $\boldsymbol{q} = 0$. If the electric field is not coupled with the mechanical field, then $\boldsymbol{e} = 0$. Even if a certain coupling does not exist in any of the constituent phases, it may appear as an effective property of a composite. For example, the interesting behavior of electromagnetoelastic composites is the overall electromagnetic coupling effect present in the composite, but entirely absent in any of the individual phases. Therefore, the electromagnetic coefficients $\boldsymbol{a}$ could be a new material properties produced by simply engineering the microstructure in such a way to combine two or more different phases.

In view of the fact that the infinite many UCs form a continuous heterogenous material, we need to enforce the continuity of the displacement field u_i, the electric potential field ϕ^e, and magnetic potential ϕ^m on the interface between adjacent UCs, which are:

$$
\begin{aligned}
u_i(n_1, n_2, n_3; d_1/2, y_2, y_3) &= u_i(n_1 + 1, n_2, n_3; -d_1/2, y_2, y_3) \\
u_i(n_1, n_2, n_3; y_1, d_2/2, y_3) &= u_i(n_1, n_2 + 1, n_3; y_1, -d_2/2, y_3) \\
u_i(n_1, n_2, n_3; y_1, y_2, d_3/2) &= u_i(n_1, n_2, n_3 + 1; y_1, y_2, -d_3/2) \\
\phi^e(n_1, n_2, n_3; d_1/2, y_2, y_3) &= \phi^e(n_1 + 1, n_2, n_3; -d_1/2, y_2, y_3) \\
\phi^e(n_1, n_2, n_3; y_1, d_2/2, y_3) &= \phi^e(n_1, n_2 + 1, n_3; y_1, -d_2/2, y_3) \\
\phi^e(n_1, n_2, n_3; y_1, y_2, d_3/2) &= \phi^e(n_1, n_2, n_3 + 1; y_1, y_2, -d_3/2) \\
\phi^m(n_1, n_2, n_3; d_1/2, y_2, y_3) &= \phi^m(n_1 + 1, n_2, n_3; -d_1/2, y_2, y_3) \\
\phi^m(n_1, n_2, n_3; y_1, d_2/2, y_3) &= \phi^m(n_1, n_2 + 1, n_3; y_1, -d_2/2, y_3) \\
\phi^m(n_1, n_2, n_3; y_1, y_2, d_3/2) &= \phi^m(n_1, n_2, n_3 + 1; y_1, y_2, -d_3/2)
\end{aligned}
\tag{3.9}
$$

The exact solution of the present problem will minimize the summation of electromagnetic enthalpy in Eq. (3.2) under the conditions in Eqs. (3.1) and (3.9). To avoid the difficulty associated with discrete integer arguments, we can reformulate the problem, including Eqs. (3.2), (3.5), (3.6), (3.7), and (3.9) in terms of continuous functions using the

idea of quasicontinuum [21]. The corresponding formulas are listed below.

$$\Pi = \int_{\mathcal{R}} \left\langle \epsilon^T D \epsilon \right\rangle \mathrm{d}\mathcal{R} \tag{3.10}$$

$$\epsilon_{ij}(\mathbf{x};\mathbf{y}) = \frac{1}{2}\left[\frac{\partial u_i(\mathbf{x};\mathbf{y})}{\partial y_j} + \frac{\partial u_j(\mathbf{x};\mathbf{y})}{\partial y_i}\right] \equiv u_{(i|j)} \tag{3.11}$$

$$E_i(\mathbf{x};\mathbf{y}) = -\frac{\partial \phi^e(\mathbf{x};\mathbf{y})}{\partial y_i} \tag{3.12}$$

$$H_i(\mathbf{x};\mathbf{y}) = -\frac{\partial \phi^m(\mathbf{x};\mathbf{y})}{\partial y_i} \tag{3.13}$$

and

$$\begin{aligned}
u_i(x_1,x_2,x_3;d_1/2,y_2,y_3) &= u_i(x_1+d_1,x_2,x_3;-d_1/2,y_2,y_3)\\
u_i(x_1,x_2,x_3;y_1,d_2/2,y_3) &= u_i(x_1,x_2+d_2,x_3;y_1,-d_2/2,y_3)\\
u_i(x_1,x_2,x_3;y_1,y_2,d_3/2) &= u_i(x_1,x_2,x_3+d_3;y_1,y_2,-d_3/2)\\
\phi^e(x_1,x_2,x_3;d_1/2,y_2,y_3) &= \phi^e(x_1+d_1,x_2,x_3;-d_1/2,y_2,y_3)\\
\phi^e(x_1,x_2,x_3;y_1,d_2/2,y_3) &= \phi^e(x_1,x_2+d_2,x_3;y_1,-d_2/2,y_3)\\
\phi^e(x_1,x_2,x_3;y_1,y_2,d_3/2) &= \phi^e(x_1,x_2,x_3+d_3;y_1,y_2,-d_3/2)\\
\phi^m(x_1,x_2,x_3;d_1/2,y_2,y_3) &= \phi^m(x_1+d_1,x_2,x_3;-d_1/2,y_2,y_3)\\
\phi^m(x_1,x_2,x_3;y_1,d_2/2,y_3) &= \phi^m(x_1,x_2+d_2,x_3;y_1,-d_2/2,y_3)\\
\phi^m(x_1,x_2,x_3;y_1,y_2,d_3/2) &= \phi^m(x_1,x_2,x_3+d_3;y_1,y_2,-d_3/2)
\end{aligned} \tag{3.14}$$

Introducing Lagrange multipliers, we can pose the variational statement of the micromechanical analysis of UC as a stationary value problem of the following functional:

$$
\begin{aligned}
J = \int_{\mathcal{R}} \Big\{ & \left\langle \epsilon^T D \epsilon \right\rangle + \lambda_i(\langle u_i \rangle - v_i) + \lambda^e(\langle \phi \rangle^e - \psi^e) + \lambda^m(\langle \phi \rangle^m - \psi^m) \\
& + \int_{S_1} \gamma_{i1} \left[u_i(x_j; d_1/2, y_2, y_3) - u_i(x_j + \delta_{j1} d_1; -d_1/2, y_2, y_3) \right] \mathrm{d}S_1 \\
& + \int_{S_2} \gamma_{i2} \left[u_i(x_j; y_1, d_2/2, y_3) - u_i(x_j + \delta_{j2} d_2; y_1, -d_2/2, y_3) \right] \mathrm{d}S_2 \\
& + \int_{S_3} \gamma_{i3} \left[u_i(x_j; y_1, y_2, d_3/2) - u_i(x_j + \delta_{j3} d_3; y_1, y_2, -d_3/2) \right] \mathrm{d}S_3 \\
& + \int_{S_1} \alpha_1 \left[\phi^e(x_j; d_1/2, y_2, y_3) - \phi^e(x_j + \delta_{j1} d_1; -d_1/2, y_2, y_3) \right] \mathrm{d}S_1 \\
& + \int_{S_2} \alpha_2 \left[\phi^e(x_j; y_1, d_2/2, y_3) - \phi^e(x_j + \delta_{j2} d_2; y_1, -d_2/2, y_3) \right] \mathrm{d}S_2 \\
& + \int_{S_3} \alpha_3 \left[\phi^e(x_j; y_1, y_2, d_3/2) - \phi^e(x_j + \delta_{j3} d_3; y_1, y_2, -d_3/2) \right] \mathrm{d}S_3 \\
& + \int_{S_1} \beta_1 \left[\phi^m(x_j; d_1/2, y_2, y_3) - \phi^m(x_j + \delta_{j1} d_1; -d_1/2, y_2, y_3) \right] \mathrm{d}S_1 \\
& + \int_{S_2} \beta_2 \left[\phi^m(x_j; y_1, d_2/2, y_3) - \phi^m(x_j + \delta_{j2} d_2; y_1, -d_2/2, y_3) \right] \mathrm{d}S_2 \\
& + \int_{S_3} \beta_3 \left[\phi^m(x_j; y_1, y_2, d_3/2) - \phi^m(x_j + \delta_{j3} d_3; y_1, y_2, -d_3/2) \right] \mathrm{d}S_3 \Big\} \mathrm{d}\mathcal{R}
\end{aligned}
\tag{3.15}
$$

where λ_i, λ^e, λ^m, γ_{ij}, α_i, and β_i are Lagrange multipliers introduced to enforce the constraints in Eqs. (3.1) and (3.14), S_i are the surfaces with $n_i = 1$, x_j represents the triplet of x_1, x_2, x_3, and δ_{ij} is the Kronecker delta. Following the general procedure of VAMUCH, we can obtain the following change of variables for u_i, ϕ^e, and ϕ^m:

$$
u_i(\mathbf{x}; \mathbf{y}) = v_i(\mathbf{x}) + y_j \frac{\partial v_i}{\partial x_j} + \chi_i(\mathbf{x}; \mathbf{y}) \tag{3.16}
$$

$$
\phi^e(\mathbf{x}; \mathbf{y}) = \psi^e(\mathbf{x}) + y_i \frac{\partial \psi^e}{\partial x_i} + \zeta^e(\mathbf{x}; \mathbf{y}) \tag{3.17}
$$

$$
\phi^m(\mathbf{x}; \mathbf{y}) = \psi^m(\mathbf{x}) + y_i \frac{\partial \psi^m}{\partial x_i} + \zeta^m(\mathbf{x}; \mathbf{y}) \tag{3.18}
$$

where χ_i, ζ^e, and ζ^m are the fluctuation functions, satisfying the following constraints in view of Eqs. (3.1) when the origin of the local coordinate system is chosen to be the center of UC:

$$
\langle \chi_i \rangle = 0 \qquad \langle \zeta^e \rangle = 0 \qquad \langle \zeta^m \rangle = 0 \tag{3.19}
$$

Substituting Eqs. (3.16), (3.17), and (3.18) into Eq. (3.15), we obtain a stationary value problem of a functional defined over UC for χ_i, ζ^e, and ζ^m according to the variational asymptotic method [15], such that:

$$\begin{aligned} J_\Omega = \left\langle \epsilon^T D \epsilon \right\rangle + \lambda_i \left\langle \chi_i \right\rangle + \lambda^e \left\langle \zeta^e \right\rangle + \lambda^m \left\langle \zeta^m \right\rangle + \sum_{j=1}^{3} \int_{S_j} \gamma_{ij} (\chi_i^{+j} - \chi_i^{-j}) \mathrm{d}S_j \\ + \sum_{j=1}^{3} \int_{S_j} \alpha_j (\zeta_{+j}^e - \zeta_{-j}^e) \mathrm{d}S_j + \sum_{j=1}^{3} \int_{S_j} \beta_j (\zeta_{+j}^m - \zeta_{-j}^m) \mathrm{d}S_j \end{aligned} \tag{3.20}$$

with

$$\chi_i^{+j} = \chi_i|_{y_j = d_j/2},\ \chi_i^{-j} = \chi_i|_{y_j = -d_j/2} \quad \text{for} \quad j = 1, 2, 3$$

$$\zeta_{+j}^e = \zeta^e|_{y_j = d_j/2},\ \zeta_{-j}^e = \zeta^e|_{y_j = -d_j/2} \quad \text{for} \quad j = 1, 2, 3$$

$$\zeta_{+j}^m = \zeta^m|_{y_j = d_j/2},\ \zeta_{-j}^m = \zeta^m|_{y_j = -d_j/2} \quad \text{for} \quad j = 1, 2, 3$$

Matrix ϵ can be expressed as

$$\epsilon = \bar{\epsilon} + \epsilon_1 \tag{3.21}$$

with

$$\begin{aligned} \bar{\epsilon} &= \lfloor \bar{\epsilon}_{11} \ \ 2\bar{\epsilon}_{12} \ \ \bar{\epsilon}_{22} \ \ 2\bar{\epsilon}_{13} \ \ 2\bar{\epsilon}_{23} \ \ \bar{\epsilon}_{33} \ \ \bar{E}_1 \ \ \bar{E}_2 \ \ \bar{E}_3 \ \ \bar{H}_1 \ \ \bar{H}_2 \ \ \bar{H}_3 \rfloor^T \\ \epsilon_1 &= \lfloor \hat{\epsilon}_{11} \ \ 2\hat{\epsilon}_{12} \ \ \hat{\epsilon}_{22} \ \ 2\hat{\epsilon}_{13} \ \ 2\hat{\epsilon}_{23} \ \ \hat{\epsilon}_{33} \ \ \hat{E}_1 \ \ \hat{E}_2 \ \ \hat{E}_3 \ \ \hat{H}_1 \ \ \hat{H}_2 \ \ \hat{H}_3 \rfloor^T \end{aligned} \tag{3.22}$$

and

$$\begin{aligned} \bar{\epsilon}_{ij} &= \frac{1}{2}\left(\frac{\partial v_i}{\partial x_j} + \frac{\partial v_j}{\partial x_i}\right) \qquad \bar{E}_i = -\frac{\partial \psi^e}{\partial x_i} \qquad \bar{H}_i = -\frac{\partial \psi^m}{\partial x_i} \\ \hat{\epsilon}_{ij} &= \frac{1}{2}\left(\frac{\partial \chi_i}{\partial y_j} + \frac{\partial \chi_j}{\partial y_i}\right) \qquad \hat{E}_i = -\frac{\partial \zeta^e}{\partial y_i} \qquad \hat{H}_i = -\frac{\partial \zeta^m}{\partial y_i} \end{aligned} \tag{3.23}$$

where $\bar{\epsilon}$ will be shown later to be the global field variable array containing the strain field, the electric field, and the magnetic field for the material with homogenized effective material properties. The functional J_Ω in Eq. (3.20) forms the backbone of the present theory. This stationary value of this functional can be solved analytically for very simple cases such as binary composites, however, for general cases we need to use numerical techniques such as the finite element method (FEM) to seek numerical solutions.

3.3 Finite Element Implementation

It is possible to formulate the FEM solution based on Eq. (3.20), however, it is not the most convenient and efficient way because Lagrange multipliers will increase the number of unknowns. To this end, we can reformulate the stationary value problem of the functional in Eq. (3.20) as the minimum value of the following functional

$$\Pi_\Omega = \frac{1}{\Omega}\int_\Omega \epsilon^T D\epsilon \mathrm{d}\Omega \tag{3.24}$$

under the following constraints

$$\chi_i^{+j} = \chi_i^{-j} \quad , \quad \zeta_{+j}^e = \zeta_{-j}^e \quad \text{, and} \quad \zeta_{+j}^m = \zeta_{-j}^m \quad \text{for} \quad j = 1,2,3 \tag{3.25}$$

The constraints in Eqs. (3.19) do not affect the minimum values of Π_Ω but help uniquely determine χ_i, ζ^e, and ζ^m. In practice, we can constrain the fluctuation function at an arbitrary node to be zero and later use this constraint to recover the unique fluctuation functions. It is fine to use penalty function method to introduce the constraints in Eqs. (3.25). However, this method introduces additional approximation and the robustness of the solution depends on the choice of large penalty numbers. Here, we choose to make the nodes on the positive boundary surface (*i.e.*, $y_i = d_i/2$) slave to the nodes on the opposite negative boundary surface (*i.e.*, $y_i = -d_i/2$). By assembling all the independent active degrees of freedom (DOFs), we can implicitly and exactly incorporate the constraints in Eqs. (3.25).

Introduce the following matrix notation

$$\epsilon_1 = \begin{bmatrix} \frac{\partial}{\partial y_1} & 0 & 0 & 0 & 0 \\ \frac{\partial}{\partial y_2} & \frac{\partial}{\partial y_1} & 0 & 0 & 0 \\ 0 & \frac{\partial}{\partial y_2} & 0 & 0 & 0 \\ \frac{\partial}{\partial y_3} & 0 & \frac{\partial}{\partial y_1} & 0 & 0 \\ 0 & \frac{\partial}{\partial y_3} & \frac{\partial}{\partial y_2} & 0 & 0 \\ 0 & 0 & \frac{\partial}{\partial y_3} & 0 & 0 \\ 0 & 0 & 0 & -\frac{\partial}{\partial y_1} & 0 \\ 0 & 0 & 0 & -\frac{\partial}{\partial y_2} & 0 \\ 0 & 0 & 0 & -\frac{\partial}{\partial y_3} & 0 \\ 0 & 0 & 0 & 0 & -\frac{\partial}{\partial y_1} \\ 0 & 0 & 0 & 0 & -\frac{\partial}{\partial y_2} \\ 0 & 0 & 0 & 0 & -\frac{\partial}{\partial y_3} \end{bmatrix} \begin{Bmatrix} \chi_1 \\ \chi_2 \\ \chi_3 \\ \zeta^e \\ \zeta^m \end{Bmatrix} \equiv \Gamma_h \chi \tag{3.26}$$

where Γ_h is an operator matrix. If we discretize χ using the finite elements as

$$\chi(x_i; y_i) = S(y_i)\mathcal{X}(x_i) \tag{3.27}$$

with S representing the shape functions and $\mathcal{X}$ a column matrix of the nodal values of the mechanical, electric, and magnetic fluctuation functions. Substituting Eqs. (3.26) and (3.27) into Eq. (3.24), we obtain a discretized version of the functional as

$$\Pi_\Omega = \frac{1}{\Omega}(\mathcal{X}^T E \mathcal{X} + 2\mathcal{X}^T D_{h\epsilon}\bar{\epsilon} + \bar{\epsilon}^T D_{\epsilon\epsilon}\bar{\epsilon}) \tag{3.28}$$

where

$$E = \int_\Omega (\Gamma_h S)^T D (\Gamma_h S) \mathrm{d}\Omega \qquad D_{h\epsilon} = \int_\Omega (\Gamma_h S)^T D \mathrm{d}\Omega \qquad D_{\epsilon\epsilon} = \int_\Omega D \mathrm{d}\Omega \tag{3.29}$$

Minimizing Π_Ω in Eq. (3.28), we obtain the following linear system

$$E\mathcal{X} = -D_{h\epsilon}\bar{\epsilon} \tag{3.30}$$

It is clear from Eq. (3.30) that the fluctuation function $\mathcal{X}$ is linearly proportional to $\bar{\epsilon}$, which means the solution can be written symbolically as

$$\mathcal{X} = \mathcal{X}_0 \bar{\epsilon} \tag{3.31}$$

Substituting Eq. (3.31) into Eq. (3.28), we can calculate the density of electromagnetic enthalpy of the UC as

$$\Pi_\Omega = \frac{1}{\Omega} \bar{\epsilon}^T \left(\mathcal{X}_0^T D_{h\epsilon} + D_{\epsilon\epsilon} \right) \bar{\epsilon} \equiv \bar{\epsilon}^T \bar{D} \bar{\epsilon} \tag{3.32}$$

It can be seen that $\bar{\epsilon}$ is a column matrix containing the global strains, global electric fields, and global magnetic fields, and $\bar{D}$ in Eq. (3.32) is a 12×12 matrix containing the effective material properties which can be expressed as

$$\bar{D} = \begin{bmatrix} \boldsymbol{C}^* & -\boldsymbol{e}^* & -\boldsymbol{q}^* \\ -\boldsymbol{e}^{*T} & -\boldsymbol{k}^* & -\boldsymbol{a}^* \\ -\boldsymbol{q}^{*T} & -\boldsymbol{a}^* & -\boldsymbol{\mu}^* \end{bmatrix} \tag{3.33}$$

If the local fields within UC are of interest, we can recover those fields, such as local displacements, electric potential, magnetic potential, stresses, electric displacements, and magnetic flux density in terms of the macroscopic behavior including the global displacements v_i, the global electric potential ψ^e, the global magnetic potential ϕ^m, the global field variables contained in $\bar{\epsilon}$, and the fluctuation functions contained in χ. First, we need to uniquely determine the fluctuation functions, which can be simply achieved using the constraints in Eq. (3.19). Then, we can recover the local displacements, electric potential, and magnetic potential using Eqs. (3.16), (3.17), and (3.18) as

$$\begin{Bmatrix} u_1 \\ u_2 \\ u_3 \\ \phi^e \\ \phi^m \end{Bmatrix} = \begin{Bmatrix} v_1 \\ v_2 \\ v_3 \\ \psi^e \\ \psi^m \end{Bmatrix} + \begin{bmatrix} \frac{\partial v_1}{\partial x_1} & \frac{\partial v_1}{\partial x_2} & \frac{\partial v_1}{\partial x_3} \\ \frac{\partial v_2}{\partial x_1} & \frac{\partial v_2}{\partial x_2} & \frac{\partial v_2}{\partial x_3} \\ \frac{\partial v_3}{\partial x_1} & \frac{\partial v_3}{\partial x_2} & \frac{\partial v_3}{\partial x_3} \\ \frac{\partial \psi^e}{\partial x_1} & \frac{\partial \psi^e}{\partial x_2} & \frac{\partial \psi^e}{\partial x_3} \\ \frac{\partial \psi^m}{\partial x_1} & \frac{\partial \psi^m}{\partial x_2} & \frac{\partial \psi^m}{\partial x_3} \end{bmatrix} \begin{Bmatrix} y_1 \\ y_2 \\ y_3 \end{Bmatrix} + \bar{S} \bar{\mathcal{X}} \tag{3.34}$$

Here $\bar{S}$ is different from S due to the recovery of slave nodes and the constrained node. The local strain field, the electric field, and the magnetic field can be recovered using Eq. (3.21)

along with Eq. (3.26) as

$$\epsilon = \bar{\epsilon} + \Gamma_h \bar{S} \bar{\mathcal{X}} \tag{3.35}$$

Finally, the local stress and electric displacement field can be recovered straightforwardly using the 3D constitutive relations for the constituent material as

$$\sigma = D\epsilon \tag{3.36}$$

with σ as a column matrix containing 3D stresses, electric displacements, and magnetic flux density such that

$$\sigma = \lfloor \sigma_{11} \;\; \sigma_{12} \;\; \sigma_{22} \;\; \sigma_{13} \;\; \sigma_{23} \;\; \sigma_{33} \;\; -T_1 \;\; -T_2 \;\; -T_3 \;\; -B_1 \;\; -B_2 \;\; -B_3 \rfloor^T \tag{3.37}$$

where σ_{ij}, T_i, and B_i denote the stress tensor, the electric flux density vector, and the magnetic flux density vector, respectively.

The present formulation is implemented in the computer program VAMUCH, a general-purpose mircomechanics analysis code. VAMUCH provides a unified analysis for periodic microstructures which are normally modeled using 1D, 2D, or 3D UCs. First, the same code VAMUCH can be used to homogenize binary composites (modeled using 1D UCs), fiber reinforced composites (modeled using 2D UCs), and particle reinforced composites (modeled using 3D UCs). Second, VAMUCH can reproduce the results for lower-dimensional UCs using higher-dimensional UCs. That is, VAMUCH predicts the same results for binary composites using 1D, 2D, or 3D UCs, and for fiber reinforced composites using 2D or 3D UCs.

3.4 Numerical Examples

In this section, we will use several examples to demonstrate the application and accuracy of the present theory and the companion code. The effective properties will be predicted and compared with available results in the literature. Furthermore, the local fields are also recovered to show the capability of VAMUCH.

Table 3.1: Material properties of the composite constituents ($BaTiO_3$, $CoFe_2O_4$, and epoxy)

	$BaTiO_3$(piezoelectric)	$CoFe_2O_4$(piezomagnetic)	Epoxy
C_{11}(GPa)	162	269.5	5.53
C_{12}(GPa)	78	170	2.97
C_{23}(GPa)	77	173	2.97
C_{22}(GPa)	166	286	5.53
C_{55}(GPa)	43	45.3	1.28
k_{11}(C/Vm)	12.6×10^{-9}	0.093×10^{-9}	0.1×10^{-9}
k_{33}(C/Vm)	11.2×10^{-9}	0.08×10^{-9}	0.1×10^{-9}
μ_{11}(Ns^2/C^2)	0.1×10^{-4}	1.57×10^{-4}	0.01×10^{-4}
μ_{33}(Ns^2/C^2)	0.05×10^{-4}	-5.9×10^{-4}	0.01×10^{-4}
e_{11}(C/m^2)	18.6	0	0
e_{21}(C/m^2)	-4.4	0	0
e_{51}(C/m^2)	11.6	0	0
q_{11}(N/Am)	0	699.7	0
q_{21}(N/Am)	0	580.3	0
q_{51}(N/Am)	0	550	0

3.4.1 Two-phase Electromagnetoelastic Composites

Following [8], we first consider a two-phase composite consisting of a $CoFe_2O_4$ piezomagnetic matrix reinforced by $BaTiO_3$ piezoelectric fibers. The piezoelectric fibers are of circular shape and arranged in a square array. Both constituents are transversely isotropic with the axis of symmetry oriented in the 1-direction. The independent material constants of constituents are given in Table 3.1. Note that the electromagnetic coefficients in both constituents are zero, i.e., $a_{ij} = 0$. The composites also exhibit transverse isotropy, characterized by 17 independent material constants including five elastic constants, three piezoelectric coefficients, three piezomagnetic coefficients, two dielectric coefficients, two electromagnetic coefficients, two magnetic permeability coefficients, which are expressed in the corresponding matrices as follows:

$$\boldsymbol{C} = \begin{bmatrix} C_{11}^* & 0 & C_{12}^* & 0 & 0 & C_{12}^* \\ 0 & C_{55}^* & 0 & 0 & 0 & 0 \\ C_{12}^* & 0 & C_{22}^* & 0 & 0 & C_{23}^* \\ 0 & 0 & 0 & C_{55}^* & 0 & 0 \\ 0 & 0 & 0 & 0 & \frac{C_{22}^* - C_{23}^*}{2} & 0 \\ C_{12}^* & 0 & C_{23}^* & 0 & 0 & C_{22}^* \end{bmatrix} \quad \boldsymbol{e} = \begin{bmatrix} e_{11}^* & 0 & 0 \\ 0 & e_{51}^* & 0 \\ e_{21}^* & 0 & 0 \\ 0 & 0 & e_{51}^* \\ 0 & 0 & 0 \\ e_{21}^* & 0 & 0 \end{bmatrix} \quad \boldsymbol{q} = \begin{bmatrix} q_{11}^* & 0 & 0 \\ 0 & q_{51}^* & 0 \\ q_{21}^* & 0 & 0 \\ 0 & 0 & q_{51}^* \\ 0 & 0 & 0 \\ q_{21}^* & 0 & 0 \end{bmatrix} \tag{3.38}$$

$$\boldsymbol{k} = \begin{bmatrix} k_{11}^* & 0 & 0 \\ 0 & k_{33}^* & 0 \\ 0 & 0 & k_{33}^* \end{bmatrix} \quad \boldsymbol{a} = \begin{bmatrix} a_{11}^* & 0 & 0 \\ 0 & a_{33}^* & 0 \\ 0 & 0 & a_{33}^* \end{bmatrix} \quad \boldsymbol{\mu} = \begin{bmatrix} \mu_{11}^* & 0 & 0 \\ 0 & \mu_{33}^* & 0 \\ 0 & 0 & \mu_{33}^* \end{bmatrix} \tag{3.39}$$

To compare with available results in the literature, we use VAMUCH to calculate these effective coefficients with the volume fraction of fibers varying between 0.1 and 0.7. For a square array with a circular fiber, the maximum achievable volume fraction of fibers is around 0.785. It is noted that we chose a square array with circular fiber for convenience to compare with available results in the literature. The present theory and VAMUCH can handle other periodic structures with arbitrarily-shaped and positioned inclusions, even voids [16]. In Figs. 3.2−3.8, we compared the results predicted by VAMUCH with those reported in [8] using the Mori-Tanaka method, where VAMUCH results are denoted using and Mori-Tanaka results are denoted as solid lines. It is clear from these plots that both VAMUCH and the Mori-Tanaka method predict almost the same set of effective material properties for this two-phase electromagnetoelastic composite. As reported previously, the electromagnetic coupling effect is present in the composite, although it is not in either of the individual phases. It is also observed in Fig. 3.6 that VAMUCH prediction for q_{51}^* is slightly different from that of the Mori-Tanaka method when the volume fraction of fibers is big. This might be due to the differences in choosing a specific microstructure (square array with circular fibers) for VAMUCH yet the information of this specific microstructure is not rigorously captured in [8].

3.4.2 Three-phase Electromagnetoelastic Composites

To show the versatility of the present model, we also consider a three-phase electromagnetoelastic composite consisting of an elastic epoxy matrix reinforced with piezoelectric ($BaTiO_3$) and piezomagnetic fibers ($CoFe_2O_4$) which is an example extensively studied in [14]. The piezomagnetic fiber is at the center of the unit cell while the piezoelectric fibers in the shape of quarter circles are located at the four corners of unit cell. A picture showing this microstructure can be found in Fig. 2 of [14]. The material properties of the three constituents are listed in Table 3.1. We investigate the effect of varying the volume fractions of piezomagnetic fibers ($BaTiO_3$) with the matrix volume fraction fixed at 0.4. Effective mate-

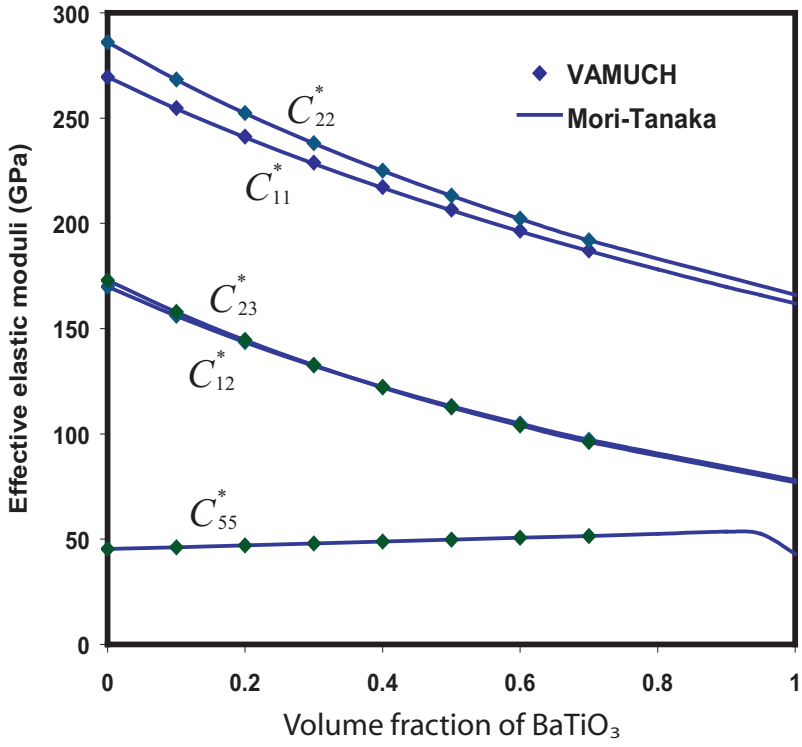

Fig. 3.2: Effective elastic constants of $BaTiO_3/CoFe_2O_4$ composites.

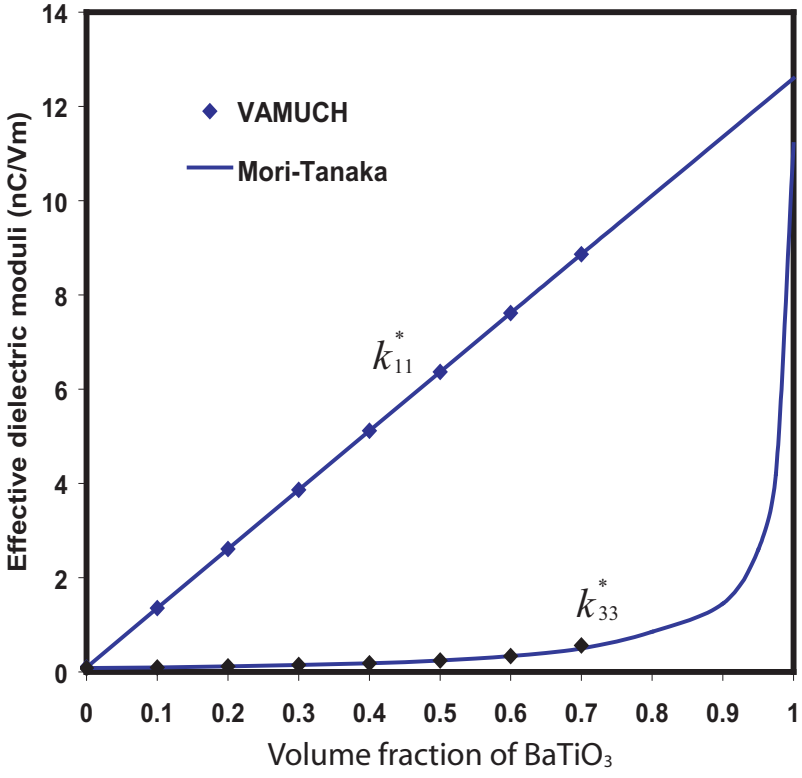

Fig. 3.3: Effective dielectric coefficients of $BaTiO_3/CoFe_2O_4$ composites.

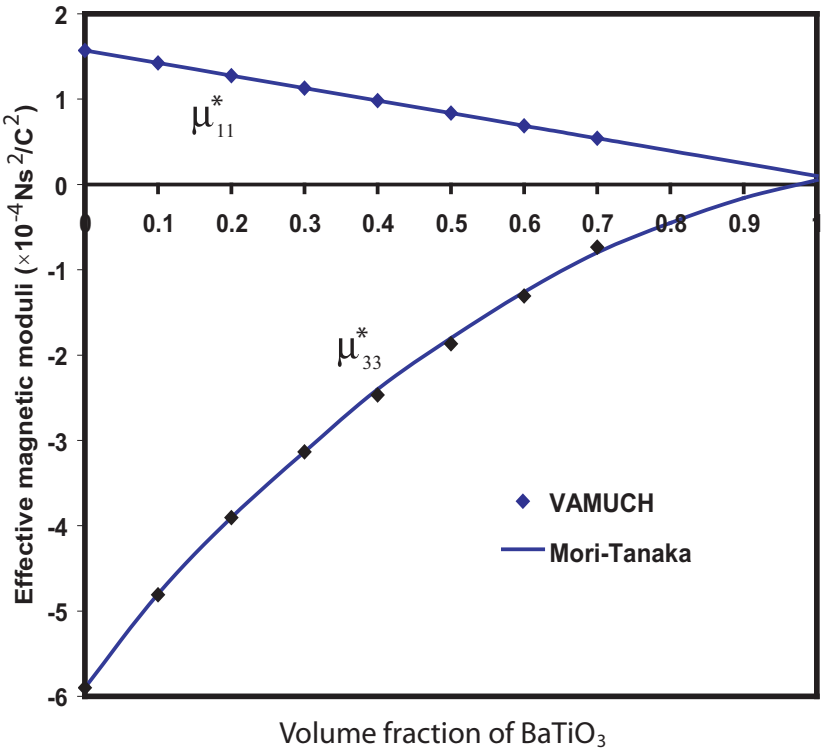

Fig. 3.4: Effective magnetic permeability coefficients of $BaTiO_3/CoFe_2O_4$ composites.

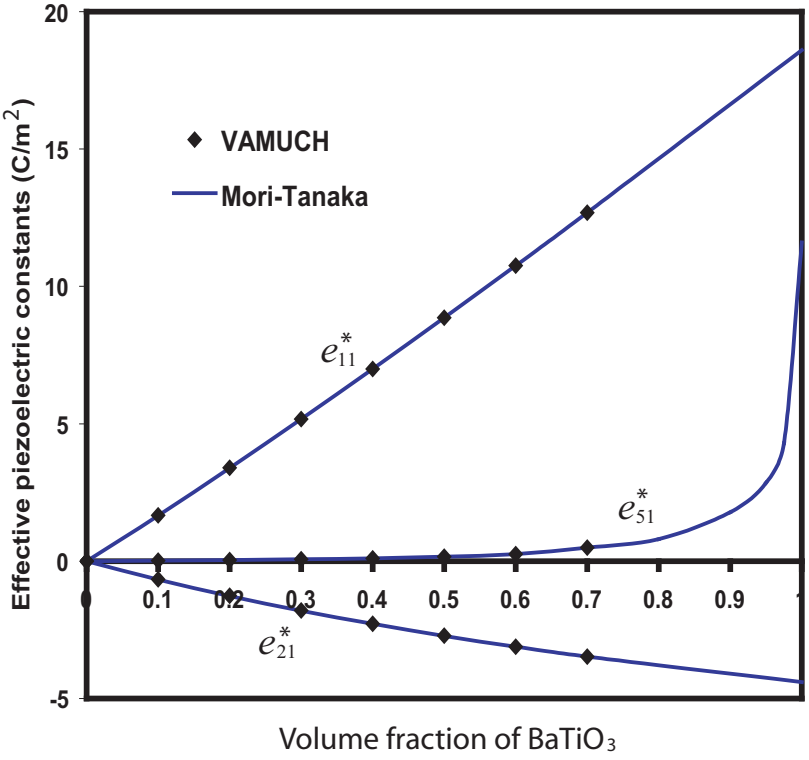

Fig. 3.5: Effective piezoelectric coefficients of $BaTiO_3/CoFe_2O_4$ composites.

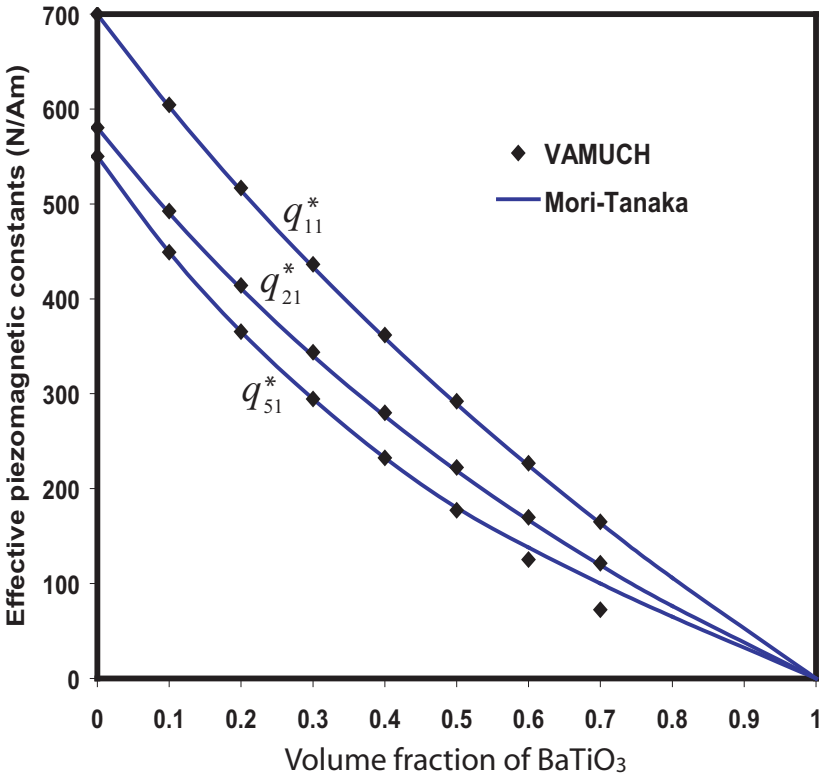

Fig. 3.6: Effective piezomagnetic coefficients of $BaTiO_3/CoFe_2O_4$ composites.

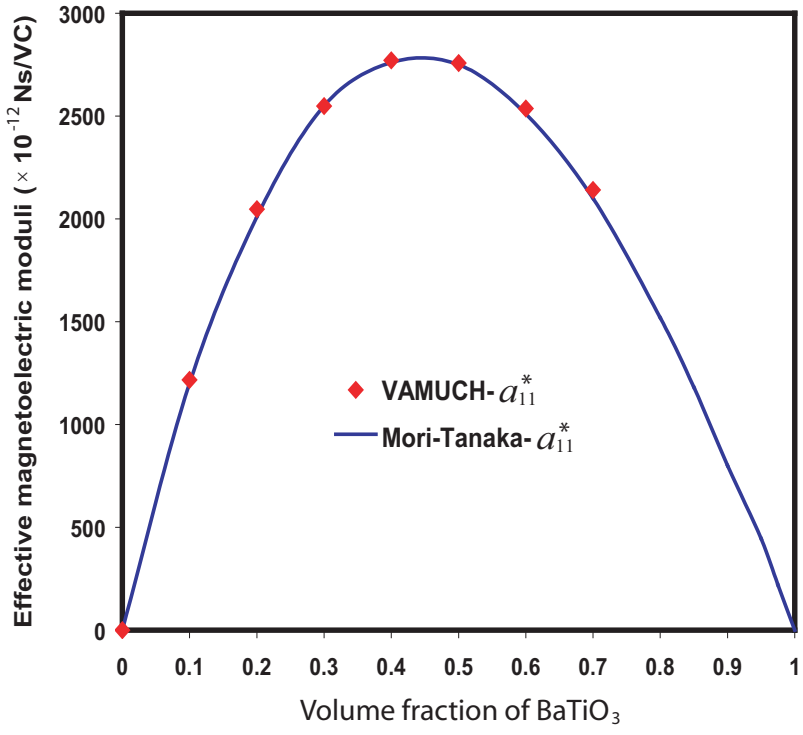

Fig. 3.7: Effective electromagnetic coefficient (a_{11}) of $BaTiO_3/CoFe_2O_4$ composites.

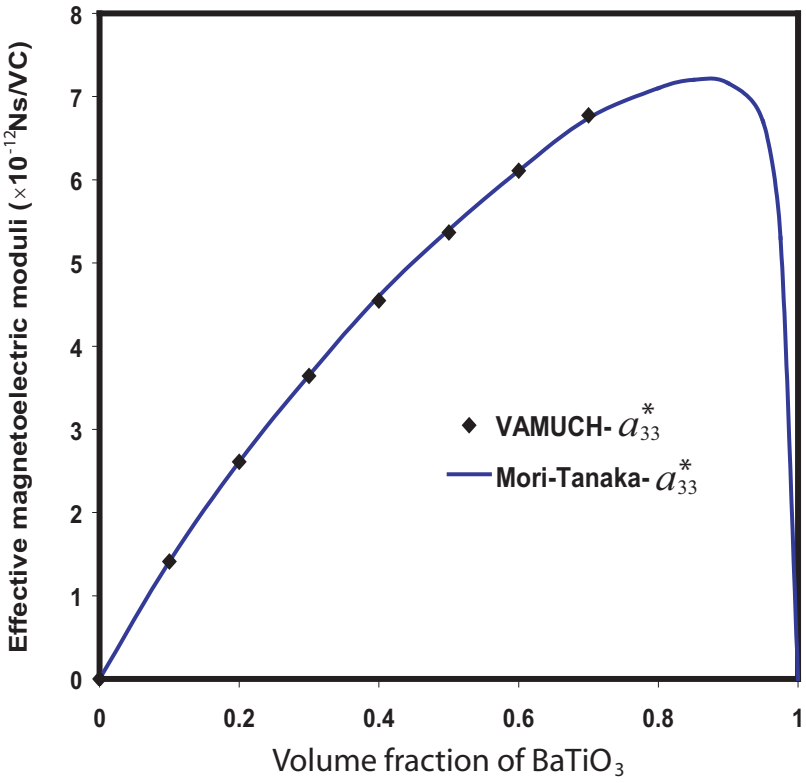

Fig. 3.8: Effective electromagnetic coefficient (a_{33}) of $BaTiO_3/CoFe_2O_4$ composites.

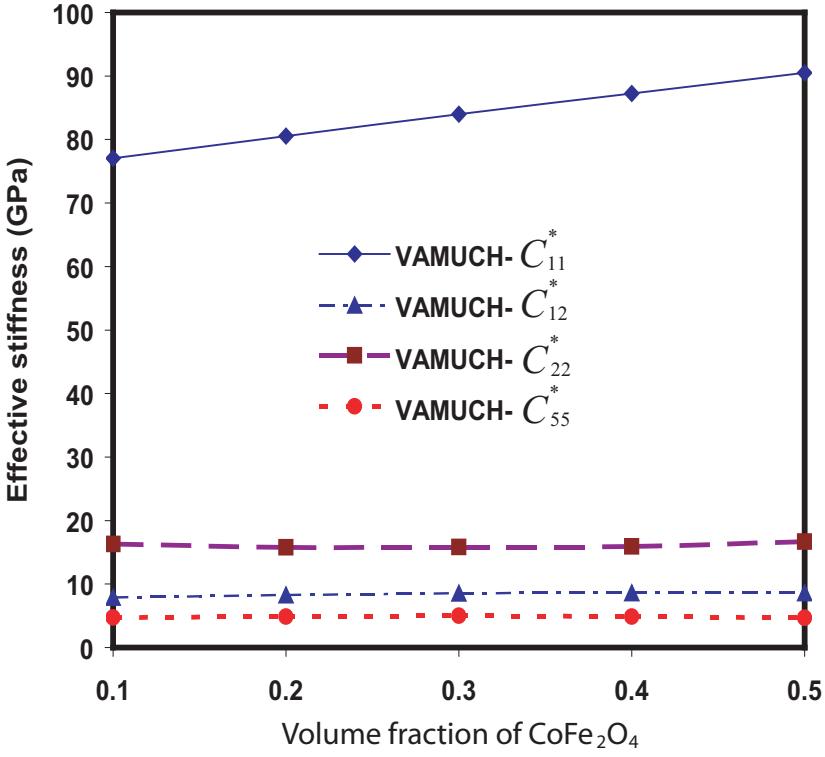

Fig. 3.9: Effective elastic constants of $BaTiO_3/CoFe_2O_4$/Epoxy composites.

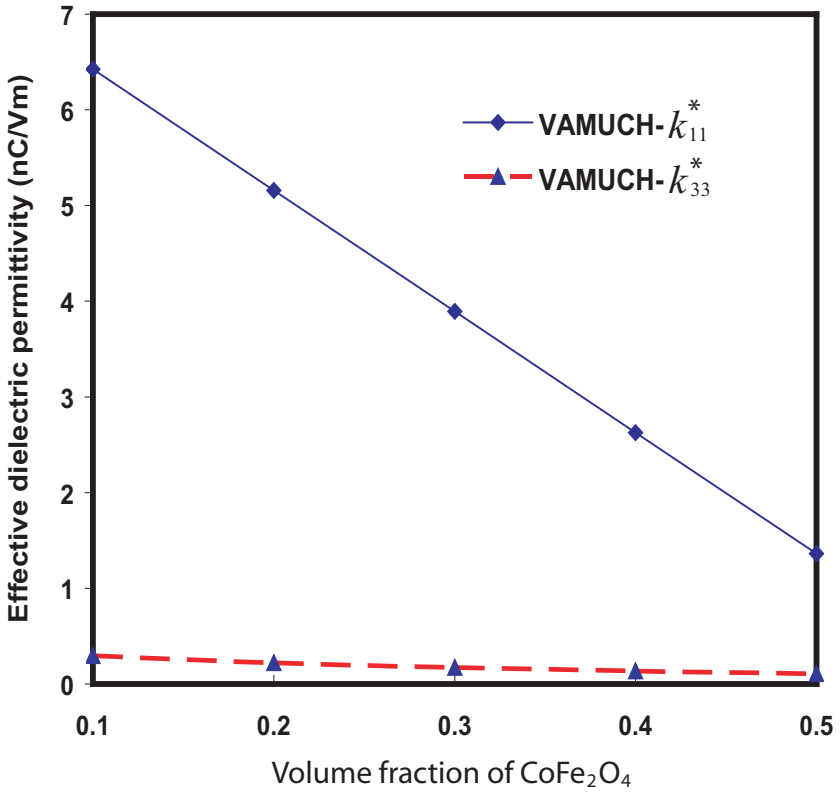

Fig. 3.10: Effective dielectric coefficients of $BaTiO_3/CoFe_2O_4$/Epoxy composites.

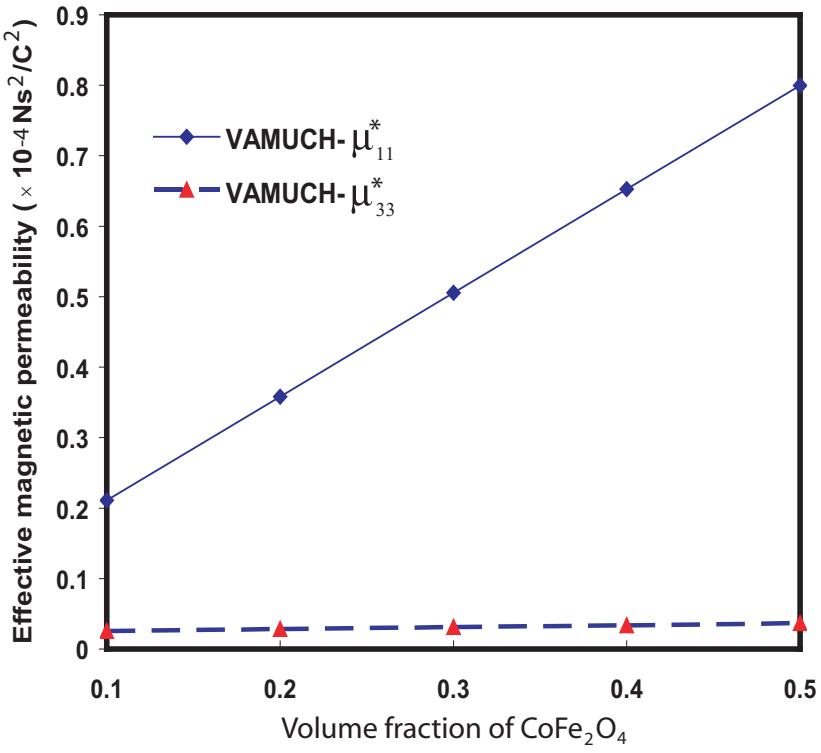

Fig. 3.11: Effective magnetic permeability coefficients of $BaTiO_3/CoFe_2O_4$/Epoxy composites.

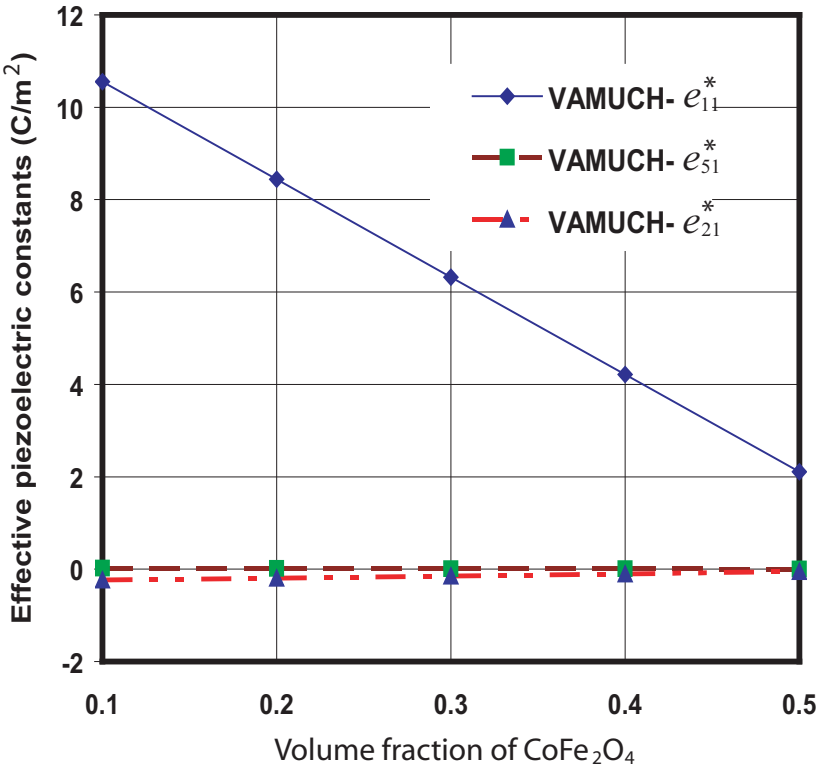

Fig. 3.12: Effective piezoelectric coefficients of $BaTiO_3/CoFe_2O_4$/Epoxy composites.

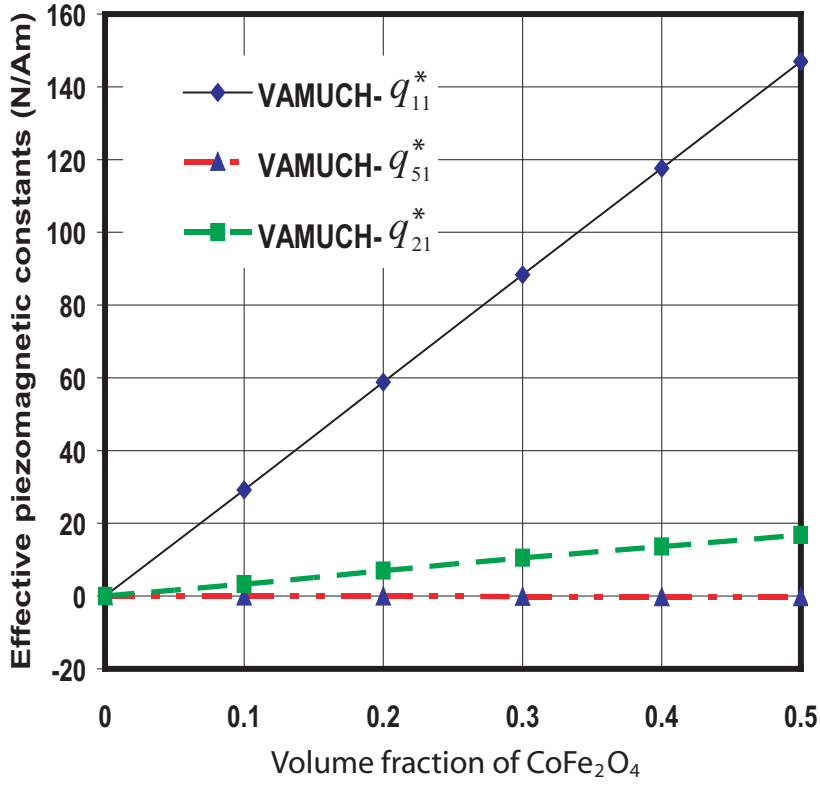

Fig. 3.13: Effective piezomagnetic coefficients of $BaTiO_3/CoFe_2O_4$/Epoxy composites.

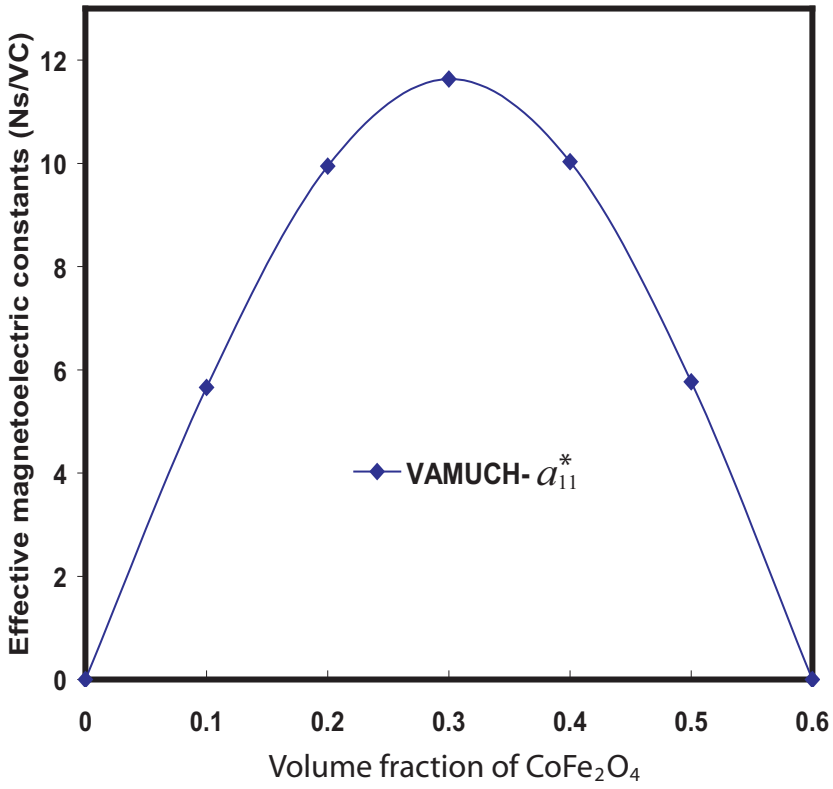

Fig. 3.14: Effective electromagnetic coefficient of $BaTiO_3/CoFe_2O_4$/Epoxy composites.

rial properties including elastic constants dielectric coefficients, magnetic permeability coefficients, piezoelectric coefficients, piezomagnetic coefficients and electromagnetic coefficients are predicted for the volume fractions of piezomagnetic fibers ($CoFe_2O_4$) between 0.1 and 0.5 using VAMUCH. Only the results predicted by VAMUCH are plotted in Figs. 3.9−3.14 because these results are almost the same as those reported in [14] except that there is a slight deviation for the electromagnetic coefficient (a_{33}^*) as shown in Fig. 3.15. The effective elastic modulus C_{23}^* is very close to C_{12}^* and the values are not presented in Fig. 3.9 for clarity. Theoretically, the present theory is very different from that of [14] because in [14] the effective properties are calculated through averaging the electromagnetoelastic fields which are obtained using a series of finite element analyses of the microstructure subjected to periodic boundary conditions and various loading conditions, while no boundary conditions on the global field variables and loading conditions are necessary for VAMUCH calculations. Furthermore, VAMUCH obtains the complete set of effective properties directly within one analysis and does not require the process of averaging the electromagnetoelastic fields.

A unique capability of VAMUCH is that it can accurately predict the local fields within

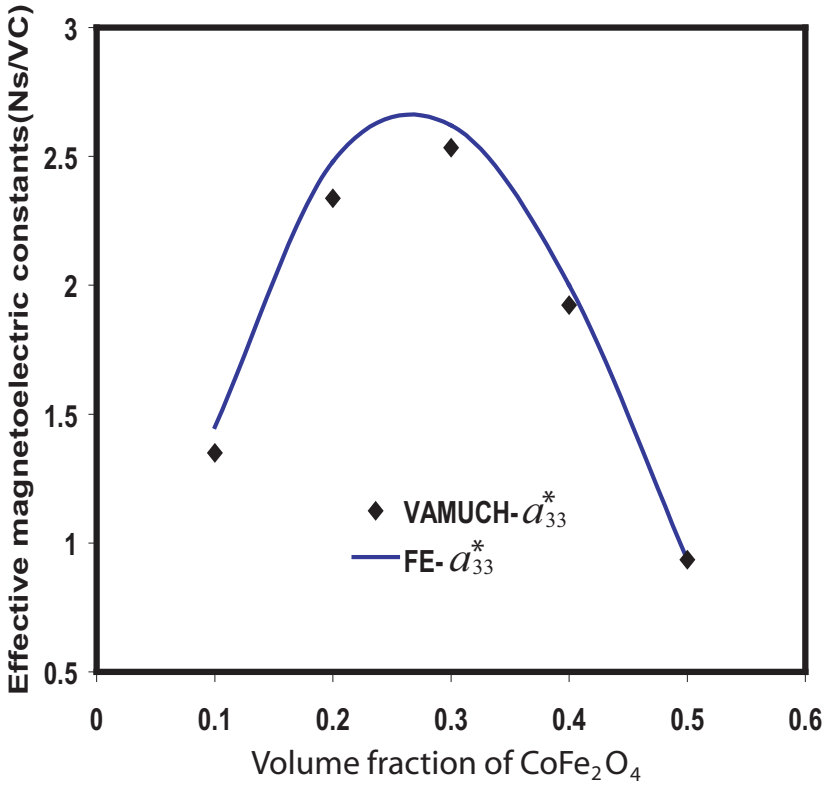

Fig. 3.15: Effective electromagnetic coefficient of $BaTiO_3/CoFe_2O_4$/Epoxy composites.

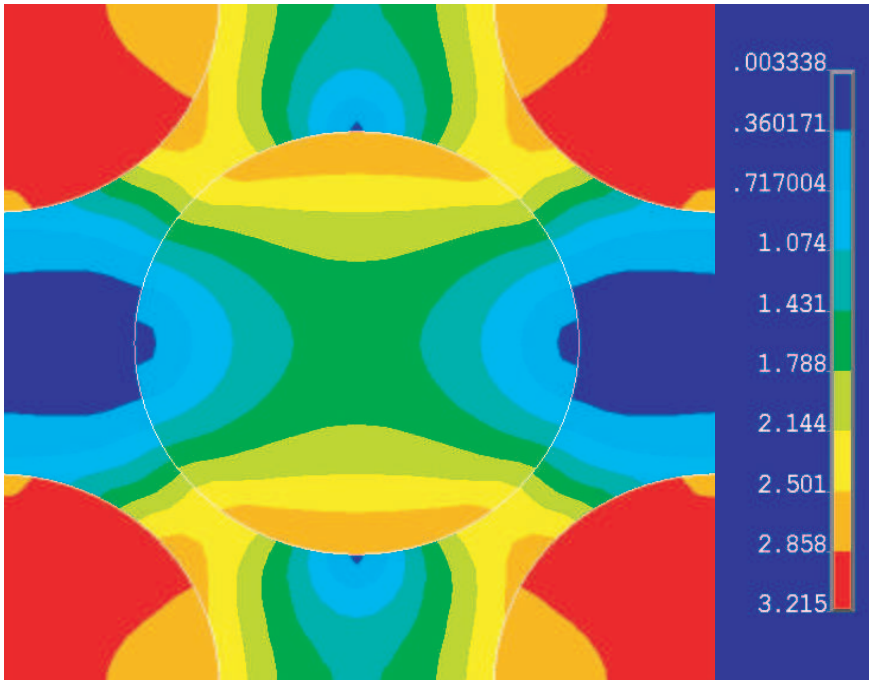

Fig. 3.16: von Mises stress (GPa) contour of $BaTiO_3/CoFe_2O_4$/Epoxy composites.

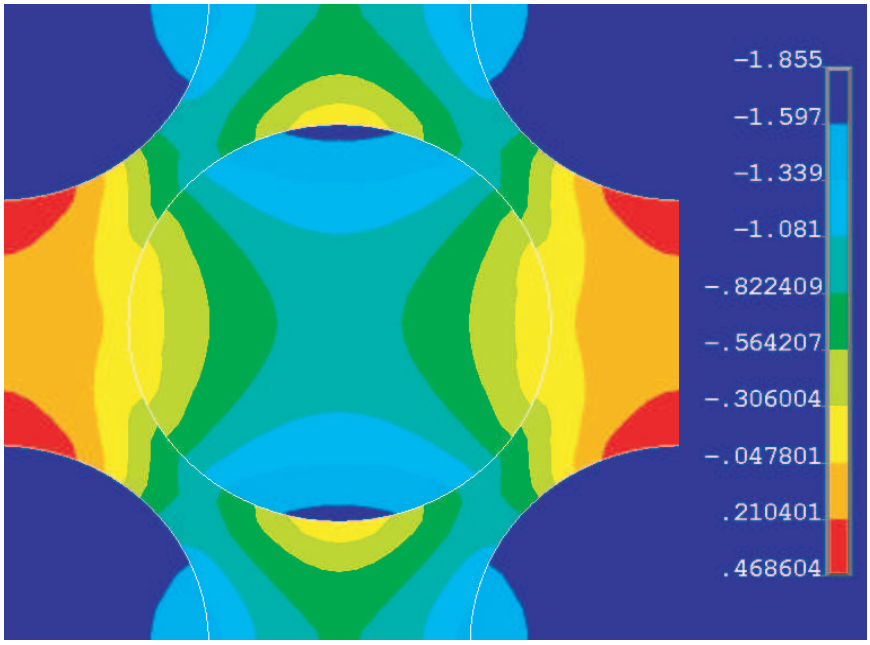

Fig. 3.17: Shear stress σ_{12}(GPa) contour of $BaTiO_3/CoFe_2O_4$/Epoxy composites.

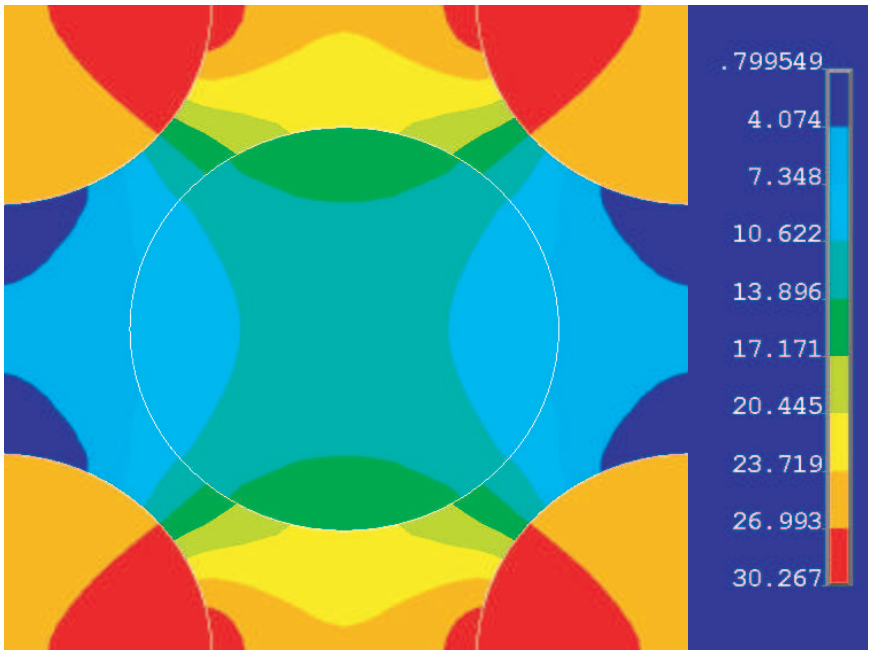

Fig. 3.18: Electric flux density T_2 (nC/Vm) contour of $BaTiO_3/CoFe_2O_4$/Epoxy composites.

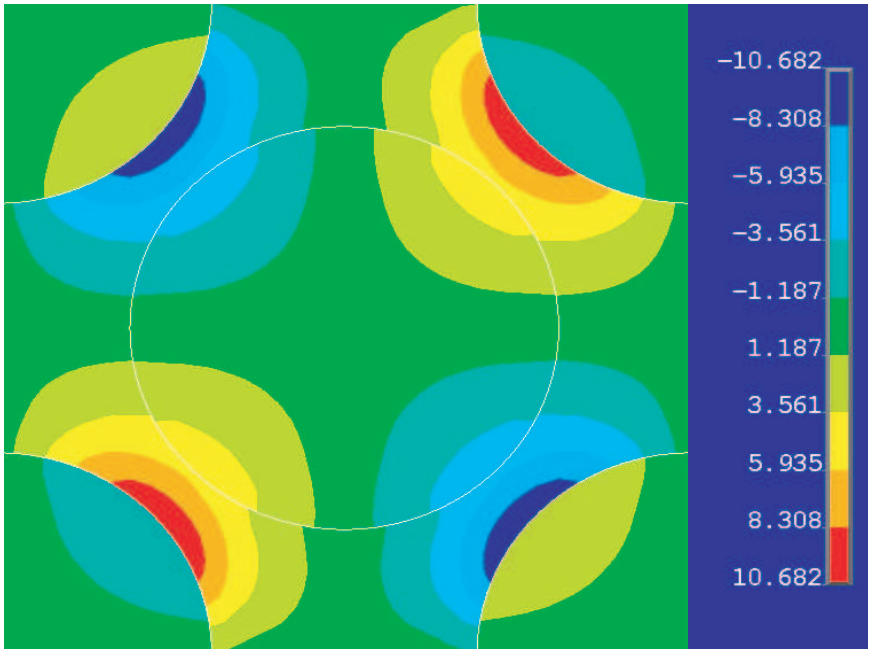

Fig. 3.19: Electric flux density T_3 (nC/Vm) contour of $BaTiO_3/CoFe_2O_4$/Epoxy composites.

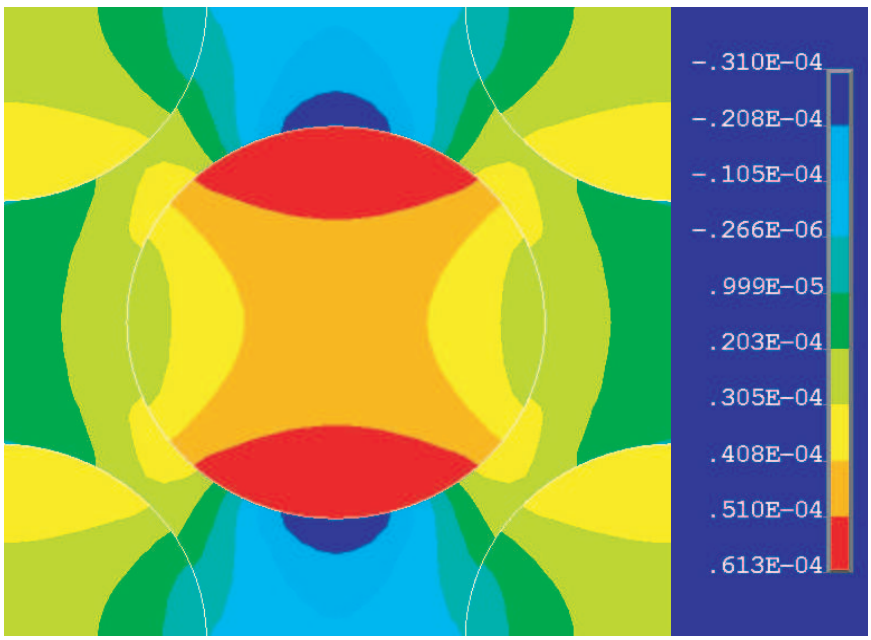

Fig. 3.20: Magnetic flux density B_2 ($\times 10^3 \mathrm{NA}^{-1}\mathrm{m}^{-1}$) contour of $BaTiO_3/CoFe_2O_4$/ Epoxy composites.

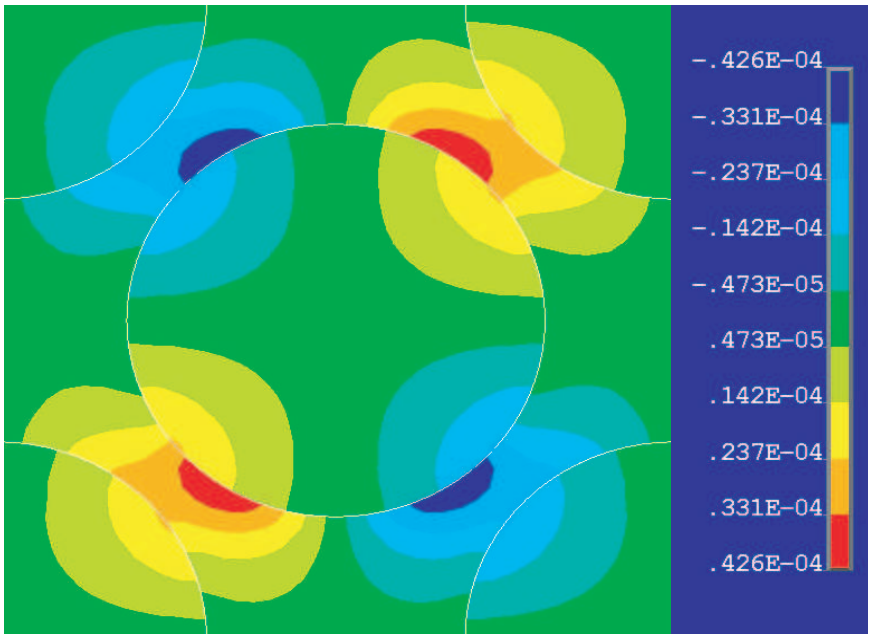

Fig. 3.21: Magnetic flux density B_3 ($\times 10^3 \mathrm{NA}^{-1}\mathrm{m}^{-1}$) contour of $BaTiO_3/CoFe_2O_4$/ Epoxy composites.

the microstructure. To this end, let us assume that the global electric field from the macroscopic analysis of the homogenized material made of the three-phase electromagnetoelastic composites are $E_2 = 100\mathrm{V/m}$ while all mechanical strains and all other electric and magnetic fields are zero. Figs. 3.16−3.21 show the distributions of Von Mises stress, shear stress σ_{12}, electric flux density, magnetic flux density within the microstructure of the three-phase electromagnetoelastic composites predicted by VAMUCH. It can be seen that all the detailed distribution of the local fields including concentrations at the interface between fibers and matrix are well captured by VAMUCH. Such information will be very helpful for design and integrity evaluation of the electromagnetoelastic composites.

3.5 Conclusion

The variational asymptotic method for unit cell homogenization (VAMUCH) has been applied to construct a general-purpose micromechanics model for predicting effective properties and local fields of periodic electromagnetoelastic composites. In comparison to existing models, the present model has the following unique features:

1. It adopts the variational asymptotic method as its mathematical foundation. It invokes only essential assumptions inherent in the concept of micromechanics.

2. It has an inherent variational nature and its numerical implementation is shown to be straightforward.

3. It handles 1D/2D/3D unit cells uniformly. The dimensionality of the problem is determined by the periodicity of the microstructure.

The present theory is implemented in the computer program, VAMUCH. Examples have been used to demonstrate its application and accuracy as a general-purpose micromechanical analysis tool for electromagnetoelastic composites. Although for the examples we have studied, VAMUCH results are almost the same as the results obtained by the finite element-based micromechanics analysis [14], VAMUCH has the following unique advantages:

1. VAMUCH can obtain the complete set of material properties within one analysis, which is more efficient than those approaches requiring multiple runs under different boundary and load conditions. Furthermore, it is not a trivial issue to apply the right boundary conditions to obtain a correct finite element-based micromechanical analysis.

2. VAMUCH calculates effective properties and local fields directly with the same accuracy as the fluctuation functions. No postprocessing calculations which introduces more approximations, such as averaging stress and electromagnetic displacement field, are needed, which are indispensable for the finite element-based micromechanical analysis.

3. VAMUCH can deal with general anisotropy for effective materials which means VAMUCH can calculate 21 constants for the effective elastic constants, 18 constants for the effective piezoelectric coefficient, 18 for the effective piezomagnetic coeffiicents, 6 for the effective dielectric constants 6 for the magnetic permeability coefficients, 6 for electromagnetic coefficients, while the finite element-based micromechanical analyses have difficult to predict effective material having constants more than orthotropic materials.

References

[1] A. Van Run, D. Terrell, J. Scholing, An in situ grown eutectic magnetoelectric composite materials, Journal of Materials Science 9 (1974) 1710-1714.

[2] L. Bracke, R. Van Vliet, A broadband magneto-electric transducer using a composite materials, International Journal of Electronics 51 (1981) 255-262.

[3] G. Harshe, J. Dougherty, R. Newnham, Theoretical modeling of 3-0/0-3 magneto-electric composites, International Journal of Applied Electromagnetics in Materials 4 (1993) 161-171.

[4] M. Avellaneda, G. Harshe, Magnetoelectric effect in piezoelectric/magnetostrictive multilayer(2-2) composites, Journal of Intelligent Material Systems and Structures 5 (1994) 501-513.

[5] C. Nan, Magnetoelectric effect in composites of piezoelectric and piezomagnetic phases, Physical Review B 50 (9) (1994) 6082-6088.

[6] Y. Benveniste, Magnetoelectric effect in fibrous composites with piezoelectric and piezomagnetic phases, Physical Review B 51 (9) (1995) 16424-16427.

[7] J. Li, M. Dunn, Anisotropic coupled-field inclusion and inhomogeneity problems, Philosophical Magazine A 77 (1998) 1341-1350.

[8] J. Li, M. Dunn, Micromechanics of magnetoelectroelastic composite materials: average fields and effective behavior, Journal of Intelligent Material Systems and Structures 9 (1998) 404-416.

[9] T. Wu, J. Huang, Closed-form solutions for the magneto-electric coupling coefficients in fibrous composites with piezoelectric and piezomagnetic phases, International Journal of Solids and Structures 37 (2000) 2981-3009.

[10] J. Huang, H. Liu, W. Dai, The optimized fiber volume fraction for magneto-electric coupling effect in piezoelectric-piezomagnetic continuous fiber reinfored composites, International Journal of Engineering Science 38 (2000) 1207-1217.

[11] J. Li, Magnetoelectroelastic multi-inclusion and inhomogeneity problems and their applications in composite materials International Journal of Engineering Science 38 (2000) 1993-2011.

[12] J. Aboudi, Micromechanical analysis of fully coupled electro-magneto-thermo-elastic multiphase composites, Smart Materials and Structures 10 (2001) 867-877.

[13] J. Boyd, C. Lagoudas, Arrays of micro-electrodes and electromagnets for proceeding of electro-magneto-elastic multifunctional composite materials, SPIE 10th Annual International Symposium on Smart Structures held at San Diego, CA March 2-6, Vol. 5055, 2005, pp. 268–277.

[14] J. Lee, J. Boyd, D. Lagoudas, Effective properties of three-phase electro-magneto-elastic composites, International Journal of Engineering Science 43 (10) (2005) 790-825.

[15] V. L. Berdichevsky, On Averaging of Periodic Systems, PMM 41 (6) (1977) 993-1006.

[16] W. Yu, T. Tang, Variational Asymptotic Method for Unit Cell Homogenization of Periodically Heterogeneous Materials, International Journal of Solids and Structures 44 (2007) 3738-3755.

[17] W. Yu, T. Tang, A Variational Asymptotic Micromechanics Model for Predicting Thermoelastic Properties of Heterogeneous Materials, International Journal of Solids and Structures 44 (22-23) (2007) 7510-7525.

[18] T. Tang, W. Yu, A Variational Asymptotic Micromechanics Model for Predicting Conductivity of Composite Materials, Journal of Mechanics of Materials and Structures 2 (9) (2007) 1813-1830.

[19] T. Tang, W. Yu, A Variational Asymptotic Model for Predicting Initial Yielding Surface and Elastoplastic Behavior of Metal Matrix Composite Materials, Proceedings of the 2007 ASME International Mechanical Engineering Congress and Exposition, ASME, Seattle, Washington, 2007. November 10-16.

[20] A. Soh, J. Liu, On the constitutive equations of magnetoelectroelastic solids, Journal of Intelligent Material Systems and Structures 16 (2005) 597-602.

[21] I. Kunin, Theory of Elastic Media with Microstructure, vols. 1-2, Springer Verlag, 1982.

Chapter 4

Variational Asymptotic Micromechanics Modeling of Heterogeneous Piezoelectric Materials

[1]

This chapter is a journal paper published in the *Mechanics of Materials*, Vol. 40, 2008, pp. 812-824.

Abstract

In this paper, a new micromechanics model is developed to predict the effective properties and local fields of heterogeneous piezoelectric materials using the variational asymptotic method for unit cell homogenization (VAMUCH), a recently developed micromechanics modeling technique. Starting from the total electric enthalpy of the heterogenous continuum, we formulate the micromechanics model as a constrained minimization problem using the variational asymptotic method. To handle realistic microstructures in engineering applications, we implement this new model using the finite element method. For validation, a few examples are used to demonstrate the application and accuracy of this theory and the companion computer program–VAMUCH.

4.1 Introduction

Piezoelectric materials such as PZT (Lead, Zirconium, Titanate) are widely used in sensors and actuators due to their property of converting electric energy into mechanical energy, and vice versa. However, bulk piezoelectric materials have several drawbacks for instance their weight, disadvantage of shape control, and acoustic impedance, therefore composite piezoelectric materials are usually a better technical solution in the case of many applications such as ultrasonic imaging, sensors, actuators and damping. Recently, piezoelectric composites are developed by combining piezoelectric materials with passive

[1] Coauthored by: Tian Tang and Wenbin Yu.

materials to form a variety of types of piezoelectric composite systems. To facilitate the design of these piezoelectric composites, convenient and accurate analysis tools are apparently indispensable.

In the past several decades, numerous approaches have been proposed to predict the effective properties of piezoelectric composites from known constituent information. Simple analytical approaches based on Voigt or Reuss hypothesis have been applied to predict the behavior of a limited class of composite geometries (Newnham et al., 1978; Banno, 1983; Chan and Unsworth, 1989; Smith and Auld, 1991). Variational bounds have been obtained for describing the complete overall behavior which are useful tools for theoretical consideration (Bisegna and Luciano, 1996, 1997; Li and Dunn, 2001). However the range between bounds can be very large for certain effective properties. Eshelby's solutions (Eshelby, 1957) have been extended to include piezoelectric constituents (Wang, 1992; Benveniste, 1992; Dunn and Taya, 1993b; Chen, 1993). Such mean field-type methods are capable of predicting the entire behavior under arbitrary loads. However, they use averaged representations of the electric and mechanical field within the constituents of the composite, i.e., they do not account for the local fluctuations of the field quantities. This restriction can be overcome by a finite element method-based micromechanical analysis (Gaudenzi, 1997; Poizat and Sester, 1999). In such models the representative unit cell and the boundary conditions are designed to capture a few special load cases which are connected to specific deformation patterns. This allows the prediction of only a few key material parameters. The finite element unit cell models which can capture the entire behavior have recently appeared (Lenglet et al., 2003; Sun et al., 2001; Pettermann and Suresh, 2000; Li, 2000; Pastor, 1997; Berger et al., 2006). Other studies (Dunn and Taya, 1993a, 1994; Huang and Kuo, 1996; Fakri et al., 2003) have focused on the classical extensions of Eshelby's solution for finite inclusion volume fractions, i.e., the Mori-Tanaka (Mori and Tanaka, 1973; Benveniste, 1987) self-consistent approach (Hill, 1965; Budiansky, 1965), differential approaches (McLaughlin, 1977; Norris, 1985), and models based on the generalized Mori-Tanako and the self-consistent approaches (Odegard, 2004).

In this paper, a novel micromechanics model based on the framework of variational asymptotic method for unit cell homogenization (VAMUCH) has been developed to predict the effective properties and local fields of piezoelectric composites. This model invokes two essential assumptions within the concept of micromechanics for composites with an

identifiable unit cell (UC):

- **Assumption 1** The exact field variables have volume average over the UC. For example, if u_i and ϕ are respectively the exact displacements and electric potential within the UC, there exist v_i and ψ such that

$$v_i = \frac{1}{\Omega}\int_\Omega u_i \, \mathrm{d}\Omega \equiv \langle u_i \rangle \tag{4.1}$$

$$\psi = \frac{1}{\Omega}\int_\Omega \phi \, \mathrm{d}\Omega \equiv \langle \phi \rangle \tag{4.2}$$

  where Ω denotes the domain occupied by the UC and its volume.

- **Assumption 2** The effective material properties obtained from the micromechanical analysis of the UC are independent of the geometry, the boundary conditions, and loading conditions of the macroscopic structure, which means that effective properties are assumed to be the intrinsic properties of the material when viewed macroscopically.

Note that these assumptions are not restrictive. The mathematical meaning of the first assumption is that the exact solutions of the field variables can be integrated over the domain of UC, which is true almost all the time. The second assumption implies that we will neglect the size effects of the material properties in the macroscopic analysis, which is an assumption often made in the conventional continuum mechanics. Of course, the micromechanical analysis of the UC is only needed and appropriate if $\eta = h/l \ll 1$, with h as the characteristic size of the UC and l as the characteristic wavelength of the deformation of the structure. Other assumptions such as particular geometry shape and arrangement of the constituents, specific boundary conditions applied to the UC, and prescribed relations between local fields and global fields are not necessary for the present study.

This new micromechanical modeling approach has been successfully used to predict the effective thermoelastic properties including elastic constants, specific heats, and coefficients of thermal expansions, and effective thermal conductivity and associated local fields (Yu and Tang, 2007a,b; Tang and Yu, 2007a). It is also applied to accurately predict the initial yielding surface and elastoplastic behavior of metal matrix composites (Tang and Yu, 2007b).

4.2 Piezoelectricity and Piezoelectric Composites

The elastic and the dielectric responses are coupled in piezoelectric materials where the mechanical variables of stress, and strain are related to each other as well as to the electric variables of electric field and electric displacement. The coupling between mechanical and electric fields is described by piezoelectric coefficients. Using the conventional indicial notation, the linear coupled constitutive equations are expressed as:

$$\begin{aligned} \sigma_{ij} &= C_{ijkl}\epsilon_{kl} - e_{ijk}E_k \\ T_i &= e_{ikl}\epsilon_{kl} + k_{ij}E_j \end{aligned} \tag{4.3}$$

where σ_{ij}, ϵ_{ij}, E_i and T_i are the stress tensor, strain tensor, electric field vector, and the electric displacement vector, respectively. C_{ijkl} denotes fourth-order elasticity tensor at constant electric field, k_{ij} is the second-order dielectric tensor at constant strain field, e_{ijk} is the third-order piezoelectric coupling tensor. To avoid the difficulty associated with heterogeneity, we can use the micromechanics approach to homogenize the material and obtain an effective constitutive model, such that

$$\begin{aligned} \bar{\sigma}_{ij} &= C^*_{ijkl}\bar{\epsilon}_{kl} - e^*_{ijk}\bar{E}_k \\ \bar{T}_i &= e^*_{ijk}\bar{\epsilon}_{kl} + k^*_{ij}\bar{E}_j \end{aligned} \tag{4.4}$$

where "over-bar" means variables which are used in the macroscopic analysis of homogenized materials, and superscripts "*" denote the effective properties whose calculation are determined by the micromechanics model one employs.

4.3 Theoretical Formulation

VAMUCH formulation uses three coordinates systems: two cartesian coordinates $\mathbf{x} = (x_1, x_2, x_3)$ and $\mathbf{y} = (y_1, y_2, y_3)$, and an integer-valued coordinate $\mathbf{n} = (n_1, n_2, n_3)$ (see Fig. 4.1). We use x_i as the global coordinates to describe the macroscopic structure and y_i parallel to x_i as the local coordinates to describe the UC (Here and throughout the paper, Latin indices assume 1, 2, and 3 and repeated indices are summed over their range except where explicitly indicated). We choose the origin of the local coordinates y_i to be

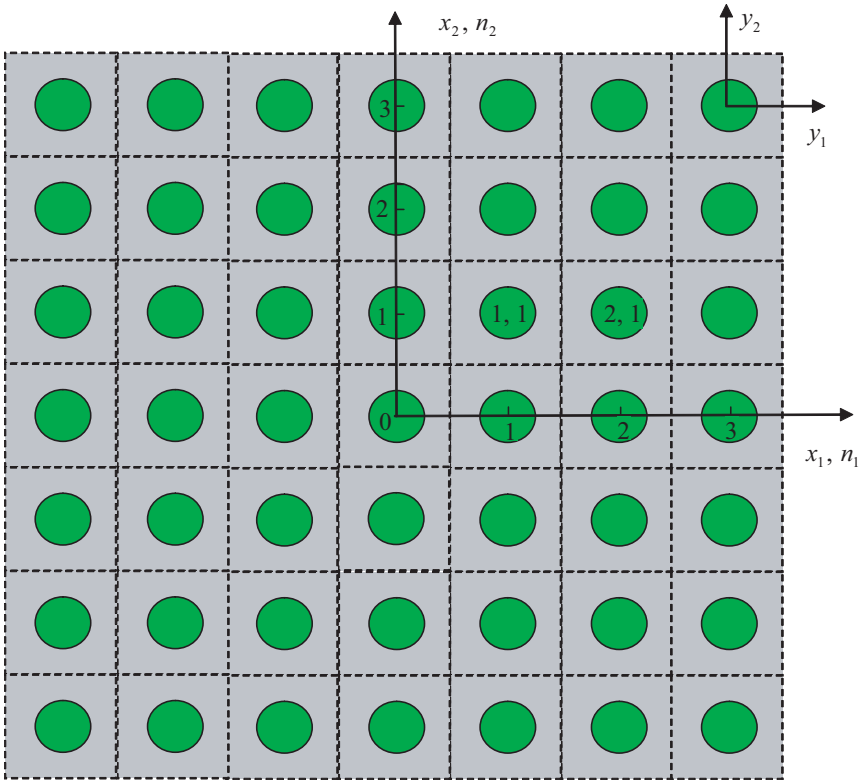

Fig. 4.1: Coordinate systems for heterogenous materials (only two-dimensional (2D) UC is drawn for clarity).

the geometric center of UC. For example, if the UC is a cube with dimensions as d_i, then $y_i \in [-\frac{d_i}{2}, \frac{d_i}{2}]$. To uniquely locate a UC in the heterogeneous material we also introduce integer coordinates n_i. The integer coordinates are related to the global coordinates in such a way that $n_i = x_i/d_i$ (no summation over i). It is emphasized although only square array is sketched in Fig. 4.1, the present theory has no such limitations.

As implied by Assumption 2, we can obtain the same effective properties from an imaginary, unbounded, and unloaded heterogeneous material with the same microstrucutre as the real, loaded, and bounded one. Hence we could derive the micromechanics model from an imaginary, unloaded, heterogeneous material which completely occupies the three-dimensional (3D) space $\mathcal{R}$ and composes of infinite many repeating UCs. For piezoelectric composites, the total electric enthalpy is equal to the summation of the electric enthalpy stored in all the UCs, which is

$$\Pi = \sum_{n=-\infty}^{\infty} \int_{\Omega} 2H \mathrm{d}\Omega \tag{4.5}$$

where $2H$ is twice the electric enthalpy, given by

$$2H = \epsilon^T D \epsilon \tag{4.6}$$

where

$$\epsilon = \lfloor \epsilon_{11} \;\; 2\epsilon_{12} \;\; \epsilon_{22} \;\; 2\epsilon_{13} \;\; 2\epsilon_{23} \;\; \epsilon_{33} \;\; E_1 \;\; E_2 \;\; E_3 \rfloor^T \tag{4.7}$$

containing both the 3D strain field ϵ_{ij} and the 3D electric field E_i, which are defined for a linear theory as:

$$\epsilon_{ij}(\mathbf{n};\mathbf{y}) = \frac{1}{2}\left[\frac{\partial u_i(\mathbf{n};\mathbf{y})}{\partial y_j} + \frac{\partial u_j(\mathbf{n};\mathbf{y})}{\partial y_i}\right] \tag{4.8}$$

$$E_i(\mathbf{n};\mathbf{y}) = -\frac{\partial \phi(\mathbf{n};\mathbf{y})}{\partial y_i} \tag{4.9}$$

and D is a 9×9 matrix including the elastic, piezoelectric, and dielectric properties and is expressed as

$$D = \begin{bmatrix} \boldsymbol{C} & -\boldsymbol{e} \\ -\boldsymbol{e}^T & -\boldsymbol{k} \end{bmatrix} \tag{4.10}$$

In view of the fact that the infinite many UCs form a continuous heterogenous material, we need to enforce the continuity of the displacement field u_i and the electric potential field ϕ on the interface between adjacent UCs, which are:

$$\begin{aligned} u_i(n_1, n_2, n_3; d_1/2, y_2, y_3) &= u_i(n_1+1, n_2, n_3; -d_1/2, y_2, y_3) \\ u_i(n_1, n_2, n_3; y_1, d_2/2, y_3) &= u_i(n_1, n_2+1, n_3; y_1, -d_2/2, y_3) \\ u_i(n_1, n_2, n_3; y_1, y_2, d_3/2) &= u_i(n_1, n_2, n_3+1; y_1, y_2, -d_3/2) \end{aligned} \tag{4.11}$$

$$\begin{aligned} \phi(n_1, n_2, n_3; d_1/2, y_2, y_3) &= \phi(n_1+1, n_2, n_3; -d_1/2, y_2, y_3) \\ \phi(n_1, n_2, n_3; y_1, d_2/2, y_3) &= \phi(n_1, n_2+1, n_3; y_1, -d_2/2, y_3) \\ \phi(n_1, n_2, n_3; y_1, y_2, d_3/2) &= \phi(n_1, n_2, n_3+1; y_1, y_2, -d_3/2) \end{aligned} \tag{4.12}$$

The exact solution of the present problem will minimize the summation of electric enthalpy in Eq. (4.5) under the constraints in Eqs. (4.1), Eqs. (4.2), (4.11), and (4.12). Due to discrete integer arguments, the problem is very difficult to solve. To avoid the difficulty associated with discrete integer arguments, we can reformulate the problem, including Eqs. (4.5), (4.8),

(4.9), (4.11) and (4.12), in terms of continuous functions using the idea of quasicontinuum (Kunin, 1982). The corresponding formulas are listed below.

$$\Pi = \int_{\mathcal{R}} \left\langle \epsilon^T D \epsilon \right\rangle \mathrm{d}\mathcal{R} \tag{4.13}$$

$$\epsilon_{ij}(\mathbf{x};\mathbf{y}) = \frac{1}{2}\left[\frac{\partial u_i(\mathbf{x};\mathbf{y})}{\partial y_j} + \frac{\partial u_j(\mathbf{x};\mathbf{y})}{\partial y_i}\right] \equiv u_{(i|j)} \tag{4.14}$$

$$E_i(\mathbf{x};\mathbf{y}) = -\frac{\partial \phi(\mathbf{x};\mathbf{y})}{\partial y_i} \tag{4.15}$$

and

$$\begin{aligned} u_i(x_1,x_2,x_3;d_1/2,y_2,y_3) &= u_i(x_1+d_1,x_2,x_3;-d_1/2,y_2,y_3) \\ u_i(x_1,x_2,x_3;y_1,d_2/2,y_3) &= u_i(x_1,x_2+d_2,x_3;y_1,-d_2/2,y_3) \\ u_i(x_1,x_2,x_3;y_1,y_2,d_3/2) &= u_i(x_1,x_2,x_3+d_3;y_1,y_2,-d_3/2) \end{aligned} \tag{4.16}$$

$$\begin{aligned} \phi(x_1,x_2,x_3;d_1/2,y_2,y_3) &= \phi(x_1+d_1,x_2,x_3;-d_1/2,y_2,y_3) \\ \phi(x_1,x_2,x_3;y_1,d_2/2,y_3) &= \phi(x_1,x_2+d_2,x_3;y_1,-d_2/2,y_3) \\ \phi(x_1,x_2,x_3;y_1,y_2,d_3/2) &= \phi(x_1,x_2,x_3+d_3;y_1,y_2,-d_3/2) \end{aligned} \tag{4.17}$$

Introducing Lagrange multipliers, we can pose the variational statement of the micromechanical analysis of UC as a stationary value problem of the following functional:

$$\begin{aligned} J = \int_{\mathcal{R}} \Big\{ & \left\langle \epsilon^T D \epsilon \right\rangle + \lambda_i(\langle u_i \rangle - v_i) + \lambda(\langle \phi \rangle - \psi) \\ & + \int_{S_1} \gamma_{i1} \left[u_i(x_j; d_1/2, y_2, y_3) - u_i(x_j + d_1; -d_1/2, y_2, y_3) \right] \mathrm{d}S_1 \\ & + \int_{S_2} \gamma_{i2} \left[u_i(x_j; y_1, d_2/2, y_3) - u_i(x_j + d_2; y_1, -d_2/2, y_3) \right] \mathrm{d}S_2 \\ & + \int_{S_3} \gamma_{i3} \left[u_i(x_j; y_1, y_2, d_3/2) - u_i(x_j + d_3; y_1, y_2, -d_3/2) \right] \mathrm{d}S_3 \\ & + \int_{S_1} \beta_1 \left[\phi(x_j; d_1/2, y_2, y_3) - \phi(x_j + d_1; -d_1/2, y_2, y_3) \right] \mathrm{d}S_1 \\ & + \int_{S_2} \beta_2 \left[\phi(x_j; y_1, d_2/2, y_3) - \phi(x_j + d_2; y_1, -d_2/2, y_3) \right] \mathrm{d}S_2 \\ & + \int_{S_3} \beta_3 \left[\phi(x_j; y_1, y_2, d_3/2) - \phi(x_j + d_3; y_1, y_2, -d_3/2) \right] \mathrm{d}S_3 \Big\} \mathrm{d}\mathcal{R} \end{aligned} \tag{4.18}$$

where λ_i, λ, γ_{ij}, and β_i are Lagrange multipliers introduced to enforce the constraints in Eqs. (4.1), (4.2), (4.16) and (4.17), respectively, S_i are the surfaces with $n_i = 1$, x_j represents the triplet of x_1, x_2, x_3, and δ_{ij} is the Kronecker delta. Following the general procedure of VAMUCH, we can obtain the following change of variables for u_i and ϕ:

$$u_i(\mathbf{x}; \mathbf{y}) = v_i(\mathbf{x}) + y_j \frac{\partial v_i}{\partial x_j} + \chi_i(\mathbf{x}; \mathbf{y}) \tag{4.19}$$

$$\phi(\mathbf{x}; \mathbf{y}) = \psi(\mathbf{x}) + y_i \frac{\partial \psi}{\partial x_i} + \zeta(\mathbf{x}; \mathbf{y}) \tag{4.20}$$

where χ_i and ζ are the fluctuation functions, satisfying the following constraints in view of Eqs. (4.1), (4.19), and Eqs. (4.2), (4.20) when the origin of the local coordinate system is chosen to be the center of UC:

$$\langle \chi_i \rangle = 0 \tag{4.21}$$

$$\langle \zeta \rangle = 0 \tag{4.22}$$

Substituting Eqs. (4.19) and (4.20) into Eq. (4.18), we obtain a stationary value problem defined over UC for χ_i and ζ according to the variational asymptotic method (Berdichevsky,

1977), such that:

$$J_\Omega = \left\langle \epsilon^T D \epsilon \right\rangle + \lambda_i \left\langle \chi_i \right\rangle + \lambda \left\langle \zeta \right\rangle + \sum_{j=1}^{3} \int_{S_j} \gamma_{ij} (\chi_i^{+j} - \chi_i^{-j}) \mathrm{d}S_j + \sum_{j=1}^{3} \int_{S_j} \beta_j (\zeta^{+j} - \zeta^{-j}) \mathrm{d}S_j \tag{4.23}$$

with

$$\chi_i^{+j} = \chi_i|_{y_j = d_j/2},\ \chi_i^{-j} = \chi_i|_{y_j = -d_j/2} \quad \text{for} \quad j = 1, 2, 3$$

$$\zeta^{+j} = \zeta|_{y_j = d_j/2},\ \zeta^{-j} = \zeta|_{y_j = -d_j/2} \quad \text{for} \quad j = 1, 2, 3$$

Matrix ϵ can be expressed as

$$\epsilon = \bar{\epsilon} + \epsilon_1 \tag{4.24}$$

with

$$\bar{\epsilon} = \lfloor \frac{\partial v_1}{\partial x_1}, \frac{\partial v_1}{\partial x_2} + \frac{\partial v_2}{\partial x_1}, \frac{\partial v_2}{\partial x_2}, \frac{\partial v_1}{\partial x_3} + \frac{\partial v_3}{\partial x_1}, \frac{\partial v_2}{\partial x_3} + \frac{\partial v_3}{\partial x_2}, \frac{\partial v_3}{\partial x_3}, -\frac{\partial \psi}{\partial x_1} \ -\frac{\partial \psi}{\partial x_2}, -\frac{\partial \psi}{\partial x_3} \rfloor^T \tag{4.25}$$

which will be shown later to be the global variables containing both the strain field and the electric field for the material with homogenized effective material properties, and

$$\epsilon_1 = \lfloor \frac{\partial \chi_1}{\partial y_1}, \frac{\partial \chi_1}{\partial y_2} + \frac{\partial \chi_2}{\partial y_1}, \frac{\partial \chi_2}{\partial y_2}, \frac{\partial \chi_1}{\partial y_3} + \frac{\partial \chi_3}{\partial y_1}, \frac{\partial \chi_2}{\partial y_3} + \frac{\partial \chi_3}{\partial y_2}, \frac{\partial \chi_3}{\partial y_3}, -\frac{\partial \zeta}{\partial y_1}, -\frac{\partial \zeta}{\partial y_2}, -\frac{\partial \zeta}{\partial y_3} \rfloor^T \tag{4.26}$$

The functional J_Ω in Eq. (4.23) forms the backbone of the present theory. This variational statement can be solved analytically for very simple cases such as binary composites, however, for general cases we need to use numerical techniques such as the finite element method (FEM) to seek numerical solutions.

4.4 Finite Element Implementation

It is possible to formulate the FEM solution based on Eq. (4.23), however, it is not the most convenient and efficient way because Lagrange multipliers will increase the number of unknowns. To this end, we can reformulate the variational statement in Eq. (4.23) as the minimum value of the following functional

$$\Pi_\Omega = \frac{1}{\Omega} \int_\Omega \epsilon^T D \epsilon \mathrm{d}\Omega \tag{4.27}$$

under the following constraints

$$\chi_i^{+j} = \chi_i^{-j} \quad \text{and} \quad \zeta^{+j} = \zeta^{-j} \quad \text{for} \quad j = 1, 2, 3 \tag{4.28}$$

The constraint in Eqs. (4.21) and (4.22) does not affect the minimum values of Π_Ω but help uniquely determine χ_i and ζ. In practice, we can constrain the fluctuation function at an arbitrary node to be zero and later use this constraint to recover the unique fluctuation function. It is fine to use penalty function method to introduce the constraints in Eqs. (4.28). However, this method introduces additional approximation and the robustness of the solution depends on the choice of large penalty numbers. Here, we make the nodes on the positive boundary surface (*i.e.*, $y_i = d_i/2$) slave to the nodes on the opposite negative boundary surface (*i.e.*, $y_i = -d_i/2$). By assembling all the independent active degrees of freedom (DOFs), we can implicitly and exactly incorporate the constraints in Eqs. (4.28).

Introduce the following matrix notation

$$\epsilon_1 = \begin{bmatrix} \frac{\partial}{\partial y_1} & 0 & 0 & 0 \\ \frac{\partial}{\partial y_2} & \frac{\partial}{\partial y_1} & 0 & 0 \\ 0 & \frac{\partial}{\partial y_2} & 0 & 0 \\ \frac{\partial}{\partial y_3} & 0 & \frac{\partial}{\partial y_1} & 0 \\ 0 & \frac{\partial}{\partial y_3} & \frac{\partial}{\partial y_2} & 0 \\ 0 & 0 & \frac{\partial}{\partial y_3} & 0 \\ 0 & 0 & 0 & -\frac{\partial}{\partial y_1} \\ 0 & 0 & 0 & -\frac{\partial}{\partial y_2} \\ 0 & 0 & 0 & -\frac{\partial}{\partial y_3} \end{bmatrix} \begin{Bmatrix} \chi_1 \\ \chi_2 \\ \chi_3 \\ \zeta \end{Bmatrix} \equiv \Gamma_h \chi \tag{4.29}$$

where Γ_h is an operator matrix. If we discretize χ using the finite elements as

$$\chi(x_i; y_i) = S(y_i)\mathcal{X}(x_i) \tag{4.30}$$

where S representing the shape functions and $\mathcal{X}$ a column matrix of the nodal values of both the mechanical and electric fluctuation functions. Substituting Eqs. (4.29) and (4.30)

into Eq. (4.27), we obtain a discretized version of the functional as

$$\Pi_\Omega = \frac{1}{\Omega}(\mathcal{X}^T E \mathcal{X} + 2\mathcal{X}^T D_{h\epsilon}\bar{\epsilon} + \bar{\epsilon}^T D_{\epsilon\epsilon}\bar{\epsilon}) \tag{4.31}$$

where

$$E = \int_\Omega (\Gamma_h S)^T D(\Gamma_h S)\mathrm{d}\Omega \qquad D_{h\epsilon} = \int_\Omega (\Gamma_h S)^T D\mathrm{d}\Omega \qquad D_{\epsilon\epsilon} = \int_\Omega D\mathrm{d}\Omega \tag{4.32}$$

Minimizing Π_Ω in Eq. (4.31), we obtain the following linear system

$$E\mathcal{X} = -D_{h\epsilon}\bar{\epsilon} \tag{4.33}$$

It is clear from Eq. (4.33) that the fluctuation function $\mathcal{X}$ is linearly proportional to $\bar{\epsilon}$, which means the solution can be written symbolically as

$$\mathcal{X} = \mathcal{X}_0\bar{\epsilon} \tag{4.34}$$

Substituting Eq. (4.34) into Eq. (4.31), we can calculate the electric enthalpy of the UC as

$$\Pi_\Omega = \frac{1}{\Omega}\bar{\epsilon}^T \left(\mathcal{X}_0^T D_{h\epsilon} + D_{\epsilon\epsilon}\right)\bar{\epsilon} \equiv \bar{\epsilon}^T \bar{D}\bar{\epsilon} \tag{4.35}$$

It can be seen that $\bar{D}$ in Eq. (4.35) is the effective piezoelectric material properties which can be expressed using a 9×9 matrix as

$$\bar{D} = \begin{bmatrix} \boldsymbol{C}^* & -\boldsymbol{e}^* \\ -\boldsymbol{e}^{*T} & -\boldsymbol{k}^* \end{bmatrix} \tag{4.36}$$

and $\bar{\epsilon}$ is a column matrix containing both the global strains and global electric fields.

If the local fields within UC are of interest, the present VAMUCH can recover those fields, such as local displacements, electric potential, stresses, and electric displacements, in terms of the macroscopic behavior including the global displacements v_i, the global electric potential ψ, the global strain and electric field $\bar{\epsilon}$, and the fluctuation function χ. First, we need to uniquely determine the fluctuation functions. Considering the fact that we fixed an arbitrary node and made nodes on the positive boundary surfaces slave to the

corresponding negative boundary surfaces, we need to construct a new array $\tilde{\mathcal{X}}_0$ from $\mathcal{X}_0$ by assigning the values for slave nodes according to the corresponding active nodes and assign zero to the fixed node. Obviously, $\tilde{\mathcal{X}}_0$ still yield the minimum value of Π_Ω in Eq. (4.27) under constrains in Eqs. (4.28). However, $\tilde{\mathcal{X}}_0$ may not satisfy Eqs. (4.21) and (4.22). The real solution, denoted as $\bar{\mathcal{X}}_0$ can be found trivially by adding a constant corresponding to each DOF to each node so that Eqs. (4.21) and (4.22) are satisfied.

After having determined the fluctuation functions uniquely, we can recover the local displacements and electric potential using Eqs. (4.19) and (4.20) as

$$\begin{Bmatrix} u_1 \\ u_2 \\ u_3 \\ \phi \end{Bmatrix} = \begin{Bmatrix} v_1 \\ v_2 \\ v_3 \\ \psi \end{Bmatrix} + \begin{bmatrix} \frac{\partial v_1}{\partial x_1} & \frac{\partial v_1}{\partial x_2} & \frac{\partial v_1}{\partial x_3} \\ \frac{\partial v_2}{\partial x_1} & \frac{\partial v_2}{\partial x_2} & \frac{\partial v_2}{\partial x_3} \\ \frac{\partial v_3}{\partial x_1} & \frac{\partial v_3}{\partial x_2} & \frac{\partial v_3}{\partial x_3} \\ \frac{\partial \psi}{\partial x_1} & \frac{\partial \psi}{\partial x_2} & \frac{\partial \psi}{\partial x_3} \end{bmatrix} \begin{Bmatrix} y_1 \\ y_2 \\ y_3 \end{Bmatrix} + \bar{S}\bar{\mathcal{X}} \tag{4.37}$$

Here $\bar{S}$ is different from S due to the recovery of slave nodes and the constrained node. The local strain field and electric field can be recovered using Eqs. (4.14), (4.15), (4.19), (4.20) and (4.29) as

$$\epsilon = \bar{\epsilon} + \Gamma_h \bar{S}\bar{\mathcal{X}} \tag{4.38}$$

Finally, the local stress and electric displacement field can be recovered straightforwardly using the 3D constitutive relations for the constituent material as

$$\sigma = D\epsilon \tag{4.39}$$

with σ as a column matrix containing both 3D stresses and electric displacements such that

$$\sigma = \lfloor \sigma_{11}, \sigma_{12}, \sigma_{22}, \sigma_{13}, \sigma_{23}, \sigma_{33}, -T_1, -T_2, -T_3 \rfloor^T \tag{4.40}$$

We have implemented this formulation in the computer program VAMUCH. To demonstrate the application, accuracy, and efficiency of this theory and the companion code, we will analyze several examples using VAMUCH in the next section.

4.5 Numerical Examples

VAMUCH provides a unified analysis for general 1D, 2D, or 3D UCs. First, the same

Table 4.1: Material properties of the composite constituents (PZT-7A, Epoxy, SiC, LaRC-SI, and PVDF)

	PZT-7A	Epoxy	SiC	LaRC-SI	PVDF
C_{11}	131.39	8.0	483.7	8.1	1.2
C_{12}	82.712	4.4	99.1	5.4	1.0
C_{23}	83.237	4.4	99.1	5.4	1.9
C_{22}	154.837	8.0	483.7	8.1	3.8
C_{44}	35.8	1.8	192.3	1.4	0.7
C_{55}	25.696	1.8	192.3	1.4	0.9
C_{66}	25.696	1.8	192.3	1.4	0.9
e_{11}	9.52183	–	–	–	-0.027
e_{21}	-2.12058	–	–	–	0.024
e_{31}	-2.12058	–	–	–	0.001
e_{51}	9.34959	–	–	–	0.000
k_{11}	2.079	0.0372	0.085	0.025	0.067
k_{22}	4.065	0.0372	0.085	0.025	0.065
k_{33}	4.065	0.0372	0.085	0.025	0.082

code VAMUCH can be used to homogenize binary composites (modeled using 1D UCs), fiber reinforced composites (modeled using 2D UCs), and particle reinforced composites (modeled using 3D UCs). Second, VAMUCH can reproduce the results for lower-dimensional UCs using higher-dimensional UCs. That is, VAMUCH predicts the same results for binary composites using 1D, 2D, or 3D UCs, and for fiber reinforced composites using 2D or 3D UCs.

In this section, several examples will be used to demonstrate the accuracy of VAMUCH for predicting the effective properties and calculating the local stress and electric displacement fields within UC.

4.5.1 Predict Effective Properties of Composites

At first the piezoelectric composite considered is composed of piezoceramic (PZT) fibers embedded in soft non-piezoelectric materials (epoxy) in which the fibers are of circular shape. The epoxy matrix is isotropic while the fibers are transversely isotropic. The material properties of both constituents are taken from (Pettermann and Suresh, 2000) and shown in Table 4.1. The units of the elastic constants, piezoelectric constants, and dielectric constants are given in GPa, Cm^{-2}, and $nCV^{-1}m^{-1}$, respectively. For transversely isotropic piezoelectric materials, there are 11 independent coefficients remained in the total material

matrix and the matrix form of constitutive equation can be written as

$$\begin{Bmatrix} \sigma_{11} \\ \sigma_{12} \\ \sigma_{22} \\ \sigma_{13} \\ \sigma_{23} \\ \sigma_{33} \\ -T_1 \\ -T_2 \\ -T_3 \end{Bmatrix} = \begin{bmatrix} C_{11} & 0 & C_{12} & 0 & 0 & C_{12} & -e_{11} & 0 & 0 \\ 0 & C_{66} & 0 & 0 & 0 & 0 & 0 & -e_{51} & 0 \\ C_{12} & 0 & C_{22} & 0 & 0 & C_{23} & -e_{21} & 0 & 0 \\ 0 & 0 & 0 & C_{55} & 0 & 0 & 0 & 0 & -e_{51} \\ 0 & 0 & 0 & 0 & C_{44} & 0 & 0 & 0 & 0 \\ C_{12} & 0 & C_{23} & 0 & 0 & C_{22} & -e_{21} & 0 & 0 \\ -e_{11} & 0 & -e_{21} & 0 & 0 & -e_{21} & -k_{11} & 0 & 0 \\ 0 & -e_{51} & 0 & 0 & 0 & 0 & 0 & -k_{22} & 0 \\ 0 & 0 & 0 & -e_{51} & 0 & 0 & 0 & 0 & -k_{22} \end{bmatrix} \begin{Bmatrix} \epsilon_{11} \\ \epsilon_{12} \\ \epsilon_{22} \\ \epsilon_{13} \\ \epsilon_{23} \\ \epsilon_{33} \\ E_1 \\ E_2 \\ E_3 \end{Bmatrix} \tag{4.41}$$

All effective coefficients were calculated for the volume fraction of fibers in a range between 0.1 and 0.7 using VAMUCH and ANSYS, a commercial finite element package capable of multiphysics simulation. The constituents of unit cell were meshed using three-dimensional 8-node brick elements with three displacement DOFs and an additional electric potential DOF when using ANSYS. The ANSYS FEM model was set up following the procedure described in Berger et al. (2006). The results of different approaches were evaluated for composites with periodic square (SQU) or periodic hexagonal (HEX) piezoelectric fiber arrangements. The effective coefficients of composites are shown in Figs. 4.2, 4.3, 4.4, 4.5, and 4.6. We found out that the predictions of all effective coefficients from VAMUCH have excellent agreement with those using ANSYS following Berger et al. (2006).

To provide a more extensive validation for VAMUCH, we considered a composite body reinforced by parallel square fibers with a square arrangement, which is the same example as in Bisegna and Luciano (1997). The matrix and the fibers are isotropic epoxy polymer and piezoelectric ceramic PZT-7A, respectively. The volume fraction of fibers is 60%. To facilitate the comparison, the effective coefficients calculated by VAMUCH are transformed

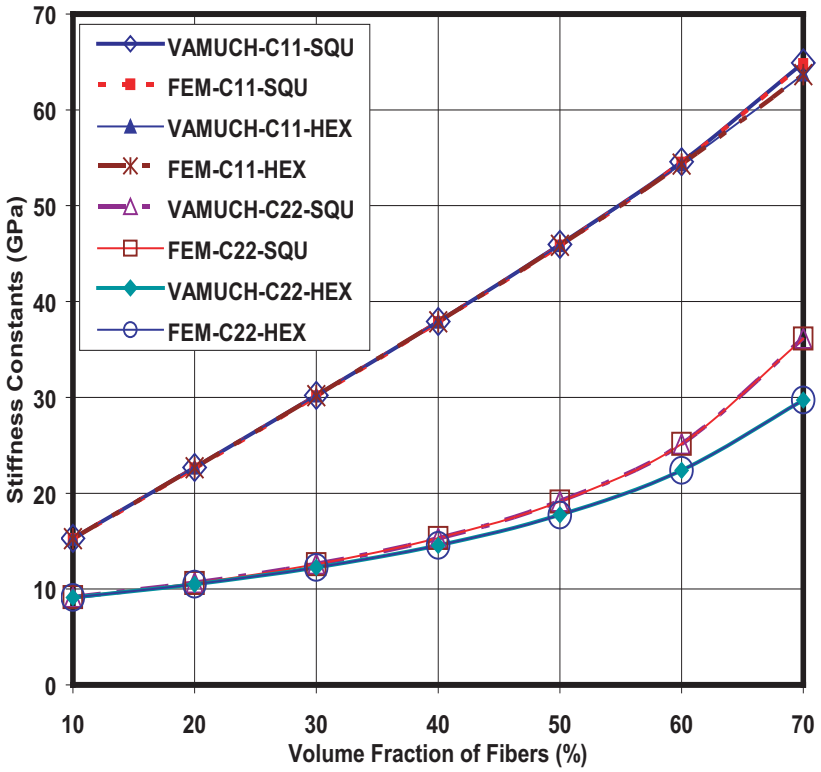

Fig. 4.2: Effective stiffness constants C_{11} and C_{22}

according to the following formulas as listed in Berger et al. (2006):

$$
\begin{aligned}
\beta_{11}^{\text{eff}} &= 1/\epsilon_{11}^{\text{eff}} & \beta_{22}^{\text{eff}} &= 1/\epsilon_{22}^{\text{eff}} \\
C_{11}^{\text{effD}} &= C_{11}^{\text{eff}} + (e_{11}^{\text{eff}})^2 \beta_{11}^{\text{eff}} & C_{12}^{\text{effD}} &= C_{12}^{\text{eff}} + e_{21}^{\text{eff}} e_{11}^{\text{eff}} \beta_{11}^{\text{eff}} \\
C_{22}^{\text{effD}} &= C_{22}^{\text{eff}} + (e_{21}^{\text{eff}})^2 \beta_{11}^{\text{eff}} & C_{23}^{\text{effD}} &= C_{23}^{\text{eff}} + (e_{21}^{\text{eff}})^2 \beta_{11}^{\text{eff}} \\
C_{44}^{\text{effD}} &= C_{44}^{\text{eff}} & C_{55}^{\text{effD}} &= C_{55}^{\text{eff}} + (e_{51}^{\text{eff}})^2 \beta_{11}^{\text{eff}} \\
h_{11}^{\text{effD}} &= e_{11}^{\text{eff}} \beta_{11}^{\text{eff}} & h_{21}^{\text{effD}} &= e_{21}^{\text{eff}} \beta_{11}^{\text{eff}} \\
h_{51}^{\text{effD}} &= e_{51}^{\text{eff}} \beta_{22}^{\text{eff}} &&
\end{aligned}
\tag{4.42}
$$

In Table 4.2, VAMUCH results are compared with ANSYS following the micromechanical analysis of Berger et al. (2006) (denoted as Berger), the results in Pettermann and Suresh (2000) (denoted as Pettermann), Bisegna-Luciano bounds in Bisegna and Luciano (1997) (denoted as BL), and Hashin-Shtrikman bounds for piezoelectric materials derived in Bisegna and Luciano (1997) (denoted as HS). From Table 4.2 one can observe that the predictions of VAMUCH agree very well with those of FEM-based micromechanical analyses (Pettermann and Suresh, 2000; Berger et al., 2006) and nicely fall in the between the

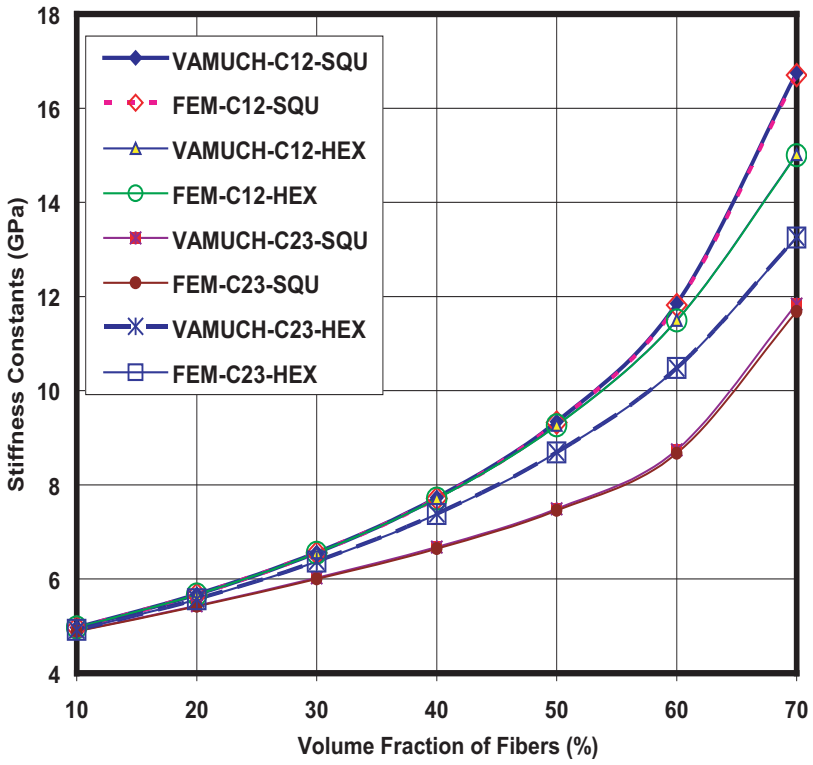

Fig. 4.3: Effective stiffness constants C_{12} and C_{23}.

tightest BL bounds.

To further demonstrate the reliability and accuracy of present model for more realistic heterogeneous materials, we choose a more complex microstructure as shown in Fig. 4.7. There are four different materials within one UC. The reinforcements are PZT-7A square fiber and a thin-wall circular SiC frame around the square fiber. The matrix between reinforcements is LaRC-SI, while the matrix outside thin-wall frame is PVDF. The material properties of the four constituents are shown in Table 4.1. There are no analytical solutions for this kind of microstructure. Here, we use ANSYS to calculate all the effective properties following the approach described in Berger et al. (2006). Table 4.3 lists the effective properties predicted by VAMUCH and ANSYS. Both methods produce almost identical results.

4.5.2 Predict Local Fields

VAMUCH can accurately recover the local stresses and the electric displacement distribution within the UC. In this study, we will use the direct multiphysics simulation in ANSYS as benchmark to verify the prediction of VAMUCH. The first example is PZT-

Table 4.2: Comparison of the effective properties for 60% volume fraction of fibers

	VAMUCH	Berger	Pettermann	BL	HS
C_{11}^{effD}(GPa)	86.982	86.982	86.98	76.1/87.0	79.0/87.8
C_{12}^{effD}(GPa)	10.630	10.631	10.64	8.89/12.3	6.12/16.5
C_{22}^{effD}(GPa)	25.322	25.322	25.42	25.2/25.5	24.9/28.7
C_{23}^{effD}(GPa)	7.931	7.930	7.86	7.72/8.15	5.00/12.0
C_{44}^{effD}(GPa)	4.39	4.39	4.41	4.39/4.41	4.37/4.92
C_{55}^{effD}(GPa)	6.481	6.477	6.51	6.45/6.52	6.40/7.67
β_{11}^{eff}(GVm/C)	0.780	0.780	0.780	0.730/0.844	0.742/0.951
β_{22}^{eff}(GVm/C)	6.614	6.60	6.572	6.57/6.66	2.54/6.73
h_{11}^{eff}(GV/m)	5.039	5.039	5.037	3.91/5.42	3.63/5.85
h_{21}^{eff}(GV/m)	-0.1524	-0.1524	-0.153	-0.337/0.024	-1.03/0.719
h_{51}^{eff}(GV/m)	0.3068	0.3063	0.311	0.229/0.384	-1.92/2.67

Table 4.3: Effective coefficients of piezoelectric composite with a complex microstructure

	C_{11}^{eff}(GPa)	C_{12}^{eff}(GPa)	C_{23}^{eff}(GPa)	C_{22}^{eff}(GPa)	C_{44}^{eff}(GPa)	C_{55}^{eff}(GPa)
VAMUCH	75.51	3.33	5.173	10.916	1.871	3.86
ANSYS	75.51	3.33	5.167	10.920	1.871	3.82
	e_{11}^{eff}(C/m^2)	e_{21}^{eff}(C/m^2)	e_{51}^{eff}(C/m^2)	k_{11}^{eff}(nC/Vm)	k_{22}^{eff}(nC/Vm)	k_{33}^{eff}(nC/Vm)
VAMUCH	1.7387	0.009275	0.000735	0.3827	0.06011	0.06555
ANSYS	1.7387	0.009291	0.000753	0.3827	0.06013	0.06558

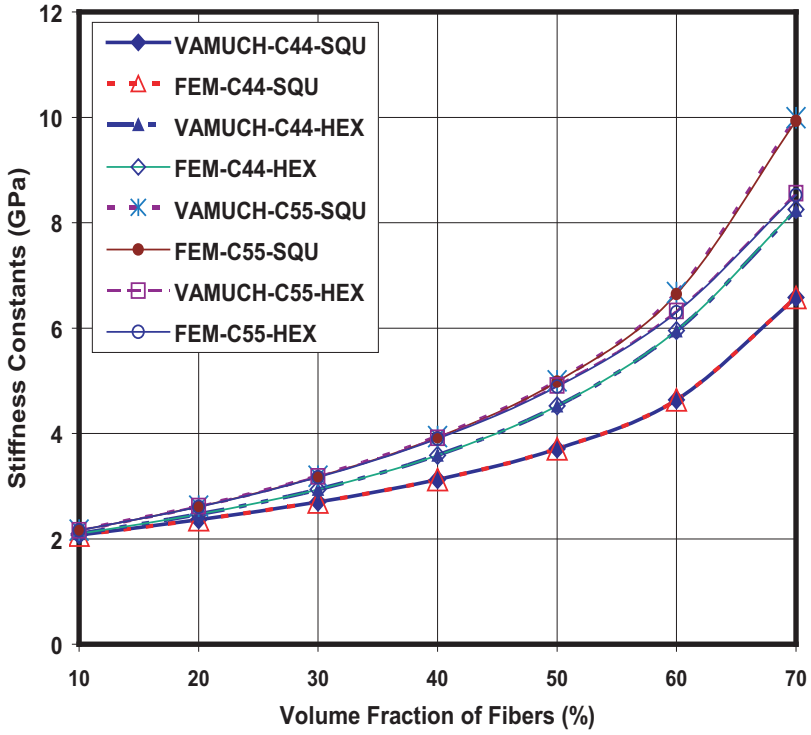

Fig. 4.4: Effective stiffness constants C_{44} and C_{55}.

7A/epoxy fiber reinforced composites with fiber volume fraction as 0.2. The boundary conditions applied to the UC are $\epsilon_{22} = 1.0\%$ and $E_2 = 100\text{V/m}$ and all other mechanical strains and gradients of electric potential are set to zero. Due to the difference of material properties of two constituents, the distribution of local stresses is not uniform within the UC. Figs. 4.8 and 4.9 show the contour plots of the distributions of σ_{22} and σ_{23}. All sudden changes of local stresses at the interface between fibers and matrix are well captured by VAMUCH. For quantitative comparison, we also plot σ_{22} predicted by VAMUCH and the direct multiphysics simulation of ANSYS along the lines $y_3 = 0$ and $y_2 = 0$ in Figs. 4.10 and 4.11, respectively. It is obvious that the predictions of VAMUCH have excellent agreement with those of ANSYS.

The second example is the composite with complex microstructure as shown in Fig. 4.7. The mechanical strains on all surfaces of UC are constrained. The contours of local electric displacement distribution T_3 and T_2 resulting from 100V/m in the y_3 direction predicted by VAMUCH is shown in Fig. 4.12 and 4.13. For a quantitative comparison, we also plot the local electric displacement distribution T_3 along $y_3 = 0$ predicted by VAMUCH and ANSYS as shown in Fig. 4.14. It can be observed that there is excellent agreement between

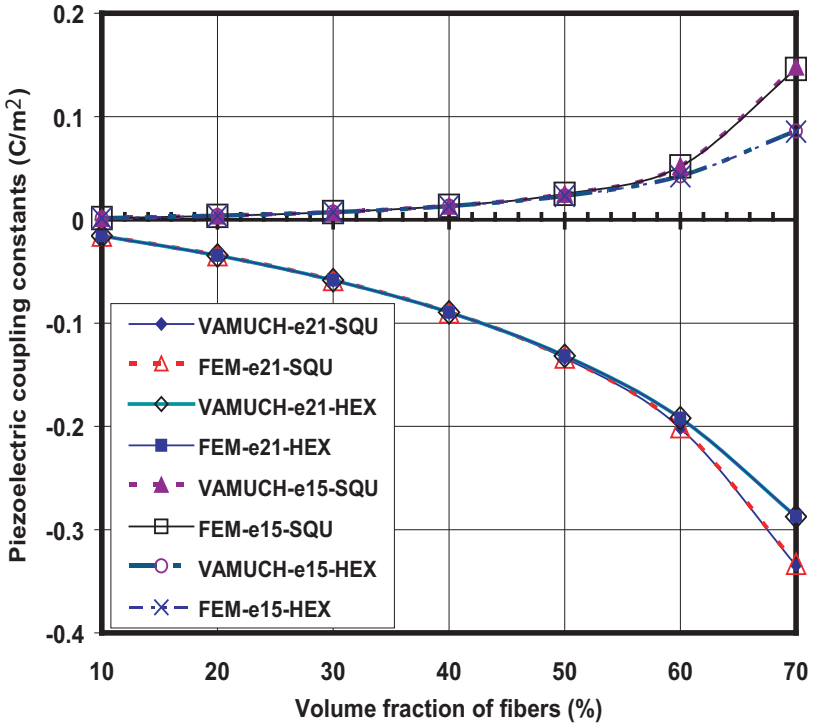

Fig. 4.5: Effective electric coupling constants.

these two sets of results.

It is emphasized here that ANSYS results are obtained through the direct multiphysics simulation of the unit cell using piezoelectric elements under specified loading without using a micromechanics approach to obtain the effective properties first, while VAMUCH calculates the effective material properties first and use these effective properties to carry out a macroscopic analysis of the homogenized microstructure to obtain the global fields and then recover the local fields within the original heterogeneous microstructure.

4.6 Conclusion

The variational asymptotic method for unit cell homogenization (VAMUCH) has been applied to construct a micromechanics model for predicting the effective properties and local fields of piezoelectric composites. In comparison to existing models, the present model has the following unique features:

1. It adopts the variational asymptotic method as its mathematical foundation. It invokes only essential assumptions inherent in the concept of micromechanics.

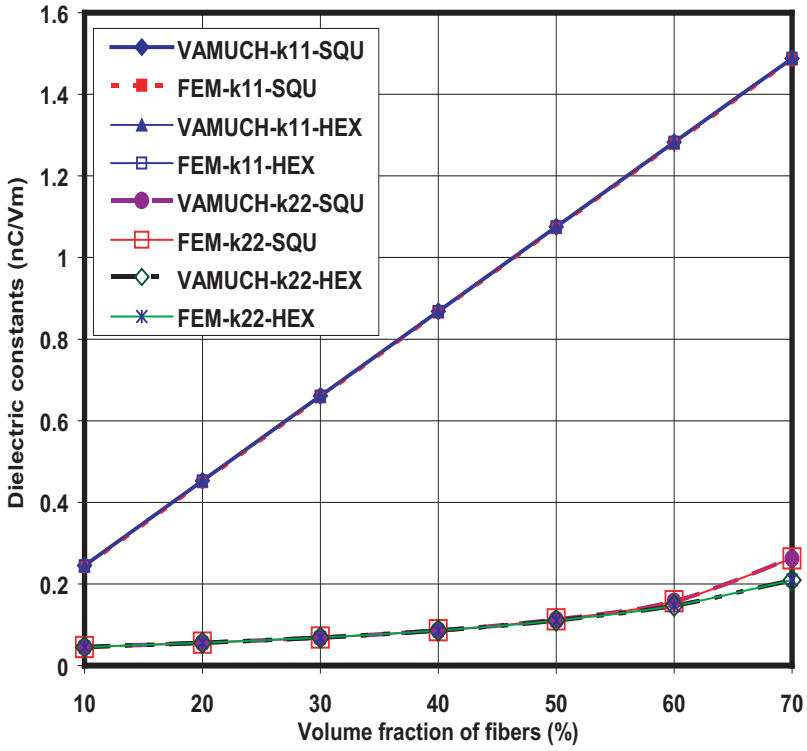

Fig. 4.6: Effective dielectric constants.

2. It has an inherent variational nature and its numerical implementation is shown to be straightforward.

3. It handles 1D/2D/3D unit cells uniformly. The dimensionality of the problem is determined by the periodicity of the unit cell.

The present theory is implemented in the computer program, VAMUCH. Numerous examples have clearly demonstrated its application and accuracy as a general-purpose micromechanical analysis tool. Although for the examples we have studied, VAMUCH results are almost identical to the results obtained by some FEM-based micromechanics analysis (Pettermann and Suresh, 2000; Berger et al., 2006), VAMUCH has the following advantages:

1. VAMUCH can obtain the complete set of material properties within one analysis, which is more efficient than those approaches requiring multiple runs under different boundary and load conditions. Furthermore, it is not a trivial issue to apply the right boundary conditions to obtain a correct FEM-based micromechanical analysis.

2. VAMUCH calculates effective properties and local fields directly with the same accuracy as the fluctuation functions. No postprocessing calculations which introduces

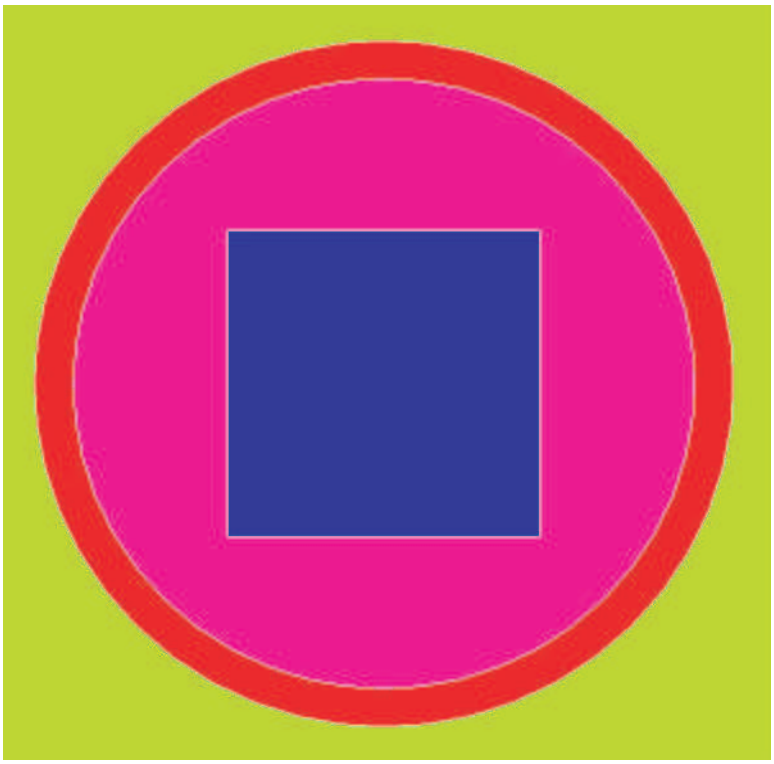

Fig. 4.7: Piezoelectric composite with a complex microstructure.

more approximations, such as averaging stress and electric displacement field, are needed, which are indispensable for FEM-based micromechanical analysis.

3. VAMUCH can deal with general anisotropy for effective materials which means VAMUCH can calculate 21 constants for the effective elastic constants, 18 constants for the effective piezoelectric constants, 6 for the effective dielectric constants, while FEM-based micromechanical analyses have difficult to predict the effective material having constants more than orthotropic materials.

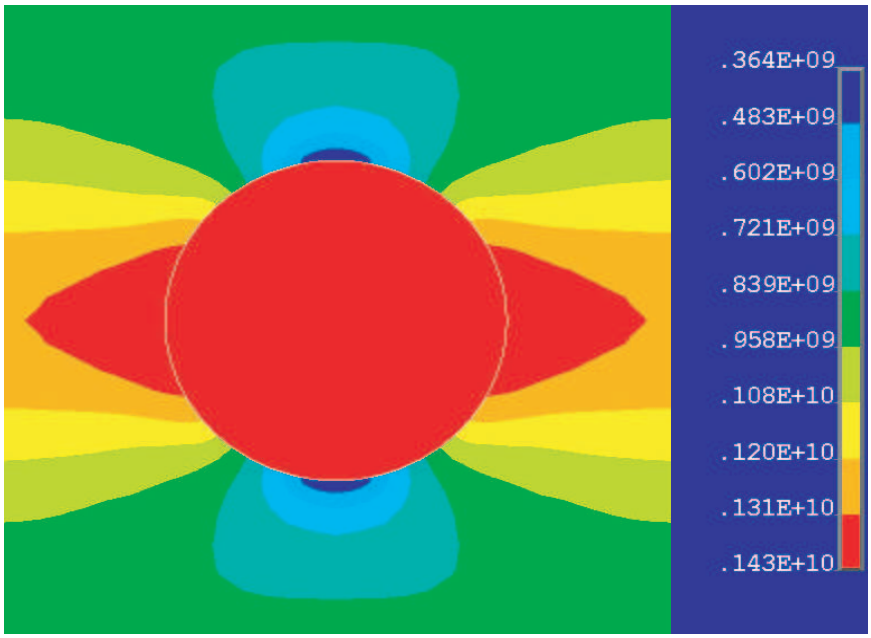

Fig. 4.8: Contour plot of σ_{22} (Pa) within UC.

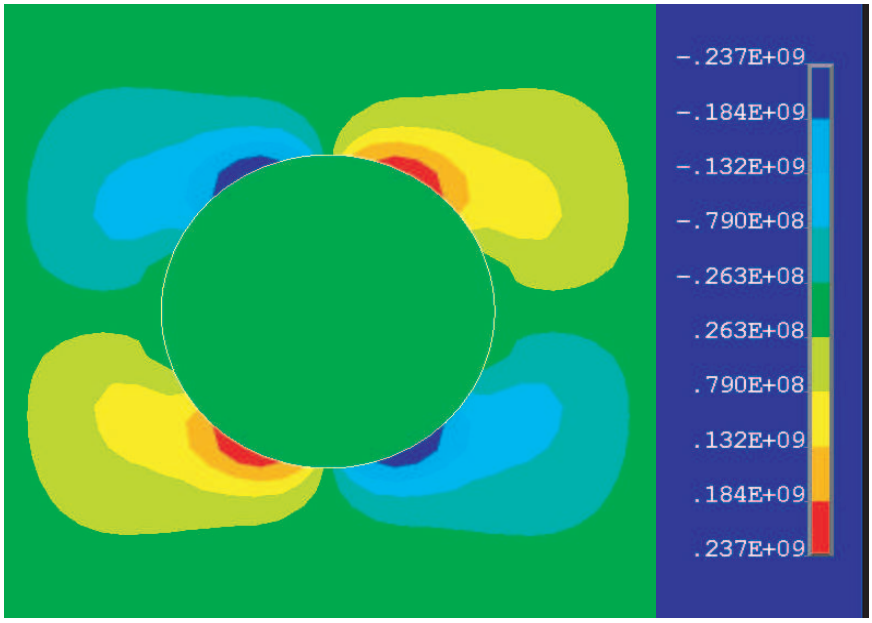

Fig. 4.9: Contour plot of σ_{23} (Pa) within UC.

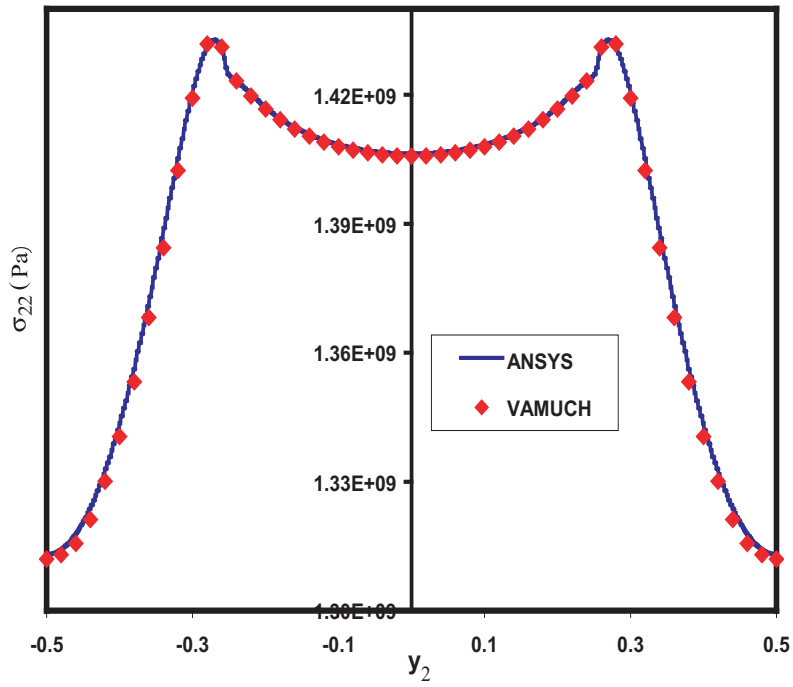

Fig. 4.10: Comparison of normal stress σ_{22} distribution along $y_3 = 0$.

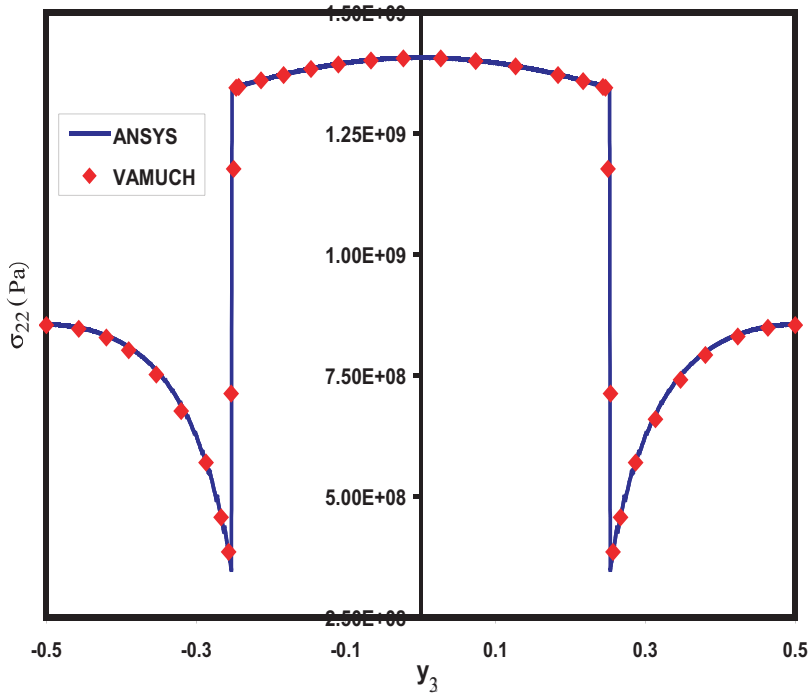

Fig. 4.11: Comparison of normal stress σ_{22} distribution along $y_2 = 0$.

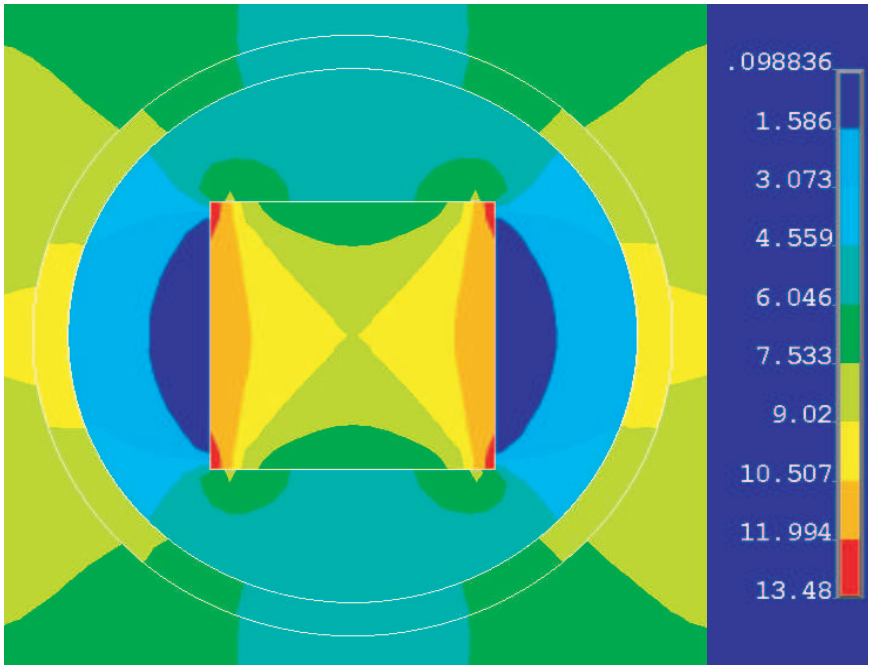

Fig. 4.12: Contour plot of electric flux density T_3 (nC/Vm) in a piezoelectric composite with complex microstructure.

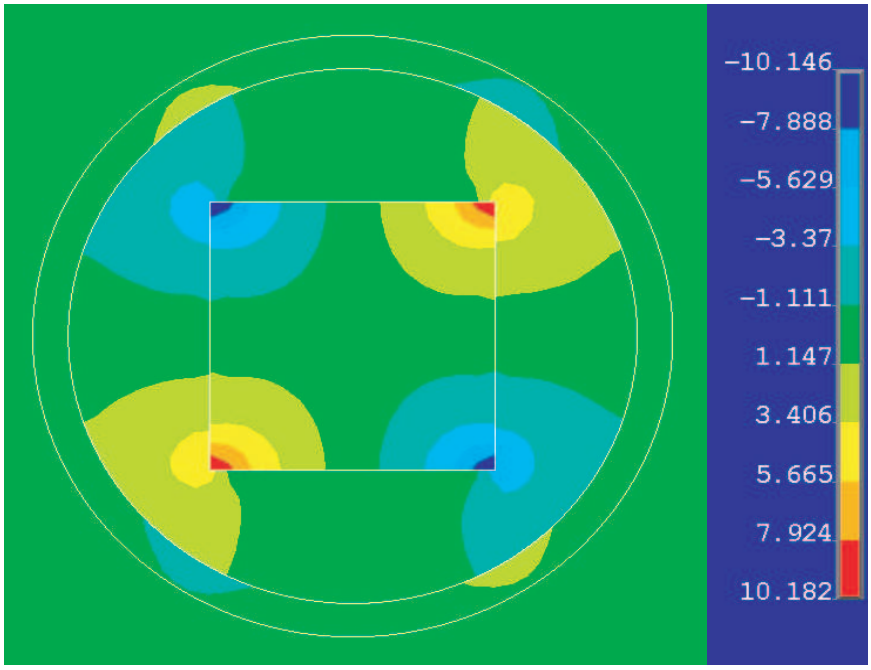

Fig. 4.13: Contour plot of electric flux density T_2 (nC/Vm) in a piezoelectric composite with complex microstructure.

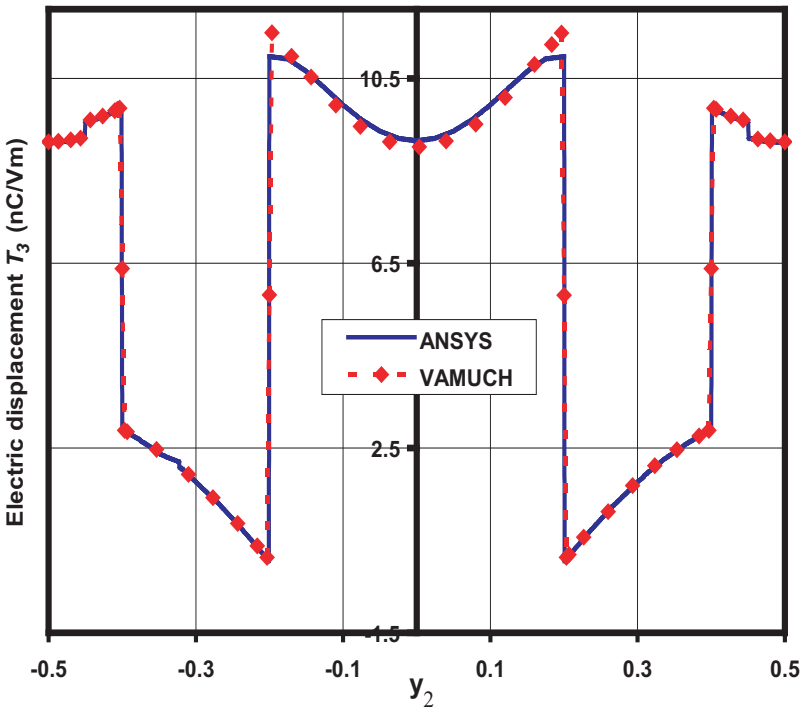

Fig. 4.14: Electric flux density T_3 distribution along $y_3 = 0$ in a piezoelectric composite with complex microstructure.

References

Banno, H., 1983. Recent developments of piezoelectric ceramic products and composites of synthetic rubber and piezoelectric ceramic particles. Ferroelectrics 50, 329–338.

Benveniste, Y., 1987. A new approach to the application of mori-tanaka's theory in composite materials. Mechanics of Materials 6, 147–157.

Benveniste, Y., 1992. The determination of the elastic and electric fields in a piezoelectric inhomogeneity. Journal of Applied Physics 72, 1086–1095.

Berdichevsky, V. L., 1977. On averaging of periodic systems. PMM 41 (6), 993–1006.

Berger, H., Kari, S., Gabbert, U., Rodriguez-Ramos, R., Bravo-Castillero, J., Guinovart-Diaz, R., Sabina, F., Maugin, G., 2006. Unit cell models of piezoelectric fiber composites for numerical and analytical calculation of effective properties. Smart Materials and Structures 15, 451–458.

Bisegna, P., Luciano, R., 1996. Variational bounds for the overall properties of piezoelectric composites. Journal of the Mechanics and Physics of Solids 44, 583–602.

Bisegna, P., Luciano, R., 1997. On methods for bounding the overall properties of periodic piezoelectic fibrous composites. Journal of the Mechanics and Physics of Solids 45, 1329–1356.

Budiansky, B., 1965. On the elastic moduli of some heterogeneous materials. Journal of the Mechanics and Physics of Solids 13, 223–227.

Chan, H., Unsworth, J., 1989. Simple model for piezoelectric ceramic/polymer 1-3 composites used in ultrasonic transducer applications. IEEE Transactions on Ultrasonics, Ferroelectrics, and Frequency Control 36, 434–441.

Chen, T., 1993. Piezoelectric properties of multiphase fibrous composites: some theoretical results. Journal of the Mechanics and Physics of Solids 41, 1781–1794.

Dunn, M., Taya, M., 1993a. An analysis of piezoelectric composite materials containing ellipsoidal inhomogeneities. Proceedings of the Royal Society of London, Series A 443, 265–287.

Dunn, M., Taya, M., 1993b. Micromechanics predictions of the effective electroelastic moduli of piezoelectric composites. International Journal of Solids and Structures 30, 161–175.

Dunn, M., Taya, M., 1994. Micromechanical estimates of the overall thermoelectroelastic moduli of multiphase fibrous composites. International Journal of Solids and Structures 31, 3099–3111.

Eshelby, J., 1957. The determination of the elastic field of an ellipsoidal inclusion, and related problems. Proceedings of the Royal Society of London, Series A 241, 376–396.

Fakri, N., Azrar, L., El Bakkali, L., 2003. Electroelastic behavior modeling of piezoelectric composite materials containing spatiallly oritented reinforcements. International Journal of Solids and Structures 40, 361–384.

Gaudenzi, P., 1997. On the electromechanical response of active composite materials with piezoelectic inclusions. Computers and Structures 65, 157–168.

Hill, R., 1965. A self-consistent mechanics of composite materials. Journal of the Mechanics and Physics of Solids 13, 213–222.

Huang, J., Kuo, W., 1996. Micromechanics determination of the effective properties of piezoelectric composites containing spatially oriented short fibers. Acta Materialia 44, 4889–4898.

Kunin, I., 1982. Theory of Elastic Media with Microstructure, vols. 1 and 2. Springer Verlag.

Lenglet, E., Hladky-Hennion, A., Debus, J., 2003. Numerical homogenization techniques applied to piezoelectric composites. Journal of the Acoustical Society of America 113, 826–833.

Li, J., Dunn, M., 2001. Variational bounds for the effective moduli of heterogeneous piezoelectric solids. Philosophical Magazine 81, 903–926.

Li, S., 2000. General unit cells for micromechanical analysis of unidirectional composites. Composites A 32, 815–826.

McLaughlin, R., 1977. A study of the differential scheme for composite materials. International Journal of Engineering Science 15, 237–244.

Mori, T., Tanaka, K., 1973. Average stress in matrix and average elastic energy of materials with misfitting inclusions. Acta Metallurgica 21, 571–574.

Newnham, R., Skinner, D., Cross, L., 1978. Connectivity and piezoelectri-pyroelectric composites. Materials Research Bulletin 13, 525–536.

Norris, A., 1985. A differential scheme for the effective moduli of composites. Mechanics of Materials 4, 1–16.

Odegard, G. M., 2004. Constitutive modeling of piezoelectric polymer composites. Acta Materialia 52 (18), 5315–5330.

Pastor, J., 1997. Homogenization of linear piezoelectric media. Mechanics Research Communications 24, 145–150.

Pettermann, H., Suresh, S., 2000. A comprehensive unit cell model: A study of coupled effects in piezoelectric 1-3 composites. International Journal of Solids and Structures 37, 5447–5464.

Poizat, C., Sester, M., 1999. Effective properties of composites with embedded piezoelectric fibers. Computational Materials Science 16, 89–97.

Smith, W., Auld, B., 1991. Modeling 1-3 composites piezoelectrics: Thickness-mode oscillations. IEEE Transactions on Ultrasonics, Ferroelectrics, and Frequency Control 38, 40–47.

Sun, H., Di, S., Zhang, N., Wu, C., 2001. Micromechanics of composite materials using multivariable finite element method and homogenization theory. International Journal of Solids and Structures 38, 3007–3020.

Tang, T., Yu, W., 2007a. A variational asymptotic micromechanics model for predicting conductivity of composite materials. Journal of Mechanics of Materials and Structures, in press.

Tang, T., Yu, W., Nov. 10–16 2007b. A variational asymptotic model for predicting initial yielding surface and elastoplastic behavior of metal matrix composite materials. In: Proceedings of the 2007 ASME International Mechanical Engineering Congress and Exposition. ASME, Seattle, Washington.

Wang, B., 1992. Three dimensional analysis of an ellipsoidal inclusion in a piezoelectic material. International Journal of Solids and Structures 29, 293–308.

Yu, W., Tang, T., 2007a. Variational asymptotic method for unit cell homogenization of periodically heterogeneous materials. International Journal of Solids and Structures 44, 3738–3755.

Yu, W., Tang, T., 2007b. A variational asymptotic micromechanics model for predicting thermoelastic properties of heterogeneous materials. International Journal of Solids and Structures 44, 7510–7525.

Chapter 5

A Variational Asymptotic Micromechanics Model for Predicting Conductivity of Composite Materials

[1]

This chapter is a journal paper published in the *Journal of Mechanics of Materials and Structures*, Vol. 2, No. 9, 2007, pp. 1813-1830.

Abstract

The focus of this paper is to extend the variational asymptotic method for unit cell homogenization (VAMUCH) to predict the effective thermal conductivity and local distribution of temperature field of heterogeneous materials. Starting from a variational statement of the conduction problem of the heterogenous continuum, we formulate the micromechanics model as a constrained minimization problem using the variational asymptotic method. To handle realistic microstructures in applications, we implement this new model using the finite element method. For validation, a few examples are used to demonstrate the application and accuracy of this theory and companion code. Since heat conduction is mathematically analogous to electrostatics, magnetostatics, and diffusion, the present model can also be used to predict effective dielectric, magnetic, and diffusion properties of heterogeneous materials.

5.1 Introduction

Along with increased knowledge and manufacturing techniques for materials, more and more materials are made with engineered microstructures to achieve better performance. To successfully design and fabricate these materials, we need efficient high-fidelity analysis tools to predict their effective properties. Many composites are applied in temperature sensitive environments such as electronic packaging and thermal protection systems. Accurate prediction of thermal properties such as the specific heat, coefficients of thermal expansion,

[1] Coauthored by: Tian Tang and Wenbin Yu.

and thermal conductivity becomes important for such applications. In this paper, we focus on developing a model to predict effective thermal conductivity and associated local temperature and heat flux distribution within the heterogeneous materials.

The effective thermal conductivity of composites is strongly affected by many parameters including the properties, volume fractions, distributions, and orientations of constituents. Numerous models have been proposed to predict the effective thermal conductivity (Progelhof et al., 1976). These models include simple rules of mixtures, self consistent scheme (Hashin, 1968), generalized self consistent scheme (Lee et al., 2006), finite element method (Islam and Pramila, 1999; Ramani and Vaidyanathan, 1995; Xu and Yagi, 2004; Kumlutas and Tavman, 2006), effective unit cell approach (Ganapathy et al., 2005) and variational bounds (Hashin and Shtrikman, 1962). Very recently, a new framework for micromechanics modeling, namely variational asymptotic method for unit cell homogenization (VAMUCH) (Yu and Tang, 2007a), has been introduced using two essential assumptions in the context of micromechanics for composites with an identifiable unit cell (UC):

- **Assumption 1** The exact field variable has volume average over the UC. For example, if ϕ is the exact temperature within the UC, there exist ψ such that

$$\psi = \frac{1}{\Omega}\int_{\Omega} \phi \, \mathrm{d}\Omega \equiv \langle \phi \rangle \tag{5.1}$$

  where Ω denotes the domain occupied by the UC and its volume, and symbol $\equiv$ denotes a definition.

- **Assumption 2** The effective material properties obtained from the micromechanical analysis of the UC are independent of the geometry, the boundary conditions, and loading conditions of the macroscopic structure, which means that effective properties are assumed to be the intrinsic properties of the material when viewed macroscopically.

Note that these assumptions are not restrictive. The mathematical meaning of the first assumption is that the exact solutions of the field are integrable over the domain of UC, which is true almost all the time. The second assumption implies that we will neglect the size effects of the material properties in the macroscopic analysis, which is an assumption often made in the conventional continuum mechanics. Of course, the micromechanical analysis

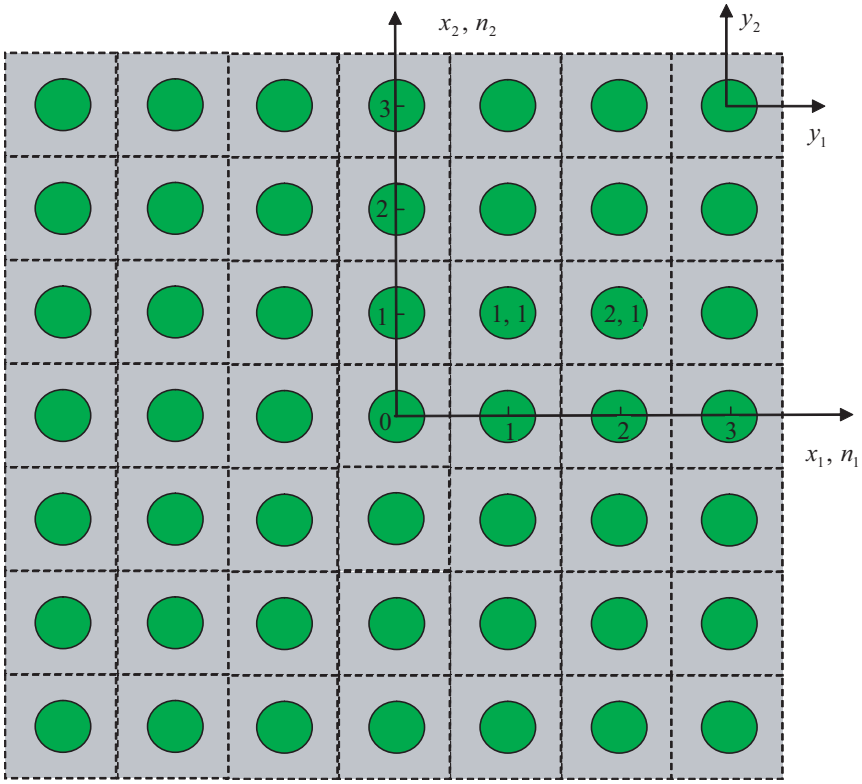

Fig. 5.1: Coordinate systems for heterogenous materials (only two-dimensional (2D) square array UC is drawn for clarity).

of the UC is only needed and appropriate if $\eta = h/l \ll 1$, with h as the characteristic size of the UC and l as the macroscopic size of the macroscopic material.

This new micromechanical modeling approach has been successfully applied to predict thermo-mechanical properties including elastic properties, coefficients of thermal expansion, and specific heats (Yu and Tang, 2007a,b). In this work, we will use this approach to construct micromechanics models for effective thermal conductivity and the corresponding local fields such as temperature and heat flux within UC.

5.2 Theoretical Formulation

VAMUCH formulation uses three coordinates systems: two Cartesian coordinates $\mathbf{x} = (x_1, x_2, x_3)$ and $\mathbf{y} = (y_1, y_2, y_3)$, and an integer-valued coordinate $\mathbf{n} = (n_1, n_2, n_3)$ (see Fig. 5.1). We use x_i as the global coordinates to describe the macroscopic structure and y_i parallel to x_i as the local coordinates to describe the UC (Here and throughout the paper, Latin indices assume 1, 2, and 3 and repeated indices are summed over their range except where explicitly indicated). We choose the origin of the local coordinates y_i to be the geometric center of UC. For example, if the UC is a cube with edge lengths d_i, then

$y_i \in [-\frac{d_i}{2}, \frac{d_i}{2}]$. To uniquely locate a UC in the heterogeneous material we also introduce integer coordinates n_i. The integer coordinates are related to the global coordinates in such a way that $n_i = x_i/d_i$ (no summation over i). It is emphasized although only square array is sketched in Fig. 5.1, the present theory has not such limitations.

As implied by Assumption 2, we can obtain the same effective properties from an imaginary, unbounded, and unloaded heterogeneous material with the same microstrucutre as the real, loaded, and bounded one. Hence we could derive the micromechanics model from an imaginary, unloaded, heterogeneous material which completely occupies the three-dimensional (3D) space $\mathcal{R}$ and composes of infinitely many repeating UCs. The solution of steady-state conduction problem, which is sufficient for us to find the effective thermal conductivity, can be obtained by the stationary value problem of the summation of "energy" integral of all the UCs (Hashin, 1968; Berdichevsky, 1977), which is:

$$\Pi = \sum_{n=-\infty}^{\infty} \frac{1}{2} \int_{\Omega} K_{ij}\, \phi_{,i}\, \phi_{,j} \mathrm{d}\Omega \tag{5.2}$$

where K_{ij} are components of the second-order thermal conductivity tensor, and

$$\phi_{,i}(\mathbf{n}; \mathbf{y}) = \frac{\partial \phi(\mathbf{n}; \mathbf{y})}{\partial y_i} \tag{5.3}$$

with $()_{,i} \equiv \frac{\partial ( )}{\partial y_i}$. Here ϕ is a function of the integer coordinates and the local coordinates for each UC. In view of the fact that the infinite many UCs form a continuous heterogeneous material, we need to enforce the continuity of the temperature field ϕ on the interface between adjacent UCs, which is:

$$\begin{aligned}
\phi(n_1, n_2, n_3; d_1/2, y_2, y_3) &= \phi(n_1 + 1, n_2, n_3; -d_1/2, y_2, y_3) \\
\phi(n_1, n_2, n_3; y_1, d_2/2, y_3) &= \phi(n_1, n_2 + 1, n_3; y_1, -d_2/2, y_3) \\
\phi(n_1, n_2, n_3; y_1, y_2, d_3/2) &= \phi(n_1, n_2, n_3 + 1; y_1, y_2, -d_3/2)
\end{aligned} \tag{5.4}$$

The exact solution of steady heat conduction problem will minimize the summation of "energy" integral in Eq. (5.2) under the constraints in Eqs. (5.1), (5.4). To avoid the difficulty associated with discrete integer arguments, we can reformulate the problem, including

Eqs. (5.2), (5.3), and (5.4), in terms of continuous functions using the idea of quasicontinuum (Kunin, 1982). The corresponding formulas are listed below.

$$\Pi = \frac{1}{2}\int_{\mathcal{R}} \langle K_{ij}\ \phi_{,i}\ \phi_{,j}\rangle \,\mathrm{d}\mathcal{R} \tag{5.5}$$

$$\phi_{,i}(\mathbf{x};\mathbf{y}) = \frac{\partial \phi(\mathbf{x};\mathbf{y})}{\partial y_i} \tag{5.6}$$

and

$$\begin{aligned}
&\phi(x_1,x_2,x_3;d_1/2,y_2,y_3) = \phi(x_1+d_1,x_2,x_3;-d_1/2,y_2,y_3)\\
&\phi(x_1,x_2,x_3;y_1,d_2/2,y_3) = \phi(x_1,x_2+d_2,x_3;y_1,-d_2/2,y_3)\\
&\phi(x_1,x_2,x_3;y_1,y_2,d_3/2) = \phi(x_1,x_2,x_3+d_3;y_1,y_2,-d_3/2)
\end{aligned} \tag{5.7}$$

Using the technique of Lagrange multipliers, we can pose the thermal conduction problem as a stationary value problem of the following functional:

$$\begin{aligned}
J = \int_{\mathcal{R}} \Bigg\{ &\left\langle \frac{1}{2} K_{ij}\ \phi_{,i}\ \phi_{,j} \right\rangle + \lambda(\langle\phi\rangle - \psi)\\
&+ \int_{S_1} \gamma_1 \left[\phi(x_1,x_2,x_3;d_1/2,y_2,y_3) - \phi(x_1+d_1,x_2,x_3;-d_1/2,y_2,y_3)\right] \mathrm{d}S_1\\
&+ \int_{S_2} \gamma_2 \left[\phi(x_1,x_2,x_3;y_1,d_2/2,y_3) - \phi(x_1,x_2+d_2,x_3;y_1,-d_2/2,y_3)\right] \mathrm{d}S_2\\
&+ \int_{S_3} \gamma_3 \left[\phi(x_1,x_2,x_3;y_1,y_2,d_3/2) - \phi(x_1,x_2,x_3+d_3;y_1,y_2,-d_3/2)\right] \mathrm{d}S_3 \Bigg\} \mathrm{d}\mathcal{R}
\end{aligned} \tag{5.8}$$

where λ and γ_i are Lagrange multipliers introduced to enforce the constraints in Eqs. (5.1) and (5.7), respectively, and S_i are the surfaces with $n_i = 1$. The main objective of micromechanics is to find the real temperature field ϕ in terms of ψ, which is a very difficult problem because we have to solve this stationary problem for each point in the global system x_i as in Eq. (5.8). It will be desirable if we can formulate the variational statement posed over a single UC only. In view of Eq. (5.1), it is natural to express the exact solution ϕ as a sum of the volume average ψ plus the difference, such that

$$\phi(\mathbf{x};\mathbf{y}) = \psi(\mathbf{x}) + w(\mathbf{x};\mathbf{y}) \tag{5.9}$$

where $\langle w\rangle = 0$ according to Eq. (5.1). The very reason that the heterogenous material

can be homogenized leads us to believe that w should be asymptotically smaller than ψ, *i.e.*, $w \sim \eta\ \psi$. Substituting Eq. (5.9) into Eq. (5.8) and making use of Eq. (5.6), we can obtain the leading terms of the functional according to the variational asymptotic method (Berdichevsky, 1977) as:

$$\begin{aligned} J_1 = \int_{\mathcal{R}} \Bigg\{ & \left\langle \frac{1}{2} K_{ij}\ w_{,i}\ w_{,j} \right\rangle + \lambda \langle w \rangle \\ & + \int_{S_1} \gamma_1 \left[w(\mathbf{x}; d_1/2, y_2, y_3) - w(\mathbf{x}; -d_1/2, y_2, y_3) - \psi_{;1} d_1 \right] \mathrm{d}S_1 \\ & + \int_{S_2} \gamma_2 \left[w(\mathbf{x}; y_1, d_2/2, y_3) - w(\mathbf{x}; y_1, -d_2/2, y_3) - \psi_{;2} d_2 \right] \mathrm{d}S_2 \\ & + \int_{S_3} \gamma_3 \left[w(\mathbf{x}; y_1, y_2, d_3/2) - w(\mathbf{x}; y_1, y_2, -d_3/2) - \psi_{;3} d_3 \right] \mathrm{d}S_3 \Bigg\} \mathrm{d}\mathcal{R} \end{aligned} \tag{5.10}$$

where $()_{;i} \equiv \frac{\partial ()}{\partial x_i}$. Although it is possible to carry out the variation of J_1 and find the Euler-Lagrange equtions and associated boundary conditions for w, which results in inhomogeneous boundary conditions, it is more convenient to use change of variables to reformulate the same problem so that the boundary conditions are homogeneous. Considering the last three terms in Eq. (5.10), we use the following change of variables to express w as:

$$w(\mathbf{x}; \mathbf{y}) = y_i \psi_{;i} + \zeta(\mathbf{x}; \mathbf{y}) \tag{5.11}$$

with ζ normally termed as fluctuation functions. We are free to choose the origin of the local coordinate system to be the center of UC, which implies the following constraints on ζ:

$$\langle \zeta \rangle = 0 \tag{5.12}$$

Substituting Eq. (5.11) into Eq. (5.10), we obtain a stationary value problem defined over UC for ζ, such that

$$\begin{aligned} J_\Omega = & \frac{1}{2} \left\langle K_{ij} \left(\psi_{;i} + \zeta_{,i} \right) \left(\psi_{;j} + \zeta_{,j} \right) \right\rangle + \lambda \langle \zeta \rangle \\ & + \int_{S_1} \gamma_1 (\zeta^{+1} - \zeta^{-1}) \mathrm{d}S_1 + \int_{S_2} \gamma_2 (\zeta^{+2} - \zeta^{-2}) \mathrm{d}S_2 \\ & + \int_{S_3} \gamma_3 (\zeta^{+3} - \zeta^{-3}) \mathrm{d}S_3 \end{aligned} \tag{5.13}$$

with

$$\zeta^{+i} = \zeta|_{y_i = d_i/2} \qquad \zeta^{-i} = \zeta|_{y_i = -d_i/2} \quad \text{for} \quad i = 1, 2, 3 \tag{5.14}$$

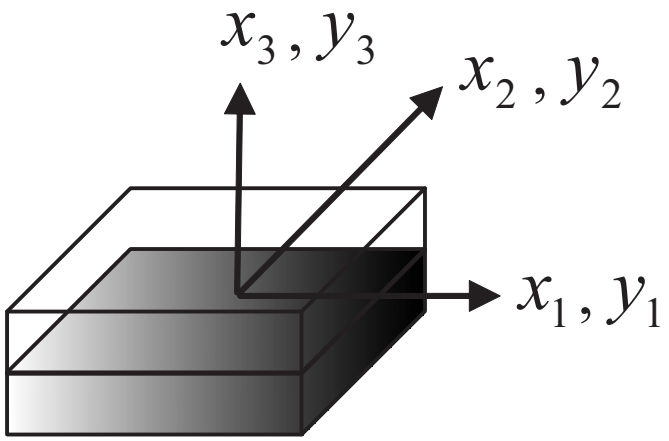

Fig. 5.2: Sketch of a binary composite.

where $\psi_{;i}$ will be shown later to be the components of the global temperature gradient vector for the effective material with homogenized material properties. The functional J_Ω in Eq. (5.13) forms the backbone of the present theory. This stationary problem can be solved analytically for very simple cases such as binary composites, however, for general cases we need to use numerical techniques such as the finite element method (FEM) to seek numerical solutions.

5.3 An Illustrative Example

To illustrate the solution procedure of the stationary problem of the functional in Eq. (5.13), we will consider a periodic binary composite made of anisotropic layers and the material axes are the same as the global coordinate x_i so that the material is uniform in the $x_1 - x_2$ plane and periodic along x_3 direction. A typical UC can be identified as shown in Fig. 5.2, with the dimension along y_3 as h and dimensions along y_1 and y_2 arbitrary. Let ϕ_1 and ϕ_2 denote the volume fraction of the first layer and the second layer, respectively, and we have $\phi_1 + \phi_2 = 1$.

Because of the uniformity of the structure in the $x_1 - x_2$ plane, we know that the solution of ζ will be independent of y_1 and y_2, and is a function of y_3 only. Taking advantage of the this fact, we can specialize the functional in Eq. (5.13) for this particular case in a matrix

form as:

$$
\begin{aligned}
J^*_\Omega = \int_{S_3} \Bigg\{ & \int_{-\frac{h}{2}}^{(\phi_1-\frac{1}{2})h} \left[\frac{1}{2} \Psi^{(1)T} K^{(1)} \Psi^{(1)} + \lambda \zeta^{(1)} \right] \mathrm{d}y_3 \\
& + \int_{(\phi_1-\frac{1}{2})h}^{\frac{h}{2}} \left[\frac{1}{2} \Psi^{(2)T} K^{(2)} \Psi^{(2)} + \lambda \zeta^{(2)} \right] \mathrm{d}y_3 \\
& + \gamma_3 \left[\zeta^{(2)}(\frac{h}{2}) - \zeta^{(1)}(-\frac{h}{2}) \right] \Bigg\} \mathrm{d}S
\end{aligned}
\tag{5.15}
$$

with $\Psi^{(\alpha)} = \lfloor \psi_{;1} \ \psi_{;2} \ \psi_{;3} + \zeta^{(\alpha)}_{,3} \rfloor^T$ for $\alpha = 1, 2$, and $\zeta^{(\alpha)}$ as the fluctuation functions of the temperature for each layer. The thermal conductivity matrix $K^{(\alpha)}$ is a fully populated symmetric matrix for a general anisotropic material, such that

$$
K^{(\alpha)} = \begin{bmatrix} K^{(\alpha)}_{11} & K^{(\alpha)}_{12} & K^{(\alpha)}_{13} \\ K^{(\alpha)}_{12} & K^{(\alpha)}_{22} & K^{(\alpha)}_{23} \\ K^{(\alpha)}_{13} & K^{(\alpha)}_{23} & K^{(\alpha)}_{33} \end{bmatrix}
\tag{5.16}
$$

The corresponding differential statement of the variational statement in Eq. (5.15) can be obtained following normal procedures of the calculus of variations, as follows:

$$
K^{(\alpha)}_{33} \zeta^{(\alpha)}_{,33} = \lambda
\tag{5.17}
$$

$$
\int_{-\frac{h}{2}}^{(\phi_1-\frac{1}{2})h} \zeta^{(1)} \, \mathrm{d}y_3 + \int_{(\frac{1}{2}-\phi_2)h}^{\frac{h}{2}} \zeta^{(2)} \, \mathrm{d}y_3 = 0
\tag{5.18}
$$

$$
\zeta^{(1)}(-\frac{h}{2}) = \zeta^{(2)}(\frac{h}{2})
\tag{5.19}
$$

$$
\zeta^{(1)}(\phi_1 h - h/2) = \zeta^{(2)}(\phi_1 h - h/2)
\tag{5.20}
$$

$$
\begin{aligned}
& K^{(1)}_{13} \psi_{;1} + K^{(1)}_{23} \psi_{;2} + K^{(1)}_{33} \left[\psi_{;3} + \zeta^{(1)}_{,3} \right] |_{y_3 = -\frac{h}{2}} \\
= & K^{(2)}_{13} \psi_{;1} + K^{(2)}_{23} \psi_{;2} + K^{(2)}_{33} \left[\psi_{;3} + \zeta^{(2)}_{,3} \right] |_{y_3 = \frac{h}{2}}
\end{aligned}
\tag{5.21}
$$

$$
\begin{aligned}
& K^{(1)}_{13} \psi_{;1} + K^{(1)}_{23} \psi_{;2} + K^{(1)}_{33} \left[\psi_{;3} + \zeta^{(1)}_{,3} \right] |_{y_3 = (\phi_1-\frac{1}{2})h} \\
= & K^{(2)}_{13} \psi_{;1} + K^{(2)}_{23} \psi_{;2} + K^{(2)}_{33} \left[\psi_{;3} + \zeta^{(2)}_{,3} \right] |_{y_3 = (\phi_1-\frac{1}{2})h}
\end{aligned}
\tag{5.22}
$$

Clearly this differential statement contains two second-order ordinary differential equations in Eq. (5.17) and five constrains to solve for $\zeta^{(\alpha)}$ and λ. The solution of λ is found to be zero and $\zeta^{(\alpha)}$ are linear functions of y_3. Having solved the fluctuation functions, $\zeta^{(\alpha)}$, the

density of "energy" integral of this effective materials can be trivially obtained as:

$$\Pi_\Omega = \frac{1}{2} \begin{Bmatrix} \psi_{;1} \\ \psi_{;2} \\ \psi_{;3} \end{Bmatrix}^T \begin{bmatrix} K^*_{11} & K^*_{12} & K^*_{13} \\ K^*_{12} & K^*_{22} & K^*_{23} \\ K^*_{13} & K^*_{23} & K^*_{33} \end{bmatrix} \begin{Bmatrix} \psi_{;1} \\ \psi_{;2} \\ \psi_{;3} \end{Bmatrix} \tag{5.23}$$

with the effective thermal conductivity coefficients K^*_{ij} as:

$$K^*_{11} = \langle K_{11} \rangle - \frac{(K^{(1)}_{13} - K^{(2)}_{13})^2 \phi_1 \phi_2}{K^{(2)}_{33}\phi_1 + K^{(1)}_{33}\phi_2} \tag{5.24}$$

$$K^*_{22} = \langle K_{22} \rangle - \frac{(K^{(1)}_{23} - K^{(2)}_{23})^2 \phi_1 \phi_2}{K^{(2)}_{33}\phi_1 + K^{(1)}_{33}\phi_2} \tag{5.25}$$

$$K^*_{33} = \frac{K^{(1)}_{33} K^{(2)}_{33}}{\phi_2 K^{(1)}_{33} + \phi_1 K^{(2)}_{33}} \tag{5.26}$$

$$K^*_{12} = \langle K_{12} \rangle - \frac{(K^{(1)}_{13} - K^{(2)}_{13})(K^{(1)}_{23} - K^{(2)}_{23}) \phi_1 \phi_2}{\phi_2 K^{(1)}_{33} + \phi_1 K^{(2)}_{33}} \tag{5.27}$$

$$K^*_{13} = \frac{K^{(1)}_{13} K^{(2)}_{33} \phi_1 + K^{(2)}_{13} K^{(1)}_{33} \phi_2}{\phi_2 K^{(1)}_{33} + \phi_1 K^{(2)}_{33}} \tag{5.28}$$

$$K^*_{23} = \frac{K^{(1)}_{23} K^{(2)}_{33} \phi_1 + K^{(2)}_{23} K^{(1)}_{33} \phi_2}{\phi_2 K^{(1)}_{33} + \phi_1 K^{(2)}_{33}} \tag{5.29}$$

It is interesting to note that K^*_{33} is the same as the rule of mixtures based on Reuss's hypothesis for this special case. If $K^{(1)}_{13} = K^{(2)}_{13}$ and $K^{(1)}_{23} = K^{(2)}_{23}$, then K^*_{11}, K^*_{22}, and K^*_{12} are the same as the rule of mixtures based on Voigt's hypothesis, and K^*_{13} and K^*_{23} are the same as the constituent properties.

5.4 Finite Element Implementation

For more general cases, we need to rely on numerical solutions. Here, we will implement the variational statement in Eq. (5.13) using the well-established FEM. It is possible to formulate the FEM solution based on Eq. (5.13), however, it is not the most convenient and efficient way because Lagrange multipliers will increase the number of unknowns. To this end, we can reformulate the variational statement in Eq. (5.13) as the stationary value of the following functional

$$\Pi_\Omega = \frac{1}{2\Omega} \int_\Omega K_{ij} \left(\psi_{;i} + \zeta_{,i}\right) \left(\psi_{;j} + \zeta_{,j}\right) \mathrm{d}\Omega \tag{5.30}$$

under the following three constraints

$$\zeta^{+i} = \zeta^{-i} \quad \text{for} \quad i = 1, 2, 3 \tag{5.31}$$

The constraint in Eq. (5.12) does not affect the minimum value of Π_Ω but help uniquely determine ζ. In practice, we can constrain the fluctuation function at an arbitrary node to be zero and later use this constraint to recover the unique fluctuation function. It is fine to use penalty function method to introduce the constraints in Eqs. (5.31). However, this method introduces additional approximation and the robustness of the solution depends on the choice of large penalty numbers. Here, we choose to make the nodes on the positive boundary surface (*i.e.*, $y_i = d_i/2$) slave to the nodes on the opposite negative boundary surface (*i.e.*, $y_i = -d_i/2$). By assembling all the independent active degrees of freedom, we can implicitly and exactly incorporate the constraints in Eqs. (5.31). In this way, we also reduce the total number of unknowns in the linear system which will be formulated as follows.

Introduce the following matrix notations

$$\Phi = \lfloor \psi_{;1} \ \psi_{;2} \ \psi_{;3} \rfloor^T \tag{5.32}$$

$$\Phi_1 = \left\{ \begin{array}{c} \frac{\partial \zeta}{\partial y_1} \\ \frac{\partial \zeta}{\partial y_2} \\ \frac{\partial \zeta}{\partial y_3} \end{array} \right\} = \left\{ \begin{array}{c} \frac{\partial}{\partial y_1} \\ \frac{\partial}{\partial y_2} \\ \frac{\partial}{\partial y_3} \end{array} \right\} \zeta \equiv \Gamma_h \zeta \tag{5.33}$$

where Γ_h is an operator matrix. If we discretize ζ using the finite elements as:

$$\zeta(x_i; y_i) = G(y_i)\xi(x_i) \tag{5.34}$$

where G representing the shape functions and ξ a column matrix of the nodal values of the fluctuation function. Substituting Eqs. (5.32), (5.33), and (5.34) into Eq. (5.30), we obtain a discretized version of the functional as:

$$\Pi_\Omega = \frac{1}{2\Omega}(\xi^T F \xi + 2\xi^T K_{h\Phi} \Phi + \Phi^T K_{\Phi\Phi} \Phi) \tag{5.35}$$

where

$$F = \int_{\Omega} (\Gamma_h G)^T K (\Gamma_h G) \mathrm{d}\Omega \qquad K_{h\Phi} = \int_{\Omega} (\Gamma_h G)^T K \mathrm{d}\Omega \qquad K_{\Phi\Phi} = \int_{\Omega} K \mathrm{d}\Omega \tag{5.36}$$

with K as the 3×3 matrix of K_{ij}. Minimizing Π_Ω in Eq. (5.35), we obtain the following linear system

$$F\xi = -K_{h\Phi}\Phi \tag{5.37}$$

It is clear from Eq. (5.37) that the fluctuation function ξ is linearly proportional to Φ, which means the solution can be written symbolically as:

$$\xi = \xi_0 \Phi \tag{5.38}$$

Substituting Eq. (5.38) into Eq. (5.35), we can calculate the density of "energy" integral of the UC as:

$$\Pi_\Omega = \frac{1}{2\Omega} \Phi^T \left(\xi_0^T K_{h\Phi} + K_{\Phi\Phi} \right) \Phi \equiv \frac{1}{2} \Phi^T K^* \Phi \tag{5.39}$$

It can be seen that K^* in Eq. (5.39) is the effective thermal conductivity matrix and Φ is the global temperature gradient.

If the local fields within UC are of interest, we can recover those fields including local temperature and heat flux in terms of the macroscopic behavior including the global temperature ψ and the corresponding gradient $\psi_{;i}$, and the fluctuation function ζ. First, we need to uniquely determine the fluctuation function. Otherwise, we could not uniquely determine the local temperature field. Because we have fixed an arbitrary node and made nodes on the positive boundary surfaces (*i.e.*, $y_i = +d_i/2$) slave to the corresponding negative boundary surfaces (*i.e.*, $y_i = -d_i/2$) in forming the linear system in Eq. (5.37), we need to construct a new array $\tilde{\xi}_0$ from ξ_0 by assigning the values for slave nodes according to the corresponding active nodes and assign zero to the fixed node. Clearly, $\tilde{\xi}_0$ corresponds to the stationary value of Π_Ω in Eq. (5.35) under constrains in Eqs. (5.31). However, $\tilde{\xi}_0$ may not satisfy Eq. (5.12). The real solution, denoted as $\bar{\xi}_0$ can be found trivially by adding a constant to each node so that Eq. (5.12) is satisfied.

After having determined the fluctuation functions uniquely, we can recover the local temperature using Eqs. (5.9) and (5.11) as:

$$\phi = \psi + y_i \psi_{;i} + \bar{G}\bar{\xi}_0 \Phi \tag{5.40}$$

where $\bar{G}$ is different from G due to the recovery of slave nodes and the constrained node. The local temperature gradient field can be recovered using Eqs. (5.6) and (5.33) as:

$$\lfloor \phi_{,1} \quad \phi_{,2} \quad \phi_{,3} \rfloor^T = \Phi + \Gamma_h \bar{G}\bar{\xi}_0 \Phi \tag{5.41}$$

Finally, the local heat flux field can be recovered straightforwardly using the 3D Fourier law for the constituent materials as:

$$q_i = -K_{ij}\phi_{,j} \tag{5.42}$$

We have implemented this formulation in the computer program VAMUCH. In the next section, we will use a few numerical examples to demonstrate the application and accuracy of this theory and code.

5.5 Numerical Examples

VAMUCH provides a unified analysis for general 1D, 2D, or 3D UCs. First, the same code VAMUCH can be used to homogenize binary composites (modeled using 1D UCs), fiber reinforced composites (modeled using 2D UCs), and particle reinforced composites (modeled using 3D UCs). Second, VAMUCH can reproduce the results for lower-dimensional UCs using higher-dimensional UCs. That is, VAMUCH predicts the same results for binary composites using 1D, 2D or 3D UCs, and for fiber reinforced composites using 2D or 3D UCs.

In this section, several examples will be used to demonstrate the accuracy of VAMUCH for predicting the effective thermal conductivity and calculating the local heat flux field within UC due to temperature gradients. To facilitate comparison with existing models in the literature, we only consider composites with isotropic constituents although the present method and code can handle general anisotropic constituents.

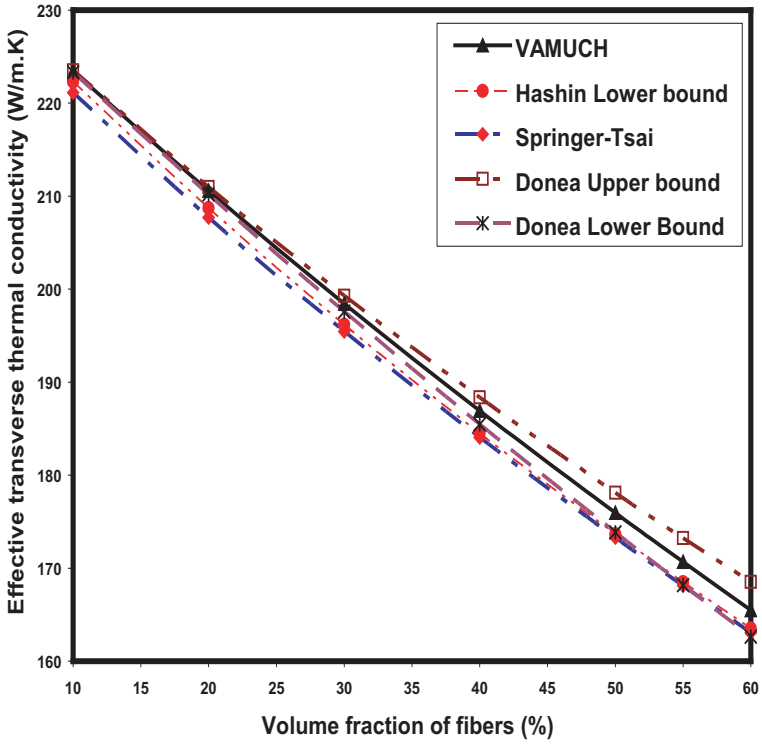

Fig. 5.3: Effective transverse thermal conductivity of the carbon/Al composite.

5.5.1 Effective Thermal Conductivity of Fiber Reinforced Composites

The first example is a carbon fiber reinforced aluminum matrix composite. Both constituents are isotropic with thermal conductivity $K = 129$ W/(m · K) for the carbon fiber, and $K = 237$ W/(m · K) for aluminum matrix. The fiber is of circular shape and arranged in a square array. The prediction of VAMUCH for the effective thermal conductivity along the fiber direction exactly obeys the rule of mixtures, which has been generally accepted as the exact solution for the longitudinal thermal conductivity for fiber reinforced composites with isotropic constituents (Hashin, 1968).

However, the effective thermal conductivity coefficients in the transverse directions (K^*_{22} and K^*_{33}) do not in general obey the rule of mixtures. To validate the present theory, we compare VAMUCH prediction with other models in the literature (Donea, 1972; Behrens, 1968; Hatta and Taya, 1986; Hashin, 1983; Springer and Tsai, 1967). As shown in Fig. 5.3, VAMUCH results are perfectly located between the variational bounds of Donea (1972), while the Springer-Tsai model (Springer and Tsai, 1967) and the lower bound of Hashin (1983) underpredict the results. We have also found out that VAMUCH results are on the top of those obtained by Behrens (1968), Hatta and Taya (1986), and the upper bound of

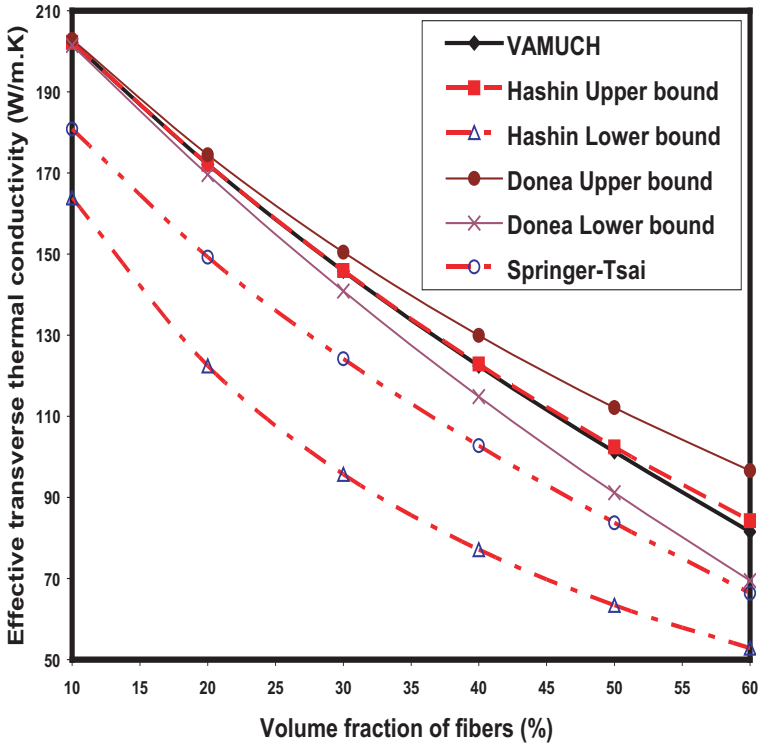

Fig. 5.4: Effective transverse thermal conductivity of the boron/Al composite.

Hashin (1983) and these results are not shown in the plot for clarity.

The second example is a boron fiber reinforced aluminum composite with constituents as isotropic with thermal conductivity $K = 27.4$ W/(m $\cdot$ K) for the boron fiber, and $K =$ 237 W/(m·K) for aluminum matrix. The fiber is still circular and arranged in a square array. The effective thermal conductivity computed by different models are plotted in Fig. 5.4. We found out that the results of Hashin upper bound (Hashin, 1983) are the same as those of Behrens (1968) and Hatta1 and Taya (1986). Hence only Hashin upper bound is plotted in the figure. It can be observed that the predictions of Hashin upper bound are slightly higher than those of VAMUCH when the fiber volume fraction is higher than 40%. We also observe that the difference between Hashin upper and lower bounds (Hashin, 1983) is significant for this case which means they are not very useful for composites with constituents having relatively high contrast ratio in thermal conductivity properties. VAMUCH results are also nicely located in the much narrower bounds of Donea (1972), while the prediction of Springer and Tsai (1967) is not accurate for this case because it is even significantly lower than the lower bound of Donea (1972).

In the two examples we just studied, the thermal conductivity of matrix is higher than

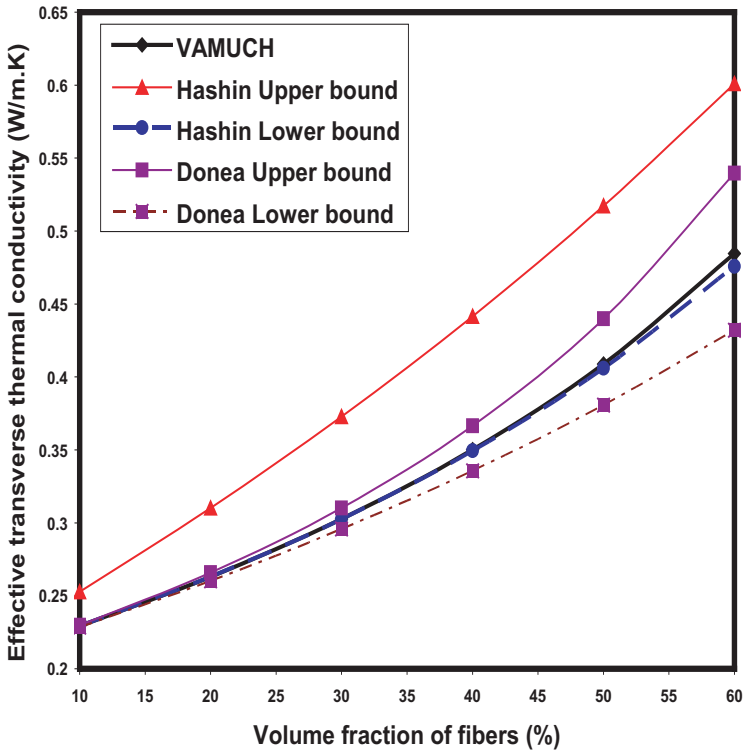

Fig. 5.5: Effective transverse thermal conductivity of the glass/polypropylene composite.

that of the fiber. Now, let us consider a glass/polypropylene composite with the thermal conductivity $K = 1.05$ W/(m $\cdot$ K) for the glass fiber, and $K = 0.2$ W/(m $\cdot$ K) for the polypropylene matrix. We plot the change of effective transverse thermal conductivity of composites with respect to volume fraction of fibers in Fig. 5.5. Again, we find out that VAMUCH results lie between the variational bounds of Donea (1972). And the results of Hashin lower bound (Hashin, 1983), Behrens (1968), and Hatta and Taya (1986) are identical but slightly lower than VAMUCH results when the volume fraction of fibers is higher than 40%. Similarly, as in the previous case, we can observe that Donea (1972) provides much narrower bounds than Hashin (1983) for this case.

We also use ANSYS, a commercial FEM package, to calculate the effective thermal conductivities of these three fiber reinforced composites. According to Islam and Pramila (1999), we apply isothermal conditions to the edges perpendicular to the direction we want to evaluate the thermal conductivity and apply adiabatic conditions to the edges parallel to this direction. The effective thermal conductivity is obtained by the ratio between the average heat flux and average temperature gradient. We found out that VAMUCH results are almost the same as the ANSYS results for similar discretization schemes.

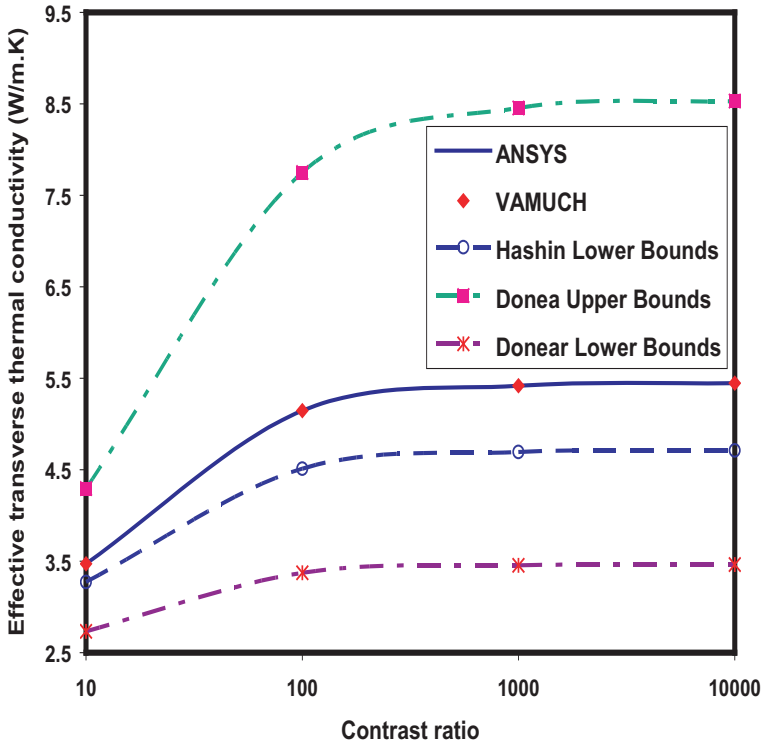

Fig. 5.6: Effective transverse thermal conductivity with respect to varying contrast ratios.

To verify whether VAMUCH can deal with composites with very high contrast ratio and high volume fraction, we choose a composite formed by circular fibers arranged in square array. The volume fraction of fibers is 65%. We fix the thermal conductivity of matrix at 1 W/(m · K), while the thermal conductivity of the fiber varies from 10 to 10^4. We plot the effective thermal conductivity computed using different approaches at different contrast ratio in Fig. 5.6. It can be seen that VAMUCH results are on the top of ANSYS results and lie between Donea variational bounds. And the results of Hashin lower bound (Hashin, 1983) are identical to those obtained from Behrens (1968), Halpin-Tsai (Progelhof et al., 1976), and Hatta and Taya (1986). It is obvious that these approaches underpredict the results. At different contrast ratio, the Hashin upper bounds are too large to be nicely plotted in the same figure.

5.5.2 Effective Thermal Conductivity of Particle Reinforced Composites

Due to special arrangements of constituents of particle reinforced composites, 3D UCs are required to accurately model the microstructures. In this section, we will use VAMUCH to analyze two typical particle reinforced composites to validate the 3D predictive capability

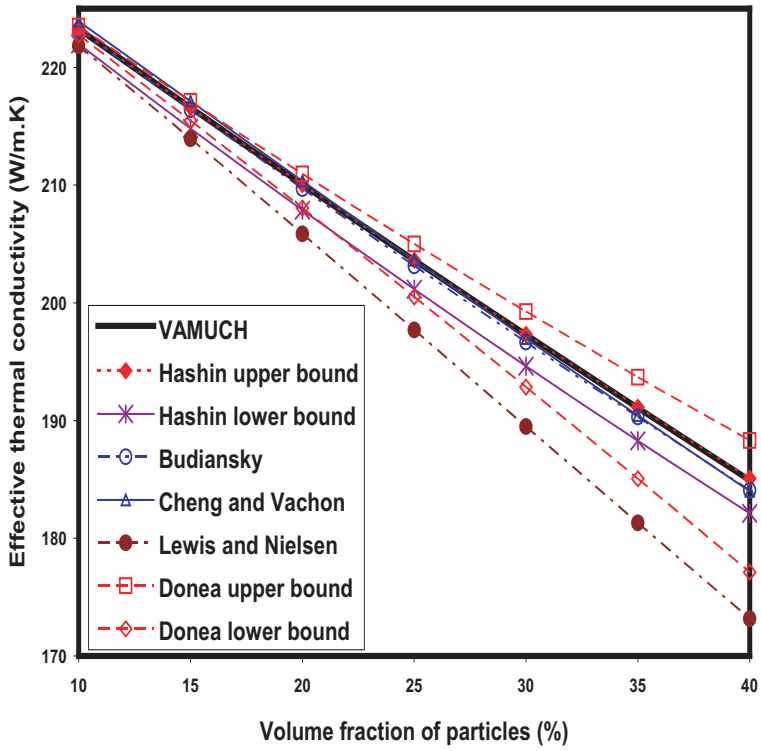

Fig. 5.7: Effective thermal conductivity of the Sic/Al composite.

of VAMUCH.

The first example is a SiC particle reinforced aluminum composite. The spherical SiC particles are embedded in a triply periodic cubic array. Both constituents are isotropic with thermal conductivity $K = 120$ W/(m $\cdot$ K) for SiC particles, and $K = 237$ W/(m $\cdot$ K) for aluminum matrix. The change of effective thermal conductivity of composites with respect to volume fraction of particles are plotted in Fig. 5.7. VAMUCH results have an excellent agreement with Hashin upper bound (Hashin, 1983), Budiansky (1970), and Cheng and Vachon (1970), although Budiansky (1970) and Cheng and Vachon (1970) slightly underpredict the results when the volume fraction of particles are higher than 20%. It was also found out that VAMUCH results are on the top of those calculated by McPhedran and Mckenzie (1978). All these predictions are perfectly located between the variational bounds of Donea (1972). It can be obviously observed that the results of Lewis and Nielsen (2003) significantly underpredict the effective thermal conductivity in comparison to other approaches.

Another example is an alumina (Al_2O_3) particle reinforced polyethylene composite. This composite has the same microstructure as the previous example. Both components

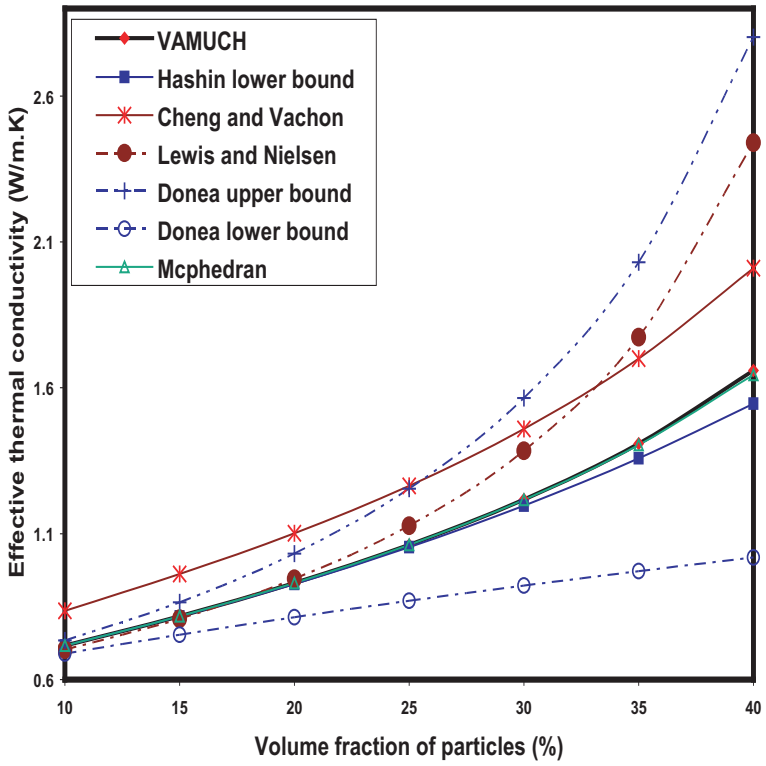

Fig. 5.8: Effective thermal conductivity of the Al_2O_3/polyethylene composite.

are also isotropic with thermal conductivity $K = 31$ W/(m $\cdot$ K) for alumina particles, and $K = 0.545$ W/(m $\cdot$ K) for the polyethylene matrix. The contrast ratio of thermal conductivity of two components is as high as 56.88. The predictions of different approaches are shown in Fig. 5.8. VAMUCH results agree with McPhedran and Mckenzie (1978) at different volume fraction and with the lower bound of Hashin (1983) very well if the volume fraction of particles is smaller than 25%. The prediction of Lewis and Nielsen (1970) is also very close to that of VAMUCH if the volume fraction of particles is very small. The difference between the variational bounds of Donea (1972) becomes too large to be useful for high volume fraction of particles. The prediction of Cheng and Vachon (1970) for this case cannot be considered as accurate because it is even not located between and lower and upper bounds of Donea (1972). We also need to point out that for this case, the results of Hashin upper bound are too different from the lower bound and cannot nicely plotted in the same figure.

We also analyzed these two examples of particle reinforced composites using ANSYS following the approach of Kumlutas and Tavman (2006). Again, we found out VAMUCH results are identical to ANSYS results if similar meshes are used for both approaches.

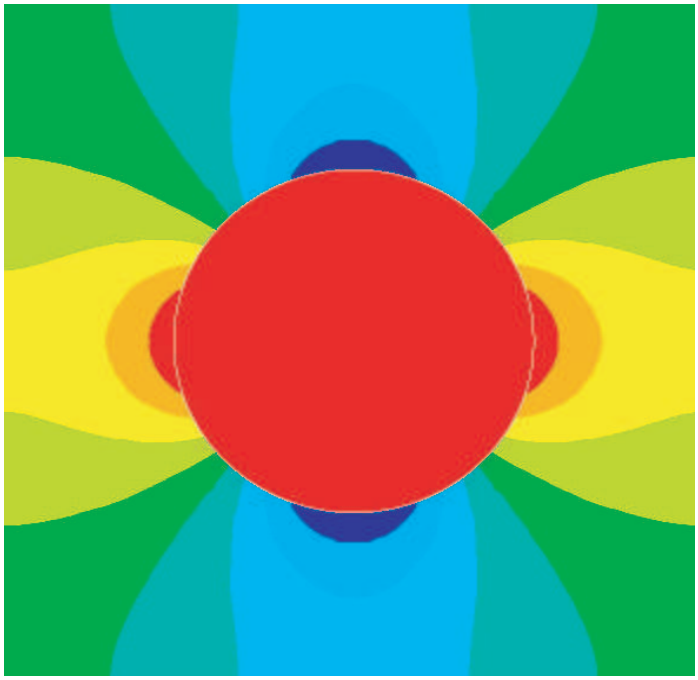

Fig. 5.9: Contour plot of heat flux q_2 in the glass/polypropylene composite.

It is noted that Hashin bounds are known to be the best possible bounds for statistically isotropic or transversely isotropic composites, when the only available geometrical information is the phase volume fractions (Hashin and Shtrikman, 1962). However, such bounds can be improved if additional information such as shape of inclusions, geometry of microstructure added into the formulation (Hashin, 1983). It has been shown that Hashin lower bound or upper bound is the exact solution for composite spheres assemblage (CSA) (Hashin, 1968), which explains why one of Hashin bounds agrees with VAMUCH very well if the inclusion volume fraction is not very large. Donea bounds (Donea, 1972) are not rigorous variational bounds. Rather the material is considered as a composition of CSA within the largest possible circle/sphere and matrix. The Voigt rule of mixtures is used to obtain the Donea upper bound and the Ruess rule of mixtures is used to obtain the Donea lower bound. The effective properties of CSA use those of Hashin (1968), which is also one of the Hashin bounds. Therefore, Donea bounds will fall outside at least one of Hashin bounds, as consistently shown in these examples. The gap between Donea bounds could be smaller that that of Hashin bounds because more information has been used in obtaining Donea bounds.

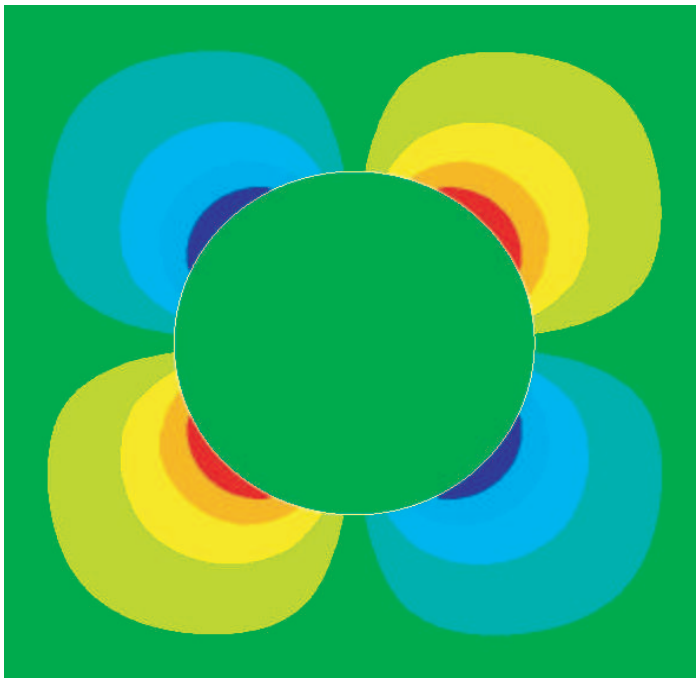

Fig. 5.10: Contour plot of heat flux q_3 in the glass/polypropylene composite.

5.5.3 Recovery of Local Heat Flux

VAMUCH can accurately recover the local heat flux distribution within the UC due to temperature gradients. We will use ANSYS results as benchmark to verify the prediction of VAMUCH. Firstly, we consider the glass/polypropylene fiber reinforced composite with fiber volume fraction as 0.2. Due to the difference of thermal conductivity of two components, the local heat flux distribution resulting from 100 K/m in the y_2 direction is not uniform within UC. The distribution contours of q_2 and q_3 are plotted in Figs. 5.9 and 5.10, respectively. The sudden changes of local heat flux around the interface between the fibers and the matrix are well captured by VAMUCH. For quantitative comparison, we also plot the local heat flux distribution q_2 along $y_2 = 0$ predicted by VAMUCH and ANSYS in Fig. 5.11. It can be seen that there are an excellent match between these two sets of results.

Secondly, we choose a special example which is a composite having an X-shape microstructure. The local heat flux distribution predicted by VAMUCH is shown in Fig. 5.12. There are narrow necks at corner contacts between the reinforcements which exhibit significant fluctuation of the local heat flux. The local heat flux distributions along the diagonal line predicted by VAMUCH and ANSYS are plotted in Fig. 5.13. Excellent match between these two approaches is clear from this plot.

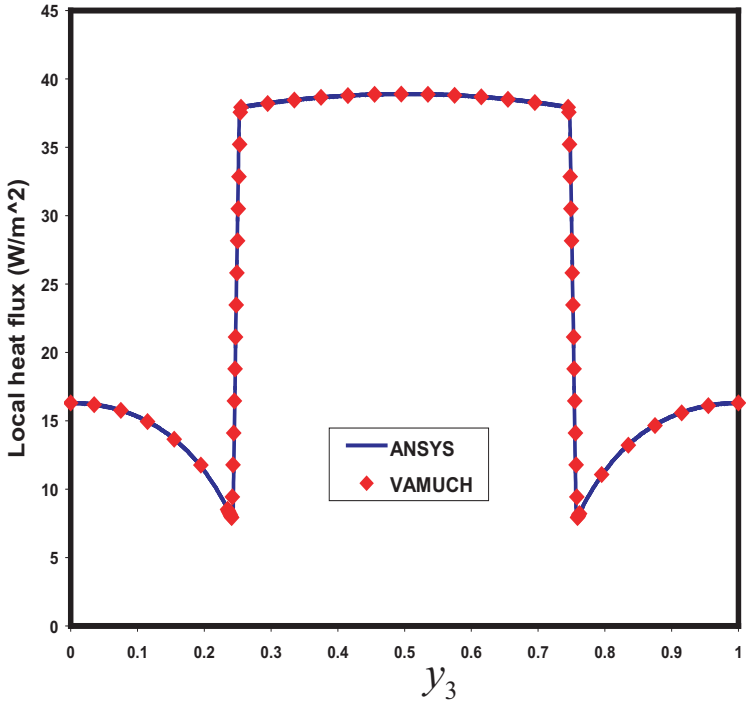

Fig. 5.11: Heat flux q_2 distribution along $y_2 = 0$ in the glass/polypropylene composite.

5.6 Conclusion

The variational asymptotic method for unit cell homogenization (VAMUCH) has been extended to predict effective thermal conductivity coefficients of composites. In comparison to existing models, the present theory has the following unique features:

1. It adopts the variational asymptotic method as its mathematical foundation. It invokes only essential assumptions inherent in the concept of micromechanics.

2. It has an inherent variational nature and its numerical implementation is shown to be straightforward.

3. It handles 1D/2D/3D unit cells uniformly. The dimensionality of the problem is determined by that of the periodicity of the unit cell.

The present theory is implemented in the computer program, VAMUCH. Numerous examples have clearly demonstrated its application and accuracy as a general-purpose micromechanical analysis tool. Although for the examples we have studied, VAMUCH results are almost identical to ANSYS results, VAMUCH has the following advantages over ANSYS for micromechanical analysis:

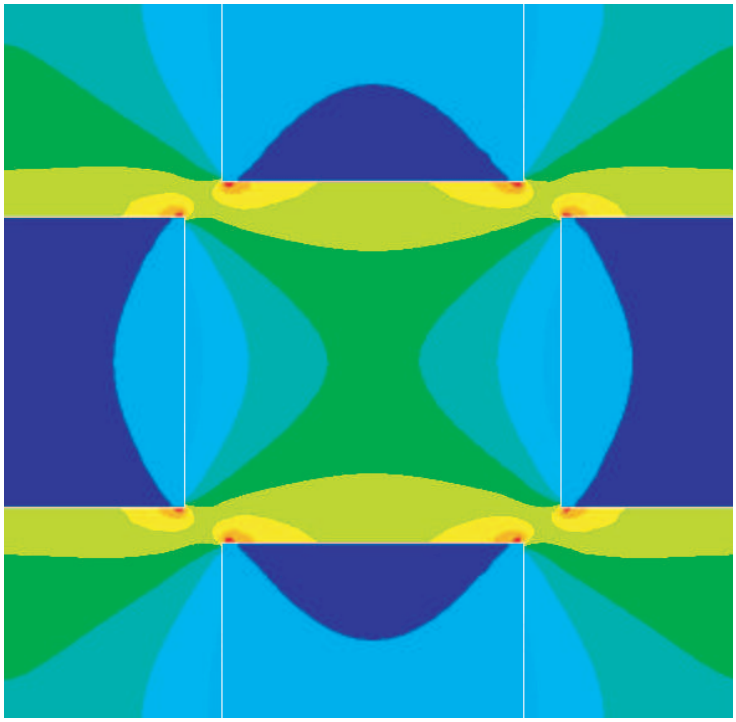

Fig. 5.12: Contour plot of heat flux of an X-shape composite.

1. VAMUCH can obtain different material properties in different directions simultaneously, which is more efficient than those approaches requiring multiple runs under different temperature conditions.

2. VAMUCH can model general anisotropic heterogeneous materials with constituents having full anisotropy (with six material constants for thermal conductivity), while ANSYS and other FEM package can only handle constituents up to orthotropic (with three material constants for thermal conductivity). The current FEM approaches for predicting thermal conductivity (Islam and Pramila, 1999; Kumlutas and Tavman, 2006) are restricted to be at most macroscopically orthotropic, which is an unnecessary restriction.

3. VAMUCH calculates effective properties and local fields directly with the same accuracy as the fluctuation functions. No postprocessing calculations which introduces more approximations, such as averaging temperature gradient and heat flux, are needed.

As a byproduct of validating VAMUCH, we also provided a brief assessment of existing models for predicting effective thermal conductivity.

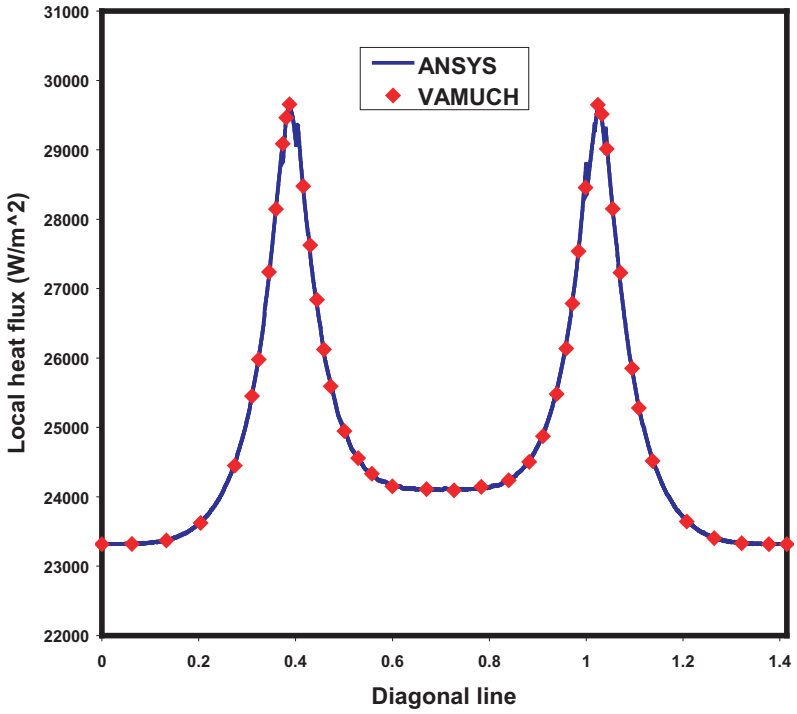

Fig. 5.13: Heat flux of of the X-shape composite along the diagonal line.

Due to the mathematical analogy of heat conduction, electrostatics, magnetostatics, and diffusion, the present theory and the companion code can also be used to predict effective dielectric, magnetic, and diffusion properties of heterogeneous materials.

References

E. Behrens, "Thermal conductivities of composite materials", *Journal of Composite Materials* **2** (1968), 2-17.

V. L. Berdichevsky, "On averaging of periodic systems", *PMM* **41**:6 (1977), 993-1006.

B. Budiansky, "Thermal and thermoelastic properties of isotropic composites", *Journal of Composite Materials* **4** (1970), 286-295.

S. Cheng and R. Vachon, "A technique for predicting the thermal conductivity of suspensions, emulsions and porous materials", *International Journal of Heat and Mass Transfer* **13** (1970), 537-546.

J. Donea, "Thermal conductivities based on variational principles", *Journal of Composite Materials* **6** (1972), 262-266.

D. Ganapathy, K. Singh, P. Phelan, R. Prasher, "An effective unit cell approach to compute the thermal conductivity of composites with cylindrical particles", *Journal of Heat Transfer* **127** (2005), 553-559.

Z. Hashin, "Assessment of the self consistent scheme approximation: conductivity of particulate composites", *Journal of Composite Materials* **2** (1968), 284-300.

Z. Hashin, "Analysis of composite materials-a survey", *Applied Mechanics Review* **50** (1983), 481-505.

Z. Hashin and S. Shtrikman, "A variational approach to the theory of the effective magnetic permeability of multiphase materials", *Journal of Applied Physics* **33** (1962), 3125-3131.

H. Hatta and M. Taya, "Thermal conductivity of coated filler composites", *Journal of Applied Physics* **59** (1986), 1851-1860.

M. R. Islam and A. Pramila, "Thermal conductivity of fiber reinforced composites by the FEM", *Journal of Composite Materials* **33** (1999), 1699-1715.

D. Kumlutas and I. Tavman, "A numerical and experimental study on thermal conductivity of particle filled polymer composites", *Journal of Thermoplastic Composite Materials* **19** (2006), 441-455.

I. Kunin, *Theory of Elastic Media with Microstructure*, vol. 1 and 2, Springer Verlag, 1982.

Y. M. Lee, R. B. Yang, and S. S. Gau, "A generalized self consistent method for calculation of effective thermal conductivity of composites with interfacial contact conductance", *International Communications in Heat and Mass Transfer* **33** (2006), 142-150.

T. Lewis and L. Nielsen, "Dynamic mechanical properties of particulate-filled composites", *Journal of Applied Polymer Science* **14** (2003), 1449-1471.

R. C. McPhedran and D. R. Mckenzie, "The conductivity of lattices of spheres I. the simple cubic lattice", *Proc. R. Soc. Lond. A* **359** (1978), 45-63.

R. Progelhof, J. Throne, and R. Ruetsch, "Methods for predicting the thermal conductivity of composite systems: a review", *Polymer Engineering and Science* **16** (1976), 615-625.

K. Ramani and A. Vaidyanathan, "Finite element analysis of effective thermal conductivity of filled polymeric composites", *Journal of Composite Materials* **29** (1995), 1725-1740.

G. Springer and S.Tsai, "Thermal conductivities of unidirectional materials", *Journal of Composite Materials* **1** (1967), 167-173.

Y. Xu and K. Yagi, "Calculation of the thermal conductivity of randomly dispersed composites using a finite element modeling method", *Materials Transactions* **45** (2004), 2602-2605.

W. Yu and T. Tang, "Variational asymptotic method for unit cell homogenization of periodically heterogeneous materials", *International Journal of Solids and Structures* **44**:11-12 (2007), 3738-3755.

W. Yu and T. Tang, "A variational asymptotic micromechanics model for predicting thermoelastic properties of heterogeneous materials", *International Journal of Solids and Structures* **44**:22-23 (2007), 7510-7525.

Chapter 6

Asymptotical Approach to Initial Yielding Surface and Elastoplasticity of Metal Matrix Composites

[1]

Abstract

The focus of this paper is to develop a micromechanics model based on the variational asymptotic method for unit cell homogenization (VAMUCH) for predicting of the initial yielding surface, overall instantaneous moduli, and elastoplastic behavior of metal matrix composites. Considering the size of the microstructure as a small parameter, we can formulate a variational statement of the unit cell through an asymptotic expansion of the energy functional. To handle realistic microstructures, we implement this new model using the finite element method. For model validation, we used a few examples to demonstrate the application and accuracy of this theory and the companion code.

6.1 Introduction

Metal matrix composites (MMC) are widely used in structural components due to their primary advantages of high stiffness, high strength, better fatigue resistance, and better elevated temperature properties. To successfully design and fabricate these materials, we need efficient high-fidelity analysis tools to predict their effective properties. Accurate prediction of initial yielding surface and uniaxial tension behavior is the major research of interest for MMC.

It is well known that the mechanical behavior of MMC is determined by many factors including the failure of fiber, interface debonding, and failure of matrix or yielding of matrix. The yielding strength and work-hardening modulus of composite system are greatly increased by the high stiffness reinforcements due to double reductions of stress and plastic strain experienced by matrix. Firstly, the hard reinforcements are main load-carrying components which sustain a higher stress so that the magnitude of stress undertaken by matrix

[1] Coauthored by: Tian Tang and Wenbin Yu.

is significantly reduced. Secondly, the plastic strain only contributed by metal matrix is further reduced due to the volume fraction of this phase. In addition, the yielding in matrix is a highly localized phenomenon due to the heterogeneity of composite system. Therefore, accurate stress prediction within the microstructure is obviously required.

Numerous models have been proposed to predict the initial yielding surface and elasto-plastic behavior of MMC. These models include the simplest vanishing fiber diameter (VFD) model [1], self consistent scheme [2,3], finite element micromechanics modeling [4-7], method of cell and its variants [8-12], and many others. A detailed review on inelastic micromechanics models is provided by [13]. Very recently, a general-purpose framework for micromechanics modeling, namely variational asymptotic method for unit cell homogenization (VAMUCH) [14], has been developed. VAMUCH adopts two essential assumptions in the context of micromechanics for composites with an identifiable unit cell (UC):

- **Assumption 1** The exact field variable has volume average over the UC. For example, if Δu_i are the exact displacement increments within the UC, there exist Δv_i such that

$$\Delta v_i = \frac{1}{\Omega}\int_{\Omega} \Delta u_i \, \mathrm{d}\Omega \equiv \langle \Delta u_i \rangle \tag{6.1}$$

  where Ω denotes the domain occupied by the UC and its volume.

- **Assumption 2** The effective material properties obtained from the micromechanical analysis of the UC are independent of the geometry, the boundary conditions, and loading conditions of the macroscopic structure, which means that effective properties are assumed to be the intrinsic properties of the material when viewed macroscopically.

Note that these assumptions are not restrictive. The mathematical meaning of the first assumption is that the exact solutions of the field are integrable over the domain of UC, which is true almost all the time. The second assumption implies that we will neglect the size effects of the material properties in the macroscopic analysis, which is an assumption often made in the conventional continuum mechanics. For clarification, it is worthwhile to point out that for nonlinear materials, the material properties is directly related with the stress state at the point we want to evaluate the material properties. Of course, the micromechanical analysis of the UC is only needed and appropriate if $\eta = h/l \ll 1$, with

h as the characteristic size of the UC and l as the macroscopic size of the macroscopic material.

This new micromechanical modeling approach has been successfully applied to predict linear thermal and mechanical properties including elastic properties, coefficients of thermal expansion, specific heats, and conductivity [14-16]. In this work, we will use this approach to construct micromechanics models for predicting the initial yielding surface and elastoplastic behavior of MMCs.

6.2 Theoretical Formulation

VAMUCH formulation uses three coordinates systems: two Cartesian coordinates $\mathbf{x} = (x_1, x_2, x_3)$ and $\mathbf{y} = (y_1, y_2, y_3)$, and an integer-valued coordinate $\mathbf{n} = (n_1, n_2, n_3)$ (see Figure 6.1). We use x_i as the global coordinates to describe the macroscopic structure and y_i parallel to x_i as the local coordinates to describe the UC (Here and throughout the paper, Latin indices assume 1, 2, and 3 and repeated indices are summed over their range except where explicitly indicated). We choose the origin of the local coordinates y_i to be the geometric center of UC. For example, if the UC is a cube with the edge lengths d_i, then $y_i \in [-\frac{d_i}{2}, \frac{d_i}{2}]$. To uniquely locate a UC in the heterogeneous material we also introduce integer coordinates n_i. The integer coordinates are related to the global coordinates in such a way that $n_i = x_i/d_i$ (no summation over i). It is emphasized although only square array is sketched in Fig. 6.1, the present theory has not such limitations.

As implied by Assumption 2, we can obtain the same effective properties from an imaginary, unbounded, and unloaded heterogeneous material with the same microstrucutre as the real, loaded, and bounded one. Hence we could derive the micromechanics model from an imaginary, unloaded, heterogeneous material which completely occupies the three-dimensional (3D) space $\mathcal{R}$ and composes of infinitely many repeating UCs. In the case of plastic loading, the total energy changes is equal to the summation of the energy changes of all the UCs [17], which is:

$$\Pi = \sum_{n=-\infty}^{\infty} \int_{\Omega} d\sigma_{ij}\ d\epsilon_{ij} \mathrm{d}\Omega = \sum_{n=-\infty}^{\infty} \frac{1}{2} \int_{\Omega} C_{ijkl} d\epsilon_{ij}\ d\epsilon_{kl} \mathrm{d}\Omega \tag{6.2}$$

where C_{ijkl} are the components of the fourth-order instantaneous tangent stiffness tensor and can be expressed as follows:

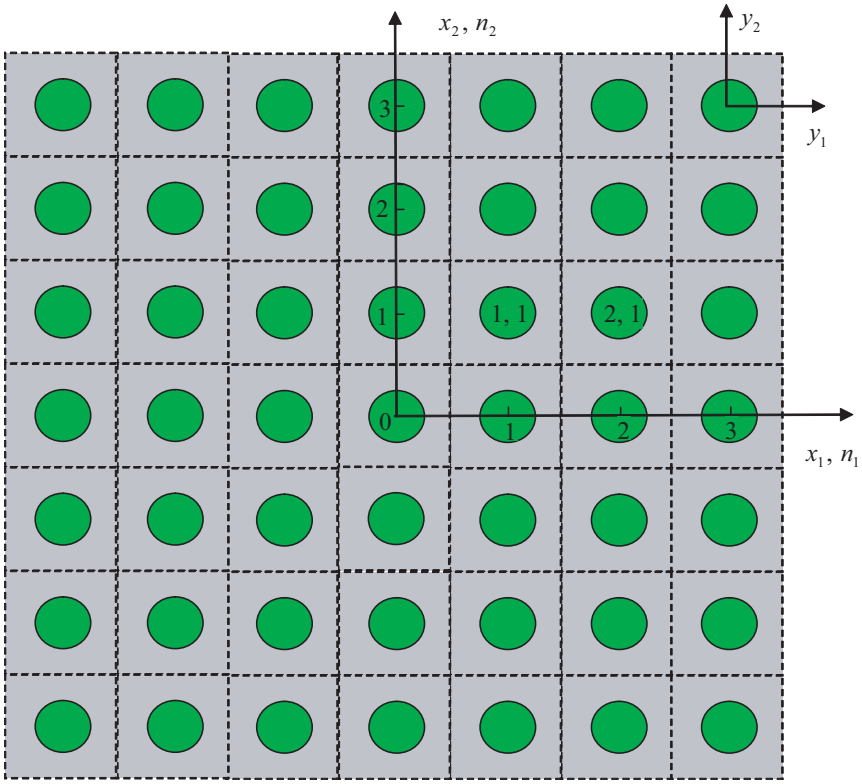

Fig. 6.1: Coordinate systems for heterogenous materials (only two-dimensional (2D) UC is drawn for clarity).

$$C_{ijkl} = \begin{cases} C^{e}_{ijkl} \text{ (elastic stiffness)} & \text{if in elastic loading} \\ C^{ep}_{ijkl} \text{ (elastic-plastic tangent stiffness)} & \text{if in plastic loading} \end{cases}$$

and

$$d\epsilon_{ij}(\mathbf{n};\mathbf{y}) = \frac{1}{2}\left[\frac{\partial \Delta u_i(\mathbf{n};\mathbf{y})}{\partial y_j} + \frac{\partial \Delta u_j(\mathbf{n};\mathbf{y})}{\partial y_i}\right] \tag{6.3}$$

Here $\Delta u_i(\mathbf{n};\mathbf{y})$ is a function of the integer coordinates and the local coordinates for each UC. In view of the fact that the infinite many UCs form a continuous heterogeneous material, we need to enforce the continuity of the displacement changes Δu_i on the interface between adjacent UCs, which can be written as follows for a UC with integer coordinates (n_1, n_2, n_3):

$$\begin{aligned} \Delta u_i(n_1, n_2, n_3; d_1/2, y_2, y_3) &= \Delta u_i(n_1+1, n_2, n_3; -d_1/2, y_2, y_3) \\ \Delta u_i(n_1, n_2, n_3; y_1, d_2/2, y_3) &= \Delta u_i(n_1, n_2+1, n_3; y_1, -d_2/2, y_3) \\ \Delta u_i(n_1, n_2, n_3; y_1, y_2, d_3/2) &= \Delta u_i(n_1, n_2, n_3+1; y_1, y_2, -d_3/2) \end{aligned} \tag{6.4}$$

According to the principle of minimum energy rate [17], the exact solution will minimize

the summation of energy changes in Eq. (6.2) under the constraints in Eqs. (6.1), (6.4). To avoid the difficulty associated with discrete integer arguments, we can reformulate the problem, including Eqs. (6.2), (6.3), and (6.4), in terms of continuous functions using the idea of quasicontinuum [18]. The basic idea is to associate a function of integer arguments defined in the integer space with a continuous function defined in $\mathcal{R}$. The corresponding formulas are listed below.

$$\Pi = \frac{1}{2}\int_{\mathcal{R}} \langle C_{ijkl}\, d\epsilon_{ij}\, d\epsilon_{kl}\rangle \,\mathrm{d}\mathcal{R} \tag{6.5}$$

$$d\epsilon_{ij}(\mathbf{x};\mathbf{y}) = \frac{1}{2}\left[\frac{\partial \Delta u_i(\mathbf{x};\mathbf{y})}{\partial y_j} + \frac{\partial \Delta u_j(\mathbf{x};\mathbf{y})}{\partial y_i}\right] \equiv \Delta u_{(i|j)} \tag{6.6}$$

and

$$\begin{aligned}
\Delta u_i(x_j; d_1/2, y_2, y_3) &= \Delta u_i(x_j + d_1\delta_{j1}; -d_1/2, y_2, y_3)\\
\Delta u_i(x_j; y_1, d_2/2, y_3) &= \Delta u_i(x_j + d_2\delta_{j2}; y_1, -d_2/2, y_3)\\
\Delta u_i(x_j; y_1, y_2, d_3/2) &= \Delta u_i(x_j + d_3\delta_{j3}; y_1, y_2, -d_3/2)
\end{aligned} \tag{6.7}$$

where δ_{ij} is the Kronecker symbol. Using the technique of Lagrange multipliers, we can pose the variational statement of the micromechanics analysis of UC as a stationary value problem of the following functional:

$$\begin{aligned}
J = \int_{\mathcal{R}} \Bigg\{ & \left\langle \frac{1}{2} C_{ijkl}\, \Delta u_{(i|j)}\, \Delta u_{(k|l)} \right\rangle + \lambda_i(\langle \Delta u_i\rangle - \Delta v_i)\\
& + \int_{S_1} \gamma_{i1}\left[\Delta u_i(x_j; d_1/2, y_2, y_3) - \Delta u_i(x_j + d_1\delta_{j1}; -d_1/2, y_2, y_3)\right] \mathrm{d}S_1\\
& + \int_{S_2} \gamma_{i2}\left[\Delta u_i(x_j; y_1, d_2/2, y_3) - \Delta u_i(x_j + d_2\delta_{j2}; y_1, -d_2/2, y_3)\right] \mathrm{d}S_2\\
& + \int_{S_3} \gamma_{i3}\left[\Delta u_i(x_j; y_1, y_2, d_3/2) - \Delta u_i(x_j + d_3\delta_{j3}; y_1, y_2, -d_3/2)\right] \mathrm{d}S_3 \Bigg\} \mathrm{d}\mathcal{R}
\end{aligned} \tag{6.8}$$

where λ_i and γ_{ij} are Lagrange multipliers introduced in Eqs. (6.1) and (6.4), respectively, and S_i is the surface normal to the corresponding y_i axis. The main objective of micromechanics is to find the real displacement change field Δu_i in terms of Δv_i, which is a very difficult problem because we have to solve this stationary problem for each point in the global system x_i as in Eq. (6.8). It will be desirable if we can formulate the variational statement posed over a single UC only. In view of Eq. (6.1), it is natural to express the

exact solution Δu_i as a sum of the volume average Δv_i plus the difference, such that

$$\Delta u_i(\mathbf{x};\mathbf{y}) = \Delta v_i(\mathbf{x}) + w_i(\mathbf{x};\mathbf{y}) \tag{6.9}$$

where $\langle w_i \rangle = 0$ according to Eq. (6.1). The very reason that the heterogenous material can be homogenized leads us to believe that w_i should be asymptotically smaller than Δv_i, *i.e.*, $w_i \sim \eta\, \Delta v_i$. Substituting Eq. (6.9) into Eq. (6.8) and making use of Eq. (6.3), we can obtain the leading terms of the functional according to the variational asymptotic method [19] as:

$$\begin{aligned} J_1 = \int_{\mathcal{R}} \Bigg\{ & \left\langle \frac{1}{2} C_{ijkl}\, w_{(i|j)}\, w_{(k|l)} \right\rangle + \lambda \langle w_i \rangle \\ & + \int_{S_1} \gamma_{i1} \left[w_i(\mathbf{x}; d_1/2, y_2, y_3) - w_i(\mathbf{x}; -d_1/2, y_2, y_3) - \Delta v_{i,1} d_1 \right] \mathrm{d}S_1 \\ & + \int_{S_2} \gamma_{i2} \left[w_i(\mathbf{x}; y_1, d_2/2, y_3) - w_i(\mathbf{x}; y_1, -d_2/2, y_3) - \Delta v_{i,2} d_2 \right] \mathrm{d}S_2 \\ & + \int_{S_3} \gamma_{i3} \left[w_i(\mathbf{x}; y_1, y_2, d_3/2) - w_i(\mathbf{x}; y_1, y_2, -d_3/2) - \Delta v_{i,3} d_3 \right] \mathrm{d}S_3 \Bigg\} \mathrm{d}\mathcal{R} \end{aligned} \tag{6.10}$$

where $()_{,i} \equiv \frac{\partial ()}{\partial x_i}$. Although it is possible to carry out the variation of J_1 and find the Euler-Lagrange equtions and associated boundary conditions for w_i, which results in inhomogeneous boundary conditions, it is more convenient to use change of variables to reformulate the same problem so that the boundary conditions are homogeneous. Considering the last three terms in Eq. (6.10), we use the following change of variables to express w_i as:

$$w_i(\mathbf{x};\mathbf{y}) = y_i \Delta v_{i,j} + \chi_i(\mathbf{x};\mathbf{y}) \tag{6.11}$$

with χ termed as fluctuation functions for displacement changes. We are free to choose the origin of the local coordinate system to be the center of UC, which implies the following constraints on χ_i:

$$\langle \chi_i \rangle = 0 \tag{6.12}$$

Now, our problem becomes to solve χ_i in terms of Δv_i, which can be posed as the stationary value problem of the following functional defined over UC:

$$\begin{aligned} J_\Omega = & \frac{1}{2}\left\langle C_{ijkl}\left[d\bar{\epsilon}_{ij}+\chi_{(i|j)}\right]\left[d\bar{\epsilon}_{kl}+\chi_{(k|l)}\right]\right\rangle + \lambda_i\left\langle\chi_i\right\rangle \\ & + \int_{S_1}\gamma_{i1}(\chi_i^{+1}-\chi_i^{-1})\mathrm{d}S_1 + \int_{S_2}\gamma_{i2}(\chi_i^{+2}-\chi_i^{-2})\mathrm{d}S_2 \\ & + \int_{S_3}\gamma_{i3}(\chi_i^{+3}-\chi_i^{-3})\mathrm{d}S_3 \end{aligned} \tag{6.13}$$

with

$$\chi_i^{+j} = \chi_i|_{y_j=d_j/2},\ \chi_i^{-j} = \chi_i|_{y_j=-d_j/2} \quad \text{for} \quad j=1,2,3$$

where $d\bar{\epsilon}_{ij} \equiv \frac{1}{2}(\Delta v_{i,j}+\Delta v_{j,i})$ will be shown later to be the components of the global strain increment tensor for the effective material with homogenized material properties. The functional J_Ω in Eq. (6.13) forms the backbone of the present theory. This stationary problem can be solved analytically for very simple cases such as binary composites, however, for general cases we need to use numerical techniques such as the finite element method (FEM) to seek numerical solutions.

6.3 Finite Element Implementation

It is possible to formulate the FEM solution based on Eq. (6.13), however, it is not the most convenient and efficient way because Lagrange multipliers will increase the number of unknowns. To this end, we can reformulate the variational statement in Eq. (6.13) as the stationary value of the following functional

$$\Pi_\Omega = \frac{1}{2\Omega}\int_\Omega C^{ep}_{ijkl}\left[d\bar{\epsilon}_{ij}+\chi_{(i|j)}\right]\left[d\bar{\epsilon}_{kl}+\chi_{(k|l)}\right]\mathrm{d}\Omega \tag{6.14}$$

under the following nine constraints

$$\chi_i^{+j} = \chi_i^{-j} \quad \text{for} \quad i,j=1,2,3 \tag{6.15}$$

The constraint in Eq. (6.12) does not affect the minimum value of Π_Ω but help uniquely determine χ_i. In practice, we can constrain the fluctuation function at an arbitrary node to be zero and later use this constraint to recover the unique fluctuation function. It is fine to use penalty function method to introduce the constraints in Eqs. (6.15). However, this

method introduces additional approximation and the robustness of the solution depends on the choice of large penalty numbers. Here, we choose to make the nodes on the positive boundary surface (*i.e.*, $y_i = d_i/2$) slave to the nodes on the opposite negative boundary surface (*i.e.*, $y_i = -d_i/2$). By assembling all the independent active degrees of freedom, we can implicitly and exactly incorporate the constraints in Eqs. (6.15). In this way, we also reduce the total number of unknowns in our finite element formulation.

Introduce the following matrix notations

$$d\bar{\epsilon} = \lfloor d\bar{\epsilon}_{11} \;\; 2d\bar{\epsilon}_{12} \;\; d\bar{\epsilon}_{22} \;\; 2d\bar{\epsilon}_{13} \;\; 2d\bar{\epsilon}_{23} \;\; d\bar{\epsilon}_{33} \rfloor^T \tag{6.16}$$

$$\epsilon_1 = \begin{Bmatrix} \frac{\partial \chi_1}{\partial y_1} \\ \frac{\partial \chi_1}{\partial y_2} + \frac{\partial \chi_2}{\partial y_1} \\ \frac{\partial \chi_2}{\partial y_2} \\ \frac{\partial \chi_1}{\partial y_3} + \frac{\partial \chi_3}{\partial y_1} \\ \frac{\partial \chi_2}{\partial y_3} + \frac{\partial \chi_3}{\partial y_2} \\ \frac{\partial \chi_3}{\partial y_3} \end{Bmatrix} = \begin{bmatrix} \frac{\partial}{\partial y_1} & 0 & 0 \\ \frac{\partial}{\partial y_2} & \frac{\partial}{\partial y_1} & 0 \\ 0 & \frac{\partial}{\partial y_2} & 0 \\ \frac{\partial}{\partial y_3} & 0 & \frac{\partial}{\partial y_1} \\ 0 & \frac{\partial}{\partial y_3} & \frac{\partial}{\partial y_2} \\ 0 & 0 & \frac{\partial}{\partial y_3} \end{bmatrix} \begin{Bmatrix} \chi_1 \\ \chi_2 \\ \chi_3 \end{Bmatrix} \equiv \Gamma_h \chi \tag{6.17}$$

where Γ_h is an operator matrix. If we discretize χ using the finite elements as

$$\chi(x_i; y_i) = G(y_i)\mathcal{X}(x_i) \tag{6.18}$$

where G representing the shape functions and $\mathcal{X}$ a column matrix of the nodal values of the fluctuation function. Substituting Eqs. (6.16), (6.17), and (6.18) into Eq. (6.14), we obtain a discretized version of the functional as

$$\Pi_\Omega = \frac{1}{2\Omega}(\mathcal{X}^T F \mathcal{X}^T + 2\mathcal{X}^T D_{h\epsilon} d\bar{\epsilon} + d\bar{\epsilon}^T D_{\epsilon\epsilon} d\bar{\epsilon}) \tag{6.19}$$

where

$$\begin{aligned} F &= \int_\Omega (\Gamma_h G)^T D (\Gamma_h G) \mathrm{d}\Omega \\ D_{h\epsilon} &= \int_\Omega (\Gamma_h G)^T D \mathrm{d}\Omega \\ D_{\epsilon\epsilon} &= \int_\Omega D \mathrm{d}\Omega \end{aligned} \tag{6.20}$$

with D as the 6×6 tangent stiffness matrix condensed from the fourth order elastoplastic

tangent stiffness tensor C^{ep}_{ijkl}. Minimizing Π_Ω in Eq. (6.19), we obtain the following linear system

$$F\mathcal{X} = -D_{h\epsilon} d\bar{\epsilon} \tag{6.21}$$

It is clear from Eq. (6.21) that the fluctuation function $\mathcal{X}$ is linearly proportional to $d\bar{\epsilon}$, which means the solution can be written symbolically as

$$\mathcal{X} = \mathcal{X}_0 \; d\bar{\epsilon} \tag{6.22}$$

Substituting Eq. (6.22) into Eq. (6.19), we can calculate the energy change density of the UC as

$$\Pi_\Omega = \frac{1}{2\Omega} d\bar{\epsilon}^T \left(\mathcal{X}_0^T D_{h\epsilon} + D_{\epsilon\epsilon} \right) d\bar{\epsilon} \equiv \frac{1}{2} d\bar{\epsilon}^T D^* d\bar{\epsilon} \tag{6.23}$$

It can be seen that D^* in Eq. (6.23) is the effective elastoplastic tangent stiffness matrix and $d\bar{\epsilon}$ global strain increments.

The increments of the local fields can be recovered in terms of the macroscopic behavior including the increments of the global displacements Δv_i and the global strain $d\epsilon_{ij}$, and the fluctuation function χ. First, we need to uniquely determine the fluctuation functions. Considering the fact that we fixed an arbitrary node and made nodes on the positive boundary surfaces slave to the corresponding negative boundary surfaces, we need to construct a new array $\tilde{\mathcal{X}}_0$ from $\mathcal{X}_0$ by assigning the values for slave nodes according to the corresponding active nodes and assign zero to the fixed node. Obviously, $\tilde{\mathcal{X}}_0$ still yield the minimum value of Π_Ω in Eq. (6.14) under constraints in Eqs. (6.15). However, $\tilde{\mathcal{X}}_0$ may not satisfy Eqs. (6.12). The real solution, denoted as $\bar{\mathcal{X}}_0$ can be found trivially by adding a constant corresponding to each DOF to each node so that Eqs. (6.12) are satisfied.

The increments of the local displacements can be recovered using the uniquely determined fluctuation function and Eqs. (6.9) and (6.11) as

$$\begin{Bmatrix} \Delta u_1 \\ \Delta u_2 \\ \Delta u_3 \end{Bmatrix} = \begin{Bmatrix} \Delta v_1 \\ \Delta v_2 \\ \Delta v_3 \end{Bmatrix} + \begin{bmatrix} \frac{\partial \Delta v_1}{\partial x_1} & \frac{\partial \Delta v_1}{\partial x_2} & \frac{\partial \Delta v_1}{\partial x_3} \\ \frac{\partial \Delta v_2}{\partial x_1} & \frac{\partial \Delta v_2}{\partial x_2} & \frac{\partial \Delta v_2}{\partial x_3} \\ \frac{\partial v_3}{\partial x_1} & \frac{\partial v_3}{\partial x_2} & \frac{\partial v_3}{\partial x_3} \end{bmatrix} \begin{Bmatrix} y_1 \\ y_2 \\ y_3 \end{Bmatrix} + \bar{S}\bar{\mathcal{X}} \tag{6.24}$$

where $\bar{S}$ is different from S due to the recovery of slave nodes and the constrained node. The local strain field and electric field can be recovered using (6.6), (6.9), (6.11), and

(6.17) as

$$d\epsilon = d\bar{\epsilon} + \Gamma_h \bar{S} \bar{\mathcal{X}} \tag{6.25}$$

The increments of the local stresses can be recovered straightforwardly using the 3D constitutive relations for the constituent material as

$$d\sigma = D^* d\epsilon \tag{6.26}$$

6.4 VAMUCH Prediction of Initial Yielding Surface

The excellent stress recover capability of VAMUCH [15] can be used to predict the initial yielding surface of MMCs under various loading conditions. If the fibers are assumed to be completely elastic, the initial yielding within matrix will occur when the most heavily loaded point reaches yielding stress. We choose the Von Mises yielding criterion given by:

$$\begin{aligned} f(\sigma_{ij}) = \Bigg\{ \frac{1}{2} \left[(\sigma_{11} - \sigma_{22})^2 + (\sigma_{11} - \sigma_{33})^2 + (\sigma_{22} - \sigma_{33})^2 \right] \\ + 3 \left(\sigma_{12}^2 + \sigma_{13}^2 + \sigma_{23}^2 \right) \Bigg\}^{\frac{1}{2}} - Y \end{aligned} \tag{6.27}$$

where$f(\sigma_{ij})$ and Y are the yielding function and the yielding strength of matrix in simple tension, respectively. In practice, the initial yielding point was determined by finding the first Gauss point within matrix at which $f(\sigma_{ij}) = 0$. The composites exhibit linear elastic behavior before initial yielding. For some situations, such as the binary composites and the stress-strain curve along the fiber direction for fiber reinforced composites, the uniaxial stress-strain curve can be described in terms of the initial yielding point and tangent moduli.

6.5 VAMUCH for the Simulation of the Elastoplastic Behavior of the Composite

The simulation of the nonlinear elastic-plastic behavior of composite materials of VAMUCH is performed in terms of incremental procedure, which is similar to those used by Aboudi [20-24] and [25] and can be described as the following steps:

1. Input the material properties of constituents to calculate the initial effective instantaneous stiffness D^*_{ijkl} of composite materials.

2. Input the given overall stress increment, evaluate the corresponding overall strain increment using $d\epsilon_{ij} = S^*_{ijkl} d\sigma_{kl}$, where $S^*_{ijkl} = D^{*-1}_{ijkl}$.

3. Update the ovarall stresses, strains, and instantaneous stiffness of the composite at the end of the increment:

$$\bar{\sigma}_{ij} = \bar{\sigma}_{ij}|_{previous} + d\bar{\sigma}_{ij} \tag{6.28}$$

$$\bar{\epsilon}_{ij} = \bar{\epsilon}_{ij}|_{previous} + d\bar{\epsilon}_{ij} \tag{6.29}$$

4. Recover the distribution of the local fields, i.e., local stresses and local strains within UC at the end of the increment using the increments of the global field variables.

5. Evaluate the von Mises stress of material points within UC. If the material yields, the instantaneous tangent stiffness tensor is C^{ep}_{ijkl}. Otherwise, it is C^{e}_{ijkl}. Then calculate the effective instantaneous tangent stiffness D^*_{ijkl} of composite materials.

Step (2) to (5) are repeated in the next increment. The present approach has the same advantage as that of GMC and HFGMC developed by Aboudi. It does not need to impose different boundary conditions as well as symmetry conditions as is carried out in finite element unit cell procedure [26]. It also has the advantage of finite element method, namely, geometrical versatility.

6.6 Validation Examples

In this section, several examples will be used to demonstrate the accuracy of VAMUCH for predicting the initial yielding surface, effective elastoplastic tangent moduli, and uniaxial tension stress-strain curve of MMCs. In all the examples, the material of metal matrix is described by bilinear work-hardening model, but the extension of present theory to other nonlinear models is straightforward.

6.6.1 Material Properties

For simplicity, we assume the reinforcements are isotropic and perfectly elastic. The inelastic behavior of isotropic matrix is described by the classical theory of plasticity and

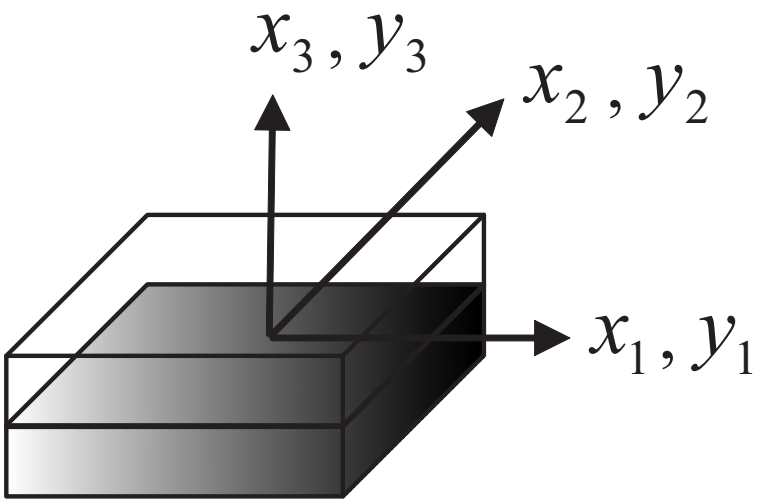

Fig. 6.2: Sketch of a binary composite.

the incremental stress-strain relation of matrix is given by:

$$d\sigma_{ij} = \left(C_{ijkl} - \frac{C_{ijmn}\frac{\partial f}{\partial \sigma_{mn}}\frac{\partial f}{\partial \sigma_{pq}}C_{pqkl}}{\frac{\partial f}{\partial \sigma_{rs}}C_{rstu}\frac{\partial f}{\partial \sigma_{tu}} - \frac{\partial f}{p}\sqrt{\frac{2}{3}\frac{\partial f}{\partial \sigma_{dw}}\frac{\partial f}{\partial \sigma_{dw}}}} \right) d\epsilon_{kl} \tag{6.30}$$

or

$$\mathbf{d}\sigma = \mathbf{C}^{ep}\mathbf{d}\epsilon \tag{6.31}$$

where $\mathbf{C}^{ep}$ is called the elastoplastic tensor of tangent moduli; f and p in Eq. (6.30) are yielding function and effective plastic strain, respectively; C_{ijkl} is the fourth-order elastic tensor.

6.6.2 Binary Composites

Firstly, we will consider a periodic binary composite made of isotropic layers and the material axes are the same as the global coordinate x_i so that the material is uniform in the $x_1 - x_2$ plane and periodic along x_3 direction. A typical UC can be identified as shown in Figure 6.2, with the dimension along y_3 as h and dimensions along y_1 and y_2 arbitrary. Let ϕ_1 and ϕ_2 denote the volume fraction of the first layer and the second layer, respectively, and we have $\phi_1 + \phi_2 = 1$.

For the sake of comparison, we also use ANSYS, a commercial FEM package, to calculate the effective tangential moduli and uniaxial stress-strain curve. To this end, we assign material properties with Young'modulus $E = 800$GPa and Poisson'ratio $\nu = 0.1$ for layer

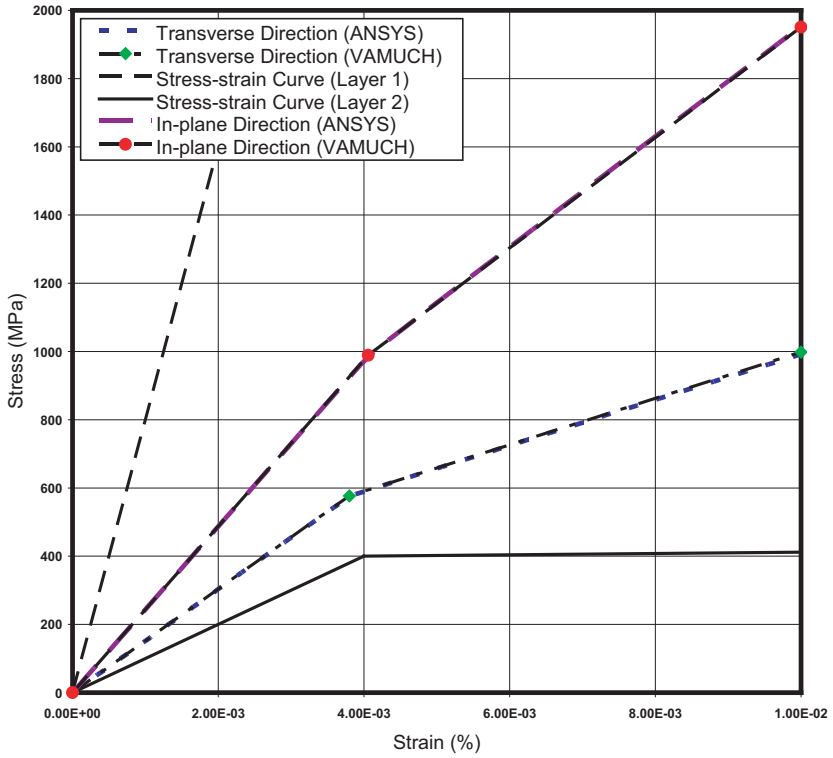

Fig. 6.3: Stress-strain curve of a binary composite.

1, and Young'modulus $E = 100$GPa, Poisson'ratio $\nu = 0.35$, tangent modulus $E_t = 2$GPa, and yielding strength $\sigma_0 = 0.4$GPa for layer 2. The volume fraction of layer 1 is 20%. Figure 6.3 shows the uniaxial stress-strain curve obtained from VAMUCH and ANSYS. It can be seen that the predictions of VAMUCH are right on the top of ANSYS results. In this special case, the global yielding point of composites is identical to that of matrix which means once the matrix reaches yielding the stress-strain curve of composites begin to occur non-linearity. VAMUCH can precisely predict this yielding point and the tangent moduli after yielding.

6.6.3 Fiber Reinforced Composites

To show the predictive capability of VAMUCH for unidirectional fiber reinforced composites, the example chosen is boron fiber reinforced aluminum matrix composites. The fiber is of circular shape and arranged in square array. Both constituents are isotropic with with Young'modulus $E = 379.3$GPa, Poisson'ratio $\nu = 0.1$, and CTE $\alpha = 8.1\ 10^{-6}$/K for boron fiber, and Young'modulus $E = 68.3$GPa, Poisson'ratio $\nu = 0.3$, tangent modulus $E_t = 2$GPa, yielding strength $\sigma_0 = 0.4$GPa, and CTE $\alpha = 23.0\ 10^{-6}$/K for aluminum

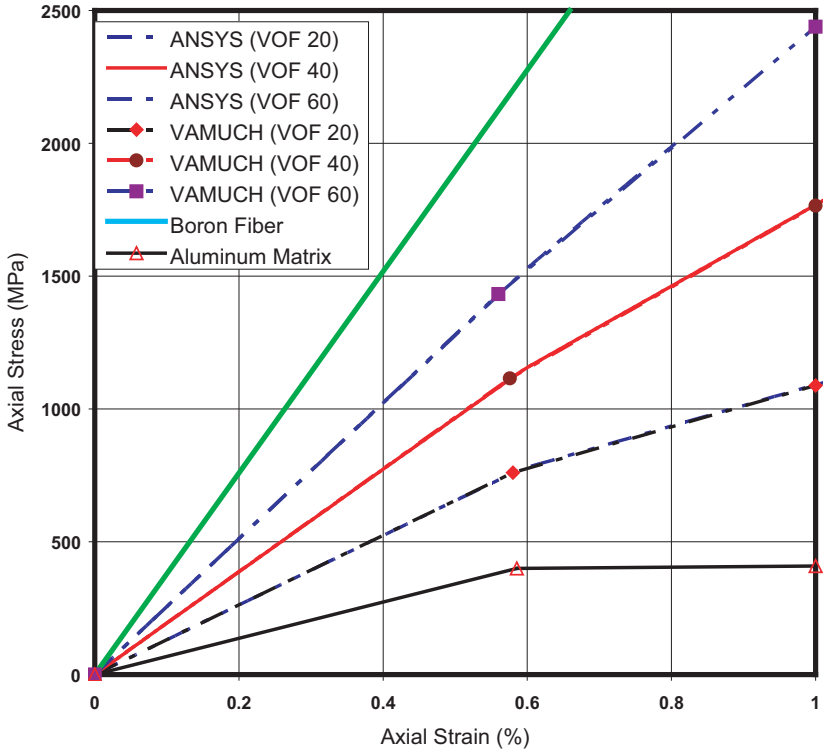

Fig. 6.4: Stress-strain curve of a Boron/Aluminum composite.

matrix.

The axial stress-strain curves of composites with three different volume fraction (VOF 20, VOF 40, and VOF 60) are plotted in Figure 6.4. Similarly as the previous binary composite example, the stress-strain curve of the effective material is simply described by the initial yielding point and tangent modulus. VAMUCH results have excellent agreement with ANSYS, although ANSYS has to trace the curve pointwisely because it has no direct means to obtain the initial yielding point and tangent modulus. The global yielding point of fiber reinforced composites in the axial direction is the same as that of matrix.

To investigate the initial yielding surface, we choose the composite with VOF 20. The initial yielding surfaces under a bi-axial loading along both transverse directions are shown in Figure 6.5. Both predictions of VAMUCH and ANSYS are plotted. The stresses are normalized with respect to the yielding strength, σ_0, of matrix which is common practice in most literature. It can be seen that the initial yielding surface is symmetric about 45° line corresponding to equal transverse stresses. Figure 6.6 depicts the yielding surfaces obtained from VAMUCH and ANSYS under axial and transverse normal loading. It can be clearly observed that VAMUCH results are exactly on the top of ANSYS results for

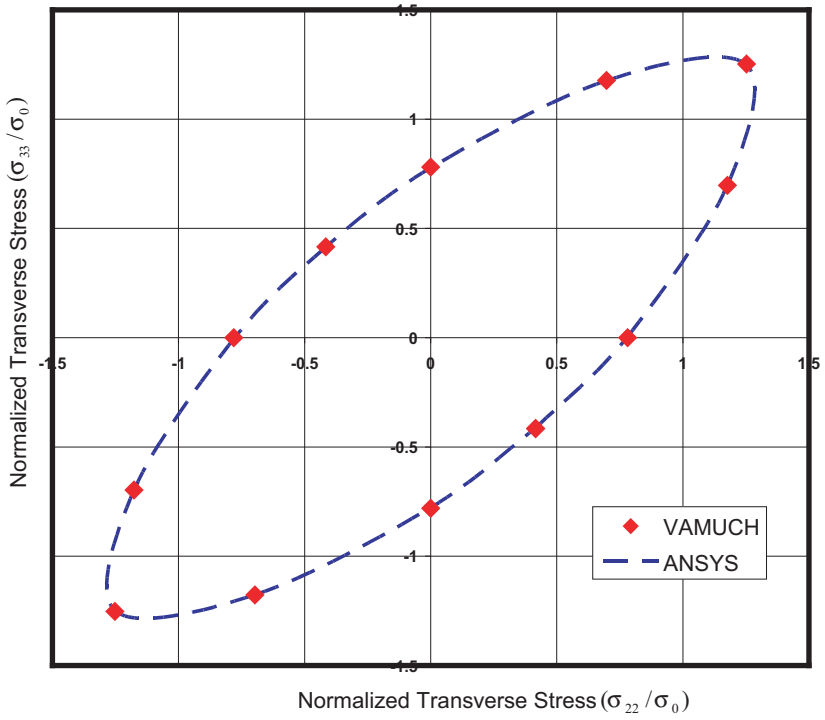

Fig. 6.5: Initial yielding surface of a Boron/Aluminum composite under transverse/transverse loading.

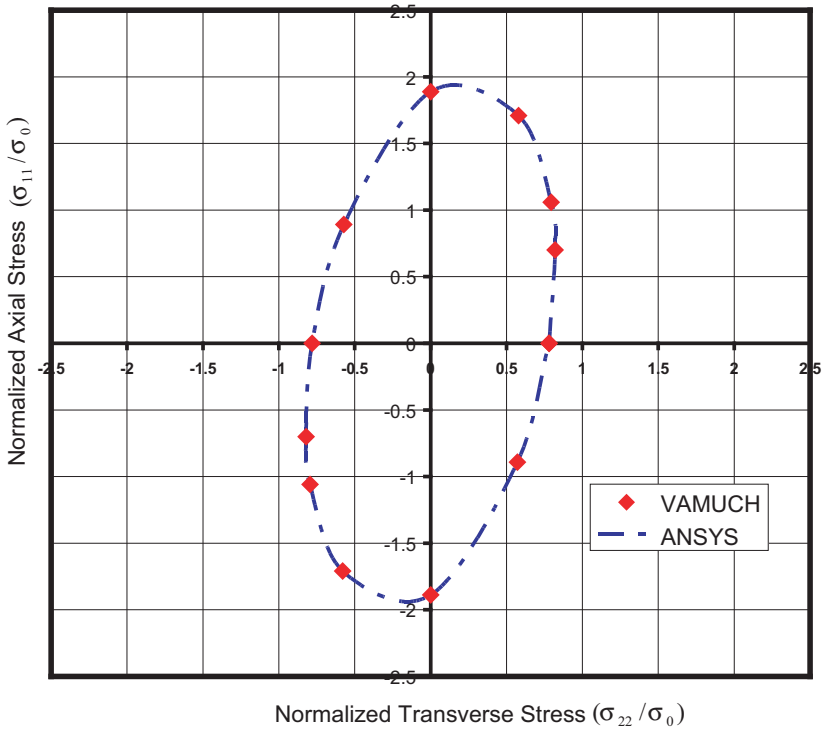

Fig. 6.6: Initial yielding surface of a Boron/Aluminum composite under axial/transverse loading.

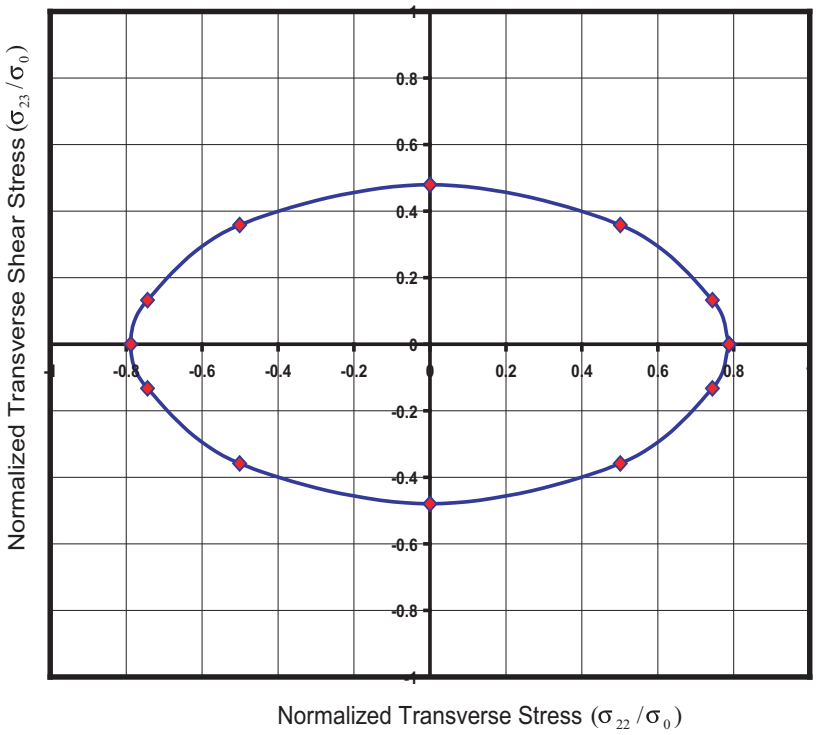

Fig. 6.7: Initial yielding surface of a Boron/Aluminum composite under transverse normal and shear loading.

these two loading conditions. The predictions of initial yielding surface of VAMUCH for other loading conditions including transverse normal and shear loading, axial normal and transverse shear loading, and axial shear loading in two directions are shown in Figures 6.7, 6.8, and 6.9, respectively. VAMUCH can also predict the initial yielding surfaces under different temperature changes of the material as shown in Figure 6.10, where the composite undergoes bi-axial external loading and unform temperature change. It can be seen that the presence of thermal stresses resulted from temperature change shifts the yielding surface along the direction corresponding to equal normal stresses. It is noted that the curve corresponding to "0 K", *i.e.*, temperature remains the same, is the same as that in Figure 6.5.

6.7 Conclusion

VAMUCH, a general-purpose micromechanics modeling framework, has been generalized to predict initial yielding surfaces, elastoplastic tangent moduli, and uniaxial stress-strain curve of composites. In comparison to existing models, the present theory has the following unique features:

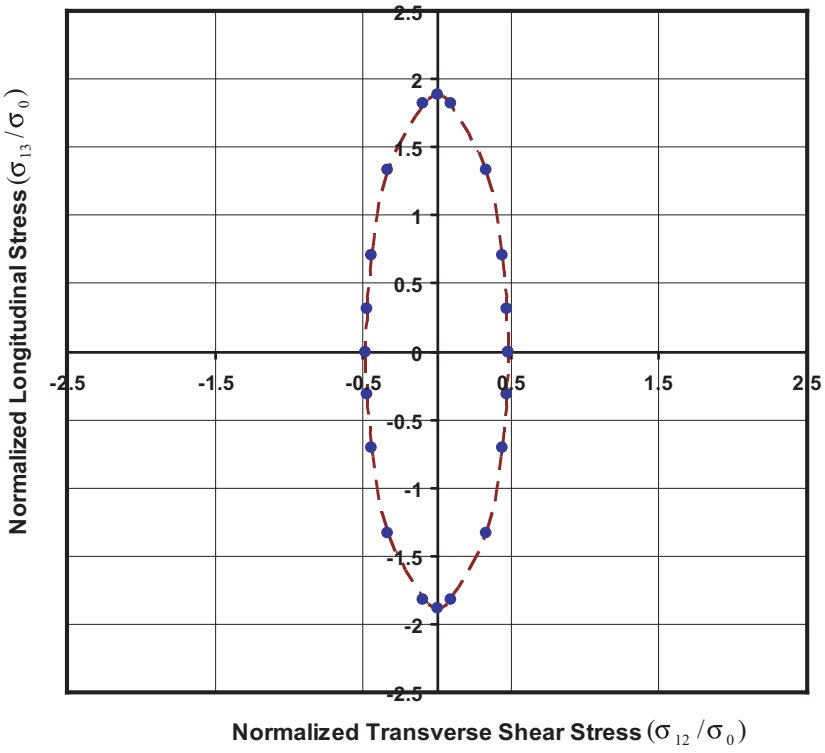

Fig. 6.8: Initial yielding surface of a Boron/Aluminum composite under axial normal and transverse shear loading.

1. It adopts the variational asymptotic method as its mathematical foundation. It invokes only essential assumptions inherent in the concept of micromechanics.

2. It has an inherent variational nature and its numerical implementation is shown to be straightforward.

3. It handles 1D/2D/3D unit cells uniformly. The dimensionality of the problem is determined by that of the periodicity of the unit cell.

The present theory is implemented in the computer program, VAMUCH. Several examples have been used to demonstrate its application and accuracy as a general-purpose micromechanical analysis tool for nonlinear composites.

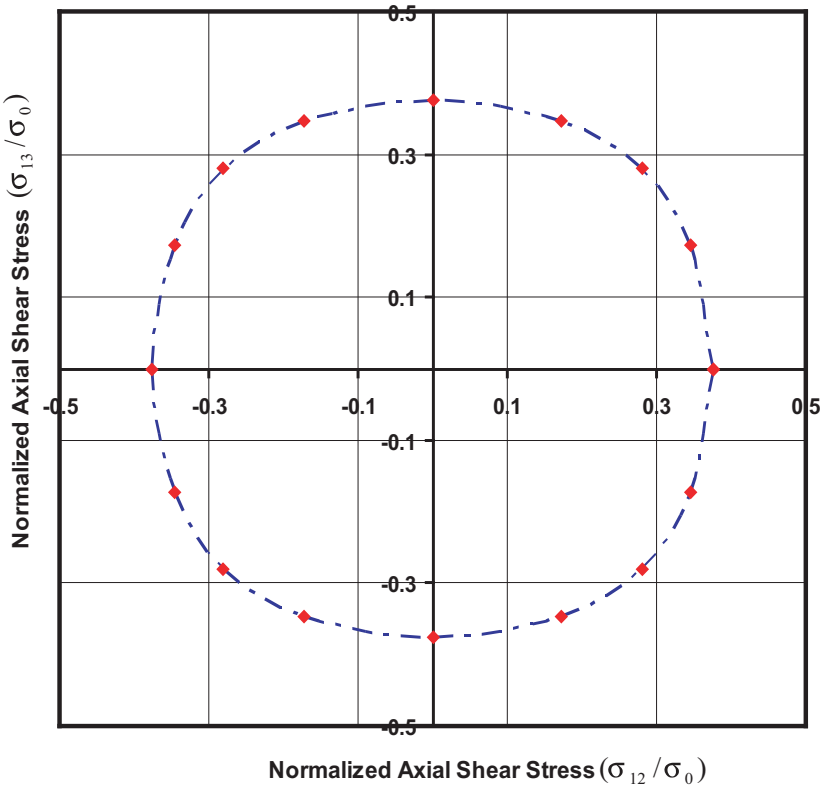

Fig. 6.9: Initial yielding surface of a Boron/Aluminum composite under axial shear loading in two directions.

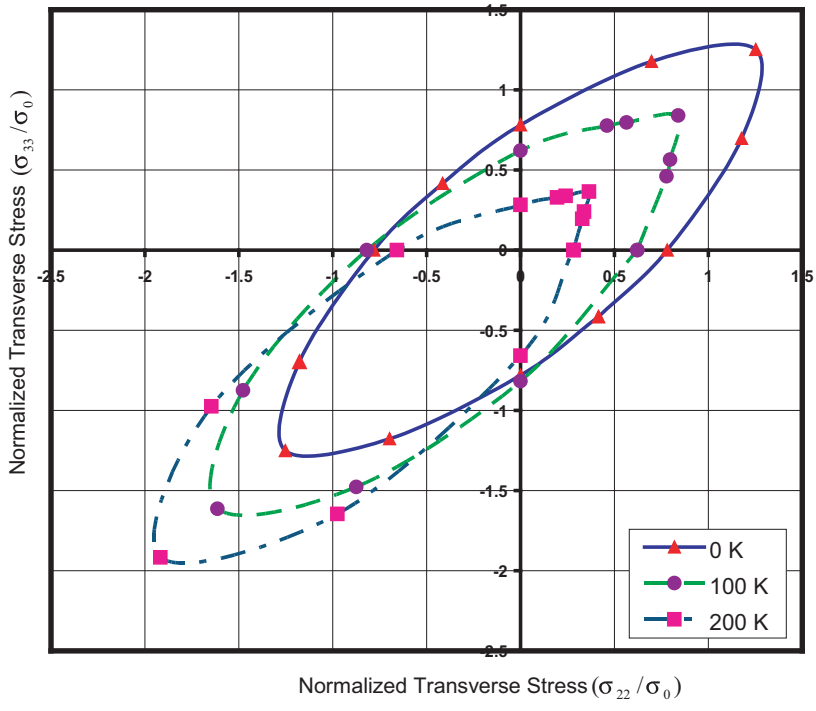

Fig. 6.10: Initial yielding surface of a Boron/Aluminum composite under transverse/transverse loading along with temperature changes.

References

1. Dvorak, G.J. and BAHEI-EL-DIN, Y.A., "Plasticity analysis of fibrous composites," *Journal of Applied Mechanics*, Vol. 49, 1982, pp. 327-335.

2. Hill, R., "A self-consistent mechanics of composite materials," *Journal of the Mechanics of Physics and Solids*, Vol. 13, 1965, pp. 213-222.

3. Budiansky, B., "On the elastic moduli of some heterogeneous materials," *Journal of the Mechanics of Physics and Solids*, Vol. 13, 1965, pp. 223-227.

4. Lin, Y. H., Salinas, D., and Ito, Y. M., "Initial yield surface of a unidirectionally reinforced composites," *Journal of Applied Mechanics*, Vol. 39, 1972, pp. 321-326.

5. Dvorak, G.J., Rao, M. S. M., and Tran, J. Q., "Yielding in unidirectional composites under external loads and temperature change," *Journal of Composite Materials*, Vol. 7, 1973, pp. 194-216.

6. Dvorak, G.J., Rao, M. S. M., and Tran, J. Q., "Generalized initial yield surfaces for unidirectional composites," *Journal of Applied Mechanics*, Vol. 41, 1974, pp. 249-253.

7. Aghdam, M. M., Smith, D. J., and Pavier, M. J., "Finite element micromechanical modeling of yield and collapse behavior of metal matrix composites," *Journal of the Mechanics of Physics and Solids*, Vol. 48, 2000, pp. 499-528.

8. Aboudi, J., "Elastoplasticity theory for composite materials," *Solid Mech.Arch.*, Vol. 11, 1986, pp. 141-183.

9. Aboudi, J., "Closed form constitutive equations for metal matrix composites," *International Journal of Engineering Science*, Vol. 25, 1987, pp. 1129-1240.

10. Aboudi, J., "Micromechanical analysis of composites by the method of cells," *Appl. Mech. Rev*, Vol. 42, 1989, pp. 193-221.

11. Aboudi, J., "Micromechanical prediction of initial and subsequent yield surfaces of metal matrix composites," *International Journal of Plasticity*, Vol. 6, 1990, pp. 471-484.

12. Aboudi, J., Pindera, M. J., and Arnold, S. M., "High-fidelity generalization method of cells for inelastic periodic multiphase materials," NASA/TM-2002-211469, Vol. 2, 2002.

13. Allen, D.H., Jones, R.H., and Boyd., J.G., "Micromechanical analysis of a continuous fiber metal matrix composite including the effects of matrix viscoplasticity and evolving damage," *Journal of the Mechanics of Physics and Solids*, Vol. 42, 1994, pp. 505–529.

14. Yu, W. and Tang, T., "Variational asymptotic method for unit cell homogenization of periodically heterogeneous materials," *International Journal of Solids and Structures*, Vol. 44, 2007, pp. 3738–3755.

15. Yu, W. and Tang, T., "A variational asymptotic micromechanics model for predicting thermoelastic properties of heterogeneous materials," *International Journal of Solids and Structures*, to appear, 2007.

16. Tang, T. and Yu, W., "A new micromechanics model for predicting effective thermal conductivity of heterogeneous materials," *Proceedings of the 48th Structures, Structural Dynamics, and Materials Conference*, Waikiki, Hawaii, April 2007.

17. Bahei-El-Din, A. Yehia and Dvorak, G.J., "A review of plasticity theory of fibrous composite materials," *Metal Matrix Composites-Testing, Analysis and Failure Modes*, ASTM International, 1989, pp. 103-130.

18. Kunin, I., *Theory of Elastic Media with Microstructure*, vols. 1 and 2, Springer Verlag, 1982.

19. Berdichevsky, V. L., "On averaging of periodic systems," *PMM*, Vol. 41, No. 6, 1977, pp. 993-1006.

20. Paley, M. and Aboudi, J., "Micromechanical analysis of composites by the generalized cells model," *Mechanics of Materials*, Vol. 14, 1992, pp. 127-139.

21. Aboudi, J., "Micromechanical prediction of the finite thermoelastic response of rubberlike matrix composites," *Z. angew. Math. Phys.*, Vol. 52, 2001, pp. 823-846.

22. Aboudi, J., "Micromechanical analysis of the finite elastic-viscoplastic response of multiphase composites," *International Journal of Solids and Structures*, Vol. 40, 2003, pp. 2793-2817.

23. Aboudi, J., "Micromechanical prediction of the response of electrostrictive multiphase composites," *Smart Materials and Structures*, Vol. 8, 1999, pp. 663-671.

24. Aboudi, J., "Hysteresis behavior of ferroelectric fiber composites," *Smart Materials and Structures*, Vol. 14, 2005, pp. 715-726.

25. Pettermann, H.E., Plankensteiner, A.F., Böhm, H.J., and Rammerstorfer, F.G., "A thermo-elasto-plastic constitutive law for inhomogeneous materials based on an incremental mori-tanaka approach," *Computers and Structures*, Vol. 71, 1999, pp. 197-214.

26. Sun, C.T., and Vaidya, R.S., "Prediction of composite properties from a representative volume element," *Composites Science and Technololy*, Vol. 56, 1996, pp. 171-179.

Chapter 7

Micromechanics Modeling of the Nonlinear Behavior of Electrostrictive Multiphase Composites

[1]

Abstract

The micromechanics modeling of the nonlinear behavior of the electrostrictive multiphase composites is developed using an incremental formulation based on the variational asymptotic method for unit cell homogenization (VAMUCH), a recently developed micromechanics modeling scheme. The microstructure of composites is assumed to be periodic. Taking advantage of the small size of the microstructure, we formulate a variational statement of energy change of the unit cell through an asymptotic analysis of the functional by invoking only two essential assumptions within the concept of micromechanics. Finally, the expression of the effective instantaneous tangential electromechanical matrix of the composites are established. Several numerical examples will be used to demonstrate the capability of the present theory.

7.1 Introduction

Electrostriction is a higher-order electro-mechanical coupling in all dielectric materials in which the strain induced by the application of the external electrical field depends on the polarization or electric field quadratically [1]. However, the electrostrictive strain generated in most dielectric materials is too small to be of practical use, while certain dielectric materials such as PMN ceramics exhibit sufficiently large electrostrictive strain in the order of 0.1% [2] that can be used in actuator applications. A detailed review on electrostrictive materials is given in [3]. Hom and Shankar [4] established a three-dimensional, electromechanical constitutive equation for electrostrictive ceramic materials. This constitutive relation depends on a manageable number of material constants instead of polynomial expansions. They [5] later incorporated the electrostrictive constitutive model into a nonlinear finite element

[1] Coauthored by: Tian Tang and Wenbin Yu.

code to analyze the performance of electrostrictive devices in composite structures. Li and Rao [6] developed a nonlinear micromechanics model that links the macroscopic behavior of ferroelectric polymer-based electrostrictive composites with their microstructural details. Aboudi [7] employed GMC for the prediction of the nonlinear behavior of electrostrictive multiphase composites of which the nonlinear electrostrictive constitutive equations were constructed by Hom and Shankar [4].

In this paper, a micromechanics model is developed for the prediction of macroscopic behavior of electrostrictive multiphase composites. This model is based on the framework of the variational asymptotic method for unit cell homogenization (VAMUCH) [8-13], which is build upon the variational asymptotic method [14] along with two essential assumptions within the concept of micromechanics for composites with an identifiable unit cell (UC):

- **Assumption 1** The exact solutions of the increments of the field variables have volume averages over the UC. For example, if Δu_i and $\Delta\phi$ are the exact increments of the displacement and electric potential within the UC, respectively, there exist Δv_i and $\Delta\psi$ such that

$$\Delta v_i = \frac{1}{\Omega}\int_\Omega \Delta u_i \, \mathrm{d}\Omega \equiv \langle \Delta u_i \rangle \tag{7.1}$$

$$\Delta\psi = \frac{1}{\Omega}\int_\Omega \Delta\phi \, \mathrm{d}\Omega \equiv \langle \Delta\phi \rangle \tag{7.2}$$

- **Assumption 2** The effective nonlinear material behavior obtained from the micromechanical analysis of the UC are independent of the geometry, the boundary conditions, and loading conditions of the macroscopic structure, which means that the effective nonlinear behavior are assumed to be the intrinsic properties of the material when viewed macroscopically.

Note that these assumptions are not restrictive. The mathematical meaning of the first assumption is that the exact solutions of the field variables can be integrated over the domain of UC, which is true almost all the time. For the second assumption, it is worthwhile to point out that for materials with nonlinear behavior, the effective tangent properties is directly related with the local micro fields such as the stress, strain, and electrical state at the point we want to evaluate the material properties. Of course, the micromechanical analysis of the UC is only needed and appropriate if $\eta = h/l \ll 1$, with h as the characteristic size of the UC and l as the macroscopic size of the material. Other assumptions such as particular

geometry shape and arrangement of the constituents, specific boundary conditions applied to the UC, and prescribed relations between local fields and global fields are not necessary for this study.

7.2 Basic Equations

The nonlinearly coupled electromechanical constitutive equations of electrostrictive materials considered here can be given by [15]:

$$\begin{aligned} \sigma_{ij} &= C_{ijkl}\epsilon_{kl} - B_{ijkl}E_kE_l \\ D_i &= \kappa_{ij}E_j + 2M_{klij}\sigma_{kl}E_j \end{aligned} \tag{7.3}$$

where σ_{ij} and ϵ_{kl} are the stress tensor and strain tensor, respectively; D_i and E_j are the vectors of electric displacement and electric field respectively; C_{ijkl}, κ_{ij}, and M_{klij} are the elastic stiffness, dielectric constant, and electrostrictive constant, respectively; and $B_{ijkl} = C_{ijmn}M_{mnkl}$.

Since the constitutive equations are nonlinear, we can transform these equations into an incremental form as:

$$d\sigma = Y\,d\epsilon \tag{7.4}$$

where

$$\begin{aligned} d\sigma &= \lfloor d\sigma_{11}, d\sigma_{12}, d\sigma_{22}, d\sigma_{13}, d\sigma_{23}, d\sigma_{33}, -dD_1, -dD_2, -dD_3 \rfloor^T \\ d\epsilon &= \lfloor d\epsilon_{11}, 2d\epsilon_{12}, d\epsilon_{22}, 2d\epsilon_{13}, 2d\epsilon_{23}, d\epsilon_{33}, dE_1, dE_2, dE_3 \rfloor^T \end{aligned} \tag{7.5}$$

and the instantaneous tangent electromechanical coupling matrix is symmetric and given by:

$$Y = \begin{bmatrix} Y_1 & Y_2 \\ Y_3 & Y_4 \end{bmatrix} \tag{7.6}$$

where Y_1 is a 6×6 elastic stiffness matrix; Y_2 is a 6×3 electromechanical coupling matrix; Y_3 is the transpose matrix of Y_2; and Y_4 is a 3×3 square matrix representing the electric behavior of the material. The elements of Y_2 and Y_3 are the function of the local electric fields, while the elements of Y_4 are the functions of the local strains and the local electric fields.

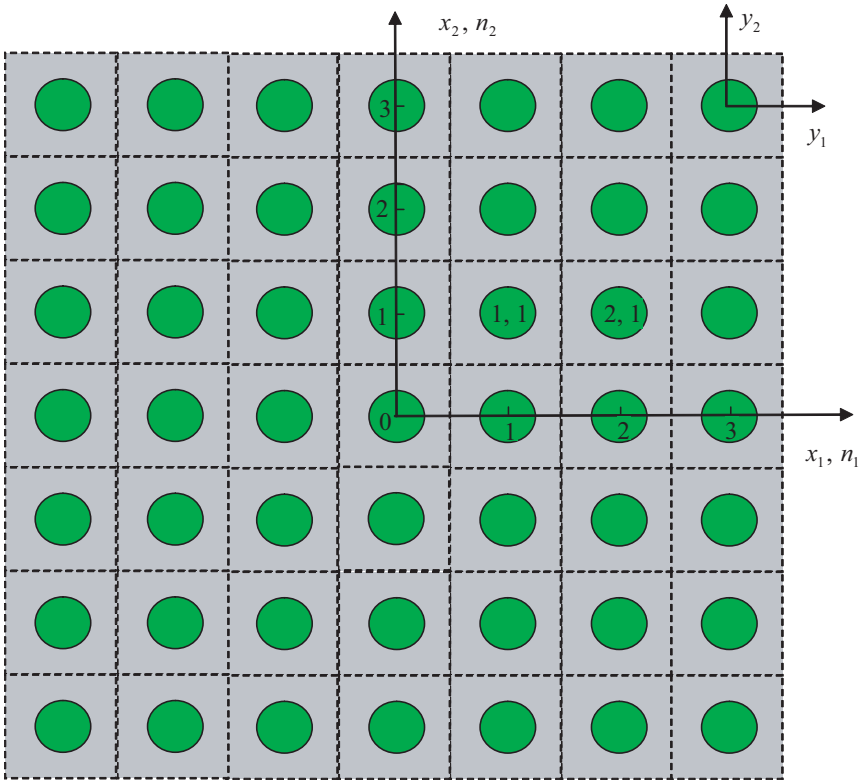

Fig. 7.1: Coordinate systems for heterogenous materials (only two-dimensional (2D) UC is drawn for clarity).

For multiphase electrostrictive composite materials, the effective tangential constitutive equation is given by:

$$d\bar{\sigma} = Y^* d\bar{\epsilon} \tag{7.7}$$

where "overbar" means the volume averaged value, and superscript "*" stands for the effective tangent properties.

7.3 Theoretical Formulation

Three coordinates systems are used in our formulation: two cartesian coordinates $\mathbf{x} = (x_1, x_2, x_3)$ and $\mathbf{y} = (y_1, y_2, y_3)$, and an integer-valued coordinates $\mathbf{n} = (n_1, n_2, n_3)$ (see Fig. 7.1). We use x_i as the global coordinates to describe the macroscopic structure and y_i parallel to x_i as the local coordinates to describe the UC (Here and throughout the paper, Latin indices assume 1, 2, and 3 and repeated indices are summed over their range except where explicitly indicated). We choose the origin of the local coordinates y_i to be the geometric center of UC. For example, if the UC is a cube with dimensions as d_i, then

$y_i \in [-\frac{d_i}{2}, \frac{d_i}{2}]$. To uniquely locate a UC in the heterogeneous material we also introduce integer coordinates n_i. The integer coordinates are related to the global coordinates in such a way that $n_i = x_i/d_i$ (no summation over i). It is emphasized although only square array is sketched in Fig. 7.1, the present theory has no such limitations.

According to the essential Assumption 2, the effective instantaneous electromechanical matrix can be obtained from an imaginary, unbounded, and unloaded heterogeneous material with the same microstrucutre as the real, loaded, and bounded one. Hence we could derive the micromechanics model from an imaginary, unloaded, heterogeneous material which completely occupies the three-dimensional (3D) space $\mathcal{R}$ and composes of infinitely many repeating UCs. The total energy changes within an electrostrictive material is equal to the summation of the energy changes of all the UCs, which is:

$$\Pi = \sum_{n=-\infty}^{\infty} \int_{\Omega} \frac{1}{2} d\sigma \; d\epsilon \mathrm{d}\Omega = \sum_{n=-\infty}^{\infty} \frac{1}{2} \int_{\Omega} \; d\epsilon^T Y \; d\epsilon \mathrm{d}\Omega \tag{7.8}$$

where $d\epsilon$ is given in Eq. (7.5) and contains both the 3D increments of strain field $d\epsilon_{ij}$ and the 3D increments of electric field dE_i, which are defined as:

$$d\epsilon_{ij}(\mathbf{n};\mathbf{y}) = \frac{1}{2}\left[\frac{\partial \Delta u_i(\mathbf{n};\mathbf{y})}{\partial y_j} + \frac{\partial \Delta u_j(\mathbf{n};\mathbf{y})}{\partial y_i}\right] \tag{7.9}$$

$$dE_i(\mathbf{n};\mathbf{y}) = -\frac{\partial \Delta \phi(\mathbf{n};\mathbf{y})}{\partial y_i} \tag{7.10}$$

Here $\Delta u_i(\mathbf{n};\mathbf{y})$ and $\Delta \phi(\mathbf{n};\mathbf{y})$ are the functions of the integer coordinates and the local coordinates for each UC, respectively. Since the infinite many UCs form a continuous heterogeneous material, the displacement changes Δu_i and the electric potential change on the interface between adjacent UCs should be continuous and can be written as follows for a UC with integer coordinates (n_1, n_2, n_3):

$$\begin{aligned}
\Delta u_i(n_1, n_2, n_3; d_1/2, y_2, y_3) &= \Delta u_i(n_1 + 1, n_2, n_3; -d_1/2, y_2, y_3) \\
\Delta u_i(n_1, n_2, n_3; y_1, d_2/2, y_3) &= \Delta u_i(n_1, n_2 + 1, n_3; y_1, -d_2/2, y_3) \\
\Delta u_i(n_1, n_2, n_3; y_1, y_2, d_3/2) &= \Delta u_i(n_1, n_2, n_3 + 1; y_1, y_2, -d_3/2)
\end{aligned} \tag{7.11}$$

$$\Delta\phi(n_1, n_2, n_3; d_1/2, y_2, y_3) = \Delta\phi(n_1 + 1, n_2, n_3; -d_1/2, y_2, y_3)$$
$$\Delta\phi(n_1, n_2, n_3; y_1, d_2/2, y_3) = \Delta\phi(n_1, n_2 + 1, n_3; y_1, -d_2/2, y_3)$$
$$\Delta\phi(n_1, n_2, n_3; y_1, y_2, d_3/2) = \Delta\phi(n_1, n_2, n_3 + 1; y_1, y_2, -d_3/2) \tag{7.12}$$

The exact solution of the present problem will minimize the summation of energy changes in Eq. (7.8) under the constraints in Eqs. (7.1), (7.2), (7.11), and (7.12). To avoid the difficulty associated with discrete integer arguments, we can reformulate the problem, including Eqs. (7.8), (7.9), (7.10), (7.11), and (7.12), in terms of continuous functions using the idea of quasicontinuum [16]. The basic idea is to associate a function of integer arguments defined in the integer space with a continuous function defined in $\mathcal{R}$. The corresponding formulas are listed below.

$$\Pi = \frac{1}{2}\int_{\mathcal{R}} \left\langle d\epsilon^T Y \; d\epsilon \right\rangle \mathrm{d}\mathcal{R} \tag{7.13}$$

$$d\epsilon_{ij}(\mathbf{x};\mathbf{y}) = \frac{1}{2}\left[\frac{\partial \Delta u_i(\mathbf{x};\mathbf{y})}{\partial y_j} + \frac{\partial \Delta u_j(\mathbf{x};\mathbf{y})}{\partial y_i}\right] \equiv \Delta u_{(i|j)} \tag{7.14}$$

$$dE_i(\mathbf{x};\mathbf{y}) = -\frac{\partial \Delta\phi(\mathbf{x};\mathbf{y})}{\partial y_i} \tag{7.15}$$

and

$$\Delta u_i(x_1, x_2, x_3; d_1/2, y_2, y_3) = \Delta u_i(x_1 + d_1, x_2, x_3; -d_1/2, y_2, y_3)$$
$$\Delta u_i(x_1, x_2, x_3; y_1, d_2/2, y_3) = \Delta u_i(x_1, x_2 + d_2, x_3; y_1, -d_2/2, y_3)$$
$$\Delta u_i(x_1, x_2, x_3; y_1, y_2, d_3/2) = \Delta u_i(x_1, x_2, x_3 + d_3; y_1, y_2, -d_3/2) \tag{7.16}$$

$$\Delta\phi(x_1, x_2, x_3; d_1/2, y_2, y_3) = \Delta\phi(x_1 + d_1, x_2, x_3; -d_1/2, y_2, y_3)$$
$$\Delta\phi(x_1, x_2, x_3; y_1, d_2/2, y_3) = \Delta\phi(x_1, x_2 + d_2, x_3; y_1, -d_2/2, y_3)$$
$$\Delta\phi(x_1, x_2, x_3; y_1, y_2, d_3/2) = \Delta\phi(x_1, x_2, x_3 + d_3; y_1, y_2, -d_3/2) \tag{7.17}$$

Using the technique of Lagrange multipliers, we can pose the variational statement of the micromechanics analysis of UC as a stationary value problem of the following functional:

$$\begin{aligned} J = \int_{\mathcal{R}} \Bigg\{ & \left\langle \frac{1}{2} d\epsilon^T Y \, d\epsilon \right\rangle + \lambda_i(\langle \Delta u_i \rangle - \Delta v_i) + +\lambda(\langle \Delta\phi \rangle - \Delta\psi) \\ & + \int_{S_1} \gamma_{i1} \left[\Delta u_i(x_j; d_1/2, y_2, y_3) - \Delta u_i(x_j + \delta_{j1} d_1; -d_1/2, y_2, y_3) \right] \mathrm{d}S_1 \\ & + \int_{S_2} \gamma_{i2} \left[\Delta u_i(x_j; y_1, d_2/2, y_3) - \Delta u_i(x_j + \delta_{j2} d_2; y_1, -d_2/2, y_3) \right] \mathrm{d}S_2 \\ & + \int_{S_3} \gamma_{i3} \left[\Delta u_i(x_j; y_1, y_2, d_3/2) - \Delta u_i(x_j + \delta_{j3} d_3; y_1, y_2, -d_3/2) \right] \mathrm{d}S_3 \\ & + \int_{S_1} \beta_1 \left[\Delta\phi(x_j; d_1/2, y_2, y_3) - \Delta\phi(x_j + \delta_{j1} d_1; -d_1/2, y_2, y_3) \right] \mathrm{d}S_1 \\ & + \int_{S_2} \beta_2 \left[\Delta\phi(x_j; y_1, d_2/2, y_3) - \Delta\phi(x_j + \delta_{j2} d_2; y_1, -d_2/2, y_3) \right] \mathrm{d}S_2 \\ & + \int_{S_3} \beta_3 \left[\Delta\phi(x_j; y_1, y_2, d_3/2) - \Delta\phi(x_j + \delta_{j3} d_3; y_1, y_2, -d_3/2) \right] \mathrm{d}S_3 \Bigg\} \mathrm{d}\mathcal{R} \end{aligned} \tag{7.18}$$

where λ_i, λ, γ_{ij}, and β_i are Lagrange multipliers introduced to enforce the constraints in Eqs. (7.1), (7.2), (7.16) and (7.17), respectively, S_i are the surfaces with $n_i = 1$, x_j represents the triplet of x_1, x_2, x_3, and δ_{ij} is the Kronecker delta. Following the general procedure of VAMUCH, we can obtain the following change of variables for Δu_i and $\Delta\phi$:

$$\Delta u_i(\mathbf{x}; \mathbf{y}) = \Delta v_i(\mathbf{x}) + y_j \frac{\partial \Delta v_i}{\partial x_j} + \chi_i(\mathbf{x}; \mathbf{y}) \tag{7.19}$$

$$\Delta\phi(\mathbf{x}; \mathbf{y}) = \Delta\psi(\mathbf{x}) + y_i \frac{\partial \Delta\psi}{\partial x_i} + \zeta(\mathbf{x}; \mathbf{y}) \tag{7.20}$$

where χ_i and ζ are the fluctuation functions for the displacement changes and electric potential changes, satisfying the following constraints in view of Eqs. (7.1), (7.19), and Eqs. (7.2), (7.20) when the origin of the local coordinate system is chosen to be the center of UC:

$$\langle \chi_i \rangle = 0 \tag{7.21}$$

$$\langle \zeta \rangle = 0 \tag{7.22}$$

Substituting Eqs. (7.19) and (7.20) into Eq. (7.18), we obtain a stationary value problem defined over UC for χ_i and ζ according to the variational asymptotic method [16], such

that:

$$J_\Omega = \left\langle \frac{1}{2} d\epsilon^T Y \, d\epsilon \right\rangle + \lambda_i \langle \chi_i \rangle + \lambda \langle \zeta \rangle + \sum_{j=1}^{3} \int_{S_j} \gamma_{ij} (\chi_i^{+j} - \chi_i^{-j}) \mathrm{d}S_j + \sum_{j=1}^{3} \int_{S_j} \beta_j (\zeta^{+j} - \zeta^{-j}) \mathrm{d}S_j \tag{7.23}$$

with

$$\chi_i^{+j} = \chi_i|_{y_j = d_j/2}, \ \chi_i^{-j} = \chi_i|_{y_j = -d_j/2} \ \text{ for } \ j = 1, 2, 3$$

$$\zeta^{+j} = \zeta|_{y_j = d_j/2}, \ \zeta^{-j} = \zeta|_{y_j = -d_j/2} \ \text{ for } \ j = 1, 2, 3$$

Matrix $d\epsilon$ can be expressed as:

$$d\epsilon = d\bar{\epsilon} + d\hat{\epsilon} \tag{7.24}$$

$d\bar{\epsilon}$ has a similar expression as Eq. (7.5):

$$d\bar{\epsilon} = \lfloor d\bar{\epsilon}_{11} \ \ 2d\bar{\epsilon}_{12} \ \ d\bar{\epsilon}_{22} \ \ 2d\bar{\epsilon}_{13} \ \ 2d\bar{\epsilon}_{23} \ \ d\bar{\epsilon}_{33} \ \ d\bar{E}_1 \ \ d\bar{E}_2 \ \ d\bar{E}_3 \rfloor^T \tag{7.25}$$

where $d\bar{\epsilon}_{ij} \equiv \frac{1}{2}(\Delta v_{i,j} + \Delta v_{j,i})$, the components of the global strain increment tensor and $d\bar{E}_i \equiv \Delta\psi_{,i}$, the components of the global electric field increment vector. $d\hat{\epsilon}$ are the strain and electric field rates due to the fluctuation functions, which is expressed as:

$$d\hat{\epsilon} = \lfloor d\hat{\epsilon}_{11} \ \ 2d\hat{\epsilon}_{12} \ \ d\hat{\epsilon}_{22} \ \ 2d\hat{\epsilon}_{13} \ \ 2d\hat{\epsilon}_{23} \ \ d\hat{\epsilon}_{33} \ \ d\hat{E}_1 \ \ d\hat{E}_2 \ \ d\hat{E}_3 \rfloor^T \tag{7.26}$$

with $d\hat{\epsilon}_{ij} \equiv \frac{1}{2}(\chi_{i,j} + \chi_{j,i})$ and $d\hat{E}_i = \zeta_{,i}$.

7.4 Finite Element Implementation

Although the FEM solutions can be possibly obtained based on Eq. (7.23), the Lagrange multipliers will increase the number of unknowns. In practice, we minimize the following functional

$$\Pi_\Omega = \frac{1}{\Omega} \int_\Omega \frac{1}{2} d\epsilon^T Y d\epsilon \mathrm{d}\Omega \tag{7.27}$$

under the following constraints

$$\chi_i^{+j} = \chi_i^{-j} \ \text{ and } \ \zeta^{+j} = \zeta^{-j} \ \text{ for } \ j = 1, 2, 3 \tag{7.28}$$

Following the general procedure of finite element implementation of VAMUCH, the fluctuation functions at an arbitrary node are restrained to be zero and later use this constraint to recover the unique fluctuation function. The nodes on the positive boundary surface (*i.e.*, $y_i = d_i/2$) are made slave to the nodes on the opposite negative boundary surface (*i.e.*, $y_i = -d_i/2$). By assembling all the independent active degrees of freedom (DOFs), we can implicitly and exactly incorporate the constraints in Eqs. (7.28).

The matrix form of $d\hat{\epsilon}$ in Eq. (7.26) can be expressed as:

$$d\hat{\epsilon} = \begin{bmatrix} \frac{\partial}{\partial y_1} & 0 & 0 & 0 \\ \frac{\partial}{\partial y_2} & \frac{\partial}{\partial y_1} & 0 & 0 \\ 0 & \frac{\partial}{\partial y_2} & 0 & 0 \\ \frac{\partial}{\partial y_3} & 0 & \frac{\partial}{\partial y_1} & 0 \\ 0 & \frac{\partial}{\partial y_3} & \frac{\partial}{\partial y_2} & 0 \\ 0 & 0 & \frac{\partial}{\partial y_3} & 0 \\ 0 & 0 & 0 & -\frac{\partial}{\partial y_1} \\ 0 & 0 & 0 & -\frac{\partial}{\partial y_2} \\ 0 & 0 & 0 & -\frac{\partial}{\partial y_3} \end{bmatrix} \begin{Bmatrix} \chi_1 \\ \chi_2 \\ \chi_3 \\ \zeta \end{Bmatrix} \equiv \Gamma_h \chi \tag{7.29}$$

where Γ_h is an operator matrix. χ is discretized as:

$$\chi(x_i; y_i) = S(y_i)\mathcal{X}(x_i) \tag{7.30}$$

where S denote the shape functions and $\mathcal{X}$ is the column matrix of the nodal values of both the mechanical and electric fluctuation functions. Substituting Eqs. (7.29), and (7.30) into Eq. (7.27), we obtain a discretized version of the functional as:

$$\Pi_\Omega = \frac{1}{\Omega}(\mathcal{X}^T E \mathcal{X} + 2\mathcal{X}^T D_{h\epsilon} d\bar{\epsilon} + d\bar{\epsilon}^T D_{\epsilon\epsilon} d\bar{\epsilon}) \tag{7.31}$$

where

$$E = \int_\Omega (\Gamma_h S)^T Y (\Gamma_h S) \mathrm{d}\Omega \qquad D_{h\epsilon} = \int_\Omega (\Gamma_h S)^T Y \mathrm{d}\Omega \qquad D_{\epsilon\epsilon} = \int_\Omega Y \mathrm{d}\Omega \tag{7.32}$$

Minimizing Π_Ω in Eq. (7.31), the following linear system is obtained as:

$$E\mathcal{X} = -D_{h\epsilon} d\bar{\epsilon} \tag{7.33}$$

The fluctuation function $\mathcal{X}$ in Eq. (7.33) is linearly proportional to $d\bar{\epsilon}$ so that the solution can be written symbolically as:

$$\mathcal{X} = \mathcal{X}_0 d\bar{\epsilon} \tag{7.34}$$

Substituting Eq. (7.34) into Eq. (7.31), we can calculate the electric enthalpy of the UC as:

$$\Pi_\Omega = \frac{1}{\Omega} d\bar{\epsilon}^T \left(\mathcal{X}_0^T D_{h\epsilon} + D_{\epsilon\epsilon} \right) d\bar{\epsilon} \equiv d\bar{\epsilon}^T Y^* d\bar{\epsilon} \tag{7.35}$$

It can be seen that Y^* in Eq. (7.35) is the 9×9 effective tangent electromechanical matrix and $d\bar{\epsilon}$ is a column matrix containing both the increments of the global strains and global electric fields.

The increments of the local fields, such as the increments of the local displacements, electric potential, stresses, and electric displacements, can be recovered in terms of the macroscopic behavior including the increments of the global displacements Δv_i, the global electric potential $\Delta\psi$, the global strain and electric field $d\bar{\epsilon}$, and the fluctuation function χ. First, we need to uniquely determine the fluctuation functions. Considering the fact that we fixed an arbitrary node and made nodes on the positive boundary surfaces slave to the corresponding negative boundary surfaces, we need to construct a new array $\tilde{\mathcal{X}}_0$ from $\mathcal{X}_0$ by assigning the values for slave nodes according to the corresponding active nodes and assign zero to the fixed node. Obviously, $\tilde{\mathcal{X}}_0$ still yield the minimum value of Π_Ω in Eq. (7.27) under constraints in Eqs. (7.28). However, $\tilde{\mathcal{X}}_0$ may not satisfy Eqs. (7.21) and (7.22). The real solution, denoted as $\bar{\mathcal{X}}_0$ can be found trivially by adding a constant corresponding to each DOF to each node so that Eqs. (7.21) and (7.22) are satisfied.

Table 7.1: Material properties of the composite constituents (P(VDF-TrFE) polymer and PZT)

	P(VDF-TrFE)	PZT
C_{11}(GPa)	1.8056	124.201
C_{12}(GPa)	0.764	96.24
C_{13}(GPa)	0.764	96.24
C_{22}(GPa)	1.8056	151.351
C_{23}(GPa)	0.764	98.3
C_{33}(GPa)	1.8056	151.351
C_{44}(GPa)	0.521	26.525
C_{55}(GPa)	0.521	22.989
C_{66}(GPa)	0.521	22.989
$M_{11}(m^2/V^2)$	-2.4×10^{-18}	0
$M_{12}(m^2/V^2)$	1.20×10^{-18}	0
κ_{11}(C/Vm)	0.606×10^{-9}	13.0×10^{-9}
κ_{33}(C/Vm)	0.606×10^{-9}	15.045×10^{-9}

The increments of the local displacements and electric potential can be recovered using the uniquely determined fluctuation function and Eqs. (7.19) and (7.20) as:

$$\begin{Bmatrix} \Delta u_1 \\ \Delta u_2 \\ \Delta u_3 \\ \Delta \phi \end{Bmatrix} = \begin{Bmatrix} \Delta v_1 \\ \Delta v_2 \\ \Delta v_3 \\ \Delta \psi \end{Bmatrix} + \begin{bmatrix} \frac{\partial \Delta v_1}{\partial x_1} & \frac{\partial \Delta v_1}{\partial x_2} & \frac{\partial \Delta v_1}{\partial x_3} \\ \frac{\partial \Delta v_2}{\partial x_1} & \frac{\partial \Delta v_2}{\partial x_2} & \frac{\partial \Delta v_2}{\partial x_3} \\ \frac{\partial v_3}{\partial x_1} & \frac{\partial v_3}{\partial x_2} & \frac{\partial v_3}{\partial x_3} \\ \frac{\partial \Delta \psi}{\partial x_1} & \frac{\partial \Delta \psi}{\partial x_2} & \frac{\partial \Delta \psi}{\partial x_3} \end{bmatrix} \begin{Bmatrix} y_1 \\ y_2 \\ y_3 \end{Bmatrix} + \bar{S}\bar{\mathcal{X}} \tag{7.36}$$

where $\bar{S}$ is different from S due to the recovery of slave nodes and the constrained node. The increments of the local strain field and electric field can be recovered using Eqs. (7.14), (7.15), (7.19), (7.20) and (7.29) as:

$$d\epsilon = d\bar{\epsilon} + \Gamma_h \bar{S}\bar{\mathcal{X}} \tag{7.37}$$

The increments of the local stress and electric displacement field can be recovered straightforwardly using the 3D constitutive relations for the constituent material as:

$$d\sigma = Y d\epsilon \tag{7.38}$$

In the first increment of the nonlinear behavior of the electrostrictive composites, the effective tangent electromechanical matrix X^* is calculated with all local field variables in

the electromechanical matrix of constituents are set to zero. The current overall stress tensor $\bar{\sigma}_{ij}$ and the current electric displacement $\bar{D}_i$ are determined from the previous values and the increments as:

$$\bar{\sigma}_{ij} = \bar{\sigma}_{ij}|_{previous} + d\bar{\sigma}_{ij} \tag{7.39}$$

and

$$\bar{D}_i = \bar{D}_i|_{previous} + d\bar{D}_i \tag{7.40}$$

In the next increment, the above process are repeated with the local field variables in the electromechanical matrix of the constituents are not zero. These local field variables can be recovered in terms of the fluctuation function and the increments of the global behavior obtained from the previous stage.

7.5 Numerical Examples

In this section, the example considered is the P(VDF-TrFE) polymer matrix reinforced by $Pb(Zr_xTi_{1-x})O_3$ (PZT) ceramics fibers which is extensively investigated in [6, 17]. The properties of both constituents are shown in Table 7.1 which are directly converted from Table 1 in [6]. The P(VDF-TrFE) polymer is isotropic and the PZT is transversely isotropic. The fiber is of circular shape and arranged in a square array. Firstly, consider the composite that is subjected to electric field $\bar{E}_1$ in 1-direction which is the axial direction of the fiber and all other electric field and mechanical strains are set to zero. Fig. 7.2 and 7.3 show the variation of the induced axial and transverse stresses $\bar{\sigma}_{11}$ and $\bar{\sigma}_{22}$ of the composites (with four different volume fraction of the fiber, namely, VOF0.0, VOF0.2, VOF0.4, VOF0.6) with respect to the applied electric field $\bar{E}_1$. It can be seen that the electromechanical coupling effects increase with the applied electric field. In this case, the resulted transverse stresses $\bar{\sigma}_{22}$ of four different volume fraction are very close.

Secondly, we consider the composite which is subjected to the traction free boundary conditions, namely, $\bar{\sigma}_{ij} = 0$ and the external electric field $\bar{E}_1$ in 1-direction. In this situation, the strains at the current stage are given by:

$$\bar{\epsilon}_{ij} = \bar{\epsilon}_{ij}|_{previous} + d\bar{\epsilon}_{ij} \tag{7.41}$$

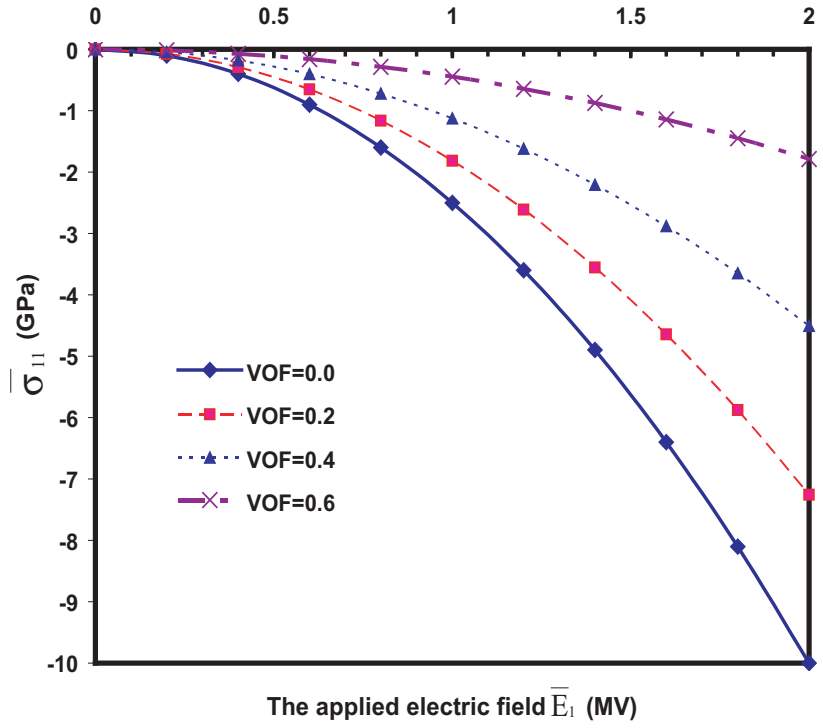

Fig. 7.2: The global stress $\bar{\sigma}_{11}$ versus the applied electric field.

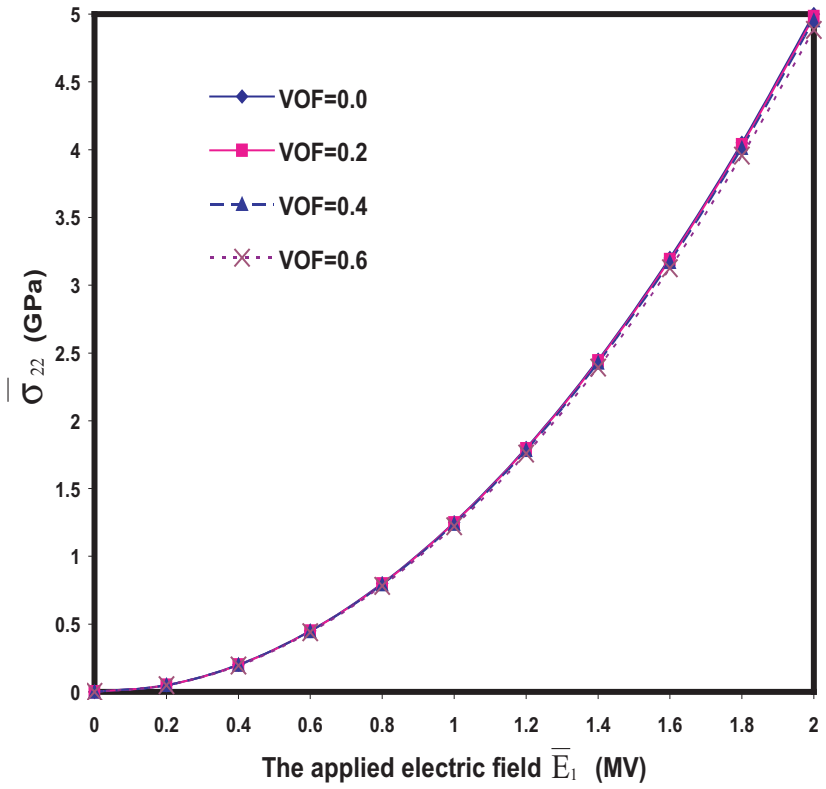

Fig. 7.3: The global stress $\bar{\sigma}_{22}$ versus the applied electric field.

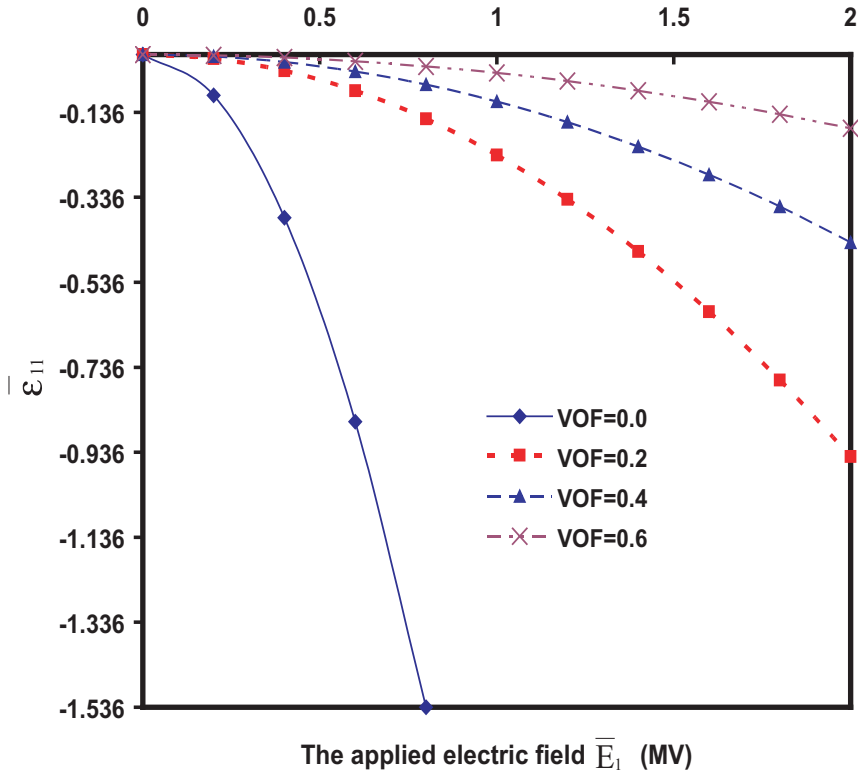

Fig. 7.4: The global strain $\bar{\epsilon}_{11}$ versus the applied electric field.

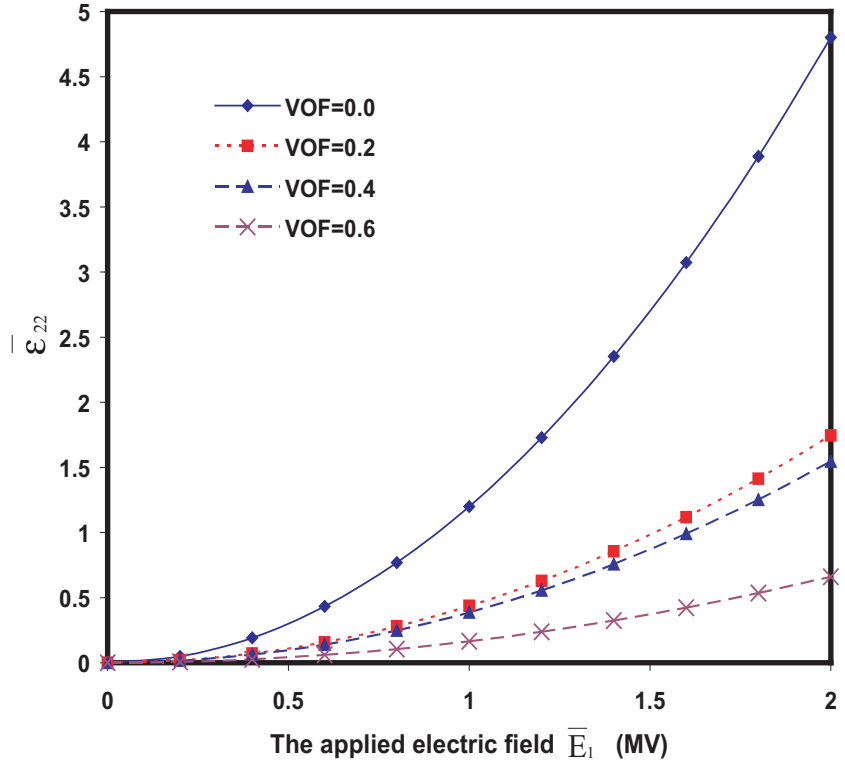

Fig. 7.5: The global stress $\bar{\epsilon}_{22}$ versus the applied electric field.

where:

$$d\bar{\epsilon}_{ij} = 2M^*_{ijkl}\bar{E}_k d\bar{E}_l \tag{7.42}$$

The variation of the induced axial and transverse strains $\bar{\epsilon}_{11}$ and $\bar{\epsilon}_{22}$ with respect to the volume fraction of the applied electric field are illustrated in Fig. 7.4 and 7.5. Both figures also show the effects of the volume fraction of the fiber. Again, it can be observed that the electromechanical coupling effects increase with the volume fractions of the fiber which impose strong effects on the resulted global strains.

7.6 Conclusions

This paper has focused on developing a micromechanics approach for the investigation of the nonlinear behavior of multiphase electrostrictive composites. The formulation of the effective instantaneous tangent electromechanical matrix is established on the basis of the variational asymptotic method. The algorithm for the nonlinear response of multiphase electrostrictive composites was constructed. The framework of this approach can be straightforwardly extended to any other nonlinear problems.

References

1. Ikeda, T., *Fundamentals of piezoelectricity.* Oxford University Press, 1996.

2. Sundar, V. and Newnham, R.E., "Electrostriction and polariztion," *Ferroelectrics*, Vol. 135, 1992, pp. 431-446.

3. Somphone, T., *Micromechanics of smart electrostrictive materials*, PhD thesis, The University of Tennessee, Knoxville, 2000.

4. Hom, C.L. and Shankar, N., "A fully coupled constitutive model for electrostrictive ceramic materials," *Journal of Intelligent Materials Systems and Structures*, Vol. 5, 1994, pp. 795-801.

5. Hom, C.L. and Shankar, N., "A finite element method for electrostrictive ceramic devices," *International Journal of Solids and Structures*, Vol. 33, 1996, pp. 1757-1779.

6. Li, J. and Rao, N., "Micromechanics of ferroelectric polyer-based electrostrictive composites," *Journal of the Mechanics and Physics of Solids*, Vol. 52, 2004, pp. 591-615.

7. Aboudi, J., "Micromechanical prediction of the response of electrostrictive multiphase composites," *Smart Materials and Structures*, Vol. 8, 1999, pp. 663-671.

8. Yu, W. and Tang, T., "Variational asymptotic method for unit cell homogenization of periodically heterogeneous materials," *International Journal of Solids and Structures*, Vol. 44, 2007, pp. 3738-3755.

9. Yu, W. and Tang, T., "A variational asymptotic micromechanics model for predicting thermoelastic properties of heterogeneous materials," *International Journal of Solids and Structures*, Vol. 44, No. 22-23, 2007, pp. 7510-7525.

10. Tang, T. and Yu, W., "A variational asymptotic micromechanics model for predicting conductivity of composite materials," *Journal of Mechanics of Materials and Structures*, Vol. 2, No. 9, 2007, pp. 1813-1830.

11. Tang, T. and Yu, W., "Variational asymptotic homogenization of heterogeneous electromagnetoelastic materials," *International Journal of Engineering Science*, Vol. 46, No. 8, 2008, pp. 741-757.

12. Tang, T. and Yu, W., "Variational asymptotic micromechanics modeling of heterogeneous piezoelectric materials," *Mechanics of Materials*, Vol. 40, 2008, pp. 812-824.

13. Tang, T. and Yu, W., "A variational asymptotic model for predicting initial yielding surface and elastoplastic behavior of metal matrix composite materials," *Proceedings of the 2007 ASME International Mechanical Engineering Congress and Exposition*, Seattle, Washington, Nov. 2007.

14. Berdichevsky, V. L., "On averaging of periodic systems," *PMM*, Vol. 41, No. 6, 1977, pp. 993-1006.

15. Blackwood, G.H. and Ealey, M.A., "Electrostrictive behavior in lead magnesium niobate (PMN) actuators. Part I: materials perspective," *Smart Materials and Structures*, Vol. 2, 1993, pp. 124-133.

16. Kunin, I., *Theory of Elastic Media with Microstructure*, vols. 1 and 2, Springer Verlag, 1982.

17. Rao, N. and Li, J., "The electrostriction of p(vdf-trfe) copolymers embedded with textured dielectric particles," *International Journal of Solids and Structures*, Vol. 41, 2004, pp. 2995-3011.

Chapter 8

Conclusions and Recommendations of Future Work

8.1 Conclusions

A series of new micromechanics models based on the framework of the variational asymptotic method for unit cell homogenization (VAMUCH) have been developed for homogenizing composite materials. In comparison with other existing models, the major advantages of VAMUCH are as follows:

1. It invokes only two essential assumptions within the concept of micromechanics for heterogeneous material with identifiable unit cells;

2. It has an inherent variational nature and its numerical implementation is shown to be straightforward;

3. It calculates the different material properties in different directions simultaneously, which is more efficient than those approaches requiring multiple runs under different loading conditions;

4. It calculates effective properties and local fields directly with the same accuracy as the fluctuation functions. No postprocessing calculations such as stress averaging and strain averaging are needed.

Although VAMUCH is as versatile as FEA-based approaches, VAMUCH is dramatically different from FEA-based approaches, both from the view point of theoreticians and from the view point of practicing engineers.

8.1.1 Differences from the View Point of Theoreticians

Taking advantage of the smallness of the microstructure of heterogeneous materials, VAMUCH formulates a variational statement of the unit cell through an asymptotic analysis of the energy functional by invoking only two essential assumptions within the concept of micromechanics of heterogeneous materials with identifiable UCs.

- **Assumption 1** The exact solutions of the field variables have volume averages over the UC.

- **Assumption 2** The effective material properties obtained from the micromechanical analysis of the UC are independent of the geometry, the boundary conditions, and loading conditions of the macroscopic structure, which means that effective material properties are assumed to be the intrinsic properties of the material when viewed macroscopically.

Please note these assumptions are not restrictive. The mathematical meaning of the first assumption is that the exact solutions of the field variables are integrable over the domain of UC, which is true almost all the time. For the second assumption, it is worthwhile to point out that for nonlinear materials, the material properties is directly related with the stress state at the point we want to evaluate the material properties. *All the other assumptions such as particular shape and arrangement of the constituents, specific boundary conditions, and prescribed relations between local fields and global fields are convenient but not essential.*

It has shown that the governing differential equations of Mathematical Homogenization Theory (MHT), which achieves the best available accuracy for periodic composites, can be derived from the variational statement of VAMUCH. The main differences between VAMUCH and MHT are:

- The periodic boundary conditions are derived in VAMUCH, while they are assumed *a priori* in MHT. MHT also assumes periodic functions, which is shown to be unnecessary in VAMUCH.

- The fluctuation functions are determined uniquely in VAMUCH, while they can only be determined up to a constant in MHT.

- VAMUCH has an inherent variational nature which is convenient for numerical implementation, while virtual quantities should be carefully chosen to make MHT variational as shown in [1].

Although the theory of VAMUCH can be compactly written as the variation of a functional, it is easier to look at the corresponding differential statement derivable from the variational statement to find out the theoretical differences between VAMUCH and

FEA-based approaches. The corresponding differential statement of VAMUCH for elastic materials includes the following governing differential equation (GDE) and boundary conditions.

$$\frac{\partial}{\partial y_l} C_{ijkl} \left(\bar{\epsilon}_{ij} + \chi_{(i|j)} \right) = 0 \quad \text{in} \quad \Omega \tag{8.1}$$

$$\chi_i(\mathbf{x}; d_1/2, y_2, y_3) = \chi_i(\mathbf{x}; -d_1/2, y_2, y_3) \tag{8.2}$$

$$\chi_i(\mathbf{x}; y_1, d_2/2, y_3) = \chi_i(\mathbf{x}; y_1, -d_2/2, y_3) \tag{8.3}$$

$$\chi_i(\mathbf{x}; y_1, y_2, d_3/2) = \chi_i(\mathbf{x}; y_1, y_2, -d_3/2) \tag{8.4}$$

$$C_{ijkl} \left(\bar{\epsilon}_{ij} + \chi_{(i|j)} \right) |_{y_1 = d_1/2} = C_{ijkl} \left(\bar{\epsilon}_{ij} + \chi_{(i|j)} \right) |_{y_1 = -d_1/2} \tag{8.5}$$

$$C_{ijkl} \left(\bar{\epsilon}_{ij} + \chi_{(i|j)} \right) |_{y_2 = d_2/2} = C_{ijkl} \left(\bar{\epsilon}_{ij} + \chi_{(i|j)} \right) |_{y_2 = -d_2/2} \tag{8.6}$$

$$C_{ijkl} \left(\bar{\epsilon}_{ij} + \chi_{(i|j)} \right) |_{y_3 = d_3/2} = C_{ijkl} \left(\bar{\epsilon}_{ij} + \chi_{(i|j)} \right) |_{y_3 = -d_3/2} \tag{8.7}$$

$$\langle \chi_i \rangle = 0 \tag{8.8}$$

where Eq. (8.1) is the governing differential equations, Eqs. (8.2)-(8.4) are the periodic boundary conditions for fluctuation functions, and Eqs. (8.5)-(8.7) are the periodic boundary conditions for local stresses. All these equations are identical to those of MHT, as listed in [2] except Eq. (8.8) which ensures a unique solution for the fluctuation functions χ_i.

The GDE of FEA-based approaches for elastic properties is the 3D equilibrium equation without body force

$$\frac{\partial}{\partial y_l} C_{ijkl} \left(u_{i,j} + u_{j,i} \right) = 0 \quad \text{in} \quad \Omega \tag{8.9}$$

Comparing this equation with the VAMUCH GDE in Eq. (8.1), one clearly observes that the fundamental variables of VAMUCH are fluctuation functions while those of FEA-based approaches are the macroscopic displacements. Furthermore, the boundary conditions for FEA-based approaches are applied on the macroscopic variables such as displacements. Different sets of displacement boundary conditions are needed for calculating different properties. Since these boundary conditions are applied a priori based on engineering intuition, it is not surprising to find out that different researchers introduced different boundary conditions for calculating the same property, see Ref. 3 for a detailed discussion on the boundary conditions for RVE. It is known that the predicted effective properties are very sensitive to boundary conditions. Another theoretical difference is that the dimensionality of VAMUCH

analysis is based on the periodicity of the microstructure. For example, we can use 1D UC to model binary composites, 2D UC to model fiber reinforced composites, and 3D UC to model particle reinforced composites. No special treatment is necessary for these different types of microstructures. However, it is not the case with FEA-based approaches, to get the complete set of 3D material properties, one has to use 3D UCs, let it be a binary composite, fiber reinforced composite, or particle reinforced composite. For example, according to the author's understanding, Sun and Vaidya [3] derived the most rigorous FEA-based approach for elastic properties, which requires 3D RVE for fiber reinforced composites.

8.1.2 Differences from the View Point of Practicing Engineers

Although there are significant theoretical difference between VAMUCH and FEA-based approaches, practicing engineers are usually more concerned with the convenience and efficiency. To use a FEA-based approach, one has to carry out multiple runs with different sets of boundary conditions and external loads for predicting different material properties. And postprocessing steps such as averaging stresses or averaging strains are needed for calculating the effective properties. If one is also interested in the local fields within the microstructure, one more run is necessary to predict local stress/strain field if the global stress/strain state is different from that used to obtain the effective properties. Comparing to FEA-based approaches, VAMUCH has the following advantages:

1. VAMUCH can obtain the complete set of material properties within one analysis without applying any load and any boundary conditions, which is far more efficient and less labor intensive than those approaches requiring multiple runs under different boundary and load conditions. It is also noted that VAMUCH can even obtain the complete set of 3D material properties using a one-dimensional analysis of the 1D UC for binary composites. It is impossible for FEA-based approaches.

2. VAMUCH calculates effective properties and local fields directly with the same accuracy as the fluctuation functions. No postprocessing calculations which introduce more approximations, such as averaging stress and electric displacement field, are needed, which are indispensable for FEM-based approaches.

3. VAMUCH can recover the local fields using a set of algebraic relations obtained in the process of calculating the effective properties. Another analysis of the microstructures

which is needed for FEA-based approaches is not necessary for VAMUCH.

It is also emphasized here that VAMUCH calculation is conceptually different from automating the multiple runs including postprocessing steps of FEA-based approaches using a macro language such as APDL of ANSYS. VAMUCH is not just a different postprocessing approach.

At this stage, we are confident to claim that VAMUCH achieves the most mathematical rigor and consequently the best available accuracy with invoking only the very essential assumptions within the micromechanics concept. VAMUCH is as versatile as FEA-based approaches because it can deal with arbitrary UC with arbitrary number of inclusions with arbitrary shape made of general anisotropic material. VAMUCH is much more convenient and efficient than FEA-based approaches. In fact, one just needs to provide a mesh with corresponding constituent properties, VAMUCH will produce the complete set of material properties with one run, which takes just a very small faction of both the model preparation time and the computational time of a FEA-based approach. Also to obtain the complete set of properties of fiber reinforced composites or binary composites, FEA-based approaches need to use 3D UC, while VAMUCH will only need to use 2D UC and 1D UC, respectively. The time saving in this dimensionality reduction is dramatic.

8.2 Recommendations of Future Work

The following topics are recommended for the future work:

- *Modeling the effects of the properties of the interfaces.* The mechanical properties of composite materials depend on the interface properties as well as the properties of constituents. The load transfer between the reinforcement and the matrix rely principally on the strength of interfaces. Strong interfaces result in good transverse strength but reduced fracture toughness. On the contrary, weak interfaces led high fracture toughness with low transverse strength. The investigation of the effects of the interfaces is absolutely significant.

- *The influences of the thermal residual stress on the overall properties of composite materials* The thermal residual stress is induced due to the differences of CTEs of the constituents during fabrication and heat treatment of the composite materials. It

imposes strong effects on the overall properties of composite materials and, therefore, is an important topic worthy to be studied.

- *Micromechanics modeling of composite materials with randomly distributed reinforcements.* In real composite materials, almost no periodic microstructure exists. Hence, the determination of effective properties of composite materials composed of statistically random distribution of reinforcements is a potentially future task.

References

1. Guedes, J. M. and Kikuchi, N., "Preprocessing and postprocessing for materials based on the homogenization method with adaptive finite element method," *Computer Methods in Applied Mechanics and Engineering*, Vol. 83, 1990, pp. 143-198.

2. Manevithch, L. I., Andrianov, I. V., and OShmyan, V. G., *Mechanics of Periodically Heterogeneous Structures*, Springer, 2002.

3. Sun, C.T. and Vaidya, R.S., "Prediction of composite properties from a representative volume element," *Composites Science and Technololy*, Vol. 56, 1996, pp. 171-179.

Appendices

Appendix A

Variational Asymptotic Method for Unit Cell Homogenization of Periodically Heterogeneous Materials

[1]

This appendix is a journal paper published in the *International Journal of Solids and Structures*, Vol. 44, 2007, pp. 3738-3755.

Abstract

A new micromechanics model, namely, the variational asymptotic method for unit cell homogenization (VAMUCH), is developed to predict the effective properties of periodically heterogeneous materials and recover the local fields. Considering the periodicity as a small parameter, we can formulate a variational statement of the unit cell through an asymptotic expansion of the energy functional. It is shown that the governing differential equations and periodic boundary conditions of mathematical homogenization theories (MHT) can be reproduced from this variational statement. In comparison to other approaches, VAMUCH does not rely on *ad hoc* assumptions, has the same rigor as MHT, has a straightforward numerical implementation, and can calculate *the complete set of properties simultaneously without using multiple loadings*. This theory is implemented using the finite element method and an engineering program, VAMUCH, is developed for micromechanical analysis of unit cells. Many examples of binary composites, fiber reinforced composites, and particle reinforced composites are used to demonstrate the application, power, and accuracy of the theory and the code of VAMUCH.

A.1 Introduction

Along with the increased knowledge and fabrication techniques for materials, more and more structures are made with heterogeneous materials with engineered microstructures to achieve the ever-increasing performance requirements. The increased complexity at the microlevel greatly complicates the analysis of the structural behavior, which is indispensable

[1] Coauthored by: Wenbin Yu and Tian Tang.

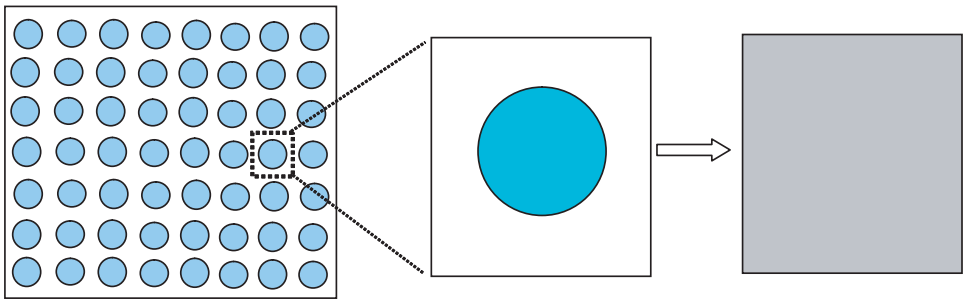

Fig. A.1: Periodic heterogeneous materials and the corresponding unit cell.

for rational designs of these structures. Although it is logically sound to use the well-established finite element method (FEM) to analyze such structures by meshing all the details of constituent materials, the size of the finite element model will easily overpower most of the computers we can access in the foreseeable future because the macroscopic structural dimensions are usually several orders of magnitude larger than the characteristic size of constituent materials.

If the structure can be idealized as a periodic assembly of *many* unit cells (UCs, see Fig. A.1), it is possible to homogenize the heterogeneous UC with a set of effective material properties obtained by a micromechanical analysis of the UC. As illustrated in Fig. A.2, the concept of UC essentially simplifies the original expensive analysis of structures made with heterogeneous materials using the following three steps:

- Identify the UC and carry out a micromechanical analysis of the UC to obtain effective material properties;
- Analyze the structure with homogenized material properties to study the macroscopic structural behavior;
- Feedback the macroscopic behavior to the micromechanical analysis to calculate local fields such as displacements, strains, and stresses within the UC, which are only needed for detailed analysis of some critical zones.

In the past several decades, numerous approaches have been proposed for the micromechanical analysis of UCs (see Hashin (1983) and references cited therein). These includes the earliest rules of mixture approaches based on Voigt and Reuss hypotheses. Hill (1952) has shown that Voigt and Reuss assumptions predict the upper and lower bounds, respectively, for the effective elastic properties of the homogenized UC. For general heterogeneous

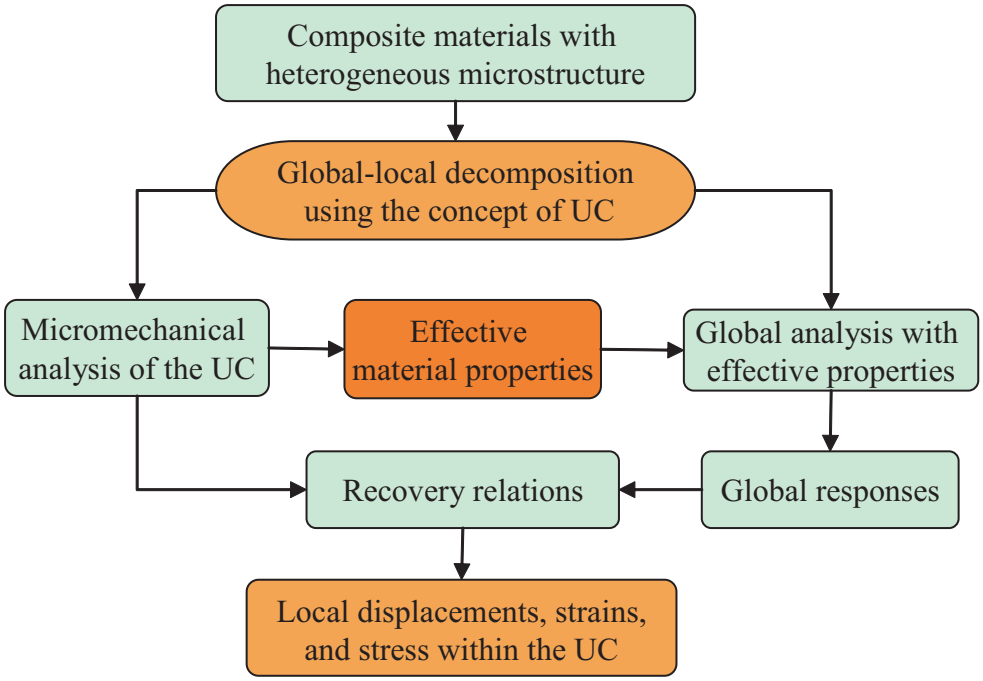

Fig. A.2: The basic steps of structure analysis with heterogeneous microstructures using the concept of unit cell.

materials, the difference between these two bounds could be too large to be of practical use. Researchers have proposed various techniques to either reduce the difference between the upper and lower bounds, or find an approximate value between the upper and lower bounds. Typical approaches are the self-consistent model (Hill, 1965) and its generalizations (Dvorak and Bahei-El-Dini, 1979; Accorsi and Nemat-Nasser, 1986), the variational approach of Hashin and Shtrikman (1962), third-order bounds (Milton, 1981), the method of cells (MOC) (Aboudi, 1982, 1989) and its variants (Paley and Aboudi, 1992; Aboudi et al., 2001; Williams, 2005b), recursive cell method (Banerjee and Adams, 2004), mathematical homogenization theories (MHT) (Bensoussan et al., 1978; Murakami and Toledano, 1990), finite element approaches using conventional stress analysis of a representative volume element (RVE) (Sun and Vaidya, 1996), and many others. Hollister and Kikuchi (1992) compared different approaches and concluded that MHT is preferable over other approaches for periodic composites even when the material is only locally periodic with a finite periodicity. Although MOC is not compared in Hollister and Kikuchi (1992), MOC expands the local displacements in terms of global displacements using the Legendre polynomial of different orders according to the required accuracy. The accuracy of MOC could be comparable to MHT if sufficient terms are used in the polynomial expansion although the asymptotical

correctness cannot be guaranteed. It is interesting to notice that the author of MOC recently developed a new micromechanical analysis (Aboudi et al., 2001) based on MHT with the solution procedure borrowed from MOC.

Although different approaches adopt different assumptions in the literature, there are only two essential assumptions associated with the micromechanical analysis of heterogeneous materials with identifiable UCs.

- **Assumption 1** The exact solutions of the field variables have volume averages over the UC. For example, if u_i are the exact displacements within the UC, there exist v_i such that

$$v_i = \frac{1}{\Omega}\int_\Omega u_i \, \mathrm{d}\Omega \equiv \langle u_i \rangle \tag{A.1}$$

  where Ω denotes the domain occupied by the UC and its volume.

- **Assumption 2** The effective material properties obtained from the micromechanical analysis of the UC are independent of the geometry, the boundary conditions, and loading conditions of the macroscopic structure, which means that effective material properties are assumed to be the intrinsic properties of the material when viewed macroscopically.

Of course, the micromechanical analysis of the UC is only needed and appropriate if $\eta = h/l \ll 1$, with h as the characteristic size of the UC and l as the the characteristic wavelength of the deformation of the structure. *All the others assumptions such as particular geometry shape and arrangement of the constituents, specific boundary conditions, and prescribed relations between local fields and global fields are convenient but not essential.*

In this study, the variational asymptotic method (VAM) of Berdichevsky (1979) will be used to develop a new unit cell homogenization technique invoking these two essential assumptions. VAM simplifies the procedure of solving physical problems that can be formulated in terms of a variational statement involving one or more small parameters. In contrast to conventional asymptotic methods, VAM carries out asymptotic analysis of the variational statement, synthesizing both merits of variational methods (*viz.*, systematic, simple, and easy to be implemented numerically) and asymptotic methods (*viz.*, without *ad hoc* assumptions). VAM has been used extensively to construct efficient high-fidelity structure models for composite beams (Yu et al., 2002c), composite and smart plates (Yu et al.,

2002a; Yu and Hodges, 2004a,b), and composite and smart shells (Yu et al., 2002b, 2005), achieving an excellent compromise between accuracy and efficiency. VAM has also been used to homogenize isotropic material with periodic cavities (Berdichevsky, 1977), which laid a foundation for the present work.

First, we extend the work of Berdichevsky (1977) to extract a variational statement for the micromechanical analysis of the UC from the three-dimensional (3D) continuum formulation of the periodically heterogeneous, anisotropic materials. This variational statement can be solved using VAM asymptotically to find the relation between the local displacements and global displacements for the purpose to predict effective material properties and local fields. Then we will implement this theory using FEM to develop an engineering code, VAMUCH, to uniformly handle general heterogeneous microstructures including one-dimensional (1D), two-dimensional (2D), or 3D UCs. Finally, many examples including binary composites, fiber reinforced composites, and particle reinforced composites, are used to demonstrate the application, power, and accuracy of the present theory and the companion code VAMUCH.

A.2 A Variational Statement for Unit Cells

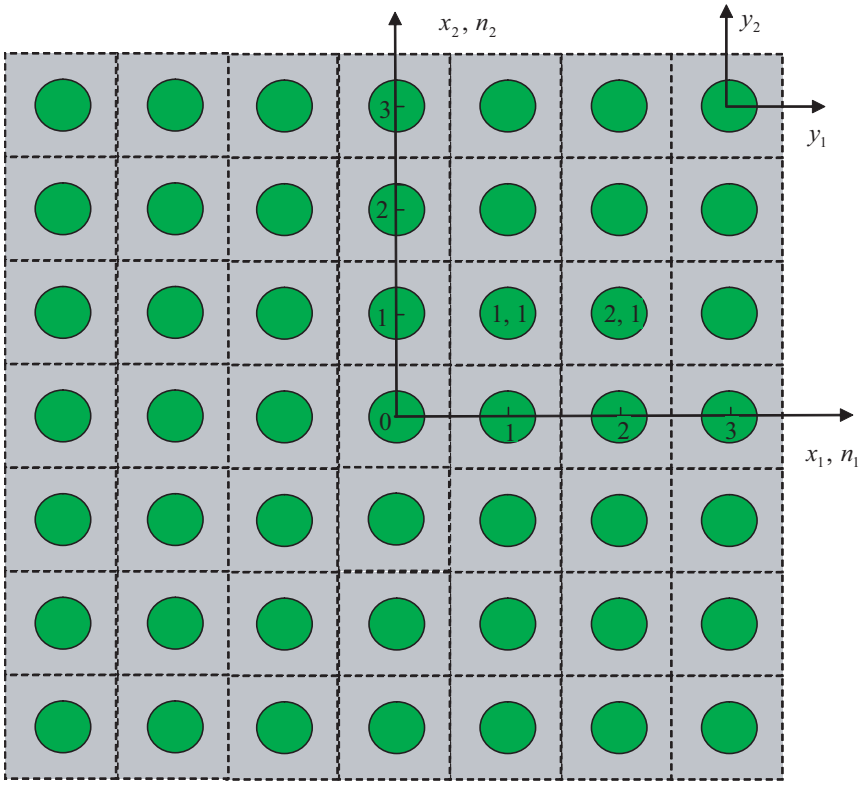

Fig. A.3: Coordinate systems for 2D heterogeneous materials.

As shown in Fig. A.3, to facilitate our formulation, we need to setup three coordinate systems: two cartesian coordinates $\mathbf{x} = (x_1, x_2, x_3)$ and $\mathbf{y} = (y_1, y_2, y_3)$, and an integer-valued coordinate $\mathbf{n} = (n_1, n_2, n_3)$. We use x_i as the global coordinates to describe the macroscopic structure and y_i parallel to x_i as the local coordinates to describe the UC (Here and throughout the paper, Latin indices assume 1, 2, and 3 and repeated indices are summed over their range except where explicitly indicated). If the UC is a cube with dimensions as d_i, we chose the local coordinates y_i in such a way that $y_i \in [-\frac{d_i}{2}, \frac{d_i}{2}]$. Since the heterogeneous material composes of many countable UCs, it is also convenient to introduce integer coordinates n_i to locate each individual UC. The integer coordinates are related to the global coordinates in such a way that $n_i = x_i/d_i$ (no summation over i). If the material is uniform in one of the directions, such as the fiber reinforced composites in the fiber direction, the dimension of that direction can be chosen to be an arbitrary length different from zero.

To formulate a variational statement for UCs, we need to use one of the energy principles, such as the principle of minimum total potential energy. The second assumption implies that we could obtain the same effective material properties from an imaginary unbounded and unloaded heterogeneous material with the same microstrucutre as the loaded and bounded one. Hence we could derive the micromechanical analysis from a heterogeneous material which could completely occupy the 3D space $\mathcal{R}$ and composes of infinite many UCs. For elastic material[2], the total potential energy is equal to the summation of the strain energy stored in all the UCs, which is:

$$\Pi = \sum_{n=-\infty}^{\infty} \int_{\Omega} \frac{1}{2} C_{ijkl}(y_1, y_2, y_3)\, \epsilon_{ij}\, \epsilon_{kl} \mathrm{d}\Omega \tag{A.2}$$

where C_{ijkl} are the components of the periodically varying fourth-order elasticity tensor and ϵ_{ij} are the components of the 3D strain tensor defined for linear theory as

$$\epsilon_{ij}(\mathbf{n}; \mathbf{y}) = \frac{1}{2} \left[\frac{\partial u_i(\mathbf{n}; \mathbf{y})}{\partial y_j} + \frac{\partial u_j(\mathbf{n}; \mathbf{y})}{\partial y_i} \right] \tag{A.3}$$

Here $u_i(\mathbf{n}; \mathbf{y})$ are functions of the integer coordinates and the local coordinates for each UC. In view of the fact that the infinite many UCs form a continuous heterogeneous material, we

[2] Although it is possible to use the present methodology to obtain inelastic properties of heterogeneous materials, we will focus on elastic properties in this study.

need to enforce the continuity of the displacement field u_i on the interface between adjacent UCs, which can be written as follows for a UC with integer coordinates (n_1, n_2, n_3):

$$\begin{aligned} u_i(n_1, n_2, n_3; d_1/2, y_2, y_3) &= u_i(n_1 + 1, n_2, n_3; -d_1/2, y_2, y_3) \\ u_i(n_1, n_2, n_3; y_1, d_2/2, y_3) &= u_i(n_1, n_2 + 1, n_3; y_1, -d_2/2, y_3) \\ u_i(n_1, n_2, n_3; y_1, y_2, d_3/2) &= u_i(n_1, n_2, n_3 + 1; y_1, y_2, -d_3/2) \end{aligned} \tag{A.4}$$

According to the principle of minimum total potential energy, the exact solution will minimize the energy in Eq. (A.2) under the constraints in Eq. (A.1) and Eqs. (A.4). Although correctly formulated, this problem is very difficult to solve due to discrete integer arguments. To take advantage of well-developed analytical techniques for continuous functions, we need to transform the formulation into a more convenient format using the idea of quasicontinuum (Kunin, 1982). The basic idea is to associate a function of integer arguments defined in the integer space with a continuous function defined in $\mathcal{R}$. Following the procedures spelled out in Berdichevsky (1977), we can reformulate Eqns. (A.2), (A.3), and (A.4) respectively as:

$$\Pi = \int_{\mathcal{R}} \left\langle \frac{1}{2} C_{ijkl}\, \epsilon_{ij}\, \epsilon_{kl} \right\rangle \mathrm{d}\mathcal{R} \tag{A.5}$$

$$\epsilon_{ij}(\mathbf{x}; \mathbf{y}) = \frac{1}{2} \left[\frac{\partial u_i(\mathbf{x}; \mathbf{y})}{\partial y_j} + \frac{\partial u_j(\mathbf{x}; \mathbf{y})}{\partial y_i} \right] \equiv u_{(i|j)} \tag{A.6}$$

and

$$\begin{aligned} u_i(x_1, x_2, x_3; d_1/2, y_2, y_3) &= u_i(x_1 + d_1, x_2, x_3; -d_1/2, y_2, y_3) \\ u_i(x_1, x_2, x_3; y_1, d_2/2, y_3) &= u_i(x_1, x_2 + d_2, x_3; y_1, -d_2/2, y_3) \\ u_i(x_1, x_2, x_3; y_1, y_2, d_3/2) &= u_i(x_1, x_2, x_3 + d_3; y_1, y_2, -d_3/2) \end{aligned} \tag{A.7}$$

Using the technique of Lagrange multipliers, we can pose the variational statement of

the micromechanical analysis of UC as a stationary value problem of the following functional:

$$\begin{aligned} J =& \frac{1}{2}\int_{\mathcal{R}} \left[\left\langle C_{ijkl}\, u_{(i|j)}\, u_{(k|l)}\right\rangle + \lambda_i(\langle u_i\rangle - v_i)\right] \mathrm{d}\mathcal{R} \\ &+ \int_{\mathcal{R}}\int_{S_1} \beta_{i1}\left[u_i(x_1,x_2,x_3;d_1/2,y_2,y_3) - u_i(x_1+d_1,x_2,x_3;-d_1/2,y_2,y_3)\right]\mathrm{d}S_1\mathrm{d}\mathcal{R} \\ &+ \int_{\mathcal{R}}\int_{S_2} \beta_{i2}\left[u_i(x_1,x_2,x_3;y_1,d_2/2,y_3) - u_i(x_1,x_2+d_2,x_3;y_1,-d_2/2,y_3)\right]\mathrm{d}S_2\mathrm{d}\mathcal{R} \\ &+ \int_{\mathcal{R}}\int_{S_3} \beta_{i3}\left[u_i(x_1,x_2,x_3;y_1,y_2,d_3/2) - u_i(x_1,x_2,x_3+d_3;y_1,y_2,-d_3/2)\right]\mathrm{d}S_3\mathrm{d}\mathcal{R} \end{aligned} \tag{A.8}$$

where λ_i and β_{ij} are Lagrange multipliers introducing constraints in Eqs. (A.1) and (A.7), respectively, and S_i are the surfaces with $n_i = 1$. Because v_i is unvarying for the UC, our problem is to find the displacement field u_i vanishing the first variation of J, which is solved asymptotically using VAM in the following section.

A.3 Variational Asymptotic Method For Unit Cell Homogenization

In view of Eq. (A.1), it is natural to express the exact solution u_i as a sum of the volume average v_i plus the difference, such that

$$u_i(\mathbf{x};\mathbf{y}) = v_i(\mathbf{x}) + w_i(\mathbf{x};\mathbf{y}) \tag{A.9}$$

where $\langle w_i\rangle = 0$ according to Eq. (A.1). The very reason that the heterogeneous material can be homogenized leads us to believe that w_i should be asymptotically smaller than v_i, *i.e.*

$$w_i \sim \eta\, v_i \tag{A.10}$$

Substituting Eq. (A.9) into Eq. (A.8) and making use of Eqs. (A.6) and (A.10), we can obtain the leading terms of the functional as:

$$\begin{aligned} J_1 =& \frac{1}{2}\int_{\mathcal{R}} \left[\left\langle C_{ijkl}\, w_{(i|j)}\, w_{(k|l)}\right\rangle + \lambda_i \langle w_i\rangle\right] \mathrm{d}\mathcal{R} \\ &+ \int_{\mathcal{R}}\int_{S_1} \beta_{i1}\left[w_i(\mathbf{x};d_1/2,y_2,y_3) - w_i(\mathbf{x};-d_1/2,y_2,y_3) - \frac{\partial v_i}{\partial x_1}d_1\right]\mathrm{d}S_1\mathrm{d}\mathcal{R} \\ &+ \int_{\mathcal{R}}\int_{S_2} \beta_{i2}\left[w_i(\mathbf{x};y_1,d_2/2,y_3) - w_i(\mathbf{x};y_1,-d_2/2,y_3) - \frac{\partial v_i}{\partial x_2}d_2\right]\mathrm{d}S_2\mathrm{d}\mathcal{R} \\ &+ \int_{\mathcal{R}}\int_{S_3} \beta_{i3}\left[w_i(\mathbf{x};y_1,y_2,d_3/2) - w_i(\mathbf{x};y_1,y_2,-d_3/2) - \frac{\partial v_i}{\partial x_3}d_3\right]\mathrm{d}S_3\mathrm{d}\mathcal{R} \end{aligned} \tag{A.11}$$

Although it is possible to carry out the variation of J_1 and find the Euler-Lagrange equations

and associated boundary conditions for w_i, which corresponds to homogenous governing differential equations along with inhomogeneous boundary conditions. It is more convenient to use change of variables to reformulate the same problem so that inhomogeneous governing differential equations along with homogeneous boundary conditions can be obtained. Considering the last three terms in Eq. (A.11), we use the following change of variables:

$$w_i(\mathbf{x};\mathbf{y}) = y_j \frac{\partial v_i}{\partial x_j} + \chi_i(\mathbf{x};\mathbf{y}) \tag{A.12}$$

with χ termed as fluctuation functions. Notice, we still have $\langle \chi_i \rangle = 0$ if the origin of the local system is chosen to be the center of UC. Then from the functional J_1 in Eq. (A.11), we can obtain the following functional defined over a UC:

$$\begin{aligned} J_1^* =& \frac{1}{2} \left\langle C_{ijkl} \left[\bar{\epsilon}_{ij} + \chi_{(i|j)}\right] \left[\bar{\epsilon}_{kl} + \chi_{(k|l)}\right] \right\rangle + \lambda_i \langle \chi_i \rangle \\ &+ \int_{S_1} \beta_{i1} \left[\chi_i(\mathbf{x}; d_1/2, y_2, y_3) - \chi_i(\mathbf{x}; -d_1/2, y_2, y_3)\right] \mathrm{d}S_1 \\ &+ \int_{S_2} \beta_{i2} \left[\chi_i(\mathbf{x}; y_1, d_2/2, y_3) - \chi_i(\mathbf{x}; y_1, -d_2/2, y_3)\right] \mathrm{d}S_2 \\ &+ \int_{S_3} \beta_{i3} \left[\chi_i(\mathbf{x}; y_1, y_2, d_3/2) - \chi_i(\mathbf{x}; y_1, y_2, -d_3/2)\right] \mathrm{d}S_3 \end{aligned} \tag{A.13}$$

where $\bar{\epsilon}_{ij} = v_{(i,j)}$ will be shown later to be the components of the global strain tensor for the structure with homogenized effective material properties. The functional J_1^* in Eq. (A.13) forms the backbone of the present theory, variational asymptotic method for unit cell homogenization (VAMUCH). Performing the variation, we can obtain conditions for J_1^* to be stationary as:

$$\frac{\partial}{\partial y_l} C_{ijkl} \left(\bar{\epsilon}_{ij} + \chi_{(i|j)}\right) = 0 \quad \text{in} \quad \Omega \tag{A.14}$$

$$\chi_i(\mathbf{x}; d_1/2, y_2, y_3) = \chi_i(\mathbf{x}; -d_1/2, y_2, y_3) \tag{A.15}$$

$$\chi_i(\mathbf{x}; y_1, d_2/2, y_3) = \chi_i(\mathbf{x}; y_1, -d_2/2, y_3) \tag{A.16}$$

$$\chi_i(\mathbf{x}; y_1, y_2, d_3/2) = \chi_i(\mathbf{x}; y_1, y_2, -d_3/2) \tag{A.17}$$

$$C_{ijkl} \left(\bar{\epsilon}_{ij} + \chi_{(i|j)}\right)|_{y_1=d_1/2} = C_{ijkl} \left(\bar{\epsilon}_{ij} + \chi_{(i|j)}\right)|_{y_1=-d_1/2} \tag{A.18}$$

$$C_{ijkl} \left(\bar{\epsilon}_{ij} + \chi_{(i|j)}\right)|_{y_2=d_2/2} = C_{ijkl} \left(\bar{\epsilon}_{ij} + \chi_{(i|j)}\right)|_{y_2=-d_2/2} \tag{A.19}$$

$$C_{ijkl} \left(\bar{\epsilon}_{ij} + \chi_{(i|j)}\right)|_{y_3=d_3/2} = C_{ijkl} \left(\bar{\epsilon}_{ij} + \chi_{(i|j)}\right)|_{y_3=-d_3/2} \tag{A.20}$$

$$\langle \chi_i \rangle = 0 \tag{A.21}$$

where Eq. (A.14) is the governing differential equations, Eqs. (A.15)-(A.17) are the periodic boundary conditions for fluctuation functions, and Eqs. (A.18)-(A.20) are the periodic boundary conditions for local stresses. All these equations are identical to those of MHT, as listed in Manevitch et al. (2002). Although VAMUCH can reproduce the results of MHT as expected, VAMUCH is different from MHT in the following aspects:

- The periodic boundary conditions are derived in VAMUCH, while they are assumed *a priori* in MHT.
- The fluctuation functions are determined uniquely in VAMUCH due to Eq. (8.8), while they can only be determined up to a constant in MHT.
- VAMUCH has an inherent variational nature which is convenient for numerical implementation, while virtual quantities should be carefully chosen to make MHT variational as shown in Guedes and Kikuchi (1990).

The difficulty of solving the variational problem in Eq. (A.13) is tantamount to 3D anisotropic elasticity problems. Closed-form solutions exist only for very simple cases. For general cases we need to turn to numerical techniques such as FEM for approximate solutions.

A.4 Finite Element Implementation of VAMUCH

It is possible to formulate the FEM solution based on Eq. (A.13), however, it is not the most convenient and efficient way. First, Lagrange multipliers will increase the number of unknowns. Second, the linear system will have zeros on the diagonal of the coefficient matrix eluding the use of common LU decomposition technique. Considering the problem governed by Eqs. (A.14)-(A.21), the last equation, Eq. (A.21), will not affect the solution obtained by the rest of equations, which means the variational statement in Eq. (A.13) can be reformulated as seeking the minimum value of the following functional Π_Ω

$$\Pi_\Omega = \frac{1}{2\Omega}\int_\Omega C_{ijkl}\left[\bar{\epsilon}_{ij} + \chi_{(i|j)}\right]\left[\bar{\epsilon}_{kl} + \chi_{(k|l)}\right] \mathrm{d}\Omega \tag{A.22}$$

under the constraints in Eqs. (A.15)-(A.17). The constraints in Eq. (A.21) do not affect the minimum value of Π_Ω but help uniquely determine χ_i. In practice, we can constrain the fluctuation functions at an arbitrary node to be zero and later use these constraints

to recover the unique fluctuation functions. It is fine to use penalty function method to introduce the periodic boundary conditions in Eqs. (A.15)-(A.17), as shown in Hollister and Kikuchi (1992). However, this method introduces additional approximation and the robustness of the solution depends on the choice of large penalty number. Here, we choose to make the nodes on the positive boundary surface (*i.e.*, $y_i = d_i/2$) slave to the nodes on the opposite negative boundary surface (*i.e.*, $y_i = -d_i/2$). By assembling all the independent active degrees of freedom, we can implicitly and exactly incorporate the periodic boundary conditions in Eqs. (A.15)-(A.17). In this way, we also reduce the total number of unknowns in the linear system.

Introduce the following matrix notations

$$\bar{\epsilon} = \lfloor \bar{\epsilon}_{11} \;\; 2\bar{\epsilon}_{12} \;\; \bar{\epsilon}_{22} \;\; 2\bar{\epsilon}_{13} \;\; 2\bar{\epsilon}_{23} \;\; \bar{\epsilon}_{33} \rfloor^T \tag{A.23}$$

$$\begin{Bmatrix} \frac{\partial \chi_1}{\partial y_1} \\ \frac{\partial \chi_1}{\partial y_2} + \frac{\partial \chi_2}{\partial y_1} \\ \frac{\partial \chi_2}{\partial y_2} \\ \frac{\partial \chi_1}{\partial y_3} + \frac{\partial \chi_3}{\partial y_1} \\ \frac{\partial \chi_2}{\partial y_3} + \frac{\partial \chi_3}{\partial y_2} \\ \frac{\partial \chi_3}{\partial y_3} \end{Bmatrix} = \begin{bmatrix} \frac{\partial}{\partial y_1} & 0 & 0 \\ \frac{\partial}{\partial y_2} & \frac{\partial}{\partial y_1} & 0 \\ 0 & \frac{\partial}{\partial y_2} & 0 \\ \frac{\partial}{\partial y_3} & 0 & \frac{\partial}{\partial y_1} \\ 0 & \frac{\partial}{\partial y_3} & \frac{\partial}{\partial y_2} \\ 0 & 0 & \frac{\partial}{\partial y_3} \end{bmatrix} \begin{Bmatrix} \chi_1 \\ \chi_2 \\ \chi_3 \end{Bmatrix} \equiv \Gamma_h \chi \tag{A.24}$$

where Γ_h is an operator matrix and χ is a column matrix containing the three components of the fluctuation functions. If we discretize χ using the finite elements as

$$\chi(x_i; y_i) = S(y_i)\mathcal{X}(x_i) \tag{A.25}$$

where S representing the shape functions (in the assembled sense disregarding the constrained node and slave nodes) and $\mathcal{X}$ a column matrix of the nodal values of the fluctuation functions for all active nodes. Substituting Eqs. (A.23)-(A.25) into Eq. (A.22), we obtain a discretized version of the functional as

$$\Pi_\Omega = \frac{1}{2\Omega}(\mathcal{X}^T E \mathcal{X} + 2\mathcal{X}^T D_{h\epsilon}\bar{\epsilon} + \bar{\epsilon}^T D_{\epsilon\epsilon}\bar{\epsilon}) \tag{A.26}$$

where

$$E = \int_{\Omega} (\Gamma_h S)^T D (\Gamma_h S) \mathrm{d}\Omega \quad D_{h\epsilon} = \int_{\Omega} (\Gamma_h S)^T D \mathrm{d}\Omega \quad D_{\epsilon\epsilon} = \int_{\Omega} D \mathrm{d}\Omega \tag{A.27}$$

with D as the 6×6 material matrix condensed from the fourth-order elasticity tensor C_{ijkl}. Since the periodic constraints have already been incorporated through assembly in Eq. (A.25), our problem becomes to minimize Π_Ω in Eq. (A.26), which gives us the following linear system

$$E\mathcal{X} = -D_{h\epsilon}\bar{\epsilon} \tag{A.28}$$

It is clear that $\mathcal{X}$ will linearly depend on $\bar{\epsilon}$, which means it is unnecessary to assign values to $\bar{\epsilon}$ (even 1's and 0's as in common practice), and they can be treated as symbols without entering the computation. The solution can be written as

$$\mathcal{X} = \mathcal{X}_0 \bar{\epsilon} \tag{A.29}$$

Substituting Eq. (2.33) into Eq. (A.26), we can calculate the energy storing in the UC

$$\Pi_\Omega = \frac{1}{2\Omega} \bar{\epsilon}^T (\mathcal{X}_0^T D_{h\epsilon} + D_{\epsilon\epsilon}) \bar{\epsilon} \equiv \frac{1}{2} \bar{\epsilon}^T \bar{D} \bar{\epsilon} \tag{A.30}$$

Clearly $\bar{D}$ is the so-called effective (or homogenized) material matrix and $\bar{\epsilon}$ the global strains. The effective medium has an energy density Π_Ω, which can be used to carry out macroscopic analyses.

If the local fields within the UC are of interest, we can recover those fields based on the global displacements v, global strains $\bar{\epsilon}$, and the fluctuation functions χ. To this end, we need to uniquely determine the fluctuation functions first, otherwise, we could not uniquely determine the local displacement field. Recall, we fixed an arbitrary node and made nodes on the positive boundary surfaces slave to facilitate the solution for the fluctuation functions. First, we need to construct a new array $\tilde{\mathcal{X}}_0$ from $\mathcal{X}_0$ by assigning the values for slave nodes according to the corresponding active nodes and assign zeros to the fixed node. Obviously, $\tilde{\mathcal{X}}_0$ still yields the minimum value of Π_Ω in Eq. (A.22) under constrains in Eqs. (A.15)-(A.17). However, $\tilde{\mathcal{X}}_0$ may not satisfy the constraints in Eq. (A.21) because it is different from the real solution by a constant. To find the real solution, denoting as $\bar{\mathcal{X}}_0$, we need to

construct a discretized version of Eq. (A.21). Let us rewrite Eq. (A.21) as

$$\int_{\Omega} \chi^T \psi \mathrm{d}\Omega = 0 \tag{A.31}$$

with ψ as the 3×3 identity matrix. It can be easily verified that ψ is the kernel matrix of Γ_h in Eq. (A.24). Both χ and ψ can discretized using the finite elements as

$$\chi = \bar{S}\bar{\mathcal{X}} \qquad \psi = \bar{S}\Psi \tag{A.32}$$

with Ψ as the discretized kernel matrix. Substituting Eq. (A.32) to Eq. (A.31), we can obtain the discretized version of the constraints as:

$$\bar{\mathcal{X}}^T H \Psi = 0 \tag{A.33}$$

with $H = \int_{\Omega} \bar{S}^T S \mathrm{d}\Omega$. Please note that we can always normalize the kernel matrix so that $\Psi^T H \Psi = \psi$.

The real solution $\bar{\mathcal{X}}$ can be expressed as

$$\bar{\mathcal{X}} = \tilde{\mathcal{X}}_0 \bar{\epsilon} + \Psi \lambda \tag{A.34}$$

where λ are constants to be determined. Substituting the above relation into Eq. (A.33), we can solve λ as

$$\lambda = -\Psi^T H \tilde{\mathcal{X}}_0 \bar{\epsilon} \tag{A.35}$$

Then, the real solution is

$$\bar{\mathcal{X}} = (I - \Psi\Psi^T H)\tilde{\mathcal{X}}_0 \bar{\epsilon} \equiv \bar{\mathcal{X}}_0 \bar{\epsilon} \tag{A.36}$$

with I as the $n \times n$ identity matrix and n is the total number of degrees of freedom.

After the fluctuation functions are determined uniquely, we can recover the local displacement based on Eqs. (A.9), (A.12), and (A.32) as

$$u = v + \begin{bmatrix} \frac{\partial v_1}{\partial x_1} & \frac{\partial v_1}{\partial x_2} & \frac{\partial v_1}{\partial x_3} \\ \frac{\partial v_2}{\partial x_1} & \frac{\partial v_2}{\partial x_2} & \frac{\partial v_2}{\partial x_3} \\ \frac{\partial v_3}{\partial x_1} & \frac{\partial v_3}{\partial x_2} & \frac{\partial v_3}{\partial x_3} \end{bmatrix} \begin{Bmatrix} y_1 \\ y_2 \\ y_3 \end{Bmatrix} + \bar{S}\bar{\mathcal{X}}_0 \bar{\epsilon} \tag{A.37}$$

with u as the column matrix of u_i and v as the column matrix of v_i. The local strain field can be recovered using Eqs. (A.6) and (A.24) as

$$\epsilon = \bar{\epsilon} + \Gamma_h \bar{S} \bar{\mathcal{X}}_0 \bar{\epsilon} \tag{A.38}$$

Finally, the local stress field can be recovered straightforwardly as

$$\sigma = D\epsilon \tag{A.39}$$

It can be easily verified that

$$\langle \sigma \rangle = \bar{D}\bar{\epsilon} \tag{A.40}$$

which is expected because the effective material matrix can be equivalently defined through the energy density of the UC or the relation between the average stress and average strain of the UC. In comparison to common numerical micromechanical simulations in the literature, the present implementation is unique in the following aspects:

- No external load is necessary to perform the simulation and the complete set of material properties can be predicted within one analysis.
- The fluctuation functions and local displacements can be determined uniquely;
- The effective material properties and recovered local fields are calculated directly with the same accuracy of the fluctuation functions. No postprocessing type calculations which introduces more approximations are needed.
- The dimensionality of the problem is determined by that of the periodicity of the UC. A complete set of 3D material properties can be obtained using a 1D analysis of microstructures with 1D periodicity such as binary composites. It is noted that the macroscopic analysis of a structure made with material having 1D periodicity could be 3D, which requires the complete set of effective material properties.

We have coded the above formulation using Fortran 90/95 into a program named VAMUCH. To demonstrate the application, accuracy, and efficiency of this theory and code, we will analyze several material systems using VAMUCH in the next section.

A.5 Validation of VAMUCH

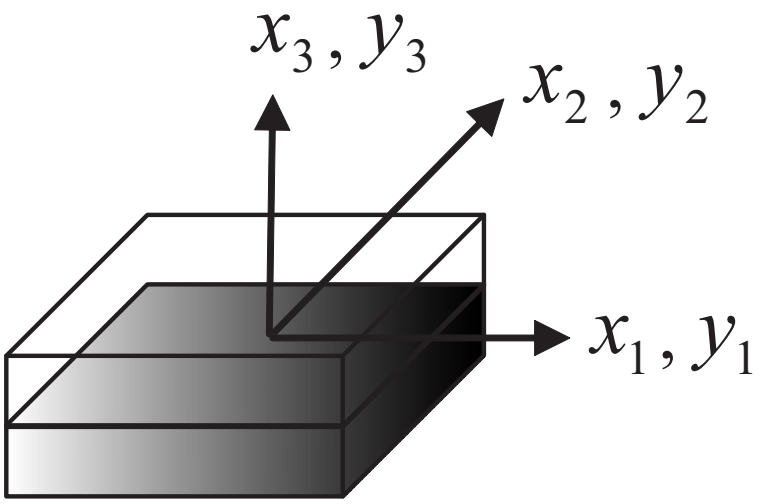

Fig. A.4: Sketch of a binary composite.

VAMUCH provides a unified analysis for general 1D, 2D, or 3D UCs. First, the same code VAMUCH can be used to homogenize binary composites (modeled using 1D UCs), fiber reinforced composites (modeled using 2D UCs), and particle reinforced composites (modeled using 3D UCs). Second, VAMUCH can reproduce the results for lower-dimensional UCs using higher-dimensional UCs. That is, VAMUCH will predict the same results for binary composites using 1D, 2D or 3D UCs, and for fiber reinforced composites using 2D or 3D UCs.

A.5.1 Binary Composites

First, let us consider a periodic binary composite formed by orthotropic layers and the material axes are the same as the global coordinates x_i so that the material is uniform in the $x_1 - x_2$ plane and periodic along x_3 direction. A typical UC can be identified as shown in Fig. A.4, the dimension along y_3 is h and dimensions along y_1 and y_2 can be arbitrary. Let ϕ_1 and ϕ_2 denote the volume fractions of the first phase and the second phase, respectively, and we have $\phi_1 + \phi_2 = 1$. This problem has been solved analytically in Yu (2005). The

strain energy density of the effective material can be obtained as:

$$\Pi_\Omega = \frac{1}{2}\begin{Bmatrix} \bar{\epsilon}_{11} \\ 2\bar{\epsilon}_{12} \\ \bar{\epsilon}_{22} \\ 2\bar{\epsilon}_{13} \\ 2\bar{\epsilon}_{23} \\ \bar{\epsilon}_{33} \end{Bmatrix}^T \begin{bmatrix} c_{11}^* & 0 & c_{13}^* & 0 & 0 & c_{16}^* \\ 0 & c_{22}^* & 0 & 0 & 0 & 0 \\ c_{13}^* & 0 & c_{33}^* & 0 & 0 & c_{36}^* \\ 0 & 0 & 0 & c_{44}^* & 0 & 0 \\ 0 & 0 & 0 & 0 & c_{55}^* & 0 \\ c_{16}^* & 0 & c_{36}^* & 0 & 0 & c_{66}^* \end{bmatrix} \begin{Bmatrix} \bar{\epsilon}_{11} \\ 2\bar{\epsilon}_{12} \\ \bar{\epsilon}_{22} \\ 2\bar{\epsilon}_{13} \\ 2\bar{\epsilon}_{23} \\ \bar{\epsilon}_{33} \end{Bmatrix} \tag{A.41}$$

It can be observed that the homogenized material properties still have the same orthotropic symmetry for this special case, although in general the homogenized material could be anisotropic, which means a fully populated 6×6 stiffness matrix. The expressions of effective material properties c_{ij}^* are listed here.

$$\begin{aligned}
c_{11}^* &= \langle c_{11} \rangle - \frac{\phi_1\phi_2(c_{16}^{(2)} - c_{16}^{(1)})^2}{\phi_1 c_{66}^{(2)} + \phi_2 c_{66}^{(1)}} \\
c_{13}^* &= \langle c_{13} \rangle - \frac{\phi_1\phi_2(c_{16}^{(2)} - c_{16}^{(1)})(c_{36}^{(2)} - c_{36}^{(1)})}{\phi_1 c_{66}^{(2)} + \phi_2 c_{66}^{(1)}} \\
c_{16}^* &= \frac{\phi_1 c_{16}^{(1)} c_{66}^{(2)} + \phi_2 c_{16}^{(2)} c_{66}^{(1)}}{\phi_1 c_{66}^{(2)} + \phi_2 c_{66}^{(1)}} \\
c_{33}^* &= \langle c_{33} \rangle - \frac{\phi_1\phi_2(c_{36}^{(2)} - c_{36}^{(1)})^2}{\phi_1 c_{66}^{(2)} + \phi_2 c_{66}^{(1)}} \\
c_{36}^* &= \frac{\phi_1 c_{36}^{(1)} c_{66}^{(2)} + \phi_2 c_{36}^{(2)} c_{66}^{(1)}}{\phi_1 c_{66}^{(2)} + \phi_2 c_{66}^{(1)}} \\
c_{66}^* &= 1/\left\langle \frac{1}{c_{66}} \right\rangle \quad c_{55}^* = 1/\left\langle \frac{1}{c_{55}} \right\rangle \quad c_{44}^* = 1/\left\langle \frac{1}{c_{44}} \right\rangle \quad c_{22}^* = \langle c_{22} \rangle
\end{aligned} \tag{A.42}$$

where the superscripted quantities are those from each phase of the composite. It can be observed that even for this simple case, only c_{22}^* is the same as the rule of mixture based on the Voigt hypothesis, and $c_{44}^*, c_{55}^*, c_{66}^*$ are the same as the rule of mixture based on the Reuss hypothesis. All the other components are different from these two rules of mixture. The effective material properties of the present theory reproduce those of a mathematical homogenization theory in Manevitch et al. (2002). When both layers are made of isotropic material, having Lamé properties λ_1, μ_1 for layer 1 and λ_2, μ_2 for layer 2, the formulas in Eq. (A.42) reproduce the well-known exact expressions listed on Page 140 of Christensen

Table A.1: Effective material properties of boron/aluminum composites

Models	E_{11} (GPa)	E_{22} (GPa)	G_{12} (GPa)	G_{23} (GPa)	ν_{12}	ν_{23}
VAMUCH	215.3	144.1	54.39	45.92	0.195	0.255
FEM	215	144	57.2	45.9	0.19	0.29
MOC	215	142.6	51.3	43.7	0.20	0.25
GMC	215.0	141.0	51.20	43.70	0.197	0.261
HFGMC	215.4	144.0	54.34	45.83	0.195	0.255
ECM	215	143.4	54.3	45.1	0.19	0.26

(1979) which was obtained by Postma (1955).

Yu (2005) shows that the fluctuation functions are piecewise linear functions for binary composites, which means we can use 2-noded line elements for 1D UC in VAMUCH to exactly, in the numerical sense, reproduce the analytical solution. We have also obtained the same results using 2D and 3D UCs numerically. For the sake of saving space, such results are not presented here. Suffice to state that the numerical results from VAMUCH are exactly the same as the analytical solution within the machine precision.

A.5.2 Fiber Reinforced Composites

To show the predictive capability of VAMUCH for unidirectional fiber reinforced composites, we choose a few examples extensively studied in the literature. For the first two examples, comparisons are made between FEM (Sun and Vaidya, 1996), method of cell (MOC) (Aboudi, 1982), generalized method of cell (GMC) (Paley and Aboudi, 1992), high-fidelity generalized method of cell (HFGMC) (Aboudi et al., 2001), and elasticity-based cell method (ECM) (Williams, 2005b). The FEM approach of Sun and Vaidya (1996) is established on a rigorous mechanics foundation and 3D RVEs with periodic boundary conditions are used for homogenization. The MOC and its variants (GMC, HFGMC, and ECM) expand the local displacements in terms of global displacements using the Legendre polynomials of different orders. ECM starts from this assumption and solve the equations of continuum mechanics in a strong form. In contrast, MOC, GMC, and HFGMC invokes additional *ad hoc* assumptions such as that the interfacial continuous conditions and periodic boundary conditions are only satisfied in the integral sense. FEM results are directly taken from Sun and Vaidya (1996), MOC and ECM results from Williams (2005b), GMC and HFGMC results from Aboudi et al. (2001).

Table A.2: Effective material properties of graphite/epoxy composites

Models	E_{11} (GPa)	E_{22} (GPa)	G_{12} (GPa)	G_{23} (GPa)	ν_{12}	ν_{23}
VAMUCH	142.9	9.61	6.10	3.12	0.252	0.350
FEM	142.6	9.60	6.00	3.10	0.25	0.35
MOC	143	9.6	5.47	3.08	0.25	0.35
GMC	143.0	9.47	5.68	3.03	0.253	0.358
HFGMC	142.9	9.61	6.09	3.10	0.252	0.350
ECM	143	9.6	5.85	3.07	0.25	0.35

The first example is a boron/aluminum composite. Both constituents are isotropic with Young's modulus $E = 379.3$ GPa and Poisson's ratio $\nu = 0.1$ for boron fibers, and $E = 68.3$ GPa and $\nu = 0.3$ for aluminum matrix. The fiber is of circular shape and arranged in a square array (see the sketch in the middle of Fig. **??**) and the fiber volume fraction is 0.47. The effective material properties predicted by different approaches are listed in Table B.1. It can be observed that MOC and GMC significantly underpredict the shear moduli G_{12} and G_{23} while FEM overpredicts the longitudinal shear modulus G_{12}. The closest correlation for all the values is found between VAMUCH and HFGMC.

The second example is graphite/epoxy composites. Graphite fiber is transversely isotropic with $E_{11} = 235$ GPa, $E_{22} = 14$ GPa, $G_{12} = 28$ GPa, $\nu_{12} = 0.2$, and $\nu_{23} = 0.25$. Epoxy matrix is isotropic with Young's modulus $E = 4.8$ GPa and Poisson's ratio $\nu = 0.34$. The fiber is circular and arranged in a square array and the fiber volume fraction is 0.6. The results from different approaches are listed in Table A.2. Again the closest correlation is found between VAMUCH and HFGMC. Considering the fact that HFGMC uses the governing equations of MHT and that VAMUCH can reproduce MHT, it is not surprising to find out that HFGMC has an excellent agreement with VAMUCH. The FEM and ECM predictions are also very close to VAMUCH results for this case. It is noted that the ECM results listed in Tables B.1 and A.2 are obtained from the 3^{rd} order model. If the 5^{th} order theory is used, the correlation between ECM and VAMUCH might be improved as shown in the following two examples.

In the following two examples, VAMUCH is compared with MOC, ECM (both 3^{rd} order and 5^{th} order), Green's function based approach (G-F) (Walker et al., 1993) and FEM. The results of MOC, ECM, and G-F are directly taken from Williams (2005b), while FEM results are calculated using ANSYS following the approach proposed in Sun and Vaidya

Table A.3: E_{22} (GPa) of W/Cu composites varying with fiber volume fraction

Models	0.0204	0.1837	0.5102	0.7511
VAMUCH	129.92	156.51	229.72	300.99
FEM	129.92	156.51	229.71	301.0
G-F	129.87	156.18	229.09	300.70
MOC	129.50	154.40	226.20	299.00
ECM (3^{rd} order)	129.50	154.60	226.60	299.10
ECM (5^{th} order)	129.80	156.50	229.50	300.80
VAMUCH (circular)	129.81	155.19	226.94	298.12
FEM (circular)	129.82	155.20	226.97	298.14

(1996). To be consistent with Williams (2005b), we use 2D UCs having square inclusions in the center for VAMUCH. As pointed out in Williams (2005b), square inclusions provide a stringent test of correct modeling the local and global behavior of heterogeneous materials due to strong gradients in the local fields induced by the corners. The two material systems we consider are tungsten/copper composite and void/copper composite. Both tungsten and copper are assumed to be isotropic with $E = 395.0$ GPa and $\nu = 0.28$ for tungsten, and $E = 127.0$ GPa and $\nu = 0.34$ for copper.

For both material systems, we calculate the effective transverse Young's modulus at different inclusion volume fractions of 0.0204, 0.1837, 0.5102, and 0.7511. The results are listed in Table A.3 for tungsten/copper composite and Table A.4 for void/copper composite. It is verified that the FEM approach of Sun and Vaidya has no size effects for E_{22}, which means this approach will provide the most accurate prediction of E_{22} with a converged mesh. As one can observe from Tables A.3 and A.4, MOC and 3^{rd} order ECM underpredict this value up to 1.6% for tungsten/copper composite and 8.6% for void/copper composite. VAMUCH, G-F, and 5^{th} order ECM have excellent agreement with FEM, with VAMUCH having the closest correlations.

To show the effect of shape of inclusions, we predict the effective transverse Young's modulus using UC with circular inclusions arranged in a square array. As shown in Tables A.3 and A.4, the shape effects of inclusions become more and more significant and cannot be neglected with large volume fraction of inclusions, particularly for void/copper composites. For example, E_{22} of void/copper composite with square holes is 80% larger than the composite with circular holes when the void volume fraction reaches 0.7511. It is interesting to note that E_{22} of the W/Cu composite with square inclusions is slightly larger

Table A.4: E_{22} (GPa) of Void/Cu composites varying with void volume fraction

Models	0.0204	0.1837	0.5102	0.7511
VAMUCH	120.22	81.73	39.75	18.25
FEM	120.22	81.70	39.75	18.25
G-F	120.63	83.50	40.48	18.40
MOC	110.20	75.27	38.22	17.99
ECM (3^{rd})	110.20	75.38	38.23	17.99
ECM (5^{th})	118.90	80.97	39.64	18.20
VAMUCH (circular)	120.34	82.67	39.08	10.31
FEM (circular)	120.34	82.64	39.08	10.31

than that with circular inclusions, with the difference getting bigger with larger fiber volume fraction. However, for the case of Void/Cu, material with square voids is slightly smaller than that with circular voids for small void volume fractions. As the void volume fraction getting bigger the trend is reversed. A parametric study is carried out to find out the point where the trend is reversed. As observed from Fig. A.5, when the void volume fraction is greater than zero and less than 0.45 (approximate), E_{22} of materials having square voids are slightly smaller than those having circular voids. When the void volume fraction is greater than 0.45 (approximate), materials with square voids have bigger E_{22} that those with circular voids.

A.5.3 Particle Reinforced Composites

Due to special arrangements of constituents of particle reinforced composites, 3D UCs are required to accurately model the microstructures. We are going to use VAMUCH to analyze several particle reinforced composites to validate its 3D capability. In previous section, we have shown that the prediction of MOC and GMC is not accurate for fiber reinforced composites and one could infer that they can not provide very accurate prediction for particle reinforced composites either. Although HFGMC and G-F provide excellent prediction for fiber reinforced composites, we could not find 3D examples analyzed by these two approaches. It is easy to verify that Sun and Vaidya's FEM approach is equally applicable to particle reinforced composites. Two other approaches we believe will provide critical evaluations for VAMUCH are the 3D version of ECM (Williams, 2005a) and an approach based on mathematical homogenization theory and finite element method (Banks-Sills et al., 1997) (later we follow Williams (2005a) to name this approach as HFE).

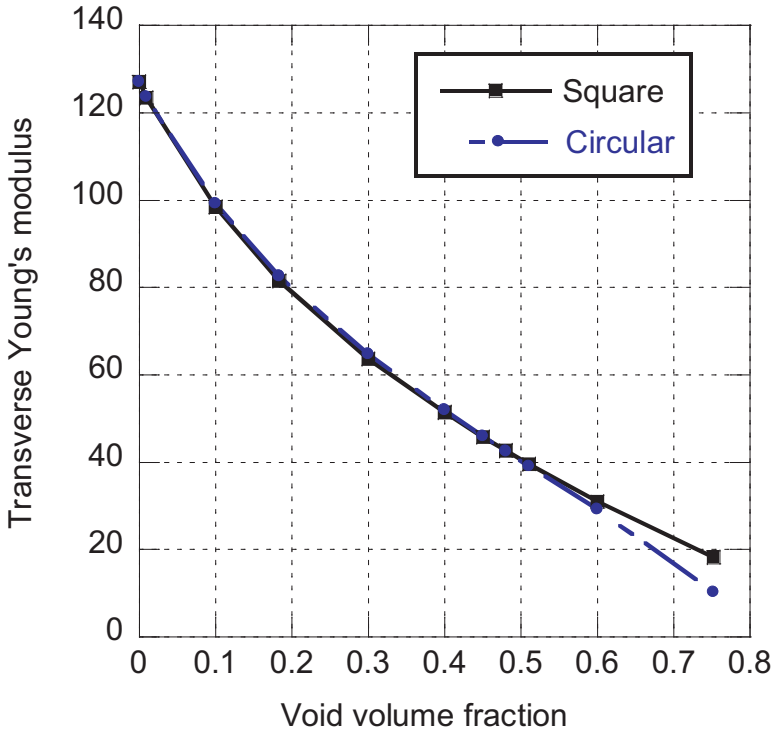

Fig. A.5: Change of Young's modulus of material with square voids and circular voids with respect to void volume fractions.

The first example is to predict the effective Young's modulus for a glass/epoxy composite. The UC of this composite is composed of glass spheres embedded in a triply periodic cubic array. Both constituents are isotropic with Young's modulus $E = 76.00$ GPa and Poisson's ratio $\nu = 0.23$ for glass, and Young's modulus $E = 3.01$ GPa and Poisson's ratio $\nu = 0.394$ for epoxy[3] We plot the change of effective Young's modulus with respect to the inclusion volume fraction in Fig. B.9. In comparison to HFE, VAMUCH outperforms ECM (both 3^{rd} order and 5^{th} order). We are surprised to find out that it is counter intuitive that the predictions of 5^{th} order ECM are worse than 3^{rd} order ECM for this particular case. It is worthy to point out that the data of HFE and ECM are provided independently by the author of Williams (2005a), where ECM data are calculated and HFE data are directly picked out from the plots in Banks-Sills et al. (1997).

The second example is a Al_2O_3/Al composite with cubic inclusions in a cubic array. Both constituents are isotropic with Young's $E = 350.00$ GPa and Poisson's ratio $\nu = 0.30$ for aluminum oxide, and Young's modulus $E = 70.00$ GPa and Poisson's ratio $\nu = 0.30$ for aluminum. The effective Young's modulus and Poisson's ratio are plotted in Fig. A.7 and

[3]The isotropic assumption is convenient for comparing with available results in the literature. VAMUCH can deal with constituents with full anisotropy with material properties characterized as many as 21 independent constants.

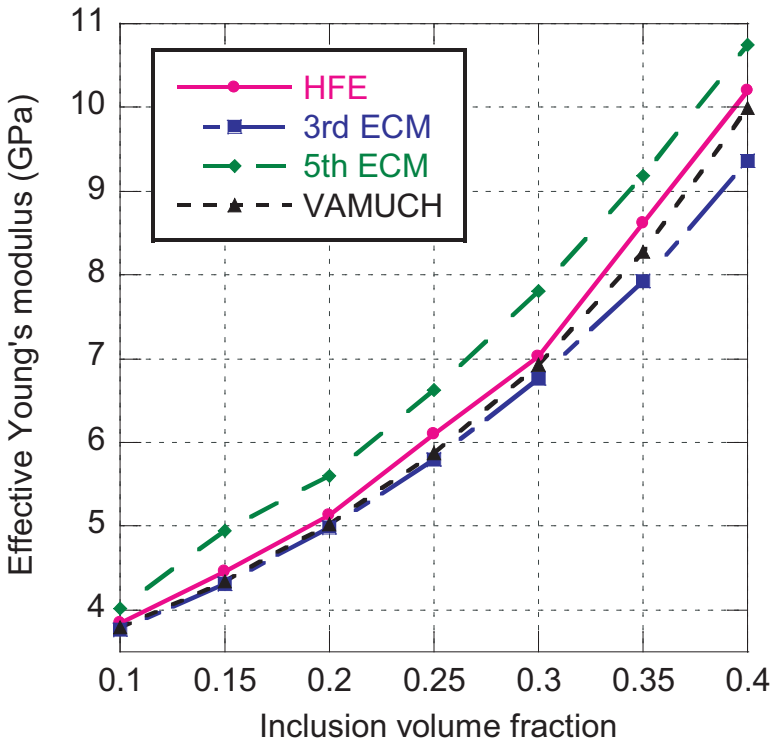

Fig. A.6: Effective Young's modulus of glass/epoxy composite with spherical inclusions.

Fig. A.8, respectively. It can be observed that both VAMUCH and 5$^{\text{th}}$ order ECM have an excellent agreement with HFE while the predictions of 3$^{\text{rd}}$ order ECM are not as accurate.

The last example is a Al_2O_3/Al composite having rectangular parallelepiped inclusions with the ratio between the three dimensions as $a_1 : a_2 : a_3 = 2 : 1 : 2$ where a_i is the dimension of the inclusion along the corresponding y_i direction. The effective material properties of this composite is not isotropic any more. For the sake of saving space, we only plot the effective Young's modulus E_{33} and effective Poisson's ratio ν_{12} as functions of inclusion volume fraction in Fig. A.9 and Fig. A.10, respectively. Again VAMUCH and 5$^{\text{th}}$ order ECM have excellent agreements with HFE and outperform 3$^{\text{rd}}$ order ECM.

A.6 Conclusion

A new micromechanics model, the variational asymptotic method for unit cell homogenization (VAMUCH), has been developed to homogenize heterogeneous materials and recover the local fields within the microstructure after obtaining the global responses of the material. VAMUCH provides a uniform analysis for microstructures which can be described using 1D, 2D, or 3D UCs, such as binary composites, fiber-reinforced composites, and particle-reinforced composites. In comparison to existing micromechanics approaches,

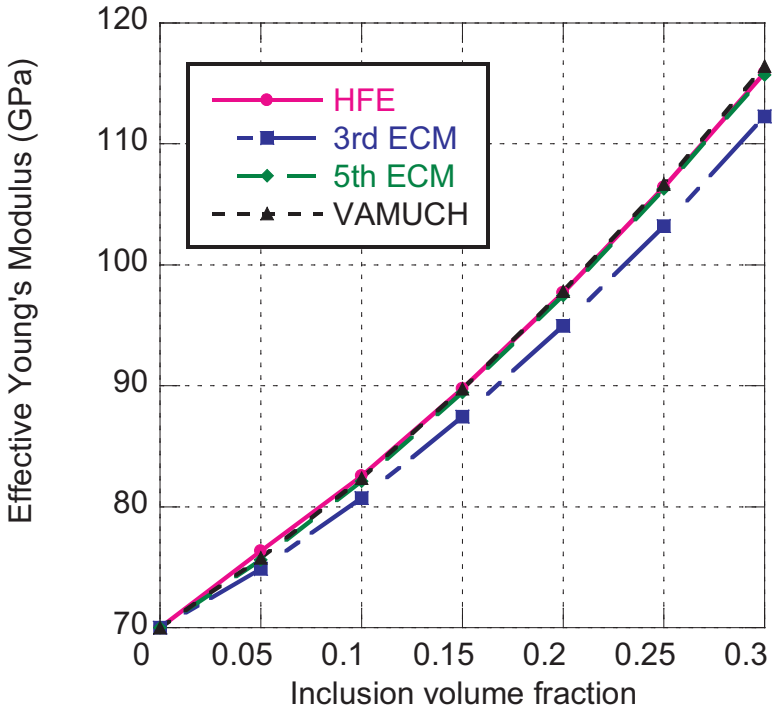

Fig. A.7: Effective Young's modulus of Al_2O_3/Al composites with cubic inclusions.

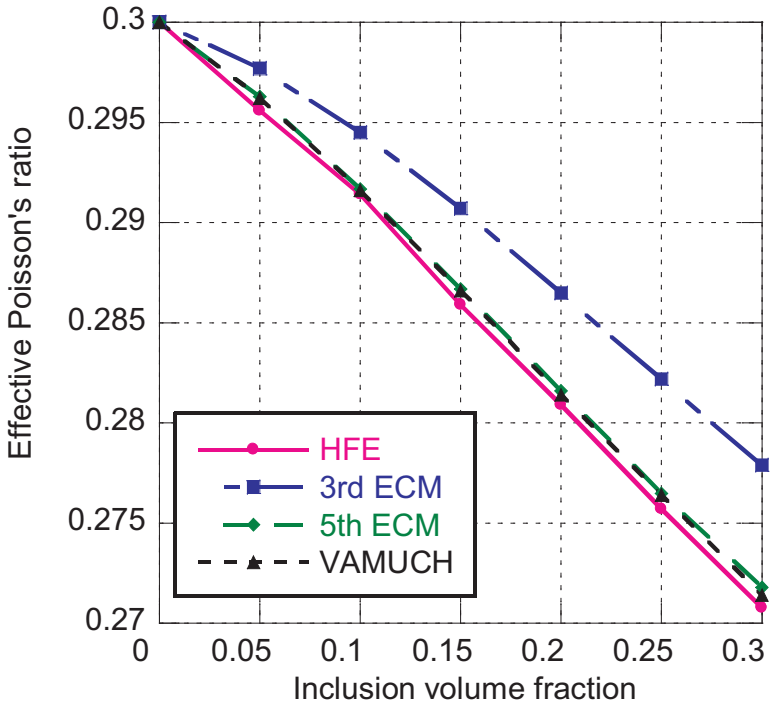

Fig. A.8: Effective Poisson's ratio of Al_2O_3/Al composites with cubic inclusions.

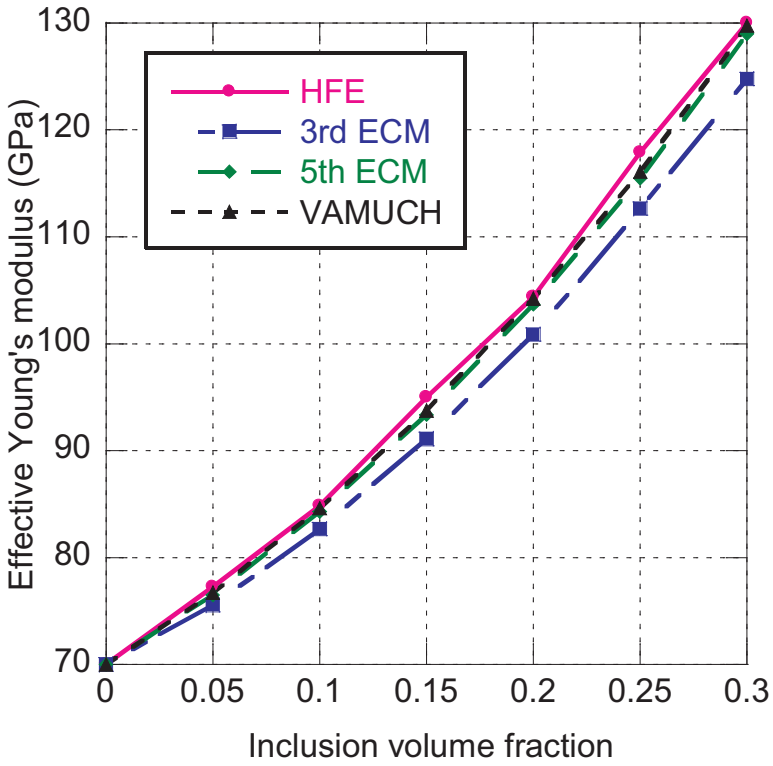

Fig. A.9: Effective Young's modulus E_{33} of Al_2O_3/Al composites with rectangular parallelepiped inclusions.

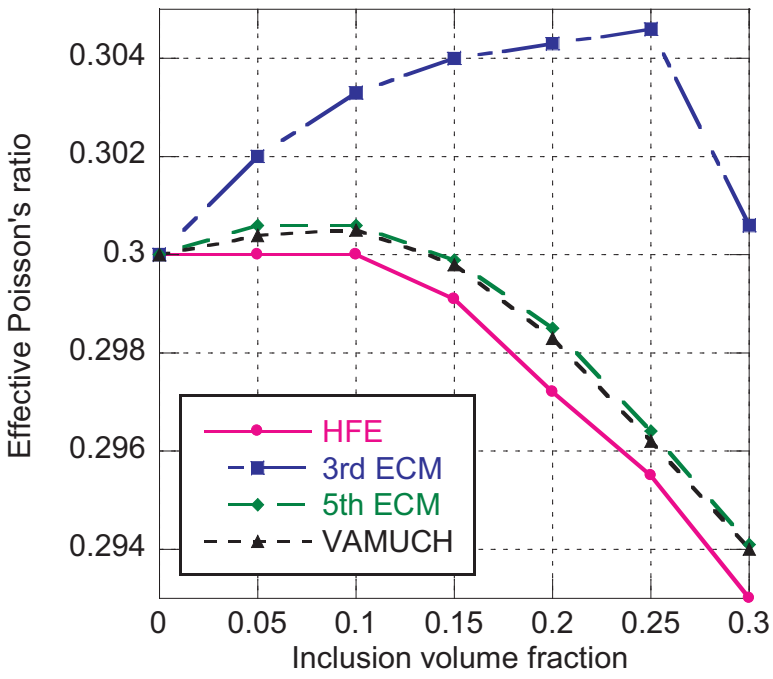

Fig. A.10: Effective Poisson's ratio ν_{12} of Al_2O_3/Al composites with rectangular parallelepiped inclusions.

VAMUCH has the following major advantages:

1. VAMUCH adopts the variational asymptotic method as its mathematical foundation. It has the same rigor as MHT without even assuming periodic fluctuation functions and boundary conditions. VAMUCH uses only assumptions inherent in micromechanics without invoking any additional *ad hoc* assumptions.

2. VAMUCH has an inherent variational nature and its numerical implementation is shown to be straightforward.

3. VAMUCH handles 1D/2D/3D unit cells uniformly. The dimensionality of the problem is determined by that of the periodicity of the unit cell.

4. VAMUCH can obtain different material properties in different directions simultaneously, which is more efficient than those approaches requiring multiple runs under different loading conditions.

5. VAMUCH calculates effective properties and local fields directly with the same accuracy as the fluctuation functions. No postprocessing calculations such as stress averaging and strain averaging are needed.

The companion code, VAMUCH, is extensively validated using various examples including binary composites, fiber reinforced composites, and particle reinforced composites. We can confidently conclude that VAMUCH provides a versatile and convenient tool for engineers to efficiently yet accurately design and analyze heterogeneous materials.

References

Aboudi, J., 1982. A continuum theory for fiber-reinforced elastic-visoplastic composites. International Journal of Engineering Science 20 (5), 605 – 621.

Aboudi, J., 1989. Micromechanical analysis of composites by the method of cells. Applied Mechanics Reviews 42 (7), 193 – 221.

Aboudi, J., Pindera, M. J., Arnold, S. M., 2001. Linear thermoelastic higher-order theory for periodic multiphase materials. Journal of Applied Mechanics 68, 697–707.

Accorsi, M. L., Nemat-Nasser, S., 1986. Bounds on the overall elastic and instantaneous elastoplastic moduli of periodic composites. Mechanics of Materials 5 (3), 209 – 220.

Banerjee, B., Adams, D. O., 2004. On predicting the effective elastic properties of polymer bonded explosives using the recursive cell method. International Journal of Solids and Structures 41 (2), 481 – 509.

Banks-Sills, L., Leiderman, V., Fang, D., 1997. On the effect of particle shape and orientation on elastic properties of metal matrix composites. Composites Part B: Engineering 28B, 465–481.

Bensoussan, A., Lions, J., Papanicolaou, G., 1978. Asymptotic Analysis for Periodic Structures. North-Holland, Amsterdam.

Berdichevsky, V. L., 1977. On averaging of periodic systems. PMM 41 (6), 993 – 1006.

Berdichevsky, V. L., 1979. Variational-asymptotic method of constructing a theory of shells. PMM 43 (4), 664 – 687.

Christensen, R. M., 1979. Mechanics of Composite Materials. Wiley-Interscience, New York.

Dvorak, G. J., Bahei-El-Din, Y. A., 1979. Elastic-plastic behavior of fibrous composites. Journal of Mechanics and Physics of Solids 27, 51–72.

Guedes, J. M., Kikuchi, N., 1990. Preprocessing and postprocessing for materials based on the homogenization method with adaptive finite element method. Computer Methods in Applied Mechanics and Engineering 83, 143–198.

Hashin, Z., 1983. Analysis of composite materials-a survey. Applied Mechanics Review 50, 481–505.

Hashin, Z., Shtrikman, S., 1962. A variational approach to the theory of the elastic behaviour of polycrystals. Journal of Mechanics and Physics of Solids 10, 343–352.

Hill, R., 1952. The elastic behavior of crystalline aggregate. Proc. Phys. Soc. London A65, 349–354.

Hill, R., 1965. Theory of mechanical properties of fibre-strengthened materials-iii. self-consistent model. Journal of Mechanics and Physics of Solids 13, 189–198.

Hollister, S. J., Kikuchi, N., 1992. A comparison of homogenization and standard mechanics analyses for periodic porous composites. Computational Mechanics.

Kunin, I., 1982. Theory of Elastic Media with Microstructure. Vol. 1 and 2. Springer Verlag.

Manevitch, L. I., Andrianov, I. V., Oshmyan, V. G., 2002. Mechanics of Periodically Heterogeneous Structures. Springer.

Milton, G. W., 1981. Bounds on the electromagentic, elastic and other properties of two component composites. Physics Review Letters 46 (8), 542 – 545.

Murakami, H., Toledano, A., 1990. A higer-order mixture homogenization of bi-laminated composites. Journal of Applied Mechanics 57, 388–396.

Paley, M., Aboudi, J., 1992. Micromechanical analysis of composites by the generalized cells model. Mechanics of Materials 14, 127–139.

Postma, G. W., 1955. Wave propagation in a stratified medium. Geophysics 20, 780.

Sun, C. T., Vaidya, R. S., 1996. Prediction of composite properties from a representative volume element. Composites Science and Technology 56, 171 – 179.

Walker, K. P., Freed, A. D., Jordan, E. H., 1993. Accuracy of the generalized self-consistent method in modeling the elastic behavior of periodic composite properties of unidirectional fiber-reinforced composites and their sensitivity coefficients. Philos. Trans. R. Soc. Lond. A345, 545–576.

Williams, T. O., 2005a. A three-dimensional, higher-oder, elasticity-based micromechanics model. International Journal of Solids and Structures 42, 971–1007.

Williams, T. O., 2005b. A two-dimensional, higher-oder, elasticity-based micromechanics model. International Journal of Solids and Structures 42, 1009–1038.

Yu, W., Nov. 5–11 2005. A variational-asymptotic cell method for periodically heterogeneous materials. In: Proceedings of the 2005 ASME International Mechanical Engineering Congress and Exposition. ASME, Orlando, Florida.

Yu, W., Hodges, D. H., 2004a. An asymptotic approach for thermoelastic analysis of laminated composite plates. Journal of Engineering Mechanics 130 (5), 531 – 540.

Yu, W., Hodges, D. H., 2004b. A simple thermopiezoelastic model for composite plates with accurate stress recovery. Smart Materials and Structures 13 (4), 926 – 938.

Yu, W., Hodges, D. H., 2005. Mathematical construction of an engineering thermopiezoelastic model for smart composite shells. Smart Materials and Structures 14 (1), 43–55.

Yu, W., Hodges, D. H., Volovoi, V. V., 2002a. Asymptotic construction of Reissner-like models for composite plates with accurate strain recovery. International Journal of Solids and Structures 39 (20), 5185 – 5203.

Yu, W., Hodges, D. H., Volovoi, V. V., Oct. 2002b. Asymptotic generalization of Reissner-Mindlin theory: accurate three-dimensional recovery for composite shells. Computer Methods in Applied Mechanics and Engineering 191 (44), 5087 – 5109.

Yu, W., Hodges, D. H., Volovoi, V. V., Cesnik, C. E. S., 2002c. On Timoshenko-like modeling of initially curved and twisted composite beams. International Journal of Solids and Structures 39 (19), 5101 – 5121.

Appendix B
A Variational Asymptotic Micromechanics Model for Predicting Thermoelastic Properties of Heterogeneous Materials

[1]

This appendix is a journal paper published in the *International Journal of Solids and Structures*, Vol. 44, No. 22-23, 2007, pp. 7510-7525.

Abstract

A variational asymptotic micromechanics model has been developed for predicting effective thermoelastic properties of composite materials, and recover the local fields within the unit cell. This theory adopts essential assumptions within the concept of micromechanics, achieves an excellent accuracy, and provides a unified treatment for one-dimensional, two-dimensional, and three-dimensional unit cells. This theory is implemented using the finite element method into the computer program, VAMUCH, a general-purpose micromechanics analysis code. Several examples are used to validate the theory and the code. The results are compared with those available in the literature and those produced by a commercial finite element package.

B.1 Introduction

In recent years, more and more structures are made of composite materials with engineered microstructure for better performance. Because the macroscopic structural dimensions are usually several orders of magnitude larger than the characteristic size of constituents, it is not very practical to analyze such structures by meshing all the details of constituent materials. Usually, the concept of unit cell (UC) is used to create a pseudo, "effective", material with homogeneous properties from the original heterogeneous materials with so-called micromechanics models; see Figure B.1.

[1] Coauthored by: Wenbin Yu and Tian Tang.

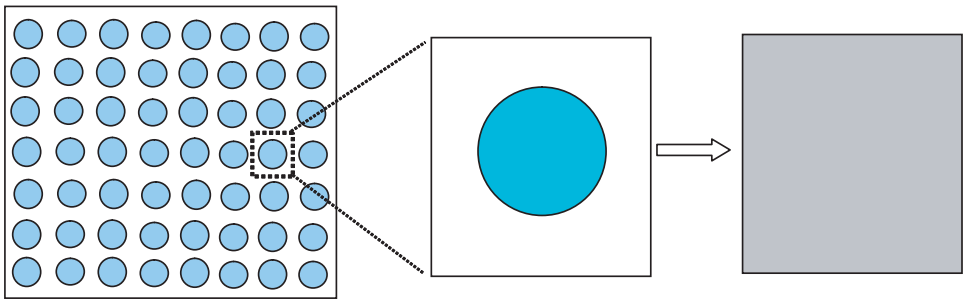

Fig. B.1: Heterogenous material, unit cell, and effective material.

In the past several decades, numerous micromechanics models have been developed; see Hashin (1983) and references cited therein. The simplest models are the rules of mixture based on Voigt and Reuss hypotheses, which provides the upper and lower bounds, respectively (Hill, 1952). The difference between these two bounds could be too large to be useful for general composite materials. To this end, researchers have proposed various techniques to either reduce the difference between the bounds, or find an approximate value between the upper and lower bounds. Typical approaches are the self-consistent model (Hill, 1965) and its generalizations (Dvorak and Bahei-El-Din, 1979; Accorsi and Nemat-Nasser, 1986), the variational approach of Hashin and Shtrikman (Hashin and Shtrikman, 1962), third-order bounds (Milton, 1981), the method of cells (MOC) (Aboudi, 1982) and its variants (Aboudi, 1989; Paley and Aboudi, 1992; Aboudi et al., 2001; Williams, 2005b), recursive cell method (Banerjee and Adams, 2004), mathematical homogenization theories (MHT) (Bensoussan et al., 1978; Murakami and Toledano, 1990), finite element approaches using conventional stress analysis of a representative volume element (RVE) (Sun and Vaidya, 1996), and many others. Although these approaches were originally introduced to predict elastic properties, most of these approaches are also extended to predict thermomechanical properties; see Schapery (1968), Rosen and Hashin (1970), and Aboudi (1984) for a few examples.

Recently, a new technique for micromechanics modeling, namely variational asymptotic method for unit cell homogenization (VAMUCH) (Yu and Tang, 2007), has been developed based on the variational asymptotic method of Berdichevsky (1979). The technique invokes two essential assumptions within the concept of micromechanics:

- **Assumption 1** The exact solutions of the field variables have volume averages over the UC. For example, if u_i are the exact displacements within the UC, there exist v_i

such that

$$v_i = \frac{1}{\Omega}\int_{\Omega} u_i \, \mathrm{d}\Omega \equiv \langle u_i \rangle \tag{B.1}$$

where Ω denotes the domain occupied by the UC and its volume.

- **Assumption 2** The effective material properties obtained from the micromechanical analysis of the UC are independent of the geometry, the boundary conditions, and loading conditions of the macroscopic structure, which means that effective material properties are assumed to be the intrinsic properties of the material when viewed macroscopically.

Please note these assumptions are not restrictive. The mathematical meaning of the first assumption is that the exact solutions of the field variables are integrable over the domain of UC, which is true almost all the time. The second assumption implies that we can neglect the size effects of the material properties in the macroscopic analysis, which is an assumption often made in the conventional continuum mechanics. Of course, the micromechanical analysis of the UC is only needed and appropriate if $\eta = h/l \ll 1$, with h as the characteristic size of the UC and l as the characteristic wavelength of the deformation of the macroscopic material.

In this paper, we will first use this modeling technique to construct a new micromechanics model for effective thermoelastic properties including elastic properties, coefficients of thermal expansion (CTEs), and specific heat for heterogeneous materials. Then we will implement the theory using the finite element method in the computer program VAMUCH to provide engineers with a general-purpose micromechanics tool for thermoelastic micromechanical analysis of composite materials.

B.2 Theoretical Formulation

We need to use three coordinate systems: two cartesian coordinates $\mathbf{x} = (x_1, x_2, x_3)$ and $\mathbf{y} = (y_1, y_2, y_3)$, and an integer-valued coordinate $\mathbf{n} = (n_1, n_2, n_3)$; see Figure B.2. We use x_i as the global coordinates to describe the macroscopic material and y_i parallel to x_i as the local coordinates to describe the UC. Here and throughout the paper, Latin indices assume 1, 2, and 3 and repeated indices are summed over their range except where explicitly indicated. We choose the origin of the local coordinates y_i to be the geometric center of UC. For example, if the UC is a cube with dimensions as d_i, then $y_i \in [-\frac{d_i}{2}, \frac{d_i}{2}]$. To

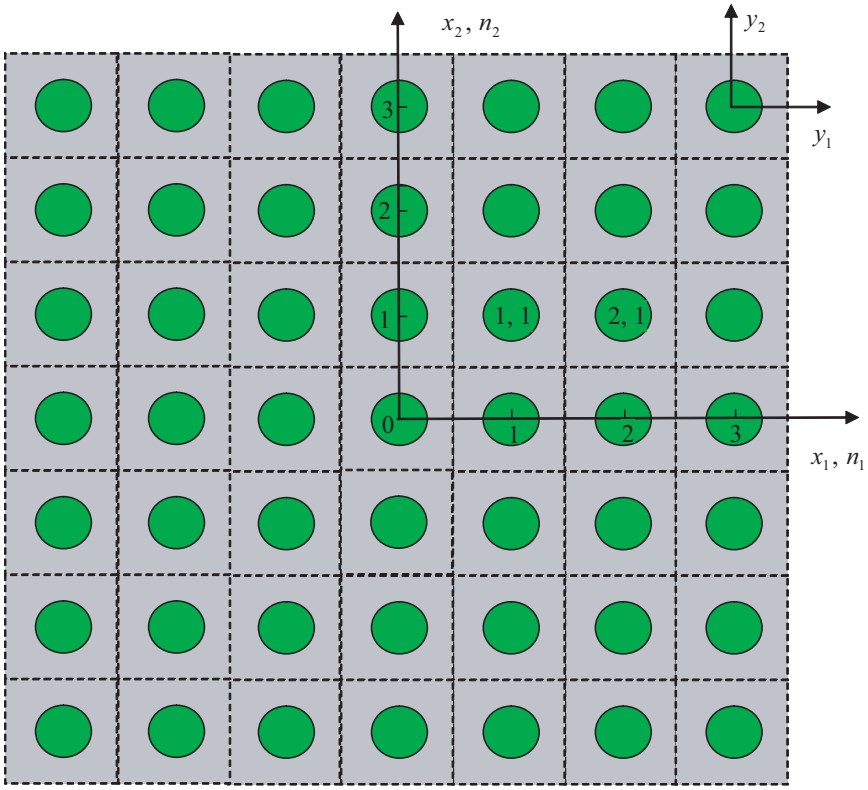

Fig. B.2: Coordinate systems for heterogenous materials (only two-dimensional (2D) UC is drawn for clarity).

uniquely locate a UC in the composite material, we also introduce integer coordinates n_i. The integer coordinates are related to the global coordinates in such a way that $n_i = x_i/d_i$ (no summation over i).

As implied by Assumption 2, we can obtain the same effective properties from an imaginary, unbounded, and unloaded composite material with the same microstrucutre as the real, loaded, and bounded one. Hence we could derive the micromechanics model from an imaginary, unloaded, composite material which completely occupies the three-dimensional (3D) space $\mathcal{R}$ and composes of infinite many repeating UCs. The total generalized potential energy of this imaginary material is equal to the summation of the Helmholtz free energy (Rosen and Hashin, 1970) stored in all the UCs, which is:

$$\Pi = \sum_{n=-\infty}^{\infty} \frac{1}{2} \int_{\Omega} (C_{ijkl}\, \epsilon_{ij}\, \epsilon_{kl} + 2\beta_{ij}\, \epsilon_{ij}\, \theta + c_v\, \frac{\theta^2}{T_0}) \mathrm{d}\Omega \tag{B.2}$$

where C_{ijkl} are components of the fourth-order elasticity tensor, β_{ij} are second-order tensor of thermal stress coefficients, c_v is the specific heat per unit volume at constant volume, T_0 is the reference temperature at which the constituent material is stress free, θ denotes the

difference between the actual temperature and the reference temperature, and ϵ_{ij} are the components of the 3D strain tensor defined for the linear theory as

$$\epsilon_{ij}(\mathbf{n};\mathbf{y}) = \frac{1}{2}\left[\frac{\partial u_i(\mathbf{n};\mathbf{y})}{\partial y_j} + \frac{\partial u_j(\mathbf{n};\mathbf{y})}{\partial y_i}\right] \tag{B.3}$$

In view of the fact that these infinite many UCs form a continuous heterogenous material, we need to enforce the continuity of the displacement field u_i on the interface between adjacent UCs, which can be written as follows for a UC with integer coordinates (n_1, n_2, n_3):

$$\begin{aligned}
u_i(n_1, n_2, n_3; d_1/2, y_2, y_3) &= u_i(n_1+1, n_2, n_3; -d_1/2, y_2, y_3)\\
u_i(n_1, n_2, n_3; y_1, d_2/2, y_3) &= u_i(n_1, n_2+1, n_3; y_1, -d_2/2, y_3)\\
u_i(n_1, n_2, n_3; y_1, y_2, d_3/2) &= u_i(n_1, n_2, n_3+1; y_1, y_2, -d_3/2)
\end{aligned} \tag{B.4}$$

For the purpose to obtain the effective CTEs and specific heat of composite materials, we assume that θ is constant with respect to time and space coordinates, which is a common practice in the literature; see Rosen and Hashin (1970) for example. Hence the continuity condition for temperature field between adjacent UCs is automatically satisfied. According to the principle of minimum total potential energy, the exact solution will minimize the energy in Eq. (B.2) under the constraints in Eq. (B.1) and Eqs. (B.4). To avoid the difficulty associated with discrete integer arguments, we can reformulate the problem, including Eqs. (B.2), (B.3), and (B.4), in terms of continuous functions using the idea of quasicontinuum introduced in Kunin (1982) as:

$$\Pi = \frac{1}{2}\int_{\mathcal{R}} \left\langle C_{ijkl}\,\epsilon_{ij}\,\epsilon_{kl} + 2\beta_{ij}\,\epsilon_{ij}\,\theta + c_v\,\frac{\theta^2}{T_0}\right\rangle \mathrm{d}\mathcal{R} \tag{B.5}$$

$$\epsilon_{ij}(\mathbf{x};\mathbf{y}) = \frac{1}{2}\left[\frac{\partial u_i(\mathbf{x};\mathbf{y})}{\partial y_j} + \frac{\partial u_j(\mathbf{x};\mathbf{y})}{\partial y_i}\right] \equiv u_{(i|j)} \tag{B.6}$$

and

$$\begin{aligned}
u_i(x_1, x_2, x_3; d_1/2, y_2, y_3) &= u_i(x_1+d_1, x_2, x_3; -d_1/2, y_2, y_3)\\
u_i(x_1, x_2, x_3; y_1, d_2/2, y_3) &= u_i(x_1, x_2+d_2, x_3; y_1, -d_2/2, y_3)\\
u_i(x_1, x_2, x_3; y_1, y_2, d_3/2) &= u_i(x_1, x_2, x_3+d_3; y_1, y_2, -d_3/2)
\end{aligned} \tag{B.7}$$

Using the technique of Lagrange multipliers, we can pose the thermoelastic analysis as a stationary value problem of the following functional:

$$\begin{aligned} J = \int_{\mathcal{R}} \Bigg\{ & \left\langle \frac{1}{2} C_{ijkl}\, u_{(i|j)}\, u_{(k|l)} + \beta_{ij}\, u_{(i|j)}\, \theta + \frac{1}{2} c_v\, \frac{\theta^2}{T_0} \right\rangle \\ & + \lambda_i (\langle u_i \rangle - v_i) + \int_{S_1} \gamma_{i1} (u_i^{+1} - u_i^{-1}) \mathrm{d}S_1 \\ & + \int_{S_2} \gamma_{i2} (u_i^{+2} - u_i^{-2}) \mathrm{d}S_2 + \int_{S_3} \gamma_{i3} (u_i^{+3} - u_i^{-3}) \mathrm{d}S_3 \Bigg\} \mathrm{d}\mathcal{R} \end{aligned} \tag{B.8}$$

with

$$u_i^{+j} = u_i|_{y_j = d_j/2},\ u_i^{-j} = u_i|_{x_j = x_j + d_j, y_j = -d_j/2} \quad \text{for} \quad j = 1, 2, 3$$

where λ_i and γ_{ij} are Lagrange multipliers introducing constraints in Eqs. (B.1) and (B.7), respectively, and S_i are the surfaces with $n_i = 1$. The main objective of micromechanics is to find the real displacements u_i in terms of v_i, which is a very difficult problem because we have to solve this stationary problem for each point in the global system x_i as in Eq. (B.8). It will be desirable if we can formulate the variational statement posed over a single UC only. In view of Eq. (B.1), it is natural to express the exact solution u_i as a sum of the volume average v_i plus the difference, such that

$$u_i(\mathbf{x}; \mathbf{y}) = v_i(\mathbf{x}) + w_i(\mathbf{x}; \mathbf{y}) \tag{B.9}$$

where $\langle w_i \rangle = 0$ according to Eq. (B.1). The very reason that the heterogenous material can be homogenized leads us to believe that w_i should be asymptotically smaller than v_i, *i.e.*, $w_i \sim \eta\, v_i$. Substituting Eq. (B.9) into Eq. (B.8) and making use of Eqs (B.6), we can obtain the leading terms of the functional as:

$$\begin{aligned} J_1 = \int_{\mathcal{R}} \Bigg\{ & \left\langle \frac{1}{2} C_{ijkl}\, w_{(i|j)}\, w_{(k|l)} + \beta_{ij}\, w_{(i|j)}\, \theta + \frac{1}{2} c_v\, \frac{\theta^2}{T_0} \right\rangle \\ & + \lambda_i \langle w_i \rangle + \int_{S_1} \gamma_{i1} (w_i^{+1} - w_i^{-1} - \frac{\partial v_i}{\partial x_1} d_1) \mathrm{d}S_1 \\ & + \int_{S_2} \gamma_{i2} (w_i^{+2} - w_i^{-2} - \frac{\partial v_i}{\partial x_2} d_2) \mathrm{d}S_2 \\ & + \int_{S_3} \gamma_{i3} (w_i^{+3} - w_i^{-3} - \frac{\partial v_i}{\partial x_3} d_3) \mathrm{d}S_3 \Bigg\} \mathrm{d}\mathcal{R} \end{aligned} \tag{B.10}$$

with

$$w_i^{+j} = w_i|_{y_j = d_j/2},\ w_i^{-j} = w_i|_{y_j = -d_j/2} \quad \text{for} \quad j = 1, 2, 3$$

Although it is possible to carry out the variation of J_1 and find the Euler-Lagrange equations and associated boundary conditions for w_i, which results in inhomogeneous boundary conditions. It is more convenient to use change of variables to reformulate the same problem so that the boundary conditions are homogeneous. Considering the last three terms in Eq. (B.10), we use the following change of variables to express w_i as:

$$w_i(\mathbf{x};\mathbf{y}) = y_j \frac{\partial v_i}{\partial x_j} + \chi_i(\mathbf{x};\mathbf{y}) \tag{B.11}$$

with χ_i termed as fluctuation functions. We are free to choose the origin of the local coordinate system to be the center of UC, which implies the following constraints on χ_i:

$$\langle \chi_i \rangle = 0 \tag{B.12}$$

Finally, according to the variational asymptotic method (Berdichevsky, 1979), the first approximation of the variational statement in Eq. (B.8) can be obtained from the following functional defined over the UC:

$$\begin{aligned} J_\Omega = & \frac{1}{2}\left\langle C_{ijkl}\left[\bar{\epsilon}_{ij} + \chi_{(i|j)}\right]\left[\bar{\epsilon}_{kl} + \chi_{(k|l)}\right]\right\rangle + \frac{1}{2}\left\langle c_v \frac{\theta^2}{T_0}\right\rangle \\ & + \left\langle \beta_{ij}\left[\bar{\epsilon}_{ij} + \chi_{(i|j)}\right]\theta\right\rangle + \lambda_i \langle \chi_i \rangle \\ & + \int_{S_1} \gamma_{i1}(\chi_i^{+1} - \chi_i^{-1})\mathrm{d}S_1 + \int_{S_2} \gamma_{i2}(\chi_i^{+2} - \chi_i^{-2})\mathrm{d}S_2 \\ & + \int_{S_3} \gamma_{i3}(\chi_i^{+3} - \chi_i^{-3})\mathrm{d}S_3 \end{aligned} \tag{B.13}$$

with

$$\chi_i^{+j} = \chi_i|_{y_j = d_j/2},\ \chi_i^{-j} = \chi_i|_{y_j = -d_j/2} \quad \text{for} \quad j = 1,2,3$$

where $\bar{\epsilon}_{ij} \equiv v_{(i,j)}$ will be shown later to be components of the global strain tensor for the structure with effective properties. The functional J_Ω in Eq. (B.13) incorporates all the information for the present thermoelastic micromechanics model. This variational statement can be solved analytically for very simple cases such as binary composites (Yu and Tang, 2007), however, for general cases, we need to use computational techniques such as the finite element method (FEM) to seek numerical solutions.

B.3 Finite Element Implementation

It is possible to formulate the FEM solution based on Eq. (B.13), however, it is not the most convenient way because Lagrange multipliers will increase the number of unknowns. To this end, we can reformulate the variational statement in Eq. (B.13) as the minimum value of the following functional

$$\begin{aligned}\Pi_\Omega = \frac{1}{2\Omega}\int_\Omega \Big\{ & C_{ijkl}\left[\bar{\epsilon}_{ij} + \chi_{(i|j)}\right]\left[\bar{\epsilon}_{kl} + \chi_{(k|l)}\right] \\ & + 2\beta_{ij}\left[\bar{\epsilon}_{ij} + \chi_{(i|j)}\right]\theta + c_v\frac{\theta^2}{T_0}\Big\}\mathrm{d}\Omega\end{aligned} \tag{B.14}$$

under the following nine constraints

$$\chi_i^{+j} = \chi_i^{-j} \quad \text{for} \quad i,j = 1,2,3 \tag{B.15}$$

It is noted that Eq. (B.15) represents the well-known periodic boundary conditions which are assumed *a priori* in other models including MHT. while in the present model, they are derived from the variational statement in Eq. (B.13). The constraints in Eq. (B.12) do not affect the minimum value of Π_Ω but help uniquely determine χ_i. In practice, we can constrain the fluctuation functions at an arbitrary node to be zero and later use these constraints to recover the unique fluctuation functions. It is fine to use penalty function method to introduce the constraints in Eqs. (B.15). However, this method introduces additional approximation and the robustness of the solution depends on the choice of large penalty numbers. Here, we choose to make the nodes on the positive boundary surface (*i.e.*, $y_i = d_i/2$) slave to the nodes on the opposite negative boundary surface (*i.e.*, $y_i = -d_i/2$). By assembling all the independent active degrees of freedom, we can implicitly and exactly incorporate the constraints in Eqs. (B.15). In this way, we also reduce the total number of unknowns in the linear system which will be formulated in the following.

Introduce the following matrix notations

$$\bar{\epsilon} = \lfloor \bar{\epsilon}_{11} \;\; 2\bar{\epsilon}_{12} \;\; \bar{\epsilon}_{22} \;\; 2\bar{\epsilon}_{13} \;\; 2\bar{\epsilon}_{23} \;\; \bar{\epsilon}_{33} \rfloor^T \tag{B.16}$$

$$\epsilon_1 = \begin{Bmatrix} \frac{\partial \chi_1}{\partial y_1} \\ \frac{\partial \chi_1}{\partial y_2} + \frac{\partial \chi_2}{\partial y_1} \\ \frac{\partial \chi_2}{\partial y_2} \\ \frac{\partial \chi_1}{\partial y_3} + \frac{\partial \chi_3}{\partial y_1} \\ \frac{\partial \chi_2}{\partial y_3} + \frac{\partial \chi_3}{\partial y_2} \\ \frac{\partial \chi_3}{\partial y_3} \end{Bmatrix} = \begin{bmatrix} \frac{\partial}{\partial y_1} & 0 & 0 \\ \frac{\partial}{\partial y_2} & \frac{\partial}{\partial y_1} & 0 \\ 0 & \frac{\partial}{\partial y_2} & 0 \\ \frac{\partial}{\partial y_3} & 0 & \frac{\partial}{\partial y_1} \\ 0 & \frac{\partial}{\partial y_3} & \frac{\partial}{\partial y_2} \\ 0 & 0 & \frac{\partial}{\partial y_3} \end{bmatrix} \begin{Bmatrix} \chi_1 \\ \chi_2 \\ \chi_3 \end{Bmatrix} \equiv \Gamma_h \chi \tag{B.17}$$

where Γ_h is an operator matrix and χ is a column matrix containing the three components of the fluctuation functions. If we discretize χ using the finite elements as

$$\chi(x_i; y_i) = S(y_i)\mathcal{X}(x_i) \tag{B.18}$$

where S representing the shape functions (in the assembled sense excluding the constrained node and slave nodes) and $\mathcal{X}$ a column matrix of the nodal values of the fluctuation functions for all active nodes. Substituting Eqs. (B.16), (B.17), and (B.18) into Eq. (B.14), we obtain a discretized version of the functional as

$$\begin{aligned} \Pi_\Omega = \frac{1}{2\Omega}(&\mathcal{X}^T E \mathcal{X} + 2\mathcal{X}^T D_{h\epsilon}\bar{\epsilon} + \bar{\epsilon}^T D_{\epsilon\epsilon}\bar{\epsilon} \\ &+ 2\mathcal{X}^T D_{h\theta}\theta + 2\bar{\epsilon}^T D_{\epsilon\theta}\theta + D_{\theta\theta}\frac{\theta^2}{T_0}) \end{aligned} \tag{B.19}$$

where

$$E = \int_\Omega (\Gamma_h S)^T D (\Gamma_h S) \mathrm{d}\Omega \qquad D_{h\epsilon} = \int_\Omega (\Gamma_h S)^T D \mathrm{d}\Omega$$
$$D_{\epsilon\epsilon} = \int_\Omega D \mathrm{d}\Omega \qquad D_{h\theta} = \int_\Omega (\Gamma_h S)^T \beta \mathrm{d}\Omega$$
$$D_{\epsilon\theta} = \int_\Omega \beta \mathrm{d}\Omega \qquad D_{\theta\theta} = \int_\Omega c_v \mathrm{d}\Omega$$

with D as the 6×6 material matrix condensed from the fourth-order elasticity tensor C_{ijkl}, and β as the 6×1 column condensed from β_{ij}. Minimizing Π_Ω in Eq. (B.19), we obtain the following linear system

$$E\mathcal{X} = -D_{h\epsilon}\bar{\epsilon} - D_{h\theta}\theta \tag{B.20}$$

It is clear from Eq. (B.20) that the fluctuation function $\mathcal{X}$ is linearly proportional to $\bar{\epsilon}$ and θ, which means the solution can be written symbolically as

$$\mathcal{X} = \mathcal{X}_0 \bar{\epsilon} + \mathcal{X}_\theta \theta \tag{B.21}$$

Substituting Eq. (B.21) into Eq. (B.19), we can calculate the Helmholtz free energy density of the UC as

$$\Pi_\Omega = \frac{1}{2}\bar{\epsilon}^T \bar{D} \bar{\epsilon} + \bar{\epsilon}^T \bar{\beta} \theta + \frac{1}{2}\bar{c}_v \frac{\theta^2}{T_0} \tag{B.22}$$

with

$$\begin{aligned}
\bar{D} &= \frac{1}{\Omega}(\mathcal{X}_0^T D_{h\epsilon} + D_{\epsilon\epsilon}) \\
\bar{\beta} &= \frac{1}{\Omega}\left[\frac{1}{2}(D_{h\epsilon}^T \mathcal{X}_\theta + \mathcal{X}_0^T D_{h\theta}) + D_{\epsilon\theta}\right] \\
\bar{c}_v &= \frac{1}{\Omega}\left[\mathcal{X}_\theta^T D_{h\theta} T_0 + D_{\theta\theta}\right]
\end{aligned}$$

Clearly $\bar{D}$ is the effective elastic material matrix, $\bar{\beta}$ contains the effective thermal stress coefficients, $\bar{c}_v$ is the effective specific heat, and $\bar{\epsilon}$ contains the global strains. It is easy to infer that the effective coefficients of thermal expansion, $\bar{\alpha}$, can be obtained using the following expression.

$$\bar{\alpha} = -\bar{D}^{-1}\bar{\beta} \tag{B.23}$$

After obtained the effective free energy density in Eq. (B.22), we can use it as the constitutive model of the effective medium to carry out various macroscopic analyses under different loading and temperature conditions.

If the local fields within the UC are of interest, we can recover those fields after we have obtained the macroscopic behavior which can be described by global displacements v_i and global temperature distribution θ.

To recover the local displacement field, we need to construct two new arrays $\tilde{\mathcal{X}}_0$ and $\tilde{\mathcal{X}}_\theta$ from $\mathcal{X}_0$ and $\mathcal{X}_\theta$, respectively, by assigning the values for slave nodes according to the corresponding active nodes and assign zeros to the constrained node. Obviously, $\tilde{\mathcal{X}}_0$ and $\tilde{\mathcal{X}}_\theta$ still yield the minimum value of Π_Ω in Eq. (B.14) under constrains in Eqs. (B.15). However, $\tilde{\mathcal{X}}_0$ and $\tilde{\mathcal{X}}_\theta$ may not satisfy the constraints in Eq. (B.12). The real solution, denoted as $\bar{\mathcal{X}}_0$ and $\bar{\mathcal{X}}_\theta$, can be found trivially by adding a constant, which is equal to the average of the

fluctuation functions, to each node so that Eq. (B.12) is satisfied. Then the real solution of the fluctuation function is

$$\bar{\mathcal{X}} = \bar{\mathcal{X}}_0 \bar{\epsilon} + \bar{\mathcal{X}}_\theta \theta \tag{B.24}$$

After having determined the fluctuation functions uniquely, we can recover the local displacement using Eqs. (B.9), (B.11), and (B.24) as

$$u = v + \begin{bmatrix} \frac{\partial v_1}{\partial x_1} & \frac{\partial v_1}{\partial x_2} & \frac{\partial v_1}{\partial x_3} \\ \frac{\partial v_2}{\partial x_1} & \frac{\partial v_2}{\partial x_2} & \frac{\partial v_2}{\partial x_3} \\ \frac{\partial v_3}{\partial x_1} & \frac{\partial v_3}{\partial x_2} & \frac{\partial v_3}{\partial x_3} \end{bmatrix} \begin{Bmatrix} y_1 \\ y_2 \\ y_3 \end{Bmatrix} + \bar{S}\bar{\mathcal{X}} \tag{B.25}$$

with u as the column matrix of u_i and v as the column matrix of v_i. Here $\bar{S}$ is different from S due to the recovery of slave nodes and the constrained node. The local strain field can be recovered using Eqs. (B.6), (B.9), (B.11), (B.17), and (B.24) as

$$\epsilon = \bar{\epsilon} + \Gamma_h \bar{S} \bar{\mathcal{X}} \tag{B.26}$$

Finally, the local stress field can be recovered straightforwardly using the 3D constitutive relations for the constituent material as

$$\sigma = D\epsilon + \beta\theta \tag{B.27}$$

Both the theoretical formulation and finite element formulation can be reduced to be those of Yu and Tang (2007) if one sets $\beta_{ij} = 0$ and $c_v = 0$. It is worthy to point out that the involved recovery procedure in Yu and Tang (2007) to obtain the unique fluctuation functions in Eq. (B.24) is avoided by recognizing the fact the differences between $\tilde{\mathcal{X}}_0$ and $\tilde{\mathcal{X}}_\theta$ and $\bar{\mathcal{X}}_0$ and $\bar{\mathcal{X}}_\theta$ are equal to the average of the fluctuation functions calculated from $\tilde{\mathcal{X}}_0$ and $\tilde{\mathcal{X}}_\theta$.

We have implemented this formulation in the computer program VAMUCH. In the next section, we will use a few examples to demonstrate the application and accuracy of the theory and code.

B.4 Numerical Examples

Numerous examples including binary composites, fiber reinforced composites, and particle reinforced composites in Yu and Tang (2007) have been used to demonstrate that VAMUCH consistently achieves excellent accuracy for predicting effective elastic properties in comparison to other existing approaches. In this paper, we will use some examples to demonstrate the predictive capability of VAMUCH to recover the local stress field within the UC, and predict effective coefficients of thermal expansions and specific heats, and recover local stress field due to temperature changes.

B.4.1 Predict local stresses

A high-fidelity micromechanics model, such as VAMUCH, should not only provide an accurate prediction for effective properties but also recover the local displacement, stress, and strain fields within the UC, which are needed for detailed analysis.

To demonstrate the accuracy of VAMUCH in predicting the local fields, we consider the classical problem of an isotropic circular fiber embedded in an infinite isotropic matrix subjected to the uniform far-field stress σ_{22}^{∞} (the so-called Eshelby problem). It is a plane strain elasticity problem and can be solved exactly. The analytical formulas can be found in Aboudi et al. (2001). To mimic this dilute case, we consider a UC with sufficiently small fiber volume fraction (we choose 0.01 for this example) so that the interaction effects due to the presence of adjacent cells are negligible. Except this restriction, the exact solution provides a convenient basis to validate the accuracy of the local fields calculated using VAMUCH.

For calculation, we choose the fiber to be glass with Young's modulus $E = 69.0$ GPa and Poisson's ratio $\nu = 0.20$, the matrix to be epoxy with Young's modulus $E = 4.80$ GPa and Poisson's ratio $\nu = 0.34$. The choice of these materials produces a high elastic moduli mismatch and thus a significant disturbance in the stress field along the interface between fiber and matrix. To obtain the stress distribution within the UC, we need to run VAMUCH first to calculate the effective properties of the composite materials. It is found out that this material is transversely isotropic with $E_1 = 5.44$ GPa, $E_2 = E_3 = 4.93$ GPa, $G_{12} = G_{13} = 1.82$ GPa, $\nu_{12} = \nu_{13}$=0.338, and $\nu_{23} = 0.357$. Then we can use these properties to solve the plane strain problem of the effective medium under the application of a far-field stress $\sigma_{22}^{\infty} = 5.5032$ MPa, which will generate a macroscopic strain field $\bar{\epsilon}_{22} = 0.1\%$ and

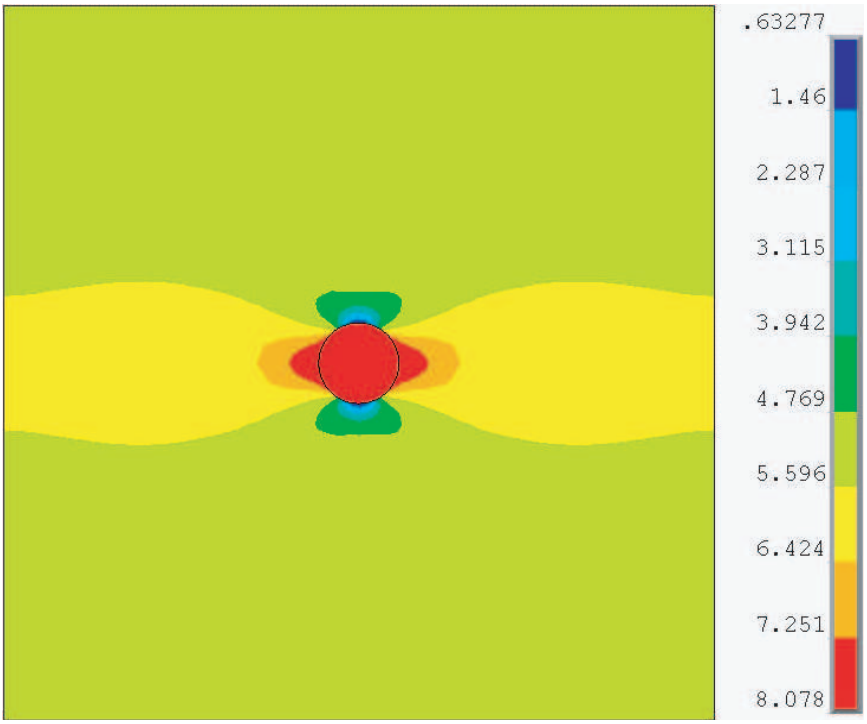

Fig. B.3: Contour plot of σ_{22} (MPa) within the UC.

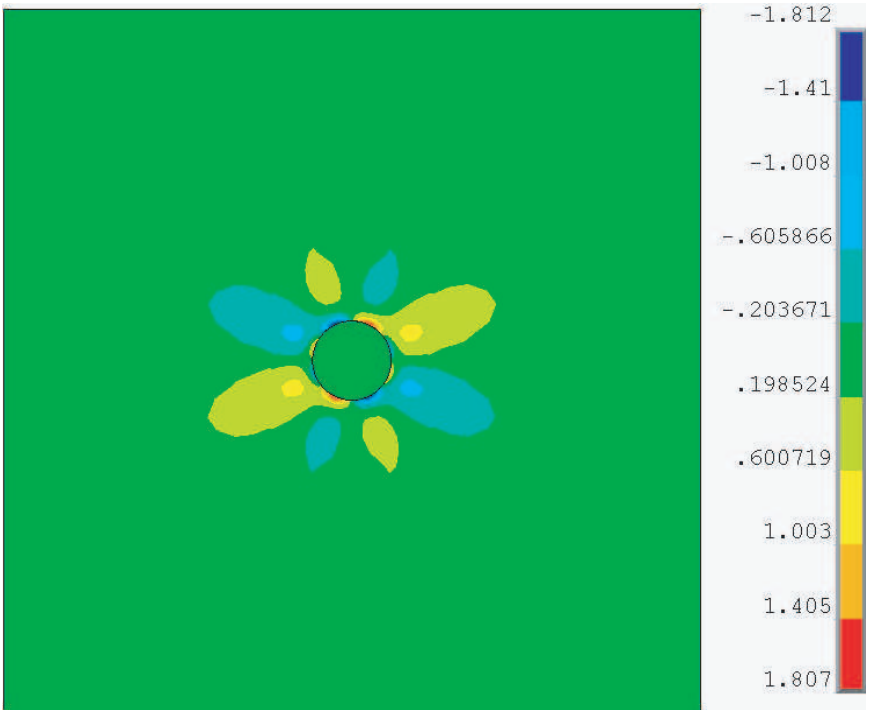

Fig. B.4: Contour plot of σ_{23} (MPa) within the UC.

$\bar{\epsilon}_{33} = -0.0514\%$ within the effective medium. Such values can be fed back to VAMUCH to recover the stress distribution within the material. Figures B.3 and B.4 show the contour plots for the distributions of σ_{22} and σ_{23} within the UC generated by VAMUCH. The contour plots of the exact solution in Aboudi et al. (2001) are not presented here for brevity because they are almost the same as those in Figures B.3 and B.4. Both stress components have sudden changes in the interface between fiber and matrix, which clearly demonstrates that VAMUCH is capable of capturing stress concentrations. Although contour plots can provide us some qualitative information, to rigorously assess the accuracy of VAMUCH, we plot σ_{22} distributions predicted by VAMUCH and the exact solution along the lines $y_2 = 0$ and $y_3 = 0$ in Figure B.5 and Figure B.6, respectively. It is evident that VAMUCH has an excellent agreement with the exact solution. Both the continuous condition along $y_3 = 0$ and discontinuous condition along $y_2 = 0$ are well captured by VAMUCH. The slight differences along the edges are caused by the interaction effects due to presence of adjacent cells because our far-field stress σ_{22}^{∞} is not really uniform along the edges which can be observed form the contour plot in Figure B.3. It has been verified that if the fiber volume fraction is as low as 0.0025, σ_{22}^{∞} will be uniform along the edges and the prediction of VAMUCH is indistinguishable from the exact solutions. The discontinuity on the interface along $y_2 = 0$ in Figure B.5 can be captured better if one refines the mesh in the vicinity. The results calculated using ANSYS following the approach in Sun and Vaidya (1996) are also plotted in the figures. All three sets of results are almost on the top of each other and ANSYS results are almost identical to VAMUCH results.

It is worthy to point out that local stress distribution is a critical assessment of micromechanics models and most of existing models cannot accurately predict the local stresses even though they may have excellent predictions for effective properties (Williams, 2005a). The fact that VAMUCH achieves an excellent agreement with the exact solution for local stresses clearly demonstrated the high-fidelity predictive capabilities of VAMUCH for micromechanical analysis of heterogeneous materials.

B.4.2 Predict effective CTEs

As reviewed by Rosen and Hashin (1970), Levin (1968) provides analytical expressions relating effective CTEs and effective elastic moduli for two phase isotropic or transversely isotropic composites having isotropic constituents. Since there are no exact formulas existing

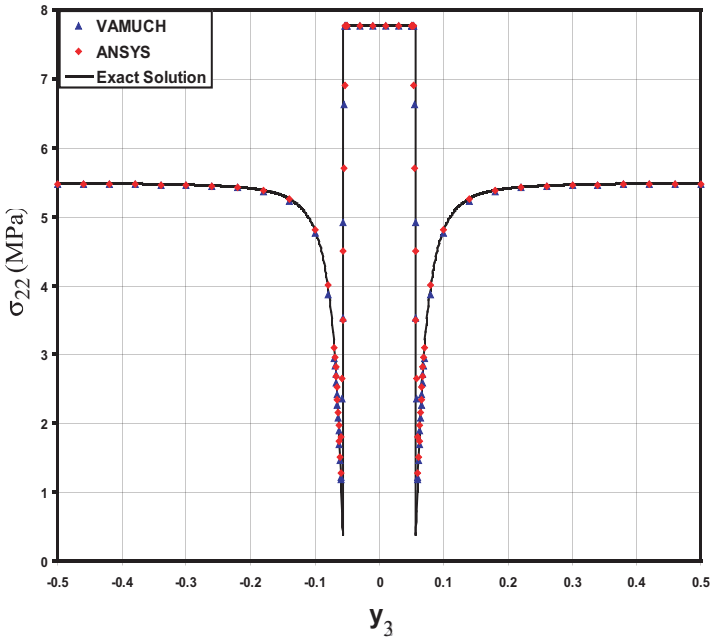

Fig. B.5: Comparison of normal stress σ_{22} distribution along $y_2 = 0$.

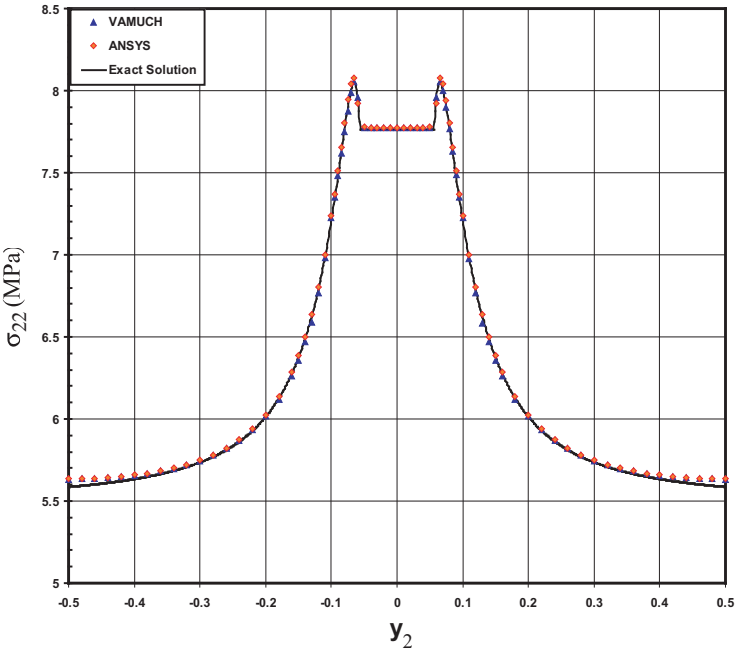

Fig. B.6: Comparison of normal stress σ_{22} distribution along $y_3 = 0$.

Table B.1: Effective CTEs of boron/aluminum composites

Models	$\alpha_{11}(10^{-6}/\text{K})$	$\alpha_{22}(10^{-6}/\text{K})$
Exact Solution (Rosen and Hashin, 1970)	10.99	16.69
VAMUCH	10.99	16.69
HFGMC (Aboudi et al., 2001)	11.00	16.70
GMC (Paley and Aboudi, 1992)	10.91	16.94
Tamma and Avila (Tamma and Avila, 1999)	10.77	17.34

for effective elastic moduli for general UCs and VAMUCH achieves excellent accuracy for predicting such properties (Yu and Tang, 2007), we will consider the elastic properties predicted by VAMUCH as exact and use them to calculate the effective CTEs following the analytical expressions given in Rosen and Hashin (1970). It is noted that these analytical expressions provide exact predictions for effective CTEs only if the corresponding elastic moduli are exact. Nevertheless, they are labeled as "exact solution" to indicate that the relations are given in exact closed-form expressions.

The first example is a boron/aluminum composite. Both constituents are isotropic with Young's modulus $E = 379.3$ GPa, Poisson's ratio $\nu = 0.1$, and CTE $\alpha = 8.1\ 10^{-6}$/K for boron fibers, and $E = 68.3$ GPa, Poisson's ratio $\nu = 0.3$, and CTE $\alpha = 23.0\ 10^{-6}$/K for aluminum matrix. The fiber is of circular shape and arranged in a square array (see the sketch in the middle of Figure B.1). The example of fiber volume fraction 0.47 is studied in several places (Aboudi et al., 2001; Tamma and Avila, 1999; Paley and Aboudi, 1992). The effective CTEs predicted by different approaches are listed in Table B.1. It can be observed that VAMUCH has a perfect match with the exact solution up to the fourth significant digit. HFGMC also has an excellent agreement with the exact solution while GMC and Tamma and Avila's results are not so accurate. To show the trend of change of effective CTEs with respect to change of the fiber volume fraction, we plot the effective CTEs for the same composite with different fiber volume fractions in Figure B.7 and Figure B.8. As it is expected, both axial CTEs and transverse CTEs are decreasing with increasing fiber volume fractions. Again the perfect match between exact solution and VAMUCH for various fiber volume fraction is observed.

The second example is to predict the effective CTE for a glass/epoxy particle reinforced composite. The UC of this composite is composed of glass spheres embedded in a triply periodic cubic array. Both constituents are isotropic with Young's modulus $E = 72.38$ GPa,

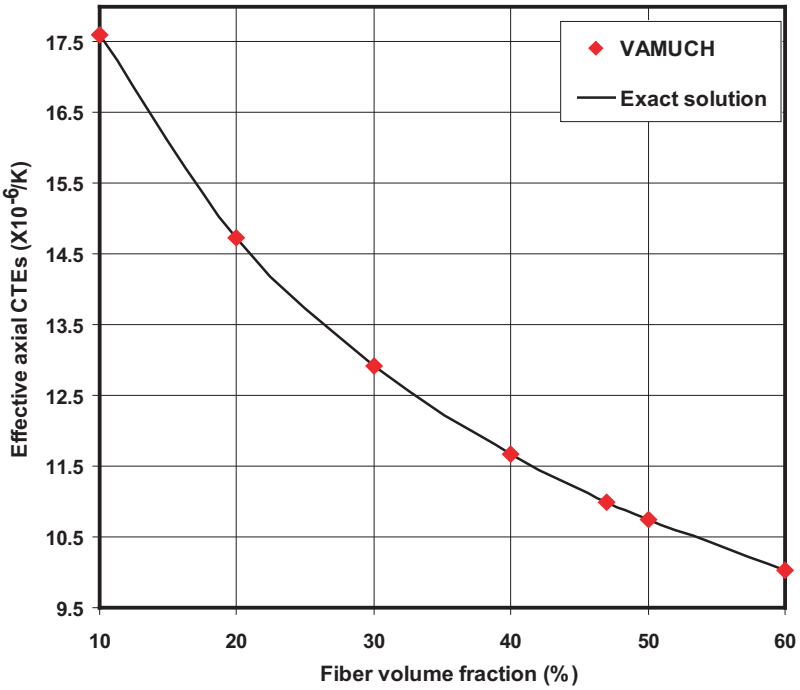

Fig. B.7: Change of effective α_{11} of the boron/aluminum composite with respect to fiber volume fractions.

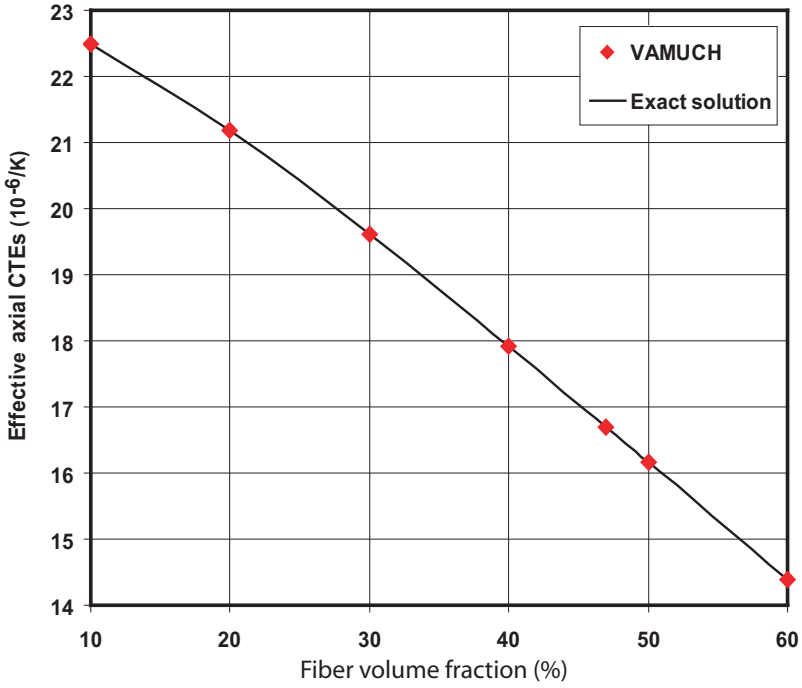

Fig. B.8: Change of effective α_{22} of the boron/aluminum composite with respect to fiber volume fractions.

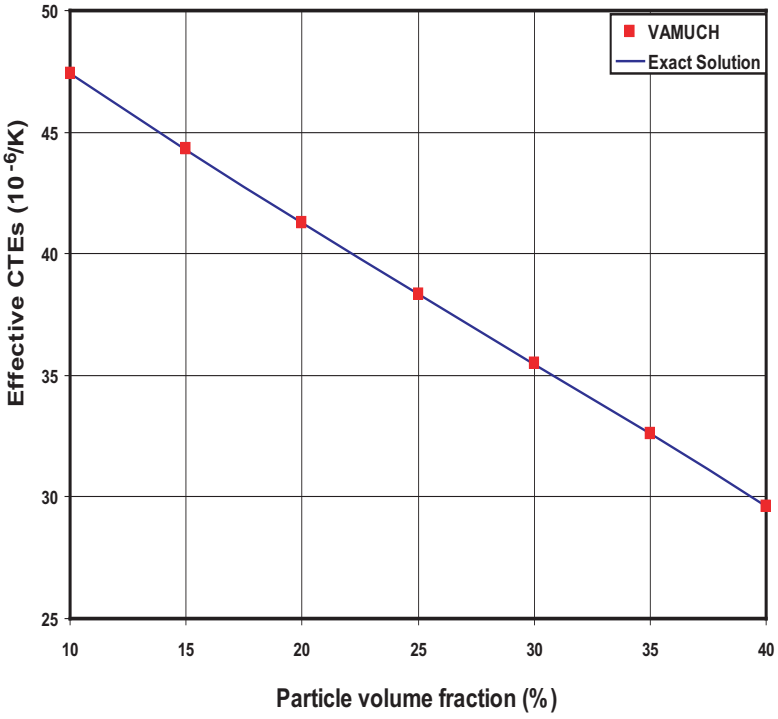

Fig. B.9: Change of effective CTEs of the glass/epoxy composite with respect to spherical inclusion volume fractions.

Poisson's ratio $\nu = 0.2$, and CTE $\alpha = 5.0\ 10^{-6}$/K for glass, and Young's modulus $E = 2.75$ GPa, Poisson's ratio $\nu = 0.35$, and CTE $\alpha = 54.0\ 10^{-6}$/K for epoxy. It is noticed that the properties are directly taken from Aboudi (1984) and different from those in Section B.4.1. We plot the change of effective CTE with respect to the particle volume fractions in Figure B.9. It is found out that VAMUCH results are right on the top of the exact solution, which demonstrates VAMUCH provides accurate predictions for CTEs for particle reinforced composites.

To demonstrate the application and accuracy of the present model for more realistic heterogeneous materials, we choose a more complex microstructure as shown in Figure B.10. Within one UC, the reinforcements are a square fiber and a thin-wall frame around the square fiber. Both matrix and reinforcements are isotropic with Young's modulus $E = 100000$ MPa, Poisson's ratio $\nu = 0.32$, and CTE $\alpha = 10.0\ 10^{-12}$/K for reinforcements, while the Young's modulus of matrix takes different values from 10 MPa, 100 MPa, 1000 MPa, 10000MPa, and 50000MPa and its Poisson'sratio and CTE are fixed at 0.49 and $\alpha = 4.0\ 10^{-6}$/K, respectively. The contrast ratio of CTEs of two constituents is as high as

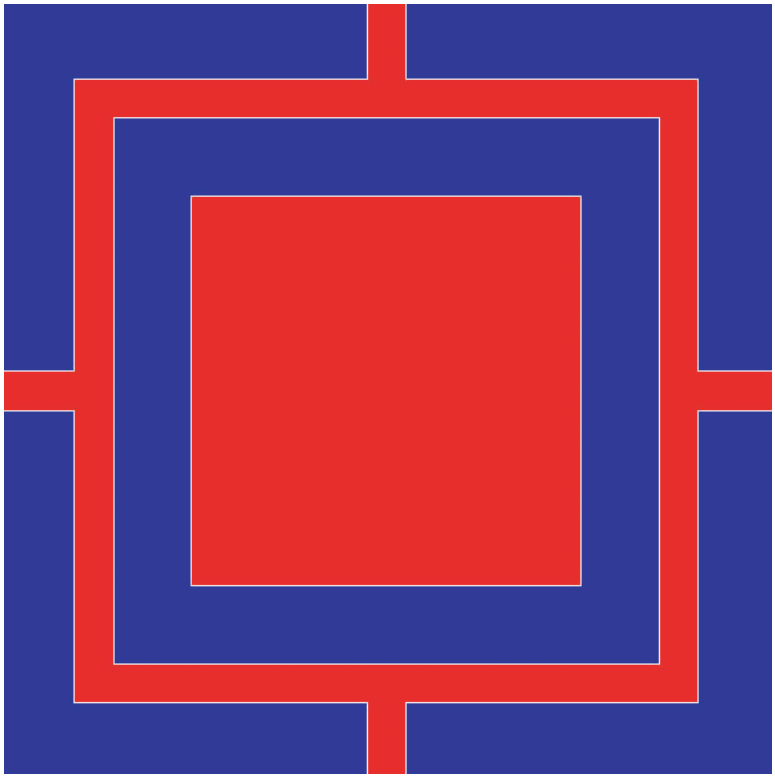

Fig. B.10: Sketch of a complex microstructure.

Table B.2: Effective CTEs of frame shape composites

Matrix Modulus	α_{11} (10^{-9}/K)		α_{22} (10^{-6}/K)	
	VAMUCH	ANSYS	VAMUCH	ANSYS
$E_m = 10$ MPa	3.92	3.90	2.22	2.23
$E_m = 100$ MPa	14.6	14.6	3.12	3.28
$E_m = 1000$ MPa	97.1	97.0	3.12	3.28
$E_m = 10000$ MPa	637	637	3.23	3.23
$E_m = 50000$ MPa	1886	1886	2.886	2.886

4×10^5. There are no analytical solution for composites with this kind of microstructure. To validate the present model, we use ANSYS, a commercial finite element code, to carry out a thermoelastic micromechanics analysis following the approach of Sun and Vaidya (1996). Table B.2 shows the effective CTEs of composites of different matrix predicted by VAMUCH and ANSYS. It can be seen that the predictions of VAMUCH are almost the same as those obtained from ANSYS at different contrast ratios of Young's modulus of the constituents.

B.4.3 Predict effective specific heat

Rosen and Hashin (1970) derived closed-form expressions for macroscopically isotropic

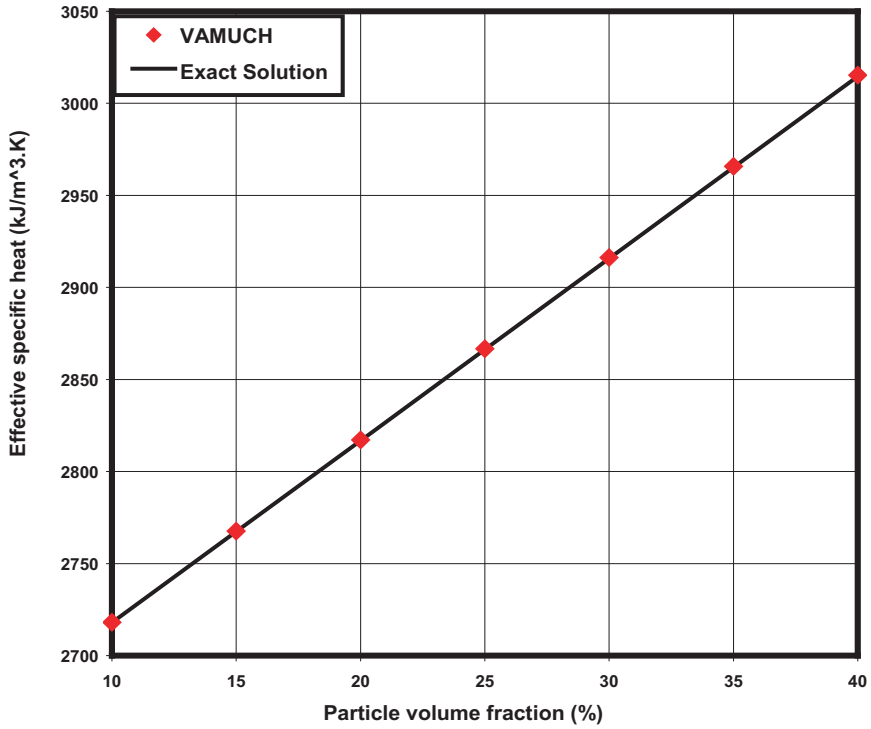

Fig. B.11: Effective specific heat c_v of steel/aluminum composite varies with particle volume fraction.

composites having two isotropic phases and bounds for macroscopically anisotropic composites relating effective specific heat and elastic moduli. Again, although those relations are in closed-form, they can predict the exact effective specific heat only if the elastic moduli predictions are exact. Here we use the elastic properties predicted by VAMUCH in these relations and label them as "exact solution" only to reflect the fact that the effective specific heats are obtained from closed-form expressions.

First, we use a steel/aluminum particle reinforced composite which can be considered as macroscopically isotropic. Both constituents are isotropic with $E = 200$ GPa, $\nu = 0.3$, $\alpha = 12\ 10^{-6}$/K, and $c_v = 3609.6$ kJ/(m^3·K) for steel particles, and $E = 68.3$ GPa, $\nu = 0.3$, $\alpha = 23.0\ 10^{-6}$/K, and $c_v = 2619.1$ kJ/(m^3·K) for aluminum matrix. To examine the agreement of VAMUCH with respect to the exact relations (Rosen and Hashin, 1970), we plot the effective specific heat c_v with different steel volume fraction as shown in Figure B.11. It can be seen that the VAMUCH results have an excellent match with the exact relations (Rosen and Hashin, 1970).

To show that VAMUCH can also predict the effective specific heat for macroscopically

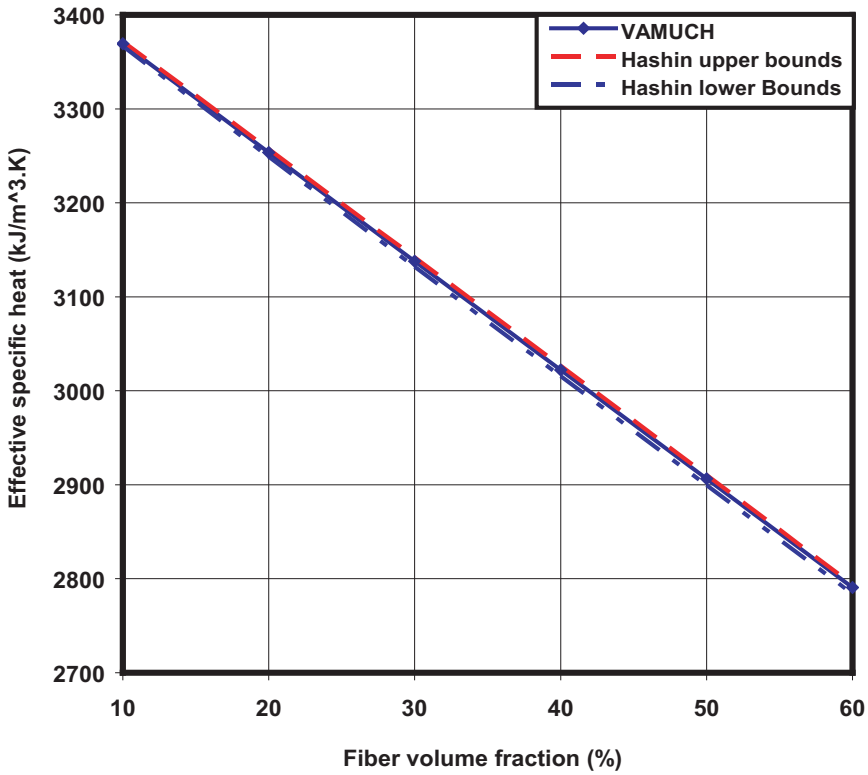

Fig. B.12: Effective specific heat c_v of SiC/Cu composite varies with particle volume fraction.

anisotropic composites, we chose the silicon carbide fiber reinforced copper matrix (SiC/Cu) composite as an example. Both constituents are also isotropic with $E = 410$ GPa, $\nu = 0.14$, $\alpha = 4.0\ 10^{-6}$/K, and $c_v = 2327.73$ kJ/(m^3·K) for silicon carbide fibers, and $E = 117$ GPa, $\nu = 0.34$, $\alpha = 22.0\ 10^{-6}$/K, and $c_v = 3485.09$ kJ/(m^3·K) for copper matrix. Only bounds are available for this type of composites. We plot the VAMUCH results along with the upper and lower bounds provided in Rosen and Hashin (1970) in Figure B.12. It can be observed that for this composite the lower and upper bounds are very close to each other and VAMUCH results are nicely located between the bounds.

B.4.4 Predict local thermal stresses

Finally, we can use VAMUCH to recover the stress distribution within the UC due to macroscopic temperature change. Consider the boron/aluminum composite with fiber volume fraction as 0.2. We use the effective thermoelastic properties to carry out a macroscopic thermoelastic analysis of the homogenized material. Suppose we know for a certain UC, it is stress free, yet the temperature is increased by 100 K. Due to the mismatch of CTEs of the

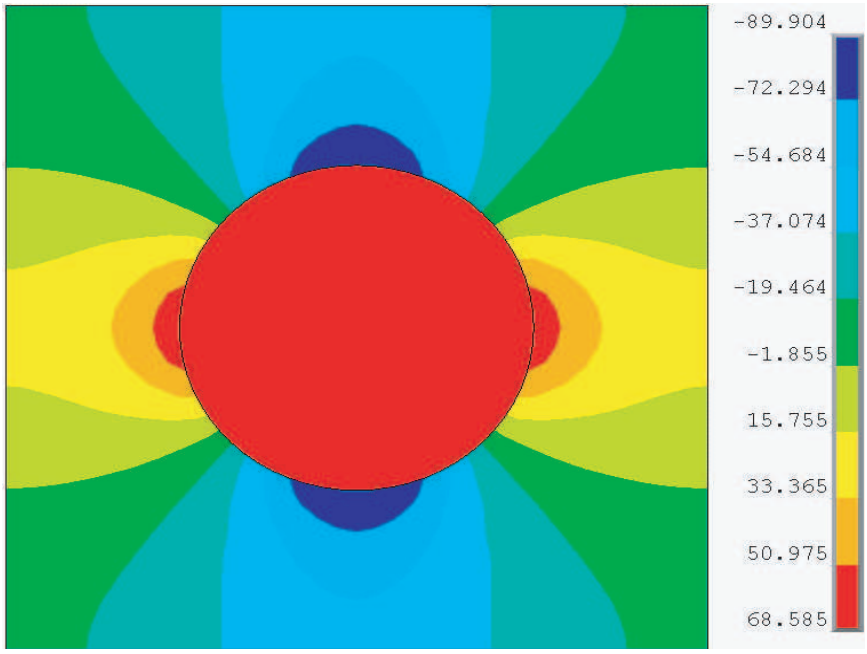

Fig. B.13: Contour plot of σ_{22} (MPa) within the UC of a boron/aluminum composite due to temperature increase of 100 K.

constituents, thermal stresses will be generated within the UC. The distributions of σ_{22} and σ_{23} are plotted in Figures B.13 and B.14, respectively. All the sudden changes of stress distributions along the fiber-matrix interface have been well captured by VAMUCH. We have also carried out a thermoelastic micromechanics analysis following the approach of Sun and Vaidya (1996) to analyze 3D RVEs using ANSYS. The local thermal stress distributions along $y_3 = 0$ and $y_2 = 0$ are plotted in Figures B.15 and B.16, respectively. Excellent match between these two approaches can be clearly observed from the plots. However, only 2D UCs are needed for VAMUCH to obtain these results. Such a capability of VAMUCH is useful for predicting residual stresses caused by temperature changes during manufacturing or operating processes.

B.5 Conclusions

A variational asymptotic model has been developed for thermoelastic micromechanical analysis of heterogeneous materials. This model can homogenize the composite materials to find effective thermoelastic properties including elastic properties, coefficients of thermal expansion, and specific heat and recover the local fields within the microstructure in terms of the global responses of the material. This model provides a uniform treatment for microstructures which can be described using 1D, 2D, or 3D UCs, such as binary composites,

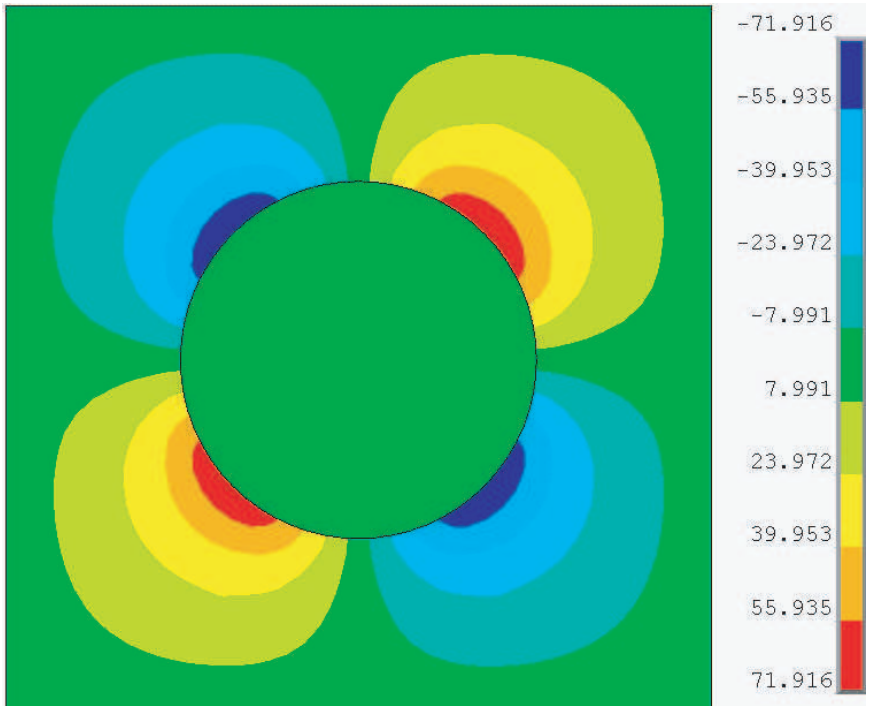

Fig. B.14: Contour plot of σ_{23} (MPa) within the UC of a boron/aluminum composite due to temperature increase of 100 K.

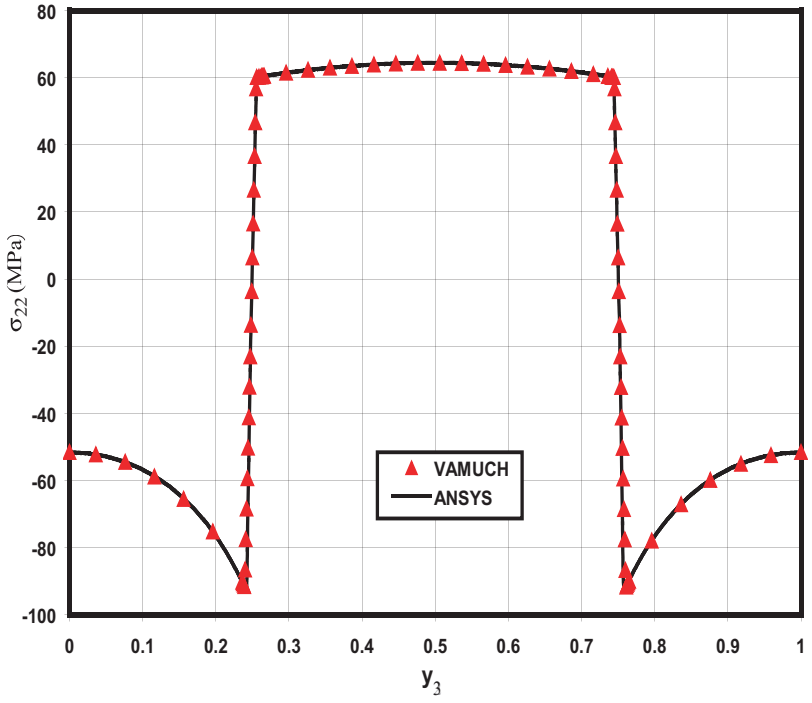

Fig. B.15: Comparison of thermal stress σ_{22} distribution along $y_2 = 0$.

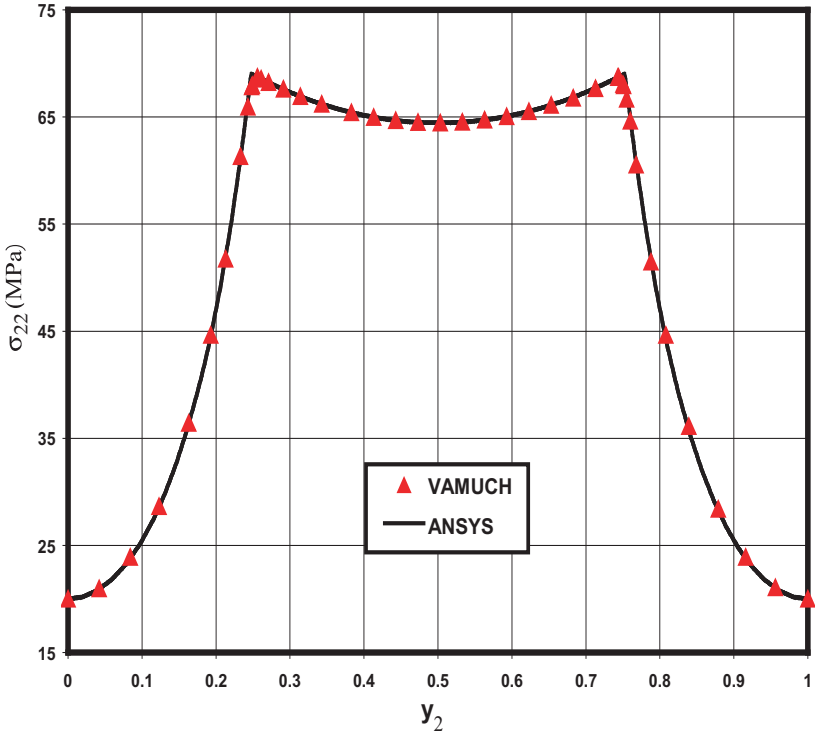

Fig. B.16: Comparison of thermal stress σ_{22} distribution along $y_3 = 0$.

fiber-reinforced composites, and particle-reinforced composites. In comparison to existing micromechanics models, this model has the following unique features:

1. It adopts the variational asymptotic method as its mathematical foundation. It has the same rigor as MHT without even assuming periodic fluctuation functions and boundary conditions.

2. It has an inherent variational nature and its numerical implementation is shown to be straightforward.

3. It handles 1D/2D/3D unit cells uniformly. The dimensionality of the problem is determined by that of the periodicity of the unit cell.

The present theory is implemented in the computer code, VAMUCH, which has the following advantages in comparison to FEM using conventional stress analysis of RVE Sun and Vaidya (1996):

1. VAMUCH can obtain different material properties in different directions simultaneously, which is more efficient than those approaches requiring multiple runs under different loading conditions.

2. VAMUCH calculates effective properties and local fields directly with the same accuracy as the fluctuation functions. No postprocessing calculations which introduces more approximations, such as averaging stresses and averaging strains, are needed.

3. VAMUCH can model composite materials with full anisotropy, while FEM can only handle at most macroscopically orthotropic material, which is an unnecessary restriction.

The application and accuracy of VAMUCH for predicting effective thermoelastic properties and local fields have been demonstrated through various examples.

References

Aboudi, J., 1982. A continuum theory for fiber-reinforced elastic-visoplastic composites. International Journal of Engineering Science 20 (5), 605 – 621.

Aboudi, J., 1984. Effective thermal constants of short fiber composites. Fibre Science and Technology 20, 211 – 225.

Aboudi, J., 1989. Micromechanical analysis of composites by the method of cells. Applied Mechanics Reviews 42 (7), 193 – 221.

Aboudi, J., Pindera, M. J., Arnold, S. M., 2001. Linear thermoelastic higher-order theory for periodic multiphase materials. Journal of Applied Mechanics 68, 697–707.

Accorsi, M. L., Nemat-Nasser, S., 1986. Bounds on the overall elastic and instantaneous elastoplastic moduli of periodic composites. Mechanics of Materials 5 (3), 209 – 220.

Banerjee, B., Adams, D. O., 2004. On predicting the effective elastic properties of polymer bonded explosives using the recursive cell method. International Journal of Solids and Structures 41 (2), 481 – 509.

Bensoussan, A., Lions, J., Papanicolaou, G., 1978. Asymptotic Analysis for Periodic Structures. North-Holland, Amsterdam.

Berdichevsky, V. L., 1979. Variational-asymptotic method of constructing a theory of shells. PMM 43 (4), 664 – 687.

Dvorak, G. J., Bahei-El-Din, Y. A., 1979. Elastic-plastic behavior of fibrous composites. Journal of Mechanics and Physics of Solids 27, 51–72.

Hashin, Z., 1983. Analysis of composite materials-a survey. Applied Mechanics Review 50, 481–505.

Hashin, Z., Shtrikman, S., 1962. A variational approach to the theory of the elastic behaviour of polycrystals. Journal of Mechanics and Physics of Solids 10, 343–352.

Hill, R., 1952. The elastic behavior of crystalline aggregate. Proc. Phys. Soc. London A65, 349–354.

Hill, R., 1965. Theory of mechanical properties of fibre-strengthened materials-iii. self-consistent model. Journal of Mechanics and Physics of Solids 13, 189–198.

Kunin, I., 1982. Theory of Elastic Media with Microstructure. Vol. 1 and 2. Springer Verlag.

Levin, V. M., 1968. Thermal expansion coefficients of heterogeneous materials. Mekhanika Tverdogo Tela 2 (1), 88 – 94.

Milton, G. W., 1981. Bounds on the electromagentic, elastic and other properties of two component composites. Physics Review Letters 46 (8), 542 – 545.

Murakami, H., Toledano, A., 1990. A higer-order mixture homogenization of bi-laminated composites. Journal of Applied Mechanics 57, 388–396.

Paley, M., Aboudi, J., 1992. Micromechanical analysis of composites by the generalized cells model. Mechanics of Materials 14, 127–139.

Rosen, B. W., Hashin, Z., 1970. Effective thermal expansion coefficients and specific heats of composite materials. International Journal of Engineering Science 8, 157 – 173.

Schapery, R. A., 1968. Thermal expansion coefficients of composite materials based on energy principles. Journal of Composite Materials 2, 380 – 404.

Sun, C. T., Vaidya, R. S., 1996. Prediction of composite properties from a representative volume element. Composites Science and Technology 56, 171 – 179.

Tamma, K. K., Avila, A. F., 1999. An integrated micro/macro modeling and computational methodology for high temperature composites. In: Hetnarski, R. B. (Ed.), Thermal Stresses 5. Lastran Corporation, Rochester, NY, pp. 143–256.

Williams, T. O., 2005a. A three-dimensional, higher-oder, elasticity-based micromechanics model. International Journal of Solids and Structures 42, 971–1007.

Williams, T. O., 2005b. A two-dimensional, higher-oder, elasticity-based micromechanics model. International Journal of Solids and Structures 42, 1009–1038.

Yu, W., Tang, T., 2007. Variational asymptotic method for unit cell homogenization of periodically heterogeneous materials. International Journal of Solids and Structures 44, 3738–3755.

Appendix C
A Critical Evaluation of the Predictive Capabilities of Various Advanced Micromechanics Models

C.1 Introduction

As structural applications become more demanding it is becoming increasingly important that the fundamental response mechanisms controlling both the microscopic and macroscopic behavior of structural materials be well understood. Properly quantified in a material model such understanding can be used to improve structural designs, make more accurate estimates of a given structure's capabilities, or engineer a material's microstructure in order to enhance desirable performance characteristics.

The fundamental response mechanisms in all heterogeneous materials are driven by the localization processes induced by the presence of the heterogeneities (the microstructures) that exist in these materials. Micromechanical theories are particularly well suited to modeling localization processes and how they influence the micro- and macroscopic material behavior since these theories predict the multiscale material response based directly on a knowledge of the behavior of the individual component materials and of the heterogeneous microstructure.

There are a number of different types of homogenization tools available. The simplest such models [1,2] which are based on strength of materials assumptions, can only be considered to give very rough estimates for a material's response characteristics. Mean field theories, such as the Mori-Tanaka theory [3,4] can provide reasonable estimates for a material's bulk elastic response but typically fail to provide good estimates for the local responses and the history-dependent responses of the material. In order to correctly predict the local and bulk response characteristics in the elastic and inelastic domains it is necessary to utilize micromechanical theories that consider both the average fields within phases as well as the fluctuating fields within the phases [5]. A set of relatively simple micromechanical models that have attempted to develop such capabilities are the so-call "Method of Cells" (MOC)

[6] and the "Generalized Method of Cells" (GMC) [7,8]. These approaches are based on the use of average strain and stress fields within discrete subvolumes of the microstructure. A review of some of the published work using these models is given in Ref.9. One shortcoming of the MOC/GMC models is the lack of coupling between the local shearing and normal responses for composites composed of phases with at least orthotropic symmetry. This lack of coupling has significant implications for predicting the history-dependent behavior of such materials. In order to overcome this lack of coupling in the local fields it is necessary to utilize theories with more accurate representations of the local fields. There are a number of such theories currently available. Two very different approaches that have been developed in an attempt to directly address the lack of coupling in the MOC/GMC set of models are the so-called "High Fidelity Generalized Method of Cells" (HFGMC) model [10] and the so-called "Elasticity-based Cell Model" [5,11,12]. Obviously, various other models that exhibit (potentially) accurate representations of the microfields in the composite exist which have no connection to the original MOC/GMC methodologies. Examples of such theories are Green's function based analyses [13] and asymptotic homogenization approaches [14]. A recently developed variant of the asymptotic homogenization approach is the Variational Asymptotic Method for Unit Cell Homogenization (VAMUCH) [15-17]. In contrast to conventional asymptotic methods, VAMUCH carries out an asymptotic analysis of the variational statement, synthesizing the merits of both variational methods and asymptotic methods. Finally, there are a number of purely numerical approaches, such as finite element analyses [18,19], and particle-in-cell methods [20], that have been used to model the micromechanical response of heterogeneous materials.

Obviously, significant effort has been expended to develop a number of approaches that can be used to consider the micromechanical responses of composite systems. However, there has been relatively little work done that compares the predictive capabilities of different approaches. One such study, carried out by Lissenden and Herakovich [21], considered the ability of various simplified micromechanical theories to predict the bulk elastic properties of continuous fiber composites. However, in today's environment of advanced applications it is no longer sufficient to consider only the predictions for the bulk characteristics. It is now necessary to consider the predictive capabilities for the local fields within the material system.

The focus of the current work is the comparison of the predictive capabilities of several

advanced micromechanical theories; the GMC theory, the HFGMC theory, the ECM theory, and VAMUCH, with each other as well as with established analytical solutions and finite element predictions. The work will consider both the local and global responses. Since accurate predictions for the elastic fields within the composite are a necessary prerequisite for accurately predicting the history-dependent behavior of heterogeneous materials the current comparisons focus on the elastic predictions.

C.2 Case Studies

These micromechanics models will be used to predict the bulk and local elastic responses of various types of fiber reinforced composites. The resulting predictions will be compared to assess the accuracy with which the different models are capable of predicting the local fields as well as the effective bulk properties of different composite systems. For the purpose of comparison, we also use a finite element based micromechanics approach (which is denoted as FEM) proposed by Sun and Vaidya [18]. This method performs the conventional stress analysis of a representative volume element by applying periodic and symmetric boundary conditions. In this work, we used ANSYS to perform all the needed finite element analysis. Using this approach, only the transverse shear moduli G_{23} can be calculated using 2D analysis, and all the other effective properties are calculated using 3D analysis. However, all the other micromechanics models reviewed in the previous section only require a 2D analysis for fiber reinforced composites.

C.2.1 Case 1: Eshelby problem

The first case is the Eshelby problem [22] which deals with an isotropic circular fiber embedded in an infinite isotropic matrix subjected to the uniform far-field stress σ_{22}^{∞}. It is a plane strain elasticity problem and can be solved exactly. Although this is not a micromechanics problem because no repeating UCs can be identified in the material, we can consider a material with repeating UCs which have sufficiently small fiber volume fraction (we choose 1% for this example) so that the interaction effects due to the presence of adjacent cells are negligible. Except for this restriction, the exact solution provides an excellent benchmark for validation of the accuracy of the local fields predicted by different micromechanics models.

For calculation, we choose the fiber to be boron with Young's modulus $E = 400.0$

Table C.1: Effective properties of boron/epoxy composites for Eshelby problem

Models	E_{11} (MPa)	E_{22} (MPa)	G_{12} (MPa)	G_{23} (MPa)	ν_{12}	ν_{23}
GMC	7465	3785	1311	1309	0.3484	0.4435
HFGMC	7466	3801	1322	1317	0.3481	0.4424
ECM (5th order)	7466	3793	1315	1313	0.3482	0.4431
VAMUCH	7466	3801	1322	1317	0.3481	0.4424
FEM	7466	3801	1322	1317	0.3481	0.4424

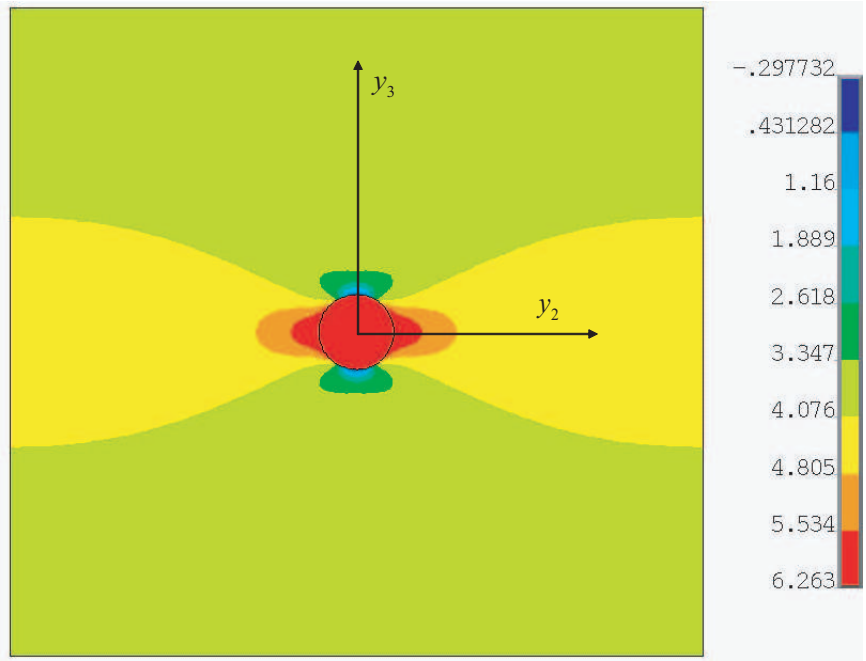

Fig. C.1: Contour plot of σ_{22} (MPa).

GPa and Poisson's ratio $\nu = 0.20$, the matrix to be epoxy with Young's modulus $E = 3.50$ GPa and Poisson's ratio $\nu = 0.35$. The choice of these materials produces a high elastic moduli mismatch and thus a significant disturbance in the stress field along the interface between fiber and matrix. To obtain the stress distribution within the UC using micromechanics approaches, we need to calculate the effective properties first, which are listed in Table C.1. It can be observed that except for GMC, which slightly under predicts the moduli (E_{22}, G_{12}, G_{23}) and over predicts the Poisson's ratios, all the other approaches obtain the same results up to the fourth significant figure.

Next we can use these properties to solve the plane strain problem of the effective, homogenized medium under the application of a far-field stress σ_{22}^{∞}, which will generate a macroscopic strain field $\bar{\epsilon}_{22} = 0.1\%$ and corresponding $\bar{\epsilon}_{33}$ due to Possion's effect. Such val-

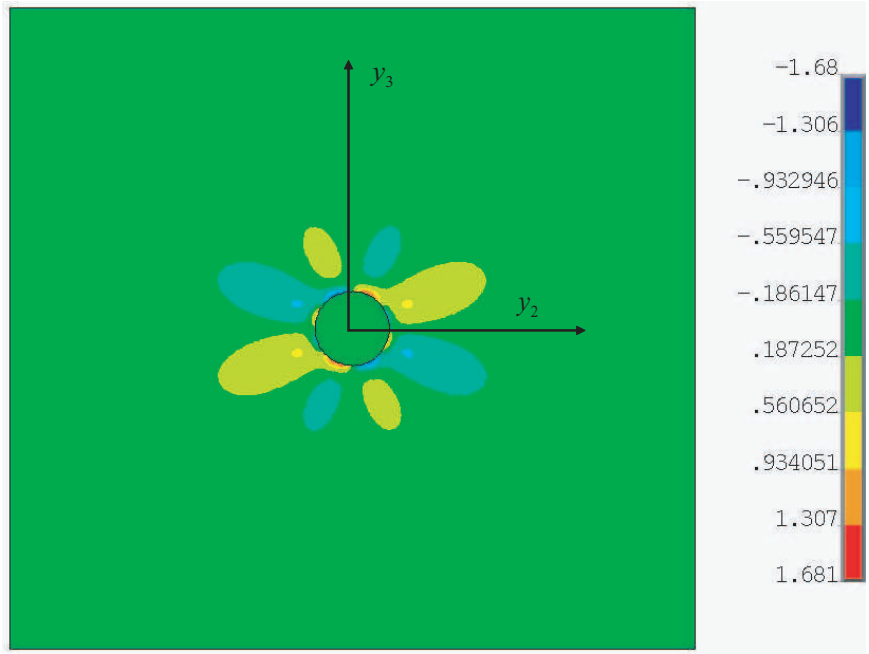

Fig. C.2: Contour plot of σ_{23} (MPa).

ues can be fed back to the micromechanics models to recover the stress distribution within the material. Figures C.1 and C.2 show the contour plots for the distributions of σ_{22} and σ_{23} directly obtained using the exact solution, in which the stress concentrations along the interface between fiber and matrix can be clearly observed. Although contour plots can provide us some qualitative information, to rigorously assess the accuracy of micromechanics approaches, we plot σ_{22} distributions predicted by micromechanics approaches (GMC, HFGMC, and VAMUCH) and the exact solution along the lines $y_2 = 0$ and $y_3 = 0$ in Figure C.3 and Figure C.4, respectively. It is evident that GMC is not predictive for the local field, yet HFGMC and VAMUCH have excellent agreements with the exact solution except that the predictions of HFGMC for the stress field inside the fiber and adjacent to the interface are slightly different from the exact solution. Both the continuous condition along $y_3 = 0$ and discontinuous condition along $y_2 = 0$ are well captured by HFGMC and VAMUCH. The slight differences along the edges are caused by the interaction effects due to presence of adjacent cells because our far-field stress σ_{22}^{∞} is not really uniform along the edges which can be observed form the contour plot in Figure C.1. It has been verified that if one chose a fiber volume fraction so low that σ_{22}^{∞} is uniform along the edges and the prediction of HFGMC and VAMUCH will be further improved. The discontinuity on the interface along $y_2 = 0$ in Figure C.3 can be captured better if one refines the mesh in the

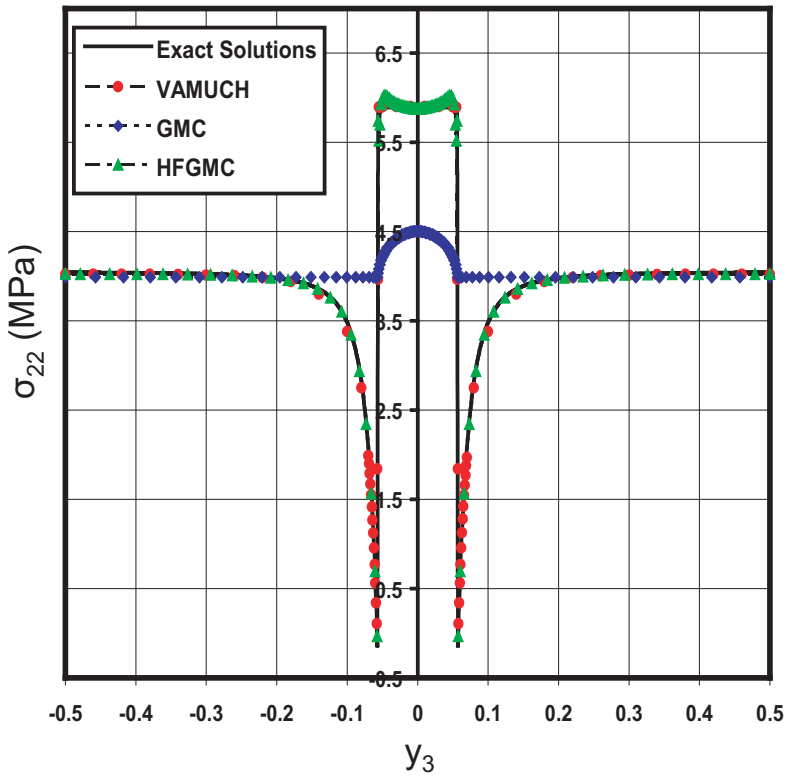

Fig. C.3: Comparison of normal stress σ_{22} distribution along $y_2 = 0$.

vicinity. Although the effective properties are not sensitive to the discretization schemes, the local fields are. In this case, we used 100×100 subcells grid for GMC and HFGMC, and a mesh of 4834 8-noded quadrilateral elements is used for VAMUCH, and the same mesh is used for ANSYS to calculate G_{23}, and the corresponding 3D mesh is extruded from this mesh with two elements along the fiber direction to calculate all the other effective properties.

C.2.2 Case 2: MOC microstructure

Next, we study a microstructure which is a square array with a square fiber in the center (Figure C.5). We called it the MOC microstructure because it is typically used by MOC, GMC and HFGMC [6]. We use the same boron fiber and epoxy matrix as the previous case. However, the fiber volume fraction is changed to be 60% so that the effective properties can be strongly affected by the fibers and their interactions with the matrix and with each other. The effective properties predicted by different approaches are listed in Table C.2. A 64×64 subcell grid is used for GMC and HFGMC, a 2×2 subcell grid is used for ECM, a mesh

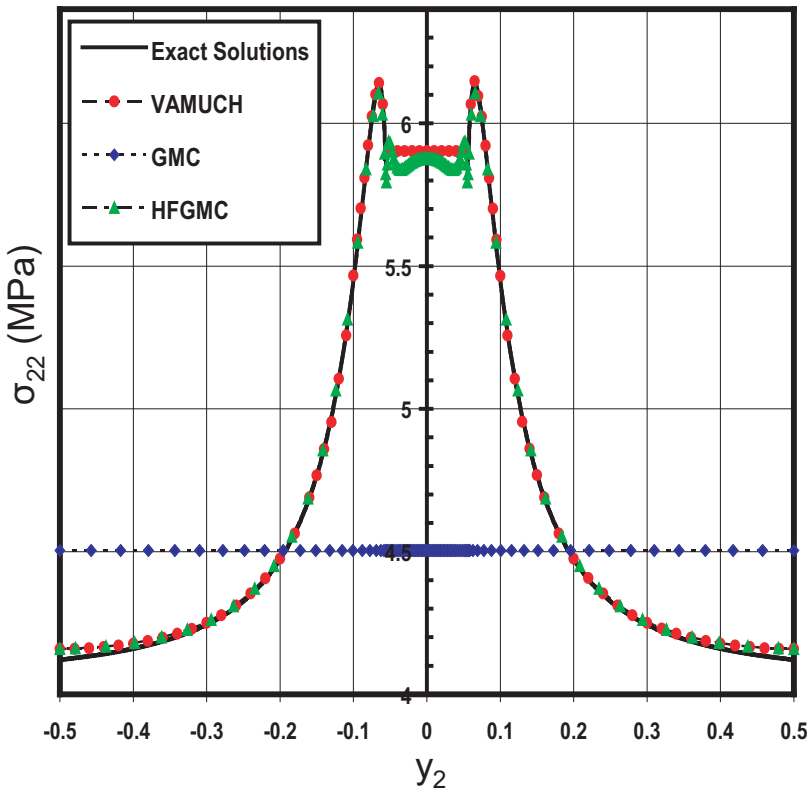

Fig. C.4: Comparison of normal stress σ_{22} distribution along $y_3 = 0$.

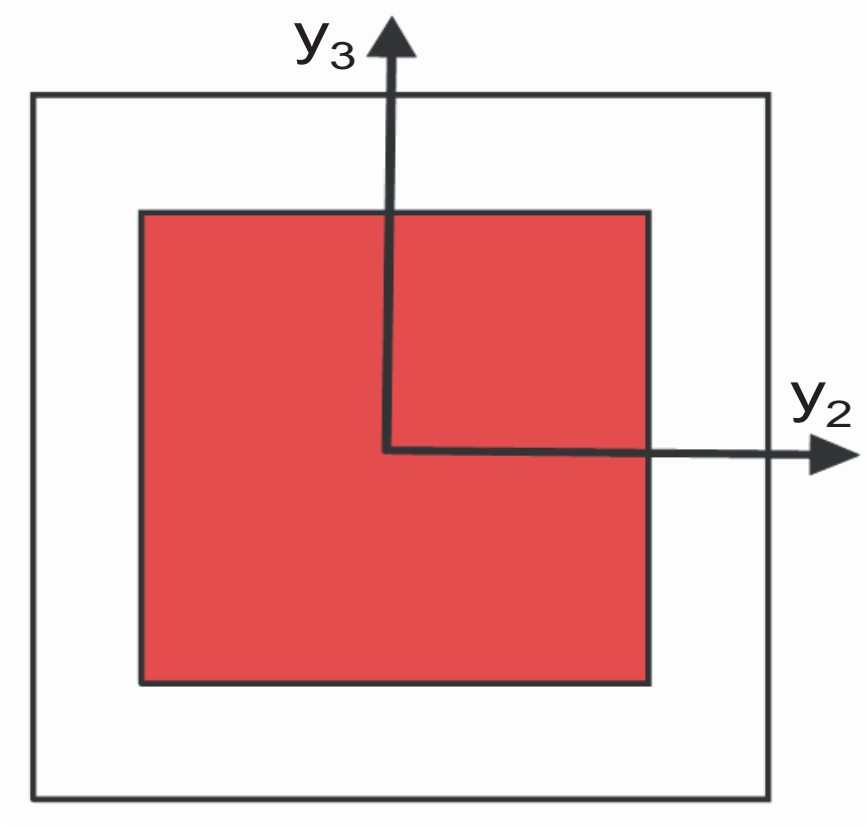

Fig. C.5: A sketch of the MOC microstructure.

Table C.2: Effective properties of boron/epoxy composites for MOC microstructure

Models	E_{11} (MPa)	E_{22} (MPa)	G_{12} (MPa)	G_{23} (MPa)	ν_{12}	ν_{23}
GMC	241422	17440	4631	3203	0.2522	0.2673
HFGMC	241428	19803	5216	3390	0.2501	0.2000
ECM (7th order)	241426	19793	5161	3368	0.2502	0.1994
VAMUCH	241426	19864	5223	3391	0.2501	0.1978
FEM	241426	19864	5223	3391	0.2501	0.1978

of 3763 8-noded elements is used for VAMUCH and the same mesh and its corresponding 3D mesh is used for FEM. It can be observed that only VAMUCH and FEM have the same predictions for all the effective properties, although all the approaches predict almost the same value for E_{11}, and HFGMC's predictions are very close to those of VAMUCH and FEM. Overall, GMC under predicts E_{22}, G_{12}, G_{23} and over predicts the Poisson's ratios. Except E_{11}, the predictions of ECM are located between GMC and HFGMC and close to those of HFGMC.

To evaluate the accuracy of the local stress field predicted by the different approaches, we use a plane strain problem by applying a biaxial loading such that $\sigma_{22} = -10$ MPa and $\sigma_{33} = 100$ MPa to the microstructure. We plot σ_{33} along $y_3 = 0$ predicted by different approaches in Figure C.6, where ANSYS results are obtained by directly solving the plane strain problem without using the effective properties. It can be clearly observed that VAMUCH and HFGMC have excellent agreements with the direct finite element analysis of ANSYS, although the predictions of HFGMC are slightly off at the interface between fiber and matrix. It is also observed that the local field obtained using GMC, although much improved compared to those of case 1, are only predictive in an average sense. We have also compared other stress components and tested with other types of loading such as transverse shear and longitudinal shear, and similar trends have been found. Those results are not reported here for conciseness.

C.2.3 Case 3: X microstructure

The last case we study is an X shaped microstructure, which is sketched in Figure C.7, where each quadrant has two square fibers of the same size and equally spaced along the diagonal. The square fibers are perfectly connected with each other through the corners.

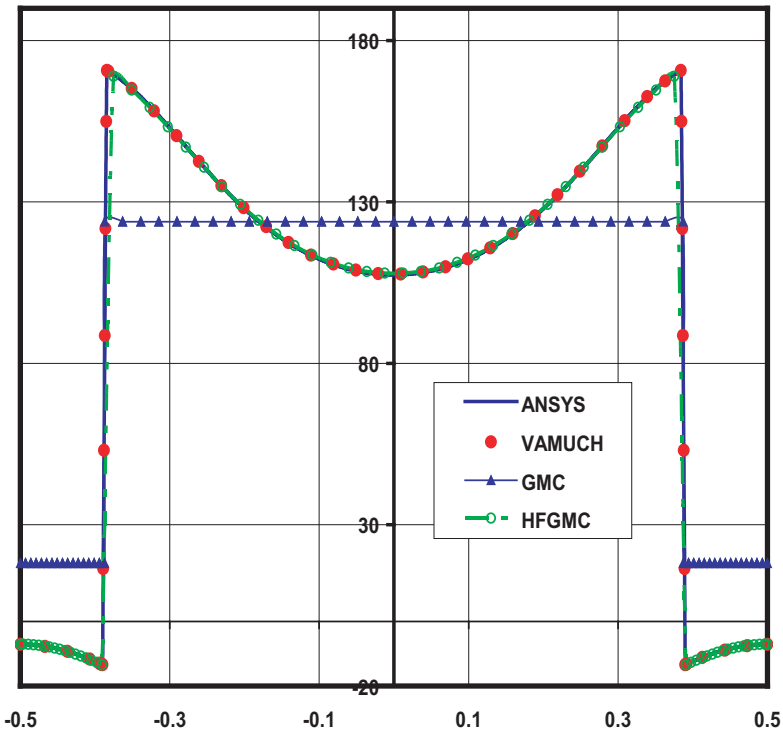

Fig. C.6: Comparison of normal stress σ_{33} distribution along $y_3 = 0$.

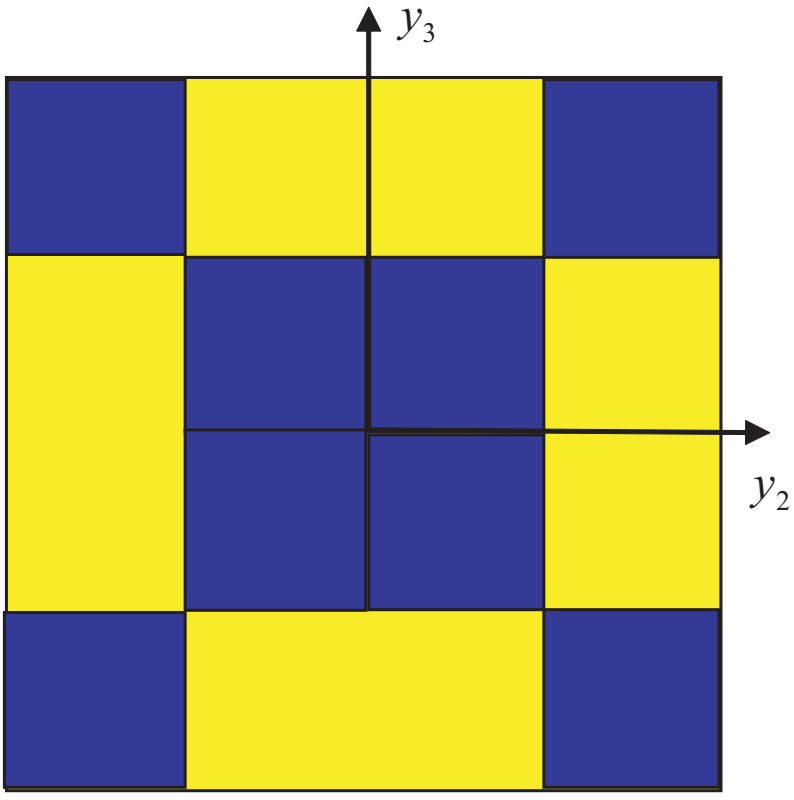

Fig. C.7: The sketch of X shape microstructure.

The composite system considered is polymer-bonded explosives (PBXs) with an explosive crystal inclusion of Young's modulus $E = 15300$ MPa and Possion's ratio $\nu = 0.32$ embedded in a binding matrix with Poisson's ratio $\nu = 0.49$. To investigate the predictions from different approaches for different ratios of elastic moduli mismatches, we choose varying binding matrix material so that its Young's modulus E_m takes different values from 0.7 MPa, 7 MPa, 70 MPa, 700 MPa, and 7000 MPa. The fiber volume fraction is fixed at 50%.

Because of the special construction of this microstructure, singularities exist at all the connecting corners of the fibers. Even the calculation of effective properties becomes sensitive to the discretization schemes used by different methods. For this case, we used a 64×64 subcell grid for GMC and HFGMC, a 3×3 subcell grid is used for ECM, a mesh of 5712 8-noded elements is used for VAMUCH and the same mesh and its corresponding 3D mesh is used for the FEM. The effective properties with different Young's modulus for the binder predicted by different approaches are listed in Tables C.3-C.7. We can observe the following from these tables:

- When $E_m = 7000$, all the approaches except GMC have excellent predictions for the effective properties. As shown in Table C.3, GMC significantly under predicts G_{12} and G_{23}, slightly under predicts E_{11}, E_{22} and ν_{12}, and over predicts ν_{23}.

- For other values of E_m, the general trend is that when the contrast ratio of the Young's moduli of fiber and matrix becomes larger, the differences among the predictions from different approaches becomes larger, although all the approaches still predict a similar value for E_{11}, which approximately obeys the Voigt rule of mixture for fiber reinforce composites.

- For other values of E_m, VAMUCH and FEM also predict the same or similar value for E_{22} and Poisson's ratios. VAMUCH predictions for G_{23} are slightly larger than those of FEM predictions, while VAMUCH predictions for G_{12} are smaller than FEM and the difference become quite significant as the contrast ratio becomes large.

- For other values of E_m, the predictions of GMC, HFGMC, and ECM for E_{22}, G_{12}, G_{23}, although very different among themselves, are significantly lower than those of VAMUCH and FEM, while Poisson's ratios predicted from GMC, HFGMC, and ECM are bigger than those from VAMUCH and FEM. As the contrast ratio becomes larger, the difference between these two sets of results become much bigger.

Table C.3: Effective properties of PBX 9501 composites for X microstructure (E_m = 7000 MPa)

Models	E_{11} (MPa)	E_{22} (MPa)	G_{12} (MPa)	G_{23} (MPa)	ν_{12}	ν_{23}
GMC	11150	10170	3343	3343	0.405	0.5212
HFGMC	11246	10530	3688	3794	0.4126	0.508
ECM (7th order)	11247	10546	3679	3804	0.4126	0.5072
VAMUCH	11247	10531	3690	3795	0.4126	0.5078
FEM	11246	10531	3690	3795	0.4126	0.5078

Table C.4: Effective properties of PBX 9501 composites for X microstructure (E_m = 700 MPa)

Models	E_{11} (MPa)	E_{22} (MPa)	G_{12} (MPa)	G_{23} (MPa)	ν_{12}	ν_{23}
GMC	8000	1687	451.5	451.5	0.405	0.8687
HFGMC	8032	2544	1025	1406	0.4039	0.8032
ECM (7th order)	8024	2089	885.3	1314	0.4042	0.8382
VAMUCH	8041	2693	1207	1525	0.4036	0.7919
FEM	8040	2694	1213	1522	0.4036	0.7919

- It is interesting to find out the GMC always predicts the same value for G_{12} and G_{23} for this microstructure for each value of E_m.

- The predictions of ECM are located between those of GMC and HFGMC for E_m = 700 MPa, 70 MPa and 7 MPa. However, such a trend is not present for E_m = 7000 MPa and 0.7 MPa. Particularly, for E_m = 0.7 MPa, the predictions of ECM for E_{22} and G_{23} are the lowest, while the method predicts the highest value for ν_{23}.

At this stage, we believe it is premature to conclude which sets of predictions are more reliable than others. First of all, it is impractical to connect two fibers through one

Table C.5: Effective properties of PBX 9501 composites for X microstructure (E_m = 70 MPa)

Models	E_{11} (MPa)	E_{22} (MPa)	G_{12} (MPa)	G_{23} (MPa)	ν_{12}	ν_{23}
GMC	7685	182.5	46.79	46.79	0.405	0.9505
HFGMC	7690	376.2	153.2	277.3	0.3991	0.9037
ECM (7th order)	7688	233.7	112.1	214.4	0.4015	0.9387
VAMUCH	7701	798	553	715	0.3854	0.8232
FEM	7704	799	664	711	0.3853	0.8229

Table C.6: Effective properties of PBX 9501 composites for X microstructure (E_m = 7 MPa)

Models	E_{11} (MPa)	E_{22} (MPa)	G_{12} (MPa)	G_{23} (MPa)	ν_{12}	ν_{23}
GMC	7654	18.41	4.696	4.696	0.405	0.9597
HFGMC	7654	40.16	18.43	33.96	0.3976	0.9197
ECM (7th order)	7654	23.67	11.53	23.00	0.4014	0.9503
VAMUCH	7658	502	468	569	0.3428	0.6839
FEM	7660	502	597	563	0.3425	0.6839

Table C.7: Effective properties of PBX 9501 composites for X microstructure (E_m = 0.7 MPa)

Models	E_{11} (MPa)	E_{22} (MPa)	G_{12} (MPa)	G_{23} (MPa)	ν_{12}	ν_{23}
GMC	7650	1.842	0.4698	0.4698	0.405	0.9607
HFGMC	7650	4.058	4.123	6.367	0.3909	0.9277
ECM (7th order)	7650	0.3535	1.146	0.3178	0.4044	0.9925
VAMUCH	7651	460	459	553	0.3228	0.6223
FEM	7651	460	590	546	0.3228	0.6223

material point (the corner). It is a mathematical idealization of small contacting areas. The singularity due to the stress bridging through the connecting corners creates difficult for all numerical approaches. Second, we are limited by resources to perform convergence studies for FEM results because its calculations except G_{23} requires 3D analysis. Although one would tend to blindly believe that the FEM results are the most reliable, this is not necessarily true. The reason is that even if all the results are converged, we have strong reasons to believe the assumed boundary conditions, particularly those applied for transverse shear and longitudinal shear, will significantly affect the results because of the extreme microstructural construction and contrast ratio of constituent properties.

Nevertheless, the aforementioned points by no means diminish the value of this case and the significance of the presented results. Due to its special construction and high contrast ratio, this case provides a great challenge to all micromechanics approaches. It clearly discloses the fallacy about micromechanics that every model "works" as far as effective properties concerned. This is a case worthy of the attention of the micromechanics community and more extensive research on issues such as convergence studies, size effects of the contacting areas, and even physical experiments, which are needed to make more authoritative conclusions.

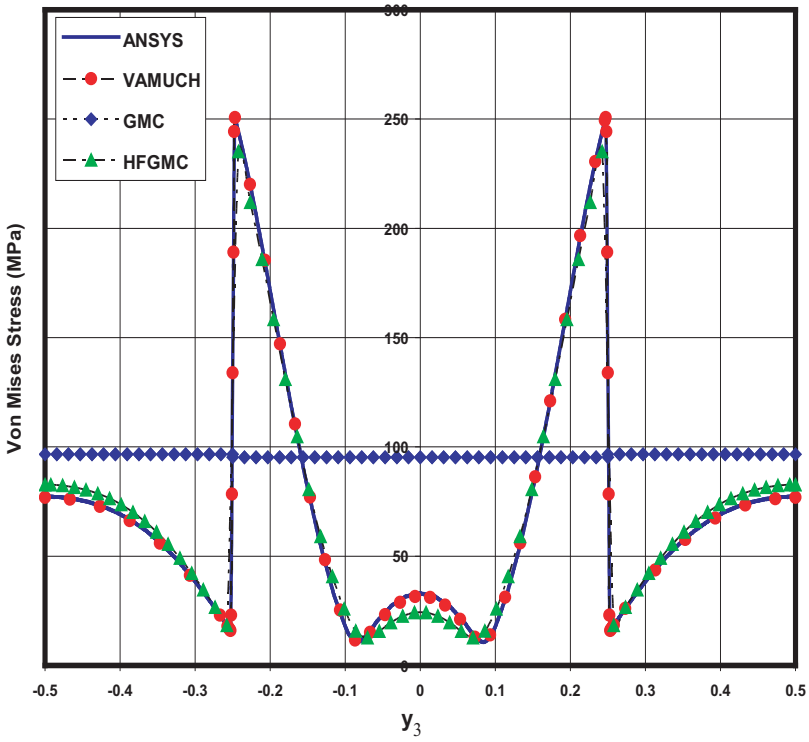

Fig. C.8: Comparison of von Mises stress distribution along $y_2 = 0$.

Although the different approaches predict different effective properties, it is interesting to observe what happens in the predictions of local fields. Here we take the moderate case with $E_m = 700$ MPa to study a plane strain problem by applying a biaxial loading such that $\sigma_{22} = -10$ MPa and $\sigma_{33} = 100$ MPa to the microstructure. We plot the von Mises stress along $y_2 = 0$ predicted by different approaches in Figure C.8, where ANSYS results are obtained by directly solving the plane strain problem without using the effective properties. It can be clearly observed that VAMUCH results are almost on the top of ANSYS results. HFGMC also has an excellent agreement with ANSYS although slight deviations have been found along the edges, fiber-matrix interfaces and the middle part of the microstructure. GMC predicts a uniform distribution which only provides an average prediction. To display the severe stress concentration around the connecting corner between inclusions, we provide a detailed contour plot around one corner in Figure C.9. Indeed, stress concentration only happens in a very small area around the connecting point.

C.3 Conclusions

For the first time, several state-of-the art micromechanics models have been critically

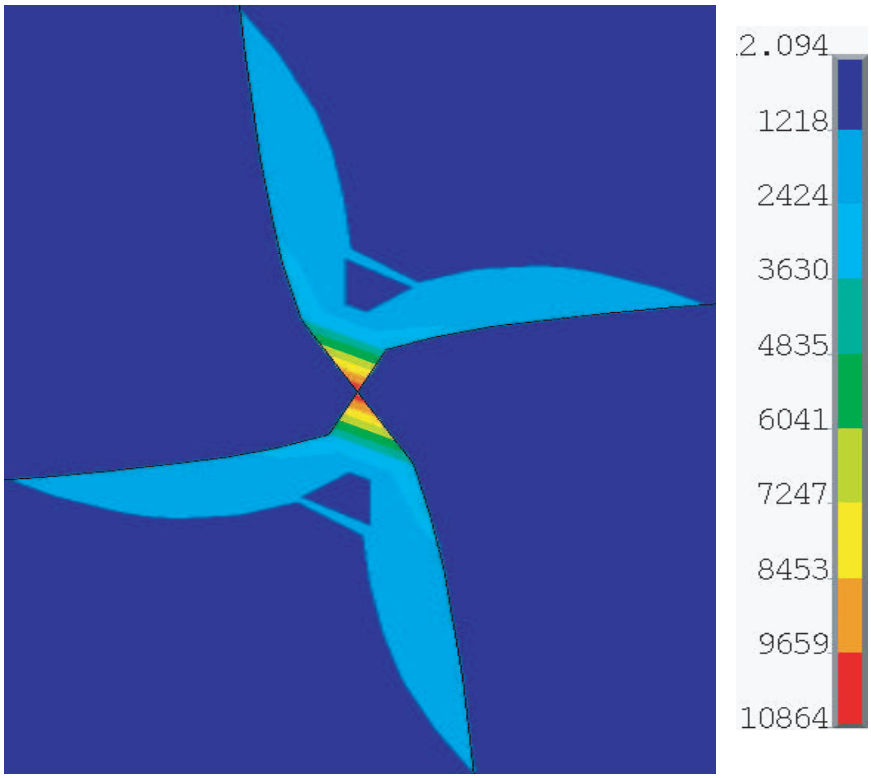

Fig. C.9: Contour plot of von Mises stress (MPa) distribution around a connecting corner.

evaluated as a joint effort among the developers of these models. Such a comparison is valuable to researchers working to adopting a model to their particular applications or to understand what the current state of the art is in predictive capabilities in the field of micromechanics. Additionally the presented results (especially the local field predictions) will represent test cases for researchers seeking to determine the accuracy of the predictive capabilities of new micromechanics models. The X shape microstructure provides a very challenging test case for all micromechanics approaches, and more research is needed to pin-point the real limits of the micromechanics approach in general, and various micromechanics models in particular.

References

1. Jones, R., *Mechanics of Composite Materials*, Hemisphere, New York, NY, 1975.

2. Herakovich, C., *Mechanics of Fibrous Composites*, John Wiley and Sons, New York, NY, 1998.

3. Mori, T. and Tanaka, K., "Average Stress in Matrix and Average Elastic Energy of Materials with Misfitting Inclusions," *Acta Materialia*, Vol. 21, 1973, pp. 571–574.

4. Benveniste, Y., "A New Approach to the Application of Mori-Tanaka's Theory in Composite Materials," *Mechanics of Materials*, Vol. 36, 1987, pp. 147–157.

5. Williams, T. O., "A Generalized, Elasticity-based Theory for the Homogenization of Hetergeneous Materials with Complex Microstructures," 2007, in preparation.

6. Aboudi, J., *Mechanics of Composite Materials: A Unified Micromechanics Approach*, Elsevier, New York, NY, 1991.

7. Paley, M. and Aboudi, J., "Micromechanical Analysis of Composites by the Generalized Method of Cells," *Mechanics of Materials*, Vol. 14, 1992, pp. 127–139.

8. Aboudi, J., "Micromechanical Analysis of Thermo-Inelastic Multiphase Short-Fiber Composites," *Composites Engineering*, Vol. 5, 1995, pp. 839–850.

9. Aboudi, J., "Micromechanical Analysis of Composites by the Method of Cells - Update," *Applied Mechanics Reviews*, Vol. 49, 1996, pp. 127–139.

10. Aboudi, J., "Micromechanical Analysis of Fully Coupled Electro-Magneto-Thermo-Elastic Multiphase Composites," *Smart Materials and Structures*, Vol. 10, 2001, pp. 867–877.

11. Williams, T. O., "A Two-dimensional, Higher-oder, Elasticity-based Micromechanics Model," *International Journal of Solids and Structures*, Vol. 42, 2005, pp. 1009–1038.

12. Williams, T. O., "A Three-dimensional, Higher-oder, Elasticity-based Micromechanics Model," *International Journal of Solids and Structures*, Vol. 42, 2005, pp. 971–1007.

13. Nemat-Nasser, S. and Hori, M., *Micromechanics: Overall Properties of Heterogeneous Materials*, North-Holland, New York, NY, 1993.

14. Bensoussan, A., Lions, J.-L., and Papanicolaou, G., *Asymptotic Analysis for Periodic Structures*, Elsevier, New York, NY, 1978.

15. Yu, W., "A Variational-Asymptotic Cell Method for Periodically Heterogeneous Materials," *Proceedings of the 2005 ASME International Mechanical Engineering Congress and Exposition*, ASME, Orlando, Florida, Nov. 5–11 2005.

16. Yu, W. and Tang, T., "Variational Asymptotic Method for Unit Cell Homogenization of Periodically Heterogeneous Materials," *International Journal of Solids and Structures*, Vol. 44, 2007, pp. 4039–4052.

17. Yu, W. and Tang, T., "A New Micromechanics Model for Predicting Thermoelastic Properties of Heterogeneous Materials," *International Journal of Solids and Structures*, 2007, submitted.

18. Sun, C. and Vaidya, R., "Prediction of Composite Properties from a Representative Volume Element," *Composites Science and Technology*, Vol. 86, 1996, pp. 171–179.

19. Brockenbrough, J., Suresh, S., and Wienecke, H., "Deformation of Metal-Matrix Composites with Continuous Fibers: Geometrical Effects of Fiber Distribution and Shape," *Acta. Metall. Mater.*, Vol. 39, 1991, pp. 735–752.

20. Brydon, A. D., Bardenhagen, S. G., Miller, E. A., and Seidler, G. T., "Simulation of the Densification of Real Open-Celled Foam Microstructures," *Journal of the Mechanics and Physics of Solids*, Vol. 53, 2005, pp. 2638–2660.

21. Lissenden, C. and Herakovich, C., "Comparison of Micromechanical Models for Elastic Properties," *Space '92, Proceedings of the 3rd International Conference, Denver, CO*, Vol. 2, 1992, pp. 1309–1322.

22. Eshelby, J. D., "The Determination of the Elastic Field of an Ellipsoidal Inclusion, and Related Problems," *Proc. R. Soc. London A*, 1957, pp. 376–396.

Appendix D

Finite Element Method for the Effective Properties of Piezoelectric Composite Materials in Chapter 4

This Appendix presents a brief introduction to the finite element method (FEM) developed by Berger et al., (2006) for calculating the effective properties of piezoelectric composite materials. The results of this FEM were compared with those of VAMUCH in **Chapter 4**.

Constitutive equation

The matrix form of constitutive equation for a transversely isotropic piezoelectric composite can be expressed as:

$$\begin{Bmatrix} \bar{\sigma}_{11} \\ \bar{\sigma}_{22} \\ \bar{\sigma}_{33} \\ \bar{\sigma}_{23} \\ \bar{\sigma}_{31} \\ \bar{\sigma}_{12} \\ \bar{T}_1 \\ \bar{T}_2 \\ \bar{T}_3 \end{Bmatrix} = \begin{bmatrix} C^*_{11} & C^*_{12} & C^*_{13} & 0 & 0 & 0 & 0 & 0 & -e^*_{13} \\ C^*_{12} & C^*_{11} & C^*_{13} & 0 & 0 & 0 & 0 & 0 & -e^*_{13} \\ C^*_{13} & C^*_{13} & C^*_{33} & 0 & 0 & 0 & 0 & 0 & -e^*_{33} \\ 0 & 0 & 0 & C^*_{44} & 0 & 0 & 0 & -e^*_{15} & 0 \\ 0 & 0 & 0 & 0 & C^*_{44} & 0 & -e^*_{15} & 0 & 0 \\ 0 & 0 & 0 & 0 & 0 & C^*_{66} & 0 & 0 & 0 \\ 0 & 0 & 0 & 0 & e^*_{15} & 0 & k^*_{11} & 0 & 0 \\ 0 & 0 & 0 & e^*_{15} & 0 & 0 & 0 & k^*_{11} & 0 \\ e^*_{13} & e^*_{13} & e^*_{33} & 0 & 0 & 0 & 0 & 0 & k^*_{33} \end{bmatrix} \begin{Bmatrix} \bar{\epsilon}_{11} \\ \bar{\epsilon}_{22} \\ \bar{\epsilon}_{33} \\ \bar{\epsilon}_{23} \\ \bar{\epsilon}_{31} \\ \bar{\epsilon}_{12} \\ \bar{E}_1 \\ \bar{E}_2 \\ \bar{E}_3 \end{Bmatrix} \tag{D.1}$$

Periodic boundary conditions for the unit cell

Composite materials are assumed to have periodic microstructure, which means that composite materials can be idealized as a periodic assembly of many unit cells. The periodic boundary conditions on the unit cell surfaces described in Cartesian coordinates can be written as:

$$u_i = \bar{\epsilon}_{ij} x_j + v_i \tag{D.2}$$

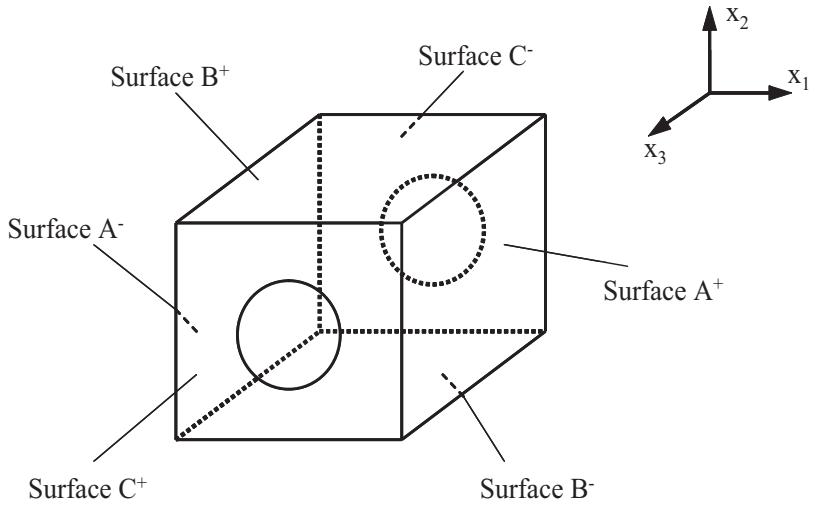

Fig. D.1: Notation for different surfaces of the unit cell.

where $\bar{\epsilon}_{ij}$ are the average strains; and v_i is the periodic part of the displacement components (local fluctuation) on the boundary surfaces. For the unit cell shown in Fig. D.1, the displacements on the opposite boundary surfaces are:

$$u_i^{K^+} = \bar{\epsilon}_{ij} x_j^{K^+} + v_i^{K^+} \tag{D.3}$$

$$u_i^{K^-} = \bar{\epsilon}_{ij} x_j^{K^-} + v_i^{K^-} \tag{D.4}$$

where the index K^+ means along the positive x_j direction and K^- means along the negative x_j direction on the corresponding surfaces A^-/A^+, B^-/B^+, and C^-/C^+. The local fluctuations $v_i^{K^+}$ and $v_i^{K^-}$ are identical on two opposing faces. Therefore the periodic boundary conditions for the displacements and the electric potential are given by:

$$u_i^{K^+} - u_i^{K^-} = \bar{\epsilon}_{ij}(x_j^{K^+} - x_j^{K^-}) \tag{D.5}$$

$$\phi^{K^+} - \phi^{K^-} = \bar{E}_i(x_i^{K^+} - x_i^{K^-}) \tag{D.6}$$

The average stresses and strains in a unit cell are defined by:

$$\bar{\sigma}_{ij} = \frac{1}{V}\int_V \sigma_{ij}\, \mathrm{d}V \tag{D.7}$$

$$\bar{\epsilon}_{ij} = \frac{1}{V}\int_V \epsilon_{ij}\, \mathrm{d}V \tag{D.8}$$

Table D.1: Boundary conditions and equations for calculation of the effective properties of transversely isotropic composite materials

Eff. Coeff.	A^-	A^+	B^-	B^+	C^-	C^+	Formula
	u_i/ϕ	u_i/ϕ	u_i/ϕ	u_i/ϕ	u_i/ϕ	u_i/ϕ	
C^*_{11}	$0/-$	$\tilde{u}_1/-$	$0/-$	$0/-$	$0/0$	$0/0$	$\bar{\sigma}_{11}/\bar{\epsilon}_{11}$
C^*_{12}	$0/-$	$\tilde{u}_1/-$	$0/-$	$0/-$	$0/0$	$0/0$	$\bar{\sigma}_{22}/\bar{\epsilon}_{11}$
C^*_{13}	$0/-$	$0/-$	$0/-$	$0/-$	$0/0$	$\tilde{u}_3/-$	$\bar{\sigma}_{11}/\bar{\epsilon}_{33}$
C^*_{33}	$0/-$	$0/-$	$0/-$	$0/-$	$0/0$	$\tilde{u}_3/-$	$\bar{\sigma}_{33}/\bar{\epsilon}_{33}$
C^*_{44}	$(\tilde{u}_3)/0$	$(\tilde{u}_3)/0$	$0/-$	$0/-$	$(\tilde{u}_1)/0$	$(\tilde{u}_1)/0$	$\bar{\sigma}_{13}/\bar{\epsilon}_{31}$
C^*_{66}	$(\tilde{u}_2)/-$	$(\tilde{u}_1)/-$	$(\tilde{u}_1)/-$	$(\tilde{u}_2)/-$	$0/0$	$0/0$	$\bar{\sigma}_{12}/\bar{\epsilon}_{12}$
e^*_{13}	$0/-$	$0/-$	$0/-$	$0/-$	$0/0$	$0/\tilde{\phi}$	$-\bar{\sigma}_{11}/\bar{E}_3$
e^*_{33}	$0/-$	$0/-$	$0/-$	$0/-$	$0/0$	$0/\tilde{\phi}$	$-\bar{\sigma}_{33}/\bar{E}_3$
e^*_{15}	$(\tilde{u}_3)/0$	$(\tilde{u}_3)/0$	$0/-$	$0/-$	$0/-$	$0/-$	$\bar{T}_1/\bar{\epsilon}_{31}$
k^*_{11}	$0/0$	$0/\tilde{\phi}$	$0/-$	$0/-$	$0/-$	$0/-$	$\bar{T}_1/\bar{E}_1$
k^*_{33}	$0/-$	$0/-$	$0/-$	$0/-$	$0/0$	$0/\tilde{\phi}$	$-\bar{T}_3/\bar{E}_3$

Finite element models and boundary conditions for evaluation of the different effective coefficients

FE package ANSYS is employed to calculate all of the effective properties. Three dimensional multi-field eight-node brick elements with three displacement degrees of freedom and an electrical potential (voltage) degree of freedom were used. To obtain the effective properties the periodic boundary conditions (equations (D.5) and (D.6)) were applied in the unit cell by coupling opposite nodes on the opposite boundary surfaces. To this end, the meshes on the opposite boundary surfaces are identical. For the computation of the effective coefficients the boundary conditions are applied to the unit cell in such a way that, except one component of the strain and electric field in Eq. (D.1), all other components are set to zero. Hence each effective coefficient is determined by multiplying the corresponding row of the material matrix by the strain and electric field. The calculation can be performed by imposing the appropriate boundary conditions and constraint equations to the different surfaces of the unit cell as shown in Table D.1. In this Table, '0' denotes a prescribed zero displacement or electric potential; '$-$' denotes a non-prescribed electric potential; $\tilde{u}_i$ stands for a non-zero prescribed displacement for the component of u_i; $\tilde{\phi}$ denotes a non-zero prescribed electric potential ϕ; $(\tilde{u}_i)$ denotes a constraint of coupling with the opposite surface for displacement component u_i.

As an example of the application of the algorithm, the calculation of the effective coefficients C^{eff}_{13} and C^{eff}_{33} is shown. The boundary conditions have to be applied to the

unit cell in such a way that, except the strain in the x_3 direction (ϵ_{33}), all other mechanical strains and the electric field ($\bar{E}_i$) are set to zero. This can be achieved by constraining the normal displacements on all the surfaces to be equal to zero except for those on the surfaces C^+ (see Fig. D.1). The periodic boundary conditions (Eq. D.5) for the opposite surfaces A^-/A^+ and B^-/B^+ are automatically satisfied since the prescribed normal displacements are zero. Due to the applied zero displacements on the surfaces C^- in the x_3 direction ($u_3^{C^-}$) the periodic boundary condition in this direction according to Eq. D.5 simplifies to:

$$u_3^{C^+} = \bar{\epsilon}_{33}(x_3^{C^+} - x_3^{C^-}) \tag{D.9}$$

Since this equation is now independent of $u_3^{C^-}$, instead of using the constraint equations, an arbitrary constant prescribed displacement can be applied on the surface C^+ to produce a strain in the x_3 direction. In order to make the electric field $\bar{E}_3$ zero, the voltage degree of freedom ϕ on the surfaces C^-/C^+ is set to zero.

For the calculation of the total average values $\bar{\epsilon}_{33}$, $\bar{\sigma}_{11}$, and $\bar{\sigma}_{33}$ according to Eqs. D.7 and D.8, the integral was replaced by a sum over averaged element values multiplied by the respective element volume. Using these total average values the coefficients C_{13}^{eff} and C_{33}^{eff} can be calculated from the matrix equation D.1. Due to the strains and electric fields being zero, except $\bar{\epsilon}_{33}$, the first row becomes $\bar{\sigma}_{11} = C_{13}^{eff}\bar{\epsilon}_{33}$. Then the C_{13}^{eff} can be calculated as the ratio $\bar{\sigma}_{11}/\bar{\epsilon}_{33}$. Similarly C_{33}^{eff} can be evaluated as the ratio $\bar{\sigma}_{33}/\bar{\epsilon}_{33}$ from the third row of matrix equation D.1. All other coefficients whose formulae are based on the average normal strain can be calculated using Table. D.1.

Special attention must be paid to the coefficients which are based on the averaged shear strains, i.e., C_{44}^{eff}, C_{66}^{eff}, and e_{15}^{eff}. Here constraint equations (coupling constraints) on two pairs of the opposite surfaces must be defined. For example, for C_{66}^{eff} which is based on the pure in-plane ($x_1 - x_2$ plane) shear state, the constraint equation for a pair of nodes on the opposite surfaces A^-/A^+ (see the notation $\tilde{u}_2$ in Table. D.1) can be written according to Eq. D.5 as $u_2^{A^+} = u_2^{A^-} + \bar{\epsilon}_{12}(x_1^{A^+} - x_1^{A^-})$. The fluctuation function $\bar{\epsilon}_{12}(x_1^{A^+} - x_1^{A^-})$ can be set to an arbitrary value. The analogous constraint equations have to be defined for the opposite surfaces B^-/B^+. To avoid rigid body motion the intersection edge between surfaces B^- and A^- is fixed in the x_1 and x_2 directions. Analogously, the coefficients C_{44}^{eff}, e_{15}^{eff}, which is based on the pure out-of-plane ($x_1 - x_3$ or $x_2 - x_3$ plane) shear state, can be

Table D.2: Boundary conditions and equations for calculation of the effective properties of transversely isotropic composite materials

	1	2	3	4	5	6
Group	C^*_{11}, C^*_{12}	C^*_{13}, C^*_{33}	C^*_{44}, e^*_{15}	C^*_{66}	e^*_{13}, e^*_{33}, k^*_{33}	k^*_{11}

calculated. Actually, the boundary conditions for C^{eff}_{44}, C^{eff}_{66}, and e^{eff}_{15} are similar to those used in Sun and Vaidya (1996) for the calculation of shear modulus.

Differences between FEM and VAMUCH

Considering the boundary conditions listed in Table. D.1, it can be seen that six groups of boundary conditions and 11 averaging processes are needed to get all 11 effective coefficients of transversely isotropic composite materials. Table. D.2 shows the groups of boundary conditions needed for calculation of the effective properties of transversely isotropic composite materials. Therefore, more groups of boundary conditions and more times of averaging processes are necessary to obtain all of the effective coefficients, if the composite is orthotropic or general anisotropic. However, VAMUCH only needs one step of calculation to get the complete set of coefficients without imposing boundary conditions and averaging processes. In addition, for unidirectional fiber composites, VAMCUH only needs two-dimensional model. Hence, it is more efficient and accurate than finite element method. That is the major difference between VAMUCH and finite element unit cell procedure.

References

Berger, H., Kari, S., Gabbert, U., Rodriguez-Ramos, R., Bravo-Castillero, J., Guinovart-Diaz, R., Sabina, F., Maugin, G.,. 2006. "Unit cell models of piezoelectric fiber composites for numerical and analytical calculation of effective properties". *Smart Materials and Structures* **15**, 451–458.

C.T. Sun and R.S. Vaidya. 1996. "Prediction of composite properties from a representative volume element." *Composites Science and Technololy*, 56:171–179.

Appendix E

Example of practical applications of VAMUCH

VAMUCH is a new micromechanics tool used for homogenizing composite materials. In this section, an example is employed to demonstrate how VAMUCH would be utilized in practical applications. The example is a composite block made of boron fibers reinforced aluminum matrix as shown in Fig. E.1, where we use (X_1, X_2, X_3) as the global coordinates to describe the macroscopic structure and (Y_1, Y_2, Y_3) parallel to (X_1, X_2, X_3) as the local coordinates to describe the unit cell. Both constituents are isotropic with Young's modulus E = 379.3GPa and Poisson's ratio $\nu = 0.1$ for the boron fibers, and Young's modulus E = 68.3GPa and Poisson's ratio $\nu = 0.3$ for the aluminum matrix. The boron fiber is arranged in a square array and the volume fraction of the fibers is 0.4. The axial direction of the disk is along X_1 direction. Uniform displacement 0.078323mm is applied at the right free boundary surface of the block. The X_2-component displacement of the left boundary surface of the block is set to zero, namely, $u_{X_2} = 0$. Fig. E.2 illustrates how VAMUCH can be used to solve this problem.

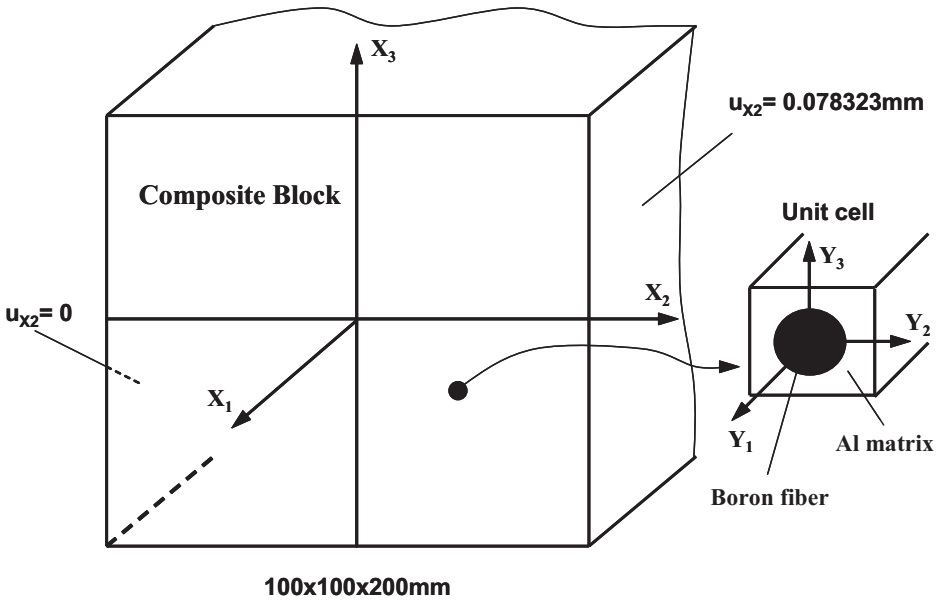

Fig. E.1: Composite plate subjected to uniform tensile displacement at the free boundary surface

Table E.1: Effective properties of the B/Al composite

E_X^*	E_Y^*	E_Z^*
127676.32 (MPa)	127676.32 (MPa)	193530.45 (MPa)
ν_{XY}^*	ν_{YZ}^*	ν_{XZ}^*
0.27776785	0.20901172	0.20901172
G_{XY}^*	G_{YZ}^*	G_{XZ}^*
41702.828(MPa)	48303.982 (MPa)	48303.982 (MPa)

1. Firstly, a unit cell (UC) should be identified as shown in Fig. E.3 and meshed. In this example, only a two dimensional model is needed because the material properties are uniform along X_1 direction.

2. Calculate the effective properties of the composite as shown Table E.1.

3. In this example, we used ANSYS to study the global response of the block with the effective properties. Fig. E.4 shows the contour plot of X_2-component of displacement of the homogenized materials.

4. If the local fields are of interest, we can recover those fields based on the global response obtained from step 3. For instance, Fig. E.5 is the contour plot of von Mises stress at a arbitrary macro material point.

We also used ANSYS to directly calculate the strain energy and averaged value of X_2-component of stress σ_{X_2} of the composite block having 1UC, 36UCs, and 81UCs, respectively. Table E.2 shows the strain engery, averaged value of X_2-component of stress σ_{X_2}, and computing time of the equivalent homogeneous materials and block having different number of UCs, respectively. It can be observed that the strain engergy and the averaged value of X_2-component of stress σ_{X_2} of the block is getting close to that of equivalent homogeneous materials as the number of unit cells increases, which means that the accuracy of micromechanics increases with the ratio of the size of RVE to that of the macroscopic structure decreasing. It can also be seen that the computational cost of equivalent homogeneous materials is much lower than that of nonhomogeneous materials. In general, VAMUCH can accurately reproduce the results of direct analysis. The saving of computational cost is much more when there are more unit cells and the microstructure of the composite is more complex.

Table E.2: Strain energy, averaged value of X_2-component stress (σ_{X_2}), and computing time of free boundary surface of the composite block having different number of UCs and equivalent homogeneous materials

Number of UCs	1UC	36UCs	81UCs	Equiv. Hom.
strain energy ($\times 10^4$ J)	7.483	7.769	7.8	7.83
averaged value of σ_{X_2} (MPa)	95.54	99.2	99.44	100
computing time (s)	20	140	320	2

One limitation of micromechanics approaches based on periodic microstructure is that they are not able to accurately recover the local fields at the boundary layer near the external surface when the composite is subjected to uniform transverse tension or compression stress. Fig. E.6 shows the distribution of von Mises stress along the X_3 axis calculated by ANSYS and VAMUCH, when the block has 81 unit cells. The results of VAMUCH are calculated from the global response of the equivalent homogeneous materials, while ANSYS results are obtained by directly solving the real problem in which the composite block contains 81 unit cells. From Figs. E.6, we can see that in real composite the actual distribution of von Mises stress (predicted by ANSYS) do not keep periodic at the boundary layer, while the predictions of VAMUCH are periodic even at the boundary layer.

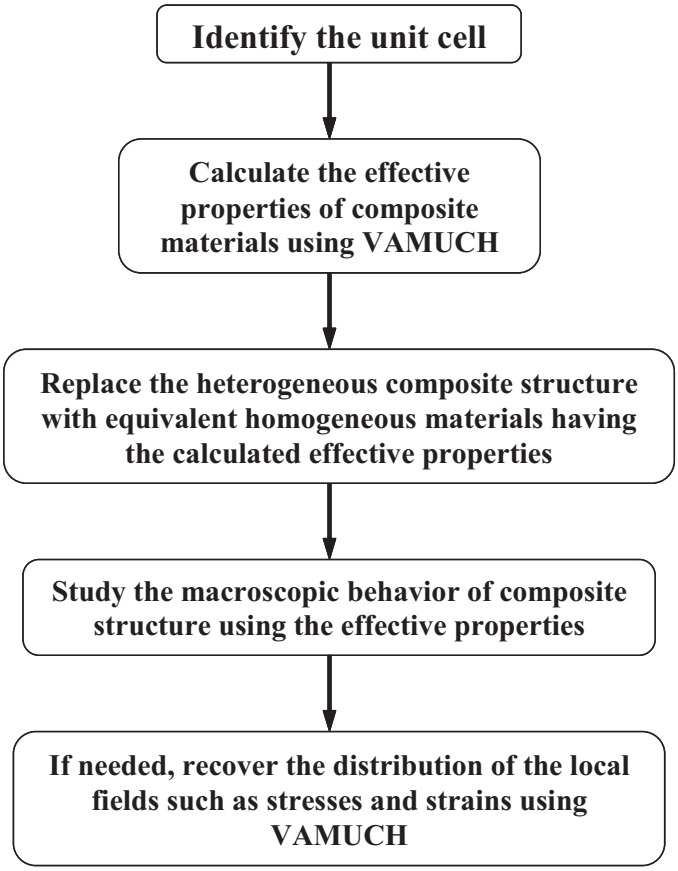

Fig. E.2: Flow chart of application of VAMUCH.

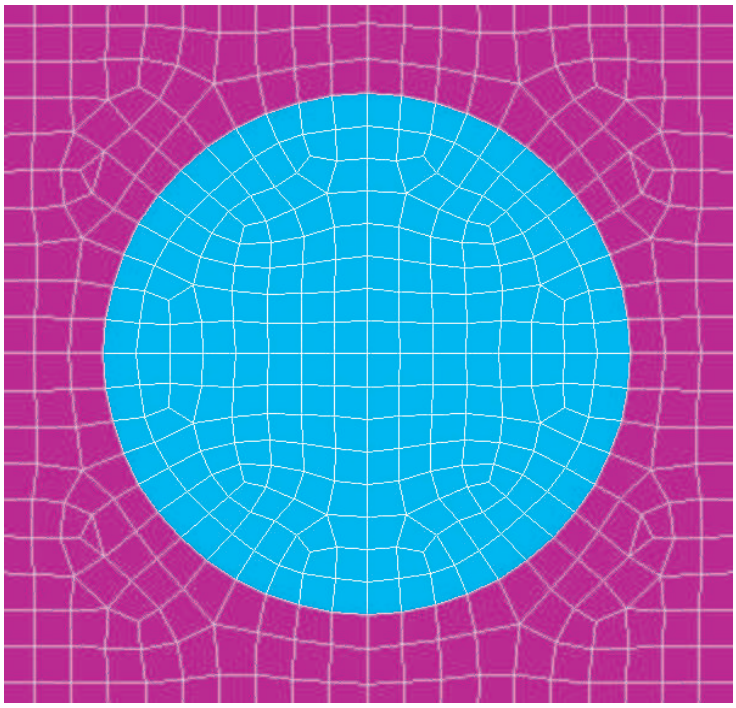

Fig. E.3: Unit cell of B/Al composites.

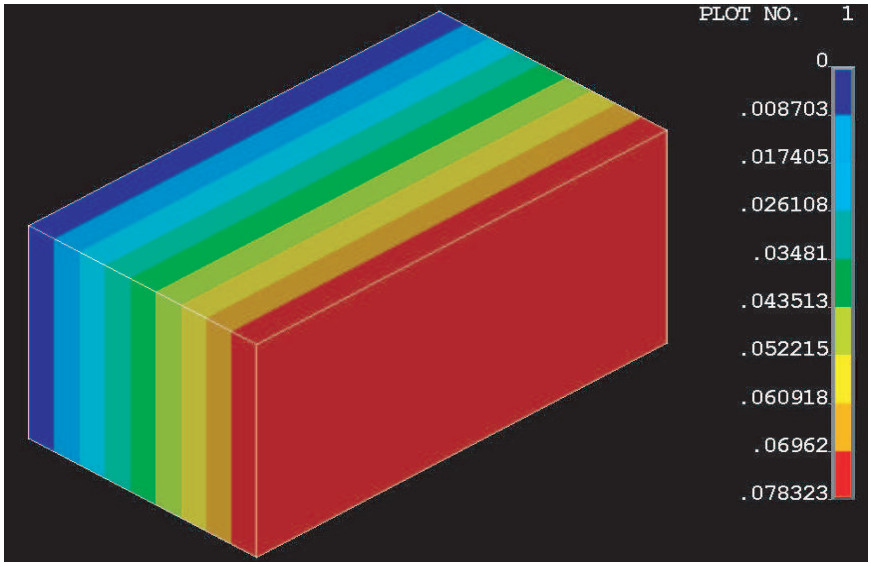

Fig. E.4: Contour plot of X_2-component displacement (mm) of the equivalent homogeneous materials.

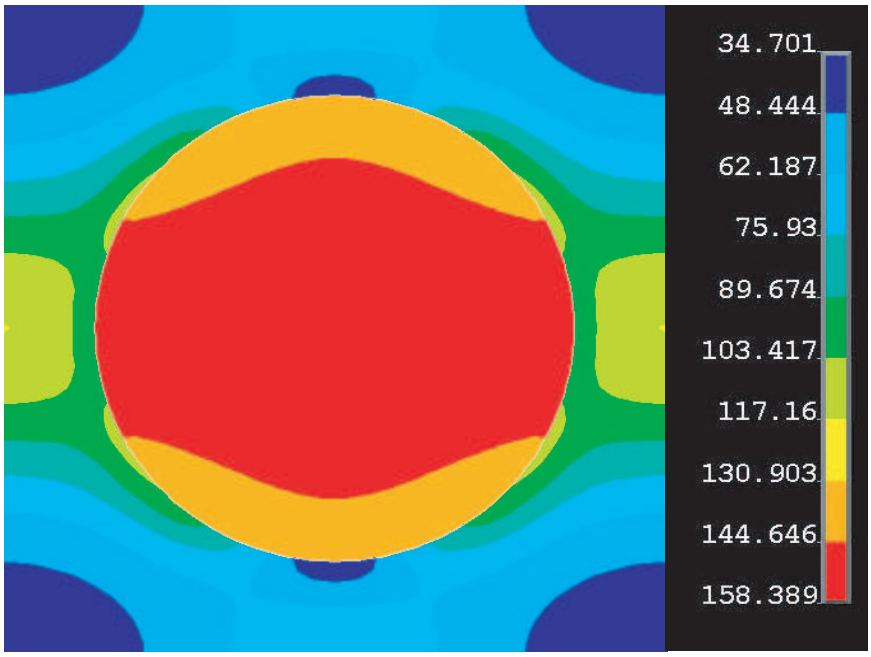

Fig. E.5: Contour plot of von Mises stress (MPa) at an arbitrary macro material point.

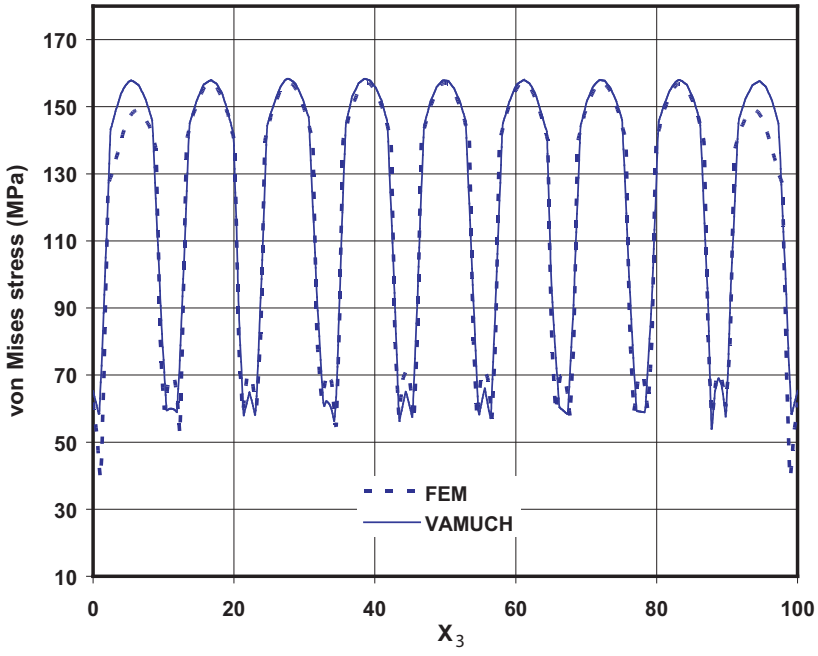

Fig. E.6: The distribution of von Mises stress along the X_3 axis.

Appendix F

Permissions

Chapter 3, 4, Appendix A, and Appendix B are journal papers published in the *International Journal of Engineering Science*–Elsevier, *Mechanics of Materials*–Elsevier, and *International Journal of Solids and Structures*–Elsevier, respectively. As a journal author, I retain the following rights presented in the website:

http://www.elsevier.com/wps/find/authorsview.authors/copyright#whatrights

What rights do I retain as a journal author*?

As a journal author, you retain rights for large number of author uses, including use by your employing institute or company. These rights are retained and permitted without the need to obtain specific permission from Elsevier. These include:

- the right to make copies (print or electric) of the journal article for their own personal use, including for their own classroom teaching use.
- the right to make copies and distribute copies (including via e-mail) of the journal article to research colleagues, for personal use by such colleagues (but not for Commercial Purposes**, as listed below).
- the right to post a pre-print version of the journal article on Internet web sites including electronic pre-print servers, and to retain indefinitely such version on such servers or sites (see also our information on electronic preprints for a more detailed discussion on these points).
- the right to post a revised personal version of the text of the final journal article (to reflect changes made in the peer review process) on the author's personal or institutional web site or server, incorporating the complete citation and with a link to the Digital Object Identifier (DOI) of the article; " the right to present the journal article at a meeting or conference and to distribute copies of such paper or article to the delegates attending the meeting.

- for the author's employer, if the journal article is a 'work for hire', made within the scope of the author's employment, the right to use all or part of the information in (any version of) the journal article for other intra-company use (e.g. training), including by posting the article on secure, internal corporate intranets.
- patent and trademark rights and rights to any process or procedure described in the journal article.
- the right to include the journal article, in full or in part, in a thesis or dissertation.
- the right to use the journal article or any part thereof in a printed compilation of works of the author, such as collected writings or lecture notes (subsequent to publication of the article in the journal).
- the right to prepare other derivative works, to extend the journal article into book-length form, or to otherwise re-use portions or excerpts in other works, with full acknowledgement of its original publication in the journal.

*****Please Note: The rights listed above apply to journal authors only. For information regarding book author rights, please contact **the Global Rights Department**.

Elsevier Global Rights Department

phone (+44) 1865 843 830

fax (+44) 1865 853 333

email: permissions@elsevier.com

Other uses by authors should be authorized by Elsevier through the Global Rights Department, and journal authors are encouraged to let Elsevier know of any particular needs or requirements.

**Commercial Purposes includes the use or posting of articles for commercial gain including the posting by companies or their employee-authored works for use by customers of such companies (e.g. pharmaceutical companies and physician-prescribers); commercial exploitation such as directly associating advertising with such postings; the charging of fees for document delivery or access; or the systematic distribution to others via e-mail lists or list servers (to parties other than known colleagues), whether for a fee or for free.

STANFORD UNIVERSITY
DEPARTMENT OF MECHANICAL ENGINEERING

To:
Mr. Tian Tang
Department of Mechanical and Aerospace Engineering
Utah State University
Logan, Utah 80322-4130

Charles R. Steele
Division of Mechanics and Computation
Durand Building, Room 262
Stanford University
Stanford, California 94305
tel: (650) 723-2844
fax: (650) 725-3377
email: chasst@stanford.edu

October 15, 2008

Dear Mr. Tang,

Thank you for your outstanding contribution:

Tang, T. and Yu, W.: "A Variational Asymptotic Micromechanics Model for Predicting Conductivity of Composite Materials," *Journal of Mechanics of Materials and Structures*, vol. 2, no. 9, 2007, pp. 1813-1830.

You have the permission from the publisher *Mathematical Sciences Publishers* to publish this in your thesis.

Sincerely yours,

Charles R Steele

Charles R. Steele, Ph.D.
Professor of Applied Mechanics, Emeritus
Chief Editor, Journal of Mechanics of Materials and Structures

Vita

About the author

Tian Tang was born in Xuanhan, Sichuan, China, on November 28, 1969. He received his B.S. degree from Beijing University of Aeronautics and Astronautics, majoring in welding technology and equipment. After his graduation, he worked in Guizhou Anshun Longyan aircraft manufacturing plant as a mechanical engineer from 1991 to 1998. He then worked in a company in Guangdong as a mechanical design engineer. He received his M.S. degree from the University of Alabama at Birmingham with emphasis in materials science and engineering in May, 2004. After that, he moved to Utah State University where he began his PhD study.

Published Journal Articles

- Yu, W. and Tang, T.: "Variational Asymptotic Method for Unit Cell Homogenization of Periodically Heterogeneous Materials", *International Journal of Solids and Structures,* vol. 44, 2007, pp. 3738-3755.

- Yu, W. and Tang, T.: "A Variational Asymptotic Micromechanics Model for Predicting Thermoelastic Properties of Heterogeneous Materials", *International Journal of Solids and Structures*, vol. 44, no. 22-23, 2007, pp. 7510-7525.

- Tang, T. and Yu, W.: "A Variational Asymptotic Micromechanics Model for Predicting Conductivity of Composite Materials", *Journal of Mechanics of Materials and Structures*, vol. 2, no. 9, 2007, pp. 1813-1830.

- Tang, T. and Yu, W.: "Variational Asymptotic Homogenization of Heterogeneous Electromagnetoelastic Materials", *International Journal of Engineering Science*, vol. 46, no. 8, 2008, pp. 741-757.

- Tang, T. and Yu, W.: "Variational Asymptotic Micromechanics Modeling of Heterogeneous Piezoelectric Materials", *Mechanics of Materials*, vol. 40, 2008, pp. 812-824.

Published Conference Papers

- Li, L., Harrison, M., and Tang, T., "Microstructure of Laser Deposited Superalloy Rene-80 on GTD-111", *International Conference on Joining of Advanced and Specialty Materials VII, ASM Materials Solutions*, 2004, Columbus, Ohio, Oct. 2004.

- Yu, W. and Tang, T., "Asymptotical Construction of a Micromechanics Model for Periodically Heterogeneous Anisotropic Materials," *Proceedings of the 47th Structures, Structural Dynamics, and Materials Conference*, Newport, Rhode Island, May 1-4, 2006.

- Yu, W. and Tang, T., "A New Micromechanics Model for Predicting Thermal Properties of Heterogeneous Materials," *Proceedings of the 2006 ASME International Mechanical Engineer-ing Congress and Exposition*, Chicago, Illinois, Nov. 5-10, 2006.

- Yu, W. and Tang, T., "A New Micromechanics Model of Heterogeneous Materials," *Proceedings of the 17th Army Solid Mechanics Symposium*, Baltimore, Maryland, Apr. 2-5, 2007 (Abstract).

- Williams, T. O.; Yu, W.; Aboudi, J.; Bednarcyk, B. A.; Tang, T.;: "A Critical Evaluation of the Predictive Capabilities of Various Advanced Micromechanics Models," *Proceedings of the 48th Structures, Structural Dynamics, and Materials Conference*, Waikiki, Hawaii, Apr. 23-26, 2007.

- Tang, T. and Yu, W., "A New Micromechanics Model for Predicting Effective Thermal Conductivity of Heterogeneous Materials," *Proceedings of the 48th Structures, Structural Dynamics, and Materials Conference*, Waikiki, Hawaii, Apr. 23-26, 2007.

- Tang, T. and Yu, W., "A Variational Asymptotic Model for Predicting Initial Yielding Surface and Elastoplastic Behavior of Metal Matrix Composite Materials," *Proceedings of the 2007 ASME International Mechanical Engineering Congress and Exposition*, Seattle, Washington, Nov. 10-16, 2007.

- Tang, T. and Yu, W., "Variational Asymptotic Micromechanics Modeling of Heterogeneous Piezoelectric Materials," *Proceedings of the 49th Structures, Structural Dynamics, and Materials Conference*, Schaumburg, Illinois, Apr. 7-10, 2008.

- Tang, T, and Yu, W., "A Multiphysics Micromechanics Model of Smart Materials Using the Variational Asymptotic Method", *Proceedings of the SMASIS08 2008 ASME Conference on Smart Materials, Adaptive Structures and Intelligent Systems*, Ellicott City, Maryland, October 28-30, 2008.

- Tang, T, and Yu, W., "Micromechanics Modeling of the Nonlinear Behavior of Electrostrictive Multiphase Composites", *Proceedings of the SMASIS08 2008 ASME Conference on Smart Materials, Adaptive Structures and Intelligent Systems*, Ellicott City, Maryland, October 28-30, 2008.